Cranfield

College of Aeronautics Report No.9114
September 1991

AN INVESTIGATION INTO THE INTERFACE BETWEEN THREE CLOSELY SPACED AXI-SYMMETRIC BODIES AT SUBSONIC SPEED

D.I.T.P. Llewelyn-Davies

College of Aeronautics
Cranfield Institute of Technology
Cranfield, Bedford MK43 0AL. England

Cranfield

College of Aeronautics Report No.9114
September 1991

AN INVESTIGATION INTO THE INTERFACE BETWEEN THREE CLOSELY SPACED AXI-SYMMETRIC BODIES AT SUBSONIC SPEED

D.I.T.P. Llewelyn-Davies

College of Aeronautics
Cranfield Institute of Technology
Cranfield, Bedford MK43 0AL. England

ISBN 1 871564 387

£10.00

CoA Report No 9114

September 1991

An investigation into the interference between three closely spaced axi-symmetric bodies at subsonic speed

by

D.I.T.P. Llewelyn-Davies

College of Aeronautics
Cranfield Institute of Technology
Cranfield, Bedford MK43 0AL, U.K.

SUMMARY

An experimental investigation has been made into the interference effects present between three closely-spaced bodies over a range of 0 to +6 degrees of either pitch or yaw. Detailed C_p distributions were obtained over the bodies and these were successively intergrated to obtain the loading distribution along the bodies and the overall forces and moments.

By analysis of contour maps representing the C_p distribution over the bodies, the loading diagrams, and the overall loads, the extent of the interference regions and their effect on the aerodynamic characteristics of the bodies were determined.

A panel method was used to estimate the C_p distributions over the bodies and, as previously, the loading distributions along the bodies and the overall forces.

There was close agreement between the estimated and experimental results over the forebody and the regions where there were appreciable interference effects, but the agreement over the rear of the afterbody was less good. Although the differences between the C_p distributions did not appear large, the differences between the afterbody loadings were appreciable at the higher attitudes with the result that the experimental loads were up to double the estimate. However, an empirical correction method was developed which resulted in the corrected estimates agreeing well with experiment.

Estimates were also made of the characteristics of the bodies when the attitude of the body combination was varied between 0 and -6 degrees pitch, and when yaw was varied between 0 and +6 degrees at pitch angles of +6 and -6 degrees.

CONTENTS

1.0 INTRODUCTION

The carriage of external stores on an aircraft has often led to aerodynamic problems such as high interference drag and poor release characteristics. These problems are most serious when the stores in close proximity to each other and the mutual interference between them becomes large. Accordingly a research programme to investigate the interference between similar axisymmetric bodies was initiated at the College of Aeronautics with MOD(PE) support.

In general, when stores are carried externally on an aircraft, they are mounted so that their axes are parallel to each other. The main parameters that then determine the geometric configuration are a) the number of stores in close proximity, b) the distance apart of their centre-lines, (separation), and their longitudinal spacing relative to each other, (stagger).

In order to determine the magnitude and extent of the interference between the bodies, the pressure distribution over the surface of an instrumented body was measured first in isolation and then in the presence of similar, but uninstrumented, bodies located in the required positions relative to it. The local loading distributions along the instrumented body and its overall aerodynamic characteristics were then obtained by successive integration of the measured pressures.

Estimates were also made using a computational fluid dynamic, (CFD), panel method, to see how well the interference effects could be predicted. Since the method used was unlikely to predict separated flow accurately, a body shape was chosen which would have attached flow over the afterbody but would also have significant viscous effects at small pitch angles.

The chosen body, Fig 1, had an ogival nose of 3:1 fineness ratio. The ogive was continued past the position of the maximum diameter until its tangent made an angle of 3.00 degrees to the body

centre-line when it blended into a 3.00 degree semi-angle conical boat tail. This was truncated at a distance of 7.665 D_{max} fron the nose to form a bluff base of diameter 0.538 D_{max} where D_{max} is the maximum diameter of the body.

Previous investigations in this series have determined:-

a) the basic characteristics of the body, ref 1

b) the effect of separation on the interference between two unstaggerd bodies at zero pitch, ref 2

c) the effect of stagger on two bodies at zero pitch whose centre-lines have a separation of 1.05 D_{max}, ref 3

d) the effect of pitch and yaw on a body combination consisting of two unstaggered bodies whose centre-lines have a separation of 1.11 D_{max}, ref 4

e) the effect of pitch and yaw on a body combination consisting of two bodies which are staggered by 3.0 D_{max} and whose centre-lines have a separation of 1.11 D_{max}, ref 5.

The purpose of the present investigation is to determine the interference between the bodies of a three-body configuration at zero pitch and the effect of pitch and yaw on this interference. The configuration chosen consisted of three unstaggered bodies whose axes were parallel. The bodies were arranged in a symmetrical triangular configuration, Fig 2, with the central body below the two outer bodies and the lines joining the centre-lines of the central and outer bodies inclined at +/- 45 degrees to the vertical. The separation between the centre-lines of the central and outer body was 1.11 D_{max}, the same as used previously in the two-body configurations. The resultant separation between the centre-lines of the two outer bodies was therefore 1.575 Dmax.

As this report is rather long due to the large amount of data to be analysed, the reader may find it advantageous to read Section 14 first and then refer to other sections as required.

2.0 EXPERIMENTAL DETAILS

2.1 Model and rig

Several modifications were made to instrumented model and the model support system.

The model was modified to have 3 additional pressure tappings added along the pressure-plotting generator at x/L = 0.9625, 0.98125 and 0.99025. In addition, another pressure tapping was inserted in the base region in the plane of the pressure-plotting generator at 0.90 of the base radius, Table 1.

The method of attaching the support stings to the rectangular cross-section strut spanning the windtunnel was altered so that the third body could be rigged.

Previously both bodies had been mounted completely independently from the strut, ref 5. This had made the alteration of the pitch of the models a very time-consuming operation as, not only was it necessary to re-rig both bodies, but the multiplicity of rigging wires made it difficult to remove the setting jig without damage to the lightweight dummy body once the position of the models had been finalised.

In the revised support system, Fig 2, the sting of the heavy, instrumented body was pivotted from the support strut and the turntable bridle wires were used to control the pitch of the model as previously. Each the lightweight models were now mounted from the sting of the instrumented body by two radius arms of variable length which were clamped to the sting on either side of the support strut. The stings from the dummy bodies were attached to the radius arms by U-bolts. In order to make the mounting system as rigid as possible, a turnbuckle was used to connect each set of radius arms and thus form a triangulated structure, Fig 2 b).

As the sting clamps and radius arms were made from rectangular bar for ease of manufacture, and the clamps used to secure the radius arms to the sting formed a large bluff addition to the sting of the instrumented body, brief tests were made to determine whether the base-pressure and/or the pressures measured over the rear of the body differed from those previously measured on the single body, ref 1. Although appreciable differences were present, it was found that they could be eliminated by fairing the front clamp-sting junction with a 10-degree semi-angle conical fairing.

The radius arm and U-bolts formed a much smaller bluff projection on the dummy-body stings. Becasuse no measurements could be made on these bodies, the radius-arm/sting junctions were not faired as it was considered that the main interference effects would be near the position of minimum gap between the bodies and thus any forward interference effects of these junctions on the afterbodies of the dummy bodies would not have any significant effect on the interference between the bodies.

As the instrumented body had to be tested in both the centre and outer positions, two different mounting arrangements had to be used as, because of its weight, the instrumented body had to be mounted directly from the support strut, Fig 2 a). When the instrumented body was in the central position, its sting was mounted 4 inches, 0.506 D_{max}, below the tunnel centre-line with the stings suporting the dummy bodies being positioned on either side of the support strut. When the instrumented body was tested in the outer position, its support sting was moved upwards along the support strut so that the bodies were in the same vertical position in the tunnel as in the previous case. However this meant that the body combination was now positioned slightly asymmetrically in the tunnel.

2.2 Model rigging

The previous method used to position the models relative to each other was to use a jig which was located in the midst of the two sets of wires supporting the bodies. Although the models were located satisfactorily, considerable care had to be taken in removing the jig to ensure that the lightweight bodies were not damaged.

For these tests, two revised setting jigs were used, one for each position of the instrumented body. In each case the jig was located by the nose and maximum diameter of the instrumented body and clamped in position so that the plane containing the centre-lines of the outer bodies was horizontal, Fig 2 c). The position of the noses of the dummy models was indicated by the jig. The positions of maximum diameter of the dummy bodies were located by two 'Vee' cutouts whose sides were at +/- 45 degrees to the horizontal. When the dummy bodies had been located, the jig was unclamped and removed forwards.

As the dummy bodies were now located relative to the sting of the instrumented body, no further adjustments were necessary when the instrumented body was moved in either pitch or yaw.

2.3 The data recoding system

The pressure measuring and data recording system was the same as that described in detail in ref 4. With this system the accuracy in measuring C_p was approximately +/- 0.0003 under static conditions. When the model was tested in the wind tunnel, the accuracy deteriorated due to tunnel unsteadiness etc., and it was estimated that most pressures were measured to within an accuracy of C_p = +/- 0.001 with an occasional reading being in error by as much as C_p = 0.003.

2.4 Data reduction

The pressure distribution around the body at each longitudinal station was integrated to give the local normal-force, side-force and axial-force loadings. These were then integrated along the length of the body to obtain the overall forces and moments acting on the body and hence the position of the lines of action of the normal and side forces.

The results are presented about the system of body axes shown in Fig 3 and whose origin is at the nose of the body.

2.5 Transition fixing

As the models were tested at a Reynolds number of approximately 3,300,000 based on model length or 430,000 based on body diameter, it was necessary to ensure a turbulent boundary layer over the bodies by fixing transition by means of a narrow, (0.1 inch), band of distributed roughness at 0.06L behind the nose as described in ref 4.

3.0 TEST PROGRAMME

The original object of the test programme was to determine the interference between the bodies over a 6 degree range of pitch and yaw.

As only one of the three bodies was instrumented, it could be necessary to move it to all three positions in order to completely determine the complete interference effects on the configuration.

As the configuration was symmetrical about the vertical centre-line, the instrumented body had to be tested in only the central and one outer position to determine the interference due to pitch at zero yaw. However it was necessary to test the configuration at both positive and negative pitch as there was no horizontal plane of symmetry.

The interference effects due to variation of yaw also could be determined with the instrumented body in only the central and one outer position if the configurations were tested at positive and negative yaw.

As sufficient wind-tunnel time was not available to complete the intended programme, it was decided to eliminate the tests at negative pitch, with one exception, and the tests at combined pitch and yaw.

The resultant test programme was:-

a) with central body instrumented.

Pitch = -2.0 → 6.0 degrees at 2.0 degree intervals at zero yaw

Yaw = 0.0 → 6.0 degrees at 2.0 degree intervals at zero pitch

b) with port body instrumented.

Pitch = 0.0 → 6.0 degrees at 2.0 degree intervals at zero pitch

Yaw = -6.0 → 6.0 degrees at 2.0 degree intervals at zero pitch

4.0 VARIATION OF THE EXPERIMENTAL LOADINGS WITH PITCH

The variation of the experimental loading distributions with pitch are shown in Fig 4. The variation of the magnitude and position of the peaks in the loading distributions are shown in Fig 5.

4.1 Normal-force and pitching-moment loading distributions at zero pitch

The normal-force loading distributions for the central and port bodies are shown in Fig 4 a).

The loading distributions are rather different for the two bodies.

Because the central body is below the two outer bodies, it has two regions of low pressure induced on the upper surface of the body due to interference from the wing bodies. These result in high positive normal-force loadings in regions centred on the positions of minimum gap between the bodies, ie centred on positions inclined at +/- 45 degrees from the top centre-line of the body at the position of maximum diameter of the body, x/L = 0.392.

Whilst this is the main region of interference due to the outer bodies, these bodies also induce a region of downwash over the nose of the central body resulting in a negative loading distribution over the nose of the body which, up to x/L = 0.16, is very similar to that over a single body, ref 2, but reaches a peak value slightly farther from the nose. The magnitude of this part of the loading distribution is roughly eqivalent to that of a single body at about -6 degrees pitch, i.e. there is a mean downwash of approximately 6 degrees over the nose of the body.

Aft of x/L = 0.2, the loading rapidly increases until the position of maximum interference is reached, x/L = 0.39. This maximum loading , $dC_N/d(x/L)$ = 2.35, agrees well with that deduced from the measured interference on two unstaggered bodies with the same separation, ref 4. Aft of this, the loading diminishes, rapidly at first and then more gradually, to reach zero at x/L = 0.55. The loading then becomes slowly more negative and reaches a minimum value at approximately x/L = 0.7 and then increases slowly to become approximately zero at x/L = 0.99. Although the shape of the distribution over the afterbody differs somewhat from that of a single body, the distribution aft of x/L = 0.7 is very similar to that of a single body at +2 degrees pitch, i.e. a mean upwash over the rear of the afterbody of approximately 2 degrees.

The normal-force loading distribution over the port body is rather different.

The main interference region is again centred on the position of maximum diameter of the bodies. This is due mainly to the considerable interference effect due to the close proximity of the central body, separation = 1.11 D_{max}, which will be centred about a point 45 degrees from the bottom centre-line of the body at the position of maximum diameter. In addition there is some interference from the starboard body. However, as the distance between the port and starboard body centre-lines is 1.57 D_{max}, the mutual interference will be about half that due to the central body, ref 2. As the centre-lines of the outer bodies are in the same horizontal plane, the mutual interference between them will mainly affect the side-force loadings, but there will be a small effect on the normal-force loadings due to the shielding effect of the central body.

The loading distribution over the front half of the nose is the same as that of the single body at a pitch of +2 degrees, i.e. a mean upwash of approximately 2 degrees over the nose of the body.

Aft of x/L = 0.2, the loading decreases to a reach a negative peak value, $dC_N/d(x/L)$ = -1.06, at x/L = 0.39, the position of minimum gap between the bodies. As x/L increases, the loading becomes less negative, fairly rapidly at first and then at a decreasing rate until it becomes zero at x/L = 0.55. Aft of this the loading increases slowly to reach a small positive peak at x/L = 0.65 and then decreases gradually to zero at the base of the body. The loading distribution over the rear of the afterbody corresponds to that over the afterbody of a single body at a pitch of about -1 degree, i.e. a mean downwash over the rear of the body of approximately 1 degree.

The pitching-moment loading distributions are shown in Fig 4 b). These loadings are obtained by multiplying the local normal-force loading at a given position by its distance from the nose of the body. Thus the shapes of the distributions are very similar to the normal-force distributions but with the variations emphasised as x/L increases.

4.2 The effect of pitch on the normal-force and pitching-moment loading distributions

The variations of the normal-force loadings with pitch, Fig 4 a), have been analysed to show the variation in magnitude and position of the maxima and minima in the distributions as pitch is varied, Fig 5 a).

There are considerable differences in the way the loading distributions over the central and port bodies alter as pitch increases.

In the case of the central body, the main interference peak, peak 3 in Fig 5 a), increases linearly by 20% as pitch increases to 6 degrees, but does not alter significantly in location from the position of maximum diameter of the body, x/L = 0.39.

As pitch changes, the alteration in loading at a given station relative to that at zero pitch, i.e. the additional loading, varies approximately linearly with increase in pitch but the variation along the body is completely different from that present on a single body. In the case of the single body, the additional loading increases gradually to reach a maximum at x/L = 0.16, decreases to become zero at the position of maximum diameter, x/L = 0.39, and then decreases further to reach a minimum value at the beginning of the conical afterbody, x/L = 0.45. Aft of this, the loading gradually increases to become approximately zero at the base of the body. In the case of the central body, the additional loading increases to reach a maximum at x/L = 0.16 as above, but then remains constant up to the position of maximum diameter before decreasing rapidly become zero at about x/L = 0.41 and then remaining small and negative along the rest of the afterbody.

It would appear therefore that the interference of the outer bodies on the central body varies appreciably with change of pitch and is not invariant as might be expected.

The variation of the normal-force loading distribution along the port body with pitch, Fig 4 a), indicates that, not only does the loading at the position of maximum diameter vary little in magnitude and position, Fig 5 a), but the additional loadings at a given station vary in a similar manner to the loading distribution along a single body. Thus it is likely that the normal-force interference on the port body due to the other bodies does not vary greatly with pitch.

The variation of the pitching-moment loading distribution with pitch is shown in Fig 4 b). As explained previously, these graphs are derived directly from the normal-force distributions and present the same information with a variable y-axis scale.

4.3 The side-force and yawing-moment distributions at zero pitch

The side-force loading distributions are shown in Fig 4 c).

As the body combination is symmetrical about the vertical centre-line of the central body, the side-force loadings along the central body are sensibly zero.

The side-force loading distribution over the port body is very similar in shape to that of the normal-force loading distribution over the central body but the magnitude of the peaks is only about 80% of that on those of the normal-force distribution. As the contribution to the interference peaks from the central body will be approximately 50% of the magnitude of the central body normal-force peaks, the remainder will be due to the interference from the starboerd body.

The shape of the forebody distribution is very similar to that of the single body at an angle of about -4 degrees indicating that there is a mean outflow of approximately that magnitude over the forebody due to the presence of the other bodies.

The distribution also indicates that there is a small inflow over the rear of the afterbody of about 1 degree.

4.4 The effect of pitch on the side-force and yawing-moment loading distributions

The variation of the side-force loading distributions over the central and port bodies with pitch is presented in Fig 4 c) and the corresponding yawing moment distributions in Fig 4 d). As the yawing-moment distributions are derived directly from the side-force distributions, only the side-force distributions will be analysed here.

As the outer bodies are symmetrically positioned about the central body, it would be expected that the side-force loading on the central body would remain zero and this is confirmed by the experimental distributions.

As pitch increases, the forebody and main interference peaks on the port body side-force loading distributions become more positive and move forwards slightly, with most of the movement occurring between 0 and 2 degrees pitch, Fig 5 b). At the same time the afterbody loading peak steadily becomes more negative and also moves forward slightly. However, the loading at the rear of the body remains small at all pitch angles.

These variations in the loading distributions indicate that the previously deduced outflows over the forebody and afterbody vary appreciably with pitch with the mean outflow over the forebody decreasing and that over the afterbody increasing with increase of pitch.

The variation in shape of the forebody loading distribution with pitch is considerably different from that expected from a single body, but, on the basis of the variation of the forebody and afterbody loading peaks, it would seem that the forebody outflow halves between 0 and 6 degrees pitch and the afterbody outflow doubles over the same range.

4.5 The axial-force loading distributions

The axial-force loading distributions of both bodies alter little in general shape with pitch, Fig 4 e).

The forebody loadings increase rapidly to reach a large positive peak at about x/L = 0.06. They then decrease equally rapidly to become zero at about x/L = 0.2, reach a negative peak at

about x/L = 0.28 and then increase rapidly to become zero at the position of maximum body diameter.

The loadings continue to increase at the same rate along the ogival part of the afterbody and reach a peak value at x/L = 0.45, the beginning of the conical part of the afterbody. Aft of the position the loading decreases, rapidly at first, to reach a slightly negative minimum value at about x/L = 0.85, before increasing to approximately zero at x/L = 0.99.

The distributions are very similar in magnitude and shape aft of the second, negative, peak but the magnitude of the first, positive, peak is appreciably greater in the case of the central body.

The variation with pitch of the magnitude and position of the loading peaks is shown in Fig 5 c).

There are significant differences in the behaviour of the first and second loading peaks on the central and port bodies as pitch varies. In the case of the central body, both the first and second peaks become more positive in value as pitch increases and move slightly aft, whilst the corresponding peaks on the port body distributions become more negative and move slightly forward as pitch increases.

Although the position and magnitude of the third and fourth loading peaks on both bodies do not vary with change of pitch, there are differences in the loading distributions aft of the fourth loading peak. In the case of the port body, there is no change in the loading distribution as pitch varies, but the central-body loading distribution becomes more positive with change in pitch with the maximum change occurring near x/L = 0.6

5.0 VARIATION OF THE AERODYNAMIC CHARACTERISTICS WITH PITCH

The variations of C^N, C_Y, C_A, C_m, C_n, X_N and X_Y with pitch are presented in Figs 6 a) - g). These variations are presented for the central and port bodies separately and for the complete 3-body configuration. In addition, the single body results are presented for comparison. In the case of the 3-body configuration, the results are non-dimensionalised using the total cross-sectional area of the three bodies as the reference area and thus making all the results directly comparable as the results for the component bodies and the single body used the cross-sectional area of a single body as the reference area.

5.1 Normal-force characteristics

The variation of C_N with pitch is non-linear for both the central and port bodies, Fig 6 a).

In the case of the central body, C_N is large and positive at all pitch angles due to the two regions of low pressure on the top of the body due to the interference from the outer bodies, and varies between 0.23 at zero pitch and 0.465 at 6 degrees pitch. The variation is linear between 0 and 4 degrees pitch but the slope increases markedly between 4 and 6 degrees. For this body only, there is an additional value available at -2 degrees pitch. This indicates that the variation is less in this region than over the linear part of the curve at positive pitch. This is not unexpected as there is no horizontal plane of symmetry.

Due to the interference between the bodies, there is a region of low pressure near the bottom of the port body which results in negative values of C_N at all pitch angles but which become more positive with increase in pitch, varying from -0.12 to -0.04 between 0 and 6 degrees pitch. Like the central body, the variation is non-linear with the slope decreasing as pitch increases.

When these results are combined to obtain the C_N variation for the 3-body combination, and compared with those of the single-body, it can be seen that the two curves are parallel to each other with the values of C_N for the 3-body combination being slightly more positive. It is possible that this may be due to differences in alignment of the bodies to the oncoming flow at the nominal zero pitch position.

The variation of C_m with pitch is shown in Fig 6 b).

The values of C_m measured on the central body are considerably negative at all pitch angles with the maximum value occurring at 0 degrees pitch. As pitch increases, C_m becomes more negative at an increasing rate.

In the case of the port body, C_m is positive at all angles of pitch and increases almost linearly with pitch.

The slope of the variation of C_m with pitch for the single body is similar in character to that of the port body, but the value of C_m at zero pitch is small and positive.

The variation of the position of the centre of normal-force, X_N, with change in pitch is shown in Fig 6 c).

The position of the centre of normal-force varies greatly both with the particular body and with pitch.

In the case of the central body, X_N = -0.58L at -2 degrees pitch and slowly becomes more positive as pitch increases to reach a value of -0.30L at 6 degrees pitch.

The position of the centre of normal-force of the port body is near the same position as that of the central body at zero

pitch, X_N = -0.37L, but X_N rapidly becomes more negative with increase in pitch to reach a value of -2.26L at 6 degrees pitch.

In the case of the single body, the value of X_N at zero pitch, -0.28, agrees reasonably well with that of the central and port bodies. However X_N increases rapidly with pitch to reach a value of +0.3 at 2 degrees pitch and then decreases slowly with further increase in pitch to a value of +0.22 at 6 degrees pitch.

It should be noted that the accuracy of measurement may be rather poor near zero pitch as unlike the other bodies, the values of C_N and C_m are both small and thus the value of C_m/C_N is sensitive to small errors in measurement with the result that the agreement at zero pitch may be fortuitous.

The large rearward movement of X_N in the case of the port and central bodies is a direct result of the large interference effects which are centred about the position of maximum diameter, 0.39L.

In the case of the central body, the loadings up to this point increase with increase in pitch, Fig 4 a), but those aft of it hardly alter thus resulting in a forward movement of the centre of normal-force.

The loading distribution over the port body behaves rather differently as pitch increases. Firstly, the main interference loading peak is negative and smaller than that of the central body. Although it is appreciably larger than the forebody loading peak at zero pitch, as pitch increases the main interference peak alters little but the forebody peak becomes increasingly more positive until, by 6 degrees pitch, it is equal in magnitude to the main interference peak.

Although the loadings at the base of the body are very small at all pitch angles and the loadings at the position of maximum interference vary little with pitch, the loadings in between these points

become appreciably more negative with increase in pitch. These changes result in the increase in C_N as pitch varies with the rate of increase falling off as pitch increases due the the changes in afterbody loading. These changes in the afterbody loadings also explain the large rearward movement of X_N as pitch increases.

5.2 Side-force characteristics

The variation of C_Y with pitch for the various configurations is shown in Fig 6 d). As would be expected, for reasons of symmetry, C_Y is very small and varies little with pitch for the single-body, three-body and central body configurations which also agree well with each other. On the other hand, the interference effects on the port body result in appreciable values of C_Y which increase slightly with increase in pitch.

The variation of C_n with pitch is shown in Fig 6 e). The values for the central and single body are small and vary little with pitch as would be expected for reasons of symmetry. In the case of the port body, C_n is -0.096 at zero pitch and increases linearly with pitch to reach a value of -0.069 at 6 degrees pitch.

From these variations of C_Y and C_n, the variation of the position of the centre of side-force, X_Y, with pitch has been obtained, Fig 6 f).

The position of the centre of side-force for the central-body becomes steadily more negative as pitch increases. Because both C_Y and C_n are small and are the result of various experimental errors, the errors in X_Y may be large and thus the linearity of the variation may be fortuitous.

In the case of the port body, the position of the centre becomes steadily more positive as pitch increases with the rate of change being approximately the same as the central body.

5.3 Axial-force characteristics

The variation of C_A with pitch for the various bodies is shown in Fig 6 g). Both the forebody and total C_A are shown with the difference between the two curves being the afterbody C_A. For ease of analysis, the variations for the central and port body results are presented separately as is the comparison between the single-body and the 3-body configuration.

In the case of the central body, both the forebody and total C_A increase appreciably with increase in pitch with the total C_A increasing at a faster rate. Thus the afterbody C_A also increases with increase in pitch but at a considerably slower rate than that of the forebody. The variation is linear over the range +/- 2 degrees for both the forebody and total C_A. At higher pitch angles, the slope of the variation decreases in both cases but more markedly in the case of the forebody. The forebody C_A is negative at pitch angles below 3½ degrees and varies between -0.035 at -2 degrees pitch and 0.006 at +6 degrees. The total C_A varies between -0.009 and + 0.056 over the same pitch range. The difference between the curves, i.e. the afterbody C_A, therefore varies between 0.026 and 0.05 over the pitch range, a considerably smaller variation than the other two.

The variation of C_A with pitch for the port body is completely different. Although the value of the forebody C_A at zero pitch is exactly the same as that of the central body, -0.02, it becomes more negative as pitch increases. The variation is linear with pitch up to 4 degrees, but falls off at an increasing rate at higher angles.

The variation of total C_A with pitch is very similar in character to that of the forebody C_A as the slope and extent of the linear part of the variation is the same, but falls off less rapidly at the higher pitch angles. The value of the total C_A at zero pitch is slightly less than the corresponding value for the central body.

The total C_A varies between 0.007 at 0 degrees pitch and -0.021 at 6 degrees with the corresponding variations for the forebody and afterbody C_A being -0.020 to -0.052 and 0.027 to 0.031 respectively.

Comparison of the comparable C_A variations for the single body and the 3-body combination shows that the variations of both the total and forebody C_A with pitch are very similar in that C_A decreases slightly over the range 0 → 3 degrees pitch and then decreases at an increasing rate. The two forebody variations are parallel as are the two total C_A variations but the rate of decrease at the higher pitch angles is appreciably greater for the forebody variations.

The variation of total C_A with pitch for the 3-body combination is from 0.0077 at 0 degrees pitch to 0.0044 at 6 degrees whilst the correspoonding variation for the single body is from 0.0042 to 0.0002.

Both the 3-body combination and single body have negative values of the forebody C_A at all pitch angles with the values for the 3-body combination being considerably more negative. The forebody C_A for the 3-body combination varies from -0.020 at zero pitch to -0.033 at -6 degrees whist the corresponding variation for the single body is from -0.003 to -0.015.

From these results it can be seen that the interference between the bodies has large effects on the distribution of C_A between the forebody and afterbody. In comparison with the single-body results, the interference effects cause a large diminution in forebody C_A and a somewhat larger increase in afterbody C_A resulting in a modest increment in total C_A. This increment however is large in percentage terms because the total C_A, being the difference between two large quantaties, is small in absolute terms.

6.0 VARIATION OF THE EXPERIMENTAL LOADINGS WITH YAW

The variation of the side-force, yawing-moment, normal-force, pitching-moment and axial-force loading distributions with yaw are presented in Figs 7 a) - e).

The presentations of the distributions for the central and outer bodies are slightly different.

As the outer bodies are symmetrically located relative to the central body, it was only necessary to obtain the central body loading distributions over the range of 0 → 6 degrees yaw to determine completely the variation of the loadings with yaw.

In the case of the outer body, the body could be either to windward or leeward of the central body and therefore, as only the port body was pressure plotted, it was necessary to obtain the distributions at both positive and negative yaw to determine the loading distributions over the windward and leeward bodies. The distributions are presented in the form that they were obtained to avoid having to make corrections for any rigging misalignments in the initial yaw setting as might be necessary if the negative yaw distributions were converted to represent those of the starboard body.

The variation in the magnitude and position of the peaks in the loading distributions over the central and port bodies is shown in Figs 8 a) → c).

6.1 Side-force and yawing-moment loading distributions

The variation of the side-force loading distributions with yaw are shown in Fig 7 a).

The loading distributions over the central and port bodies are rather different in character. The main interference between

the bodies is centred about the position of minimum gap between the bodies. As the outer bodies are positioned symmetrically about the central body, the side-force interference of these bodies on the central body is equal and opposite and thus there is no side-force loading at zero yaw. Change in yaw then results in a side-force loading distribution that is somewhat similar to that generated on a yawed single body, ref 1. In the case of the outer bodies, the interference loading is asymmetric and thus generates a complicated side-force interference loading distribution at zero yaw which is appreciable in magnitude and on which is superimposed the side-force loadings that are generated when the bodies are yawed.

6.1.1 Central-body loading distributions

Although the loading distribution along the yawed central body is superficially similar to that of the single body, there are considerable differences in detail. These are :-

a) Although the forebody loading distributions agree well up to x/L = 0.13, the peak in the single-body distribution occurs at x/L = 0.16 whilst the central-body loadings continue to increase until x/L = 0.21.

b) The loading peak in the central-body distribution is rather flatter than that of the single body.

c) As the loadings on both the central and single bodies decrease to zero at the position of maximum body diameter, x/L = 0.392, there is an appreciable increase in loading over the last half of the forebody of the central body and the rate at which the loading decreases over the rear of the forebody of the central body is much greater than that over the single body. This higher rate of decrease is continued as far as the junction between the ogive and the conical part of the afterbody where the negative loading over the central body reaches a peak that is approximately twice that present in the case of the single body.

d) The loadings then reduce smoothly along the conical part of the afterbody to approximately zero at the base of the body. The dip in the loading distributions at x/L = 0.78 noted in the case of the single-body, ref 1, had been found to be due to a programming error. This has

been corrected and thus neither the dip in the loadings or the third peak in the loading distribution are now present.

The magnitude of the forebody and afterbody peaks in the side-force loading distributions vary linearly with yaw but postion of the peaks remains constant, Fig 8 a).

Because the nose of the body was chosen as the moment-centre, the general characteristics of the yawing-moment distributions, Fig 7 b), are very similar to side-force distributions but with the differences in loading increasing gradually along the length of the body.

6.1.2 Port-body loading distributions

The side-force loading distributions over the port body are presented in Fig 7 a) for a range of yaw from -6 to +6 degrees. The variation in magnitude and position of the peaks in the loading distributions are presented in Fig 8 b).

The side-force loading distribution at zero yaw has been previous described in section 4.3.

Basically there is an outflow over the nose of the body due to the presence of the other bodies and this results in negative side-force loadings over much of the forebody. Towards the rear of the forebody the side-force loadings are dominated by the interference effects from the other bodies resulting in a large positive interference loadings which peak at the position of minimum gap between the bodies, (the position of maximum body diameter). Aft of this, the loadings decrease rapidly and are small over much of the afterbody where they are due to a small inflow over the rear of the afterbody.

When the bodies are yawed, there is very little change in the loading distribution in the immediate neighbourhood of the

position of maximum interference. However, as yaw becomes more positive, the afterbody loadings become slightly more negative and the forebody loadings become appreciably more positive.

At negative angles of yaw, the magnitude of the forebody loading peak becomes increasingly more negative as yaw becomes more negative and the general shape of the forebody distribution remains similar to that at zero yaw.

As yaw becomes increasingly positive, the forebody loading peak and the slope of the distribution near the nose of the body increase linearly. The effect of these changes is that an additional peak in the loading distributions is formed near the nose of the body at yaw angles of 4 and 6 degrees, Fig 8 a).

The afterbody loadings remain very small at the rear of the body at all yaw angles. Over the front of the afterbody the loadings increase linearly with decrease in yaw between 6 and -4 degrees, but there is only a small increase in afterbody loading between -4 and -6 degrees yaw. Between 6 and -4 degrees yaw the side-force loadings are slightly negative over the rear of the afterbody and thus there is a flat peak in the distribution as the loading at the base of the body is small. At angles of less than -4 degrees, the loadings remain positive over the whole of the afterbody and thus the 4th peak in the distribution is eliminated, Fig 8 a).

As previously, the yawing-moment distributions, Fig 7 b) are similar in character to the side-force distributions but the differences between the distributions increase with distance along the body as a result of the choice of moment centre.

6.2 Normal-force and pitching-moment loading distributions

The variation of the normal-force and pitching-moment loading distributions with yaw are presented in Figs 7 c) and d).The variations in the magnitude and position of the peaks in these loading distributions are shown in Fig 8 b).

There is virtually no change in the forbody loading distribution of the central body as yaw varies and only small changes in the afterbody distributions up to 4 degrees yaw with the loadings decreasing slightly with increase in yaw. Between 4 and 6 degrees yaw, the rate if increase becomes appreciably greater, but the overall increase is still small.

The changes in the port-body loading distributions as yaw varies are much larger.

The basic distribution at zero pitch has already been described in detail in Section 4.3. Briefly, the normal-force loading increases slowly along the forebody to reach a peak value at x/L = 0.2 and then decreases rapidly to reach a much larger negative peak at the position of maximum diameter, x/L = 0.39. Aft of this, the loading increases, rapidly at first, to reach a small positive peak at x/L = 0.65 before falling away slowly to a small positive value at the end of the body.

When yaw is varied, the forebody loadings become more positive with increase in yaw whilst, at most stations, the afterbody loadings become more negative as yaw increases. Therefore there is one position near the beginning of the afterbody at approximately x/L = 0.42, where there is very little change in loading with yaw.

Over the forebody, the normal-force loading slowly becomes more positive with increase in yaw. The magnitude of the peak loading increases approximately linearly with yaw from 0.03 at -6

degrees yaw to 0.43 at +6 degrees yaw while the peak moves aft from x/L = 0.09 at -6 degrees yaw to x/L = 0.19 at +6 degrees.

The main interference peak also becomes more positive with increase in yaw, varying approximately linearly from -1.18 at -6 degrees yaw to -0.96 at +6 degrees yaw whilst moving rearwards from x/L = 0.36 to x/L = 0.41.

The loading distribution at a given afterbody position varies most at the junction of the ogival and conical parts of the afterbody, x/L = 0.45, i.e. not very far aft of the position where the loadings vary little with yaw. At this position, the loading variation with yaw is not uniform, the variation between 2 and 6 degrees yaw being approximately equal to that between -6 and 2 degrees.

Over the first part of the conical afterbody, the variation of loading with yaw diminishes rapidly and somewhat irregularly until the peak in the afterbody loadings. The magnitude and position of this peak loading varies between 0.19 at x/L = 0.60 at -6 degrees yaw and 0.07 at x/L = 0.73 at +6 degrees yaw. Aft of the peak, the variation of the afterbody loadings with yaw decreases steadily as the rear of the body is approached as does the mean loading.

6.3 Axial-force loading distributions

The variation of the axial-force loading distributions with yaw are presented in Fig 8 e) for the central and port bodies and the variation in magnitude of the peaks in these loading distributions is shown in Fig 8 c).

Although all the loading distributions are very similar in shape, there are considerable differences in detail between the various distributions.

In general, the effect of yaw on the loading distributions is much greater on the outer bodies both in magnitude and extent.

Yaw makes very little difference to the central body loading distributions aft of x/L = 0.30, the position of the second peak in the distributions. However, although the position of the first two peaks does not alter with change in yaw, the peak loadings become more negative with increase in yaw with the first peak altering at a greater rate than the second.

The variation of the loading distributions along the port body are different in the following ways:-

1) Although the position of the first two peaks still does not alter with change in yaw, the peak loadings all become more positive as yaw increases rather than decreasing as they did along the central body.

2) The loadings alter at a slower rate at positive yaw and this rate is approximately half that at negative yaw.

3) The loadings vary little with yaw between x/L = 0.35 to 0.45 instead of aft of x/L = 0.3 for the central body.

4) Aft of the third peak at x/L = 0.45, the port body loadings again become more positive as yaw increases, except between -6 and -4 degrees yaw, but the rate of increase is considerably less than over the forebody and does not alter greatly along the afterbody.

7.0 VARIATION OF THE AERODYNAMIC CHARACTERISTICS WITH YAW

The variation of the aerodynamic characteristics of the bodies with variation of yaw at zero pitch are shown in Fig 9 a) - g). The graphs show the characteristics of each body separately and also complete combination. In some graphs, the characteristics of the single-body are also shown for comparison with the results for the complete combination.

Also shown are the estimated characteristics of the single-body and the complete combination. These results will not be discussed in this section, but will be discussed later as part of the analysis of the estimated results.

7.1 Variation of C_Y, C_n and X_v

The variation of C_Y with yaw for the various bodies and the 2-body combination are shown in Fig 9 a).

At zero yaw, the port and starboard bodies are subject to large interference effects which, for reasons of symmetry, result in large equal and opposite values of C_Y which are approximately double that of that due to yawing the body through 6 degrees. When the bodies are yawed, C_Y for the starboard, leeward, body increases linearly with yaw. The increase of C_Y with yaw for the port body is initially linear and of approximately the same slope as the starboard body, but above 4 degrees, C_Y increases at a greater rate.

The variation of C_Y with yaw for the central body is rather nonlinear, but most of the nonlinearity is due to the large value of C_Y measured at 2 degrees yaw. As the other 3 values vary linearly with yaw and the deviation of the value at 2 degrees yaw from this line is considerably greater than would be expected from experimental error, it is probable that there is some local effect causing the

increase. Examination of the loading distributions, Fig 7 a), shows that the forebody loading distributions vary regularly with yaw, but the afterbody distributions do not. It can be seen that the increments in the afterbody loadings between 0 and 2 degrees yaw are much smaller than those between 2 and 4 degrees and 4 and 6 degrees which are approximately equal. This rapid increase in the negative afterbody loadings above 2 degrees yaw results in a relative increase in C_Y at 2 degrees yaw as observed.

When the variation of C_Y with yaw is derived for the 3-body configuration, it can be seen that the variation is somewhat more linear than that of the central body and that a mean line through the data has a smaller slope that the mean through the central body data, as would be expected as the variation of C_Y with yaw is less for the outer bodies than the central body. However, the mean variation of C_Y with yaw for the 3-body combination is approximately the same as that of the single body.

The variation of C_n with yaw for the individual bodies and the single- body about their own body axes is shown in Fig 9 b). Although the values of C_n at zero yaw are very different, the variation with yaw is very similar for all the bodies and takes the form of a gradual increase in C_n with yaw which agrees well with that of the single body.

The variation of X_V,the distance from the nose of the line of action of C_Y, with yaw is shown in Fig 9 c). Where the values of C_Y are small, i.e near zero yaw in the case of the central and single bodies, the accuracy of X_V is poor and wide variations in value should be ignored.

The values of X_V for the single body and the 3-body combination are positive except at zero yaw. For the single body X_V has a value of approximately 0.23L above 4 degrees yaw, but this increases gradually at lower yaw angles until becoming negative near zero yaw.

The variation of X_Y with yaw for the central body varies between the same end values but in a more erratic way due to the irregular changes in C_Y at low angles as described above.

Because of the large interference effects, the value of X_Y for the port and starboard bodies is large and negative at zero yaw, -0.45. The variation with yaw is linear for both bodies, but of opposite slope. The slope of the variation for the starboard body is negative and its magnitude is approximately double that of the port body.

7.2 Variation of C_N, C_m, and X_N

The variation of C_N with yaw for the various bodies and the 3-body combination is shown in Fig 9 d) and the related variation of C_m with yaw is presented in Fig 9 e).

Because of the large positive interference from the outer bodies, the central body has a C_N value of 0.23 at zero pitch. With increase in yaw, this decreases in an irregular manner by about a third over the 6 degree yaw range.

The negative interference effects on the outer bodies result in the outer bodies having a C_N of -0.13 at zero yaw.

The variation of C_N with yaw is rather different for the two bodies. In the case of the starboard body, C_N becomes slighty more negative as yaw increases with the rate decreasing with increasing yaw. On the other hand, C_N becomes more positive as yaw increases in the case of the port body and, not only is the slope of variation greater than that of the starboard body, but the variation is more non-linear at yaw angles of greater than 4 degrees.

C_N does not vary with yaw in the case of the 3-body combination but has a small negative value probably due to errors in model alignment.

The variation of C_m with yaw for the individual bodies is shown in Fig 11 e). As previously the moments are measured about their individual body axes.

Because of the large interference effects between the bodies, the values of C_m at zero yaw are not zero.

In the case of the central body, the values of C_m vary between -0.103 at 0 degrees and -0.068 at +6 degrees yaw with the variation between 0 and 4 degrees being appreciably less than that between 4 and 6 degrees yaw.

The variation of C_m with yaw for the port and starboard bodies is almost identical with the values for the port body being slightly more positive than those of the starboard body. C_m for the port body varies between 0.047 at 0 degrees and 0.029 at 6 degrees yaw and that for the starboard body between 0.047 and 0.023. In both cases, the variation is rather smaller between 0 and 4 degrees yaw than between 4 and 6 degrees.

The variation of X_N with yaw for the individual bodies is shown in Fig 9 f).

The value of X_N for the central body remains constant at -0.44 between 0 and 4 degrees yaw and then becomes less negative with further increase in yaw.

The value of X_N at zero yaw for both the port and starboard bodies is -0.37, i.e rather more positive than the central body, but the variation with yaw is different. The value of X_N for the starboard becomes more positive at an increasing rate as yaw increases and reaches a value of -0.17 at 6 degrees yaw. In the case of the port body X_N becomes linearly more negative with increase in yaw and reaches a value of -0.52 at 6 degrees yaw.

7.3 Variation of C_A

The variations of both the forebody and total C_A with yaw for the various bodies are shown in Fig 9 g). The differences between the curves for corresponding bodies is thus the afterbody C_A.

The total C_A for the central body is +0.0089 at zero yaw and decreases slightly with increase in yaw to a value of +0.0060 at 6 degrees yaw. The forebody C_A is -0.020 at 0 degrees yaw and becomes more negative at an increasing rate with increase of yaw to reach a value of -0.034 at 6 degrees yaw. Thus, the afterbody C_A varies between +0.029 at 0 degrees yaw and +0.040 at 6 degrees.

The variation of C_A with yaw for the port and starboard bodies is rather different.

At zero yaw, the total C_A is +0.007 and the forebody C_A is -0.0205 for both bodies.

When yaw is increased, both the total and forebody C_A of the port body increase linearly with yaw, with the total C_A increasing at a greater rate thus indicating that the afterbody C_A also increases linearly with yaw. The total C_A increases from +0.007 at zero yaw to +0.047 at 6 degrees yaw whilst, over the same range, the forebody C_A increases from -0.0205 to +0.003. The afterbody C_A varies from +0.028 to +0.044 over the same yaw range.

Over the same range of yaw, both the total and forebody C_A of the starboard body decrease linearly with yaw with the total C_A decreasing at a greater rate. Thus the afterbody C_A will also decrease linearly with yaw. The total C_A varies from +0.007 at zero yaw to -0.036 at 6 degrees yaw. As the forebody C_A decreases from -0.0205 to -0.059 over the same range of yaw, the corresponding afterbody C_A varies from +0.028 to +0.023.

When the C_A values for the combination are obtained using the total body cross-sectional area as the non-dimensionalising area, the total C_A varies slowly from 0.008 at 0 degrees pitch to 0.006 at 6 degrees pitch while the forebody C_A varies from -0.02 to -0.030 over the same range of yaw and thus the afterbody C_A varies from +0.028 to +0.036.

In comparison, the total C_A of the single body varies from 0.004 to 0.000, the forebody C_A varies from -0.003 to -0.015 and the afterbody C_A varies from +0.007 to +0.015. Thus the total C_A of the 3-body combination is slightly greater than that of the single body and varies similarly with yaw. The forebody C_A however is also varies in the same manner as the single body but is consideably more negative. This indicates that the interference effects between the bodies has a large favourable effect on the forebody C_A. However, as the total C_A ot the 3-body combination is greater than that of the single body, the interference between the bodies has an even larger unfavourable effect on the afterbody C_A.

8.0 VARIATION OF THE INTERFERENCE EFFECTS WITH PITCH AND YAW

The interference loadings on a particular body were found by subtracting the single-body loadings from those measured on the chosen body at the same position and attitude. The changes in interference loading as attitude was altered, the 'additional interference' loading, were obtained by subtracting the corresponding interference loading at zero pitch and yaw from the interference loading at the other positions and attitudes.

Because the configuration is asymmetric, the interference characteristics were analysed for the normal-force, side-force and axial-force loadings. As loadings had only been obtained for the central and port bodies, the range of attitude examined was from 0 to 6 degrees in pitch at zero yaw and from -6 t0 +6 degrees yaw at zero pitch.

The results of the analysis are presented in Figs 10, 11 and 12.

8.1 Normal-force interference

The normal-force interference loading characteristics are presented in Fig 10.

8.1.1 Central body

The normal-force interference loading distribution for the central body at zero pitch and yaw consists of a relatively small negative region where the loading peaks at x/L = 0.16 and extends up to x/L = 0.25. This is followed by the main, positive, interference region which peaks at x/L = 0.39, extends up to x/L = 0.55, and has a peak interference loading approximately three times that of the front region. Aft of this, the interference loading is small and negative and, after peaking at x/L = 0.65, reduces to zero at the base of the body.

If the interference is examined in three regions, a) the front of the forebody up to x/L = 0.2, b) the remainder of the ogival part of the body, (up to x/L =0.45), and c) the remainder of the afterbody, it can be seen that the 'additional interference' due to change in pitch has a consistent pattern in that the 'additional interference' at the end of each region is virtually independent of change in pitch.

At 2 degrees pitch, the 'additional interference' is positive over the forebody and increases gradually over region a) and the first part of region b) to reach a peak value of about 1/20 of the basic interference loading at x/L = 0.34. It then decreases rapidly to reach a small negative value at the end of region b). The 'additional interference' then increases rapidly at the beginning of region c) to reach a small positive peak value, slightly greater than that in region a), which occurs near x/L = 0.5. Aft of this, the 'additional interference' reduces rapidly to zero at x/L = 0.6 and then remains slightly negative over the rest of the afterbody.

At 4 degrees pitch, the 'additional interference' is approximately zero over most of region a) before steadily increasing over the remainder of region a) and the beginning of region b) to reach a peak value of about double that at 2 degrees pitch but at the same position, x/L = 0.34. The 'additional interference' then falls rapidly to zero at the end of region b), the beginning of the conical afterbody, before recovering to reach a peak which is the same in magnitude and position as that at 2 degrees pitch but which is now about 2/3 the magnitude of the peak in region b). The 'additional interference' then falls gradually to zero at x/L = 0.8 and remains near zero over the remainder of the body.

The variation of the 'additional interference' along the body at 6 degrees follows the same general pattern except that it is now negative over the first part of region a), up to x/L = 0.18. The peak in the 'additional interference' loading in region b) is at the same

position as previously, x/L = 0.34, but has now doubled again in magnitude to become about 1/6 the maximum interference loading. The general form of the rest of the distribution is the same as at 4 degrees pitch except that the 'additional interference' does not become zero until x/L = 0.9.

The variation of the 'additional interference' with yaw is considerably less and does not vary so much along the body.

Up to x/L = 0.25 the 'additional interference' is small and negative. There is little difference between the 2 degree and 4 degree distributions but the increment between the distributions doubles between 4 and 6 degrees. Between x/L = 0.25 and 0.4 the 'additional interference' remains negative but increases steadily in magnitude. Between x/L = 0.4 and 0.5 the the 'additional interference' varies rather irregularly with yaw but reaches peak values approaching 8% of the maximum value of the basic interference. Aft of this, the 'additional interference' becomes much smaller, approximately the same as that at the rear of the forebody, x/L = 0.39, and slowly reduces over the rest of the afterbody. There is again relatively little difference between the 2 and 4 degree cases but a considerable difference between the 4 and 6 degree values.

8.1.2 Port body

The basic interference loading distribution over the port body is very similar to that over the central body but with the sign reversed and the magnitude halved.

The variation of the 'additional interference' loading with variation in pitch is slightly different to that of the central body.

Over the front of the forebody, (up to x/L = 0.15), the 'additional interference' increases slowly with x/L and varies little

with change in pitch. Aft of this, the distributions increase more rapidly with x/L to reach a peak value near x/L = 0.26. This peak value varies linearly with attitude with the maximum value at 6 degrees pitch being approximately 20% of the maximum interference loading at the datum condition. It must be pointed out that these maxima occur at very different positions along the body from the central body and the comparison is only intended to give a feel for the magnitude of the changes in interference taking place. The 'additional interference' then decrease rapidly to become approximately zero at the position of D_{max} and continue to fall to reach a very large negative value at the end of the ogive, approximately 40% of the maximum negative interference.

The 'additional interference' then rises very rapidly to reach a peak value near x/L = 0.5 and falls equally rapidly to a negative peak value near x/L = 0.55 before increasing slowly to reach approximately zero at the rear of the body.

At first glance, the variation of the 'additional interference' with yaw is similar to, but approximately double, the variation with pitch. Closer inspection, however, shows that there are some important differences as the distributions at positive and negative yaw are somewhat different.

Although the 'additional interference' loadings over the ogival part of the body due to positive yaw are indeed similar to those at positive pitch, but double in magnitude, the loadings over the conical afterbody are rather different in that they are zero aft of x/L = 0.60 at all yaw angles.

At negative yaw, the distributions of 'additional interference' along the body differ in that the initial slope of the variation along the body is rather greater than that at positive yaw, is yaw dependent but the peak values are only about 90% of those at positive yaw. Although the 'additional interference' loadings still peak at the beginning of the conical part of the afterbody, the magnitude of

the peak values is considerably smaller than at positive yaw and the distribution then decreases almost linearly with yaw and distance along the afterbody to a small value at the rear of the body instead of decreasing rapidly to zero as at positive yaw.

8.2 Side-force interference.

The side-force interference characteristics are shown in Fig 11.

8.2.1 Central body.

As the outer bodies are symmetrical about the vertical plane through the axis of the central body, there should be no side-force interference loading present on the central body at any pitch angle. The figure shows that the measured side-force interference loadings are generally small except near the position of D_{max}. As this is the position of greatest interference, the measured loadings are probably due to inaccuracies in rigging etc.

The variation of the distribution of the 'additional interference' along the body as yaw varies is reasonably consistent. Initially the 'additional interference' becomes more negative as x/L increases until it reaches a peak near x/L = 0.1 . The additional loading then becomes more positive with further increase in x/L until it becomes zero at about x/L = 0.17 and reaches a peak value at x/L = 0.28 before decreasing to become zero near the position of D_{max} and then falling rapidly to a large, negative, pitch-independent peak at the beginning of the conical afterbody. The additional interference then increases to a maximum near x/L = 0.55 before decreasing rapidly to small, generally negative, value at x/L = 0.6. Aft of this, the 'additional interference' remains approximately constant over the rest of the afterbody . Although the shape of the distributions are similar, the increments with yaw are not uniform, particularly near the positive peak over the rear of the forebody. In this region, the increment between the 4 and 6 degree

values is larger than the increments between 0 and 2 and 2 and 4 degrees yaw. However, over most of the conical afterbody, the 'additional interference' at 4 and 6 degrees yaw is approximately the same and appreciably more negative than that at 2 degrees yaw.

8.2.2 Port body

The variation of the interference loading with x/L at zero pitch is very similar that of the normal-force interference loading with x/L for the central body, Fig 10, except that the magnitude of the forebody loading peaks is some 10 to 15% less.

The 'additional interference' loading distributions at 2, 4 and 6 degrees pitch are very similar in character to the corresponding normal-force distributions except that the magnitudes of the side-force forebody loading peaks are approximately double that of the normal-force peaks, whilst the afterbody distributions are very similar in magnitude.

The distributions of the 'additional interference' loadings over the forebody appear, at first glance, to vary with yaw in a very similar manner to the normal-force distributions but with the peaks in the side-force distributions being about about 3/4 the magnitude of the of the corresponding normal-force distributions. However, closer inspection shows that the sign of the 'additional interference' is reversed. This means that the 'additional interference' in side-force becomes more negative with increase in yaw but the 'additional interference' in normal-force becomes more positive with increase in pitch. The variation with yaw is still different at positive and negative yaw angles, but the changes in the side-force 'additional interference' loadings with yaw are larger at negative yaw whilst the changes in the normal-force 'additional interference' loadings are larger at positive yaw.

The distributions of the side-force 'additional interference' loadings over the front of the afterbody differ appreciably at positive and negative yaw. At the end of the ogival part of the afterbody, x/L = 0.45, the 'additional interference' loadings vary little with yaw at positive yaw but vary appreciably at negative yaw. At x/L = 0.48, this is reversed and the 'additional interference' loadings vary little with yaw at negative yaw but vary appreciably with yaw at positive yaw. However, by x/L = 0.51 the variation of loading with yaw has become approximately symmetrical about zero yaw and remains so along the afterbody. The effect of yaw on the loadings diminishes rapidly so that there is little effect of yaw aft of x/L = 0.7.

8.3 Axial-force interference

The axial-force interference characteristics are shown in Fig 12.

The interference effects at zero pitch and yaw are rather different from the other forces in that, not only are the interference distributions very similar in shape for the central and port bodies but these are also very similar in character to the basic axial-force distribution along the single body, but smaller in magnitude, ref 1. All these distributions have a positive peak near x/L = 0.1, a negative peak near x/L = 0.3 and another positive peak at x/L = 0.45, the beginning of the conical part of the afterbody. The first two peaks are smooth in shape, but the third peak seems to mark a discontinuity in loading and aft of it the loadings decrease rapidly to become zero over the last 20% of the length of the body.

Thus, compared with the single body, the interference effects will cause an increase in C_A over the front half of the forebody, a decrease over the rear half of the forebody and an increase over the afterbody. As the interference loadings for the central body are more positive than for the port body over the front of the forebody, more negative over the rear of the forebody and only slightly more positive

over the afterbody, the change in C_A at zero pitch and yaw will probably be quite small.

8.3.1 Central body

The 'additional interference' loadings on the central body are very small up to x/L = 0.2 and vary somewhat irregularly with pitch and yaw. Aft of this, the 'additional interference' is negligible .

8.3.2 Port body

Pitch alterations do cause changes in the 'additional interference' loadings over the forebody.

At 4 and 6 degrees pitch, the 'additional interference' becomes more negative with increase in x/L until a negative peak is reached at x/L = 0.18. Aft of this the interference decreases to become zero at the position of D_{max}.

At 2 degrees pitch, the distribution is slightly different in that the loading initially becomes slightly positive before going negative and the negative peak in the distribution occurs rather farther aft, at x/L = 0.26.

The increase in the 'additional interference' loadings do not vary uniformly with pitch. Between 0 and 2 degrees and 2 and 4 degrees are the increments are similar but are about half that between 4 and 6 degrees pitch.

The 'additional interference' over the afterbody is constant, slightly negative and does not vary with pitch.

As yaw varies, the variations of the 'additional interference' loadings over the forebody are some 50% greater than the variations with pitch and are of opposite sign. The 'additional

interference' does not vary uniformly with yaw. At positive yaw, it increases uniformly with increase in yaw. This rate of change applies also at negative yaw until -4 degrees, but the rate of change then diminishes between -4 and -6 degrees. The position of the peak values of the 'additional interference' over the forebody is slightly further forward at -6 degrees yaw than at the other yaw angles.

The 'additional interference' over the afterbody is again of the same sign as the forebody loadings and much smaller in magnitude. However, the loadings vary linearly with yaw and and the variations are larger at negative pitch. The 'additional interference' increases slowly along the afterbody until it reaches a maximum value at about x/L = 0.6 before decreasing slightly over the remainder of the body.

9.0 ESTIMATION OF THE AERODYNAMIC CHARACTERISTICS.

The Surface Panel And Ring Source (SPARV) panel method, originated by Petrie, ref 6, was used to estimate the pressure distribution over the bodies and hence to determine the local loading distributions and the overall loads on the bodies.

This method had been used to estimate the pressures and loadings on other configurations in the series. It was found that the estimates agreed well with experiment except over the afterbody. In this region the estimates were poor when the loadings at the beginning of the afterbody were large. The reasons for this have been investigated, ref 1, and it was concluded that the reason for the poor agreement was the inability of the method to reproduce the effect of the base cavity. As no improved method is yet available, the estimates were still made using SPARV.

The panelling system used for each body was the same. The body was defined at each of 41 equally spaced longitudinal stations by 21 equally spaced circumferential points resulting in 800 panels/body. The base closure chosen as being one of the most satisfactory, ref 1, was a 8-degree semi-angle cone which was truncated 0.175L from the base of the body. This closure was defined at 10 equally spaced longitudinal stations by 21 equally spaced circumferential points, i.e. 180 panels. The number of circumferential points was chosen so that a line of influence points passed through expected positions of maximum interference on the bodies.

9.1 Comparison of the estimated and experimental loading distributions as pitch is varied, yaw = zero.

Although the loadings along all three axes were available, it was decided to present only the normal-force and axial-force loadings for the central body, Figs 13 a) and b), as the side-force loadings should be zero and not vary with pitch.

In the case of the port-body, only the normal-force and side-force loading distributions are presented, Figs 13 c) and d) as these distributions are most affected by the interference between the bodies.

9.1.2 Central body

At all pitch angles, the estimated and experimental normal-force distributions over the central body agree well as far as x/L = 0.55 which is the position where the loadings become negative at all pitch angles, Fig 13 a).

Aft of this, the experimental loadings become increasingly negative at all pitch angles until they reach a minimum value at about x/L = 0.7 and then increase to become zero at the base of the body. The magnitude of the negative loading peak increases only slowly as pitch increases.

At zero pitch, the estimated afterbody loadings agree quite well with experiment, but are slightly more negative. As pitch increases, the agreement becomes less good as the estimated loadings become increasingly more negative than the experimental loadings up to x/L = 0.7 and, aft of x/L = 0.7, the estimated loadings remain approximately constant instead of increasing steadily to become zero at the base of the body.

The estimated and experimental axial-force loadings agree well at all pitch angles except in two regions, Fig 13 b).

The first region is in the neighbourhood of the first, positive, peak in the distribution which occurs near x/l = 0.08. Here the experimental values are some 10% higher than estimated and the magnitude and position of these peaks change little with change in pitch.

The second region is over the afterbody. Here the experimental loadings are consistently slightly more negative than estimated and the sharp increase in loading that is estimated to occur aft of x/L = 0.95 is not present on the experimental distributions.

9.1.2 Port body

The estimated and experimental normal-force loading distributions for 0, 2, 4 and 6 degrees pitch are shown in Fig 13 c). There are no regions of major disagreement, but some regions of minor disagreement are present which change with change of pitch.

At zero pitch, the loadings agree well over the afterbody but the experimental loadings are slightly more negative over the forebody.

As pitch increases, the agreement between the loadings improves over the forebody and worsens over the afterbody until, at 6 degrees pitch, the agreement between the estimated and experimental forebody loading distributions is excellent but the experimental afterbody loadings becomes gradually more positive than estimated as the rear of the body is approached.

At 0 degrees pitch, the main feature of the distributions is the region of interference centred on the position of maximum diameter where the gap between the bodies is a minimum and the interference loadings rise to a large negative value. There are two other features of the distribution. Firstly, a region of positive loading at the front of the forebody due to an upflow due to the interference between the bodies and secondly, another region of positive loading over the afterbody due to an induced downflow.

When pitch increases, only small changes take place in the region of maximum interference, but the normal changes in loading distribution due to change in pitch are superimposed on the zero-pitch

loading distribution with the result that the forebody loading peak becomes more prominent and the loadings over the afterbody decrease and become negative. By 4 degrees pitch, the afterbody loadings are sufficiently large to start to interact with the interference region and the estimated loadings remain almost constant along the afterbody instead of rising steadily towards zero. This happens because the panel method cannot predict the effects of the cavity flow in the base of the body. This imposes the condition that there can be no large circumferential variation in pressure around the base of the body and thus the loading in the region of the base must be small. In the absence of this constraint, the panel method estimates almost constant loadings along the rear of the afterbody at a given pitch angle and these are not seriously affected by the type of base closure used to fair the bluff base of the body, ref 1.

The comparison of the estimated and experimental side-force loading distributions are shown in Fig 13 d).

The agreement between the distributions is good and remains good throughout the pitch range because the loading distributions alter little with variation in pitch. What little change there is is noticeable over the afterbody and, as described above, is due to the slight increase in the afterbody loadings with increase in pitch.

9.2 Comparison of the estimated and experimental loading distributions as yaw is varied, pitch = zero.

The comparisons of the estimated and experimental normal force and side-force loading distributions over the three bodies at yaw angles of 0, 2, 4 and 6 degrees are presented in Figs 14 a) - f).

9.2.1 Port body

The agreement between the estimated and experimental normal-force loading distributions at zero pitch is good over the

afterbody, but the experimental forebody loadings are slightly more negative than estimated, Fig 14 a).

As yaw is increased, little change takes place in forebody loading distributions or in the experimental afterbody distributions, but the estimated afterbody loadings steadily become more negative with increase in yaw. As a result the agreement between the afterbody loading distributions gets steadily worse as yaw increases, but the differences are relatively small.

The comparison between the estimated and experimental side-force loading distributions is shown in Fig 14 b).

At zero yaw, the agreement is very good over the main interference region, x/L = 0.3 to 0.5, but the experimental loadings over the front of the forebody are slightly more negative than estimated while those over the afterbody slightly more positive.

The side-force loading distributions in the main interference region alter very little with variation in yaw and remain well predicted.

The forebody distributions vary considerably with variation of yaw but are also well predicted when allowance is made for the differences in loading than occurred at zero yaw, i.e. the differences between the distributions do not vary with yaw and thus are probably due to an alignment error in rigging the bodies.

The afterbody loadings become slightly more negative with increase in yaw with the estimated loadings always more positive than estimated. The comparison between the estimated and experimental distributions follows the pattern previously described. As the general magnitude of the loading increases, the estimated loadings remain constant over the rear of the afterbody but the experimental loadings gradually reduce to become zero at the base of the body.

9.2.2 Central body

The comparison between the estimated and experimental normal-force loading distributions are shown in Fig 14 c).

The comparison between the loading distributions follows the general pattern, i.e. The loadings are well predicted in the region of maximum interference but the experimental forebody loadings are slightly more negative than predicted and the afterbody loadings are slightly more positive than estimated. For this body the distribution varies very little with change in yaw and thus there is little change in the comparison between the loadings. In fact, the comparison gets better with increase in yaw.

The estimated and experimental side-force loading distributions are shown in Fig 14 d).

As the bodies are symmetrical about the vertical centre-line of the central body, the side-force loadings at zero yaw should be zero as the interference loadings from the port body are cancelled by those from the starboard body.

The experimental loadings are very close to zero but have a small region between x/L = 0.3 and 0.5 where the loadings gradually become slightly negative and then recover to become zero.

When yaw is varied, the loadings up to x/L = 0.5 are well predicted if the difference in loadings at zero yaw is added to the estimate.

Aft of x/L = 0.5, the afterbody loadings become more negative with increase in yaw with the experimental loadings being slightly more positive than the estimate and tending to zero at the base of the body whilst the estimated loadings remain approximately constant aft of x/L = 0.5.

9.2.3 Starboard body

The variation of the estimated and experimental normal-force loading distributions with yaw are shown in Fig 14 e).

The differences between the estimated and experimental loading distributions are very similar to those previously observed on the port body, i.e. the experimental forebody loading distributions are more negative than estimated, but the agreement over the afterbody is good.

The corresponding side-force loading distributions are shown in Fig 14 f).

The agreement between the estimated and experimental loading distributions is better than those over the other two bodies. This is because the estimated afterbody loadings are smaller and so the usual disagreements that are present over the rear of the afterbody when the afterbody loadings are appreciable, are minimised and are only really noticeable at 6 degrees yaw.

9.3 Comparison of the overall aerodynamic coefficients.

The comparison of the estimated and experimental variation of C_N, C_Y and C_A with pitch at zero yaw and yaw at zero pitch are shown in Figs 6 and 9 respectively. The variations are shown for each body in the configuration, the complete configuration and also for the single body.

9.3.1 Variation with pitch at zero yaw

9.3.1.1 C_N

The variations of C_N with pitch for the various bodies is shown in Fig 6 a).

The estimated and experimental value of C_N for the central body agree well at zero pitch, but the variation with pitch are rather different.

The experimental values vary linearly with pitch up to 4 degrees after which the slope of the variation increases appreciably. The estimates, however, increase at a slower rate which is non-linear although always less than the corresponding experimental value. One experimental value was obtained at -2 degrees pitch. The slope between 0 and -2 degrees pitch was less than that from 0 to 4 degrees pitch, but was the same as the slope of the estimated variation between 0 and +2 degrees pitch.

The agreement between the estimated and experimental values of C_N at zero pitch is rather worse for the port body as the experimental value is rather more negative than estimated. The variation with pitch also is rather different. Experimentally, the initial slope of the variation of C_N with pitch reduces above 2 degrees pitch and the variation then becomes linear. It is interesting to note that, if the linear part of the variation is projected backwards to zero pitch, the intercept coincides with the estimated value of C_N. The initial slope of the estimated variation of C_N with pitch is considerably less than experiment and reduces steadily with increase in pitch.

The estimated and experimental variation of C_N with pitch were also obtained for the complete 3-body configuration and these are also plotted in Fig 6 a) as well as the variation for the single body.

The estimated variations of C_N with pitch for these two configurations are linear and virtually identical. The experimental variations are also linear but the slopes for the two configurations are different. That for the single body is approximately 60% greater than estimated whilst that for the 3-body configuration is 100% greater.

9.3.1.2 C_Y

At zero pitch, the estimated and experimental values of C_Y for the port body agree reasonably well with the experimental value being slightly higher. When pitch is varied, the estimated values of C_Y remain constant, but the experimental values increase steadily and have increased by about 10% at 6 degrees pitch.

For reasons of symmetry, C_Y should be zero at all pitch angles for the central body, and the 3-body and 1-body configurations as is estimated. The experimental values are slightly negative at all angles of pitch but agree well amongst themselves.

9.3.1.3 C_A

At zero pitch, the estimated value of the total C_A for the central body is 0.0183. C_A increases linearly with increase in pitch and has increased to 0.066 by 6 degrees pitch.

The measured value of C_A at zero pitch is 0.0089. The variation of the experimental values of the total C_A with pitch is linear between -2 and 4 degrees pitch and has a slightly greater slope than estimated . The slope then decreases gradually with further increase in pitch and C_A reaches a value of 0.0566 at 6 degrees pitch, i.e. the increment in C_A between 0 and 6 degrees pitch is approximately the same as estimated.

The variation of the total C_A with pitch for the port body is completely different as it decreases with increase in pitch. The estimated values vary non-linearly between 0.0135 at 0 degrees pitch and -0.0163 at 6 degrees, whilst the experimental values vary between 0.0071 to -0.0212 over the same pitch range but the shape of the variation is slightly different.

Because of the different character of the variation of the total C_A of the central and outer bodies, C_A for the 3-body combination changes relatively little with change of pitch, varying from 0.0077 at zero yaw to 0.0044 at 6 degrees yaw. The estimated C_A of the 3-body combination at zero pitch, 0.0151, is greater than experiment but the variation with pitch is very similar to experiment, varying from 0.0151 at zero pitch to 0.0111 at 6 degrees pitch.

In comparison, the estimated variation of the total C_A with pitch is very similar in shape to the experimental variation for the 3-body combination but slightly smaller in magnitude, varying from 0.0067 to 0.0037. The experimental variation of total C_A for the single body is similar in shape to the other variations but again is smaller in magnitude varying from 0.0042 at zero pitch to 0.0002 at 6 degrees pitch.

9.3.2 Variation with yaw at zero pitch

9.3.2.1 C_Y

The variation of the experimental and estimated values of C_Y with yaw for the various bodies is shown in Fig 9 a).

At zero yaw, the estimated value of C_Y for the port body, 0.2090, is slightly less than experiment, 0.2142. As yaw is increased, the estimated and experimental values of C_Y increase at the same rate up to 4 degrees, but above this, the experimental values increase faster than the estimated values which continue to increase at approximately the same rate as before.

In the case of the starboard body, the values of C_Y at zero yaw are the same as the port body, but are negative. The variation of C_Y as yaw is increased differs from that of the port body. The experimental variation is very similar to the estimated variation of the port body in slope and character, i.e. a steady increase in slope with

yaw without the rapid increase that was present experimentally above 4 degrees yaw. The initial slope of the estimated variation of C_Y with yaw is slightly less than experiment and reduces further as yaw increases so that, at 6 degrees yaw, C_Y is considerably less than experiment and is not much more positive than at zero yaw.

With the exception of the value at 2 degrees yaw, the experimental variation of C_Y with yaw for the central body is linear and the value at zero yaw is slightly negative instead of zero as would be expected. The estimated variation is also linear but the slope is only about 60% of experiment.

When the three bodies are considered in combination, the experimental variation of C_Y with yaw about 90% of that the central body whilst the estimated variation is the same percentage of the estimated C_Y for the central body.

However, the estimated and experimental variations of C_Y with yaw for the 3-body combination and single body agree very closely.

9.3.2.2 C_N

The variation of C_N with pitch for the various bodies is shown in Fig 9 d).

The estimated value of C_N at zero yaw for the port and starboard bodies is -0.1120 which is slightly more positive than the experimental value of -0.1284. When yaw is varied, the estimated variation of C_N is virtually the same for both the port and starboard bodies and C_N increases slowly at a gradually increasing rate as yaw increases to reach a value of -0.0857 at 6 degrees yaw.

The experimental variations of C_N with pitch for the port and starboard bodies are different, both from each other and the

estimate. C_N for the starboard body decreases slowly, but at a decreasing rate to reach a minimum value of -0.1405 at 4 degrees yaw before starting to increase slightly with further increase in yaw. In the case of the port body, C_N initially becomes more positive at a greater rate than estimated and continues to become more positive at an increasing rate as yaw increases until the estimated and experimental values are the same at 4 degrees yaw. At higher angles, the experimental C_N becomes rapidly more positive to reach a value of -0.056 at 6 degrees yaw.

The estimated and experimental values of C_N at zero yaw for the central bodies are both approximately the same, 0.229. As yaw increases, both the estimated and experimental values of C_N decrease at an increasing rate with increase in yaw. The experimental values have a certain amount of scatter, but bracket the estimated variation.

When the results for the bodies are combined to give the results for the 3-body combination, the estimated value of C_N is zero at all angles of yaw. The experimental values are approximately constant as yaw varies, but are slightly negative, c. -0.08.

9.3.2.3 C_A

The variation of C_A with yaw for the various bodies is shown in Fig 9 g).

As mentioned above, at zero yaw, the estimated value of the total C_A for the port body is approximately twice the measured value. The estimated and experimental values of total C_A both vary almost linearly with yaw with the slope of the estimated variation being slightly the greater. The estimated C_A varies between 0.0135 at zero yaw and 0.0552 at 6 degrees yaw whilst the experimental values vary between 0.0071 and 0.0474 over the same range.

In the case of the starboard body, the estimated and experimental values of C_A at zero yaw are the same as those of the port body. Both values of C_A become linearly more negative with increase of yaw with the slope of the both the estimated and experimental values corresponding with those for the port body. As a result, the estimated and experimental values of C_A are the same at slightly less than 6 degrees yaw.

The estimated value of the total C_A for the central body is again about double the experimental value at zero yaw, but both decrease slightly as yaw varies. The estimated C_A varies from 0.0183 at zero yaw to 0.0147 at 6 degrees yaw with the corresponding experimental values being 0.0089 and 0.006.

From the above results, the variation of the estimated and experimental values of the total C_A for the 3-body combination were obtained. At zero yaw, the estimated C_A, 0.0151, is greater than the experimental value, 0.0077. As yaw varies, both values decrease slowly to reach values of 0.0116 and 0.0051 respectively.

In comparison, the estimated and experimental values of C_A for the single body at zero yaw are 0.0067 an 0.0042 respectively and 0.0037 and 0.0002 at 6 degrees yaw.

Thus, in spite of the different variations of the total C_A for the component bodies with pitch and yaw, it makes very little difference to the variation of the total C_A of the 3-body configuration whether the combination is pitched or yawed.

10.0 EXAMINATION OF THE C_p DISTRIBUTIONS OVER THE BODIES

So far, the effects of the interference between the bodies have been assessed by the changes in the local loading distributions and the aerodynamic characteristics of the bodies. However the physical magnitude and extent of the interference regions can best be assessed by examination of the basic data, i.e. the pressure distributions over the bodies. In the previous tests in the series, this has been done by presenting both contour plots and isometric representations of the pressure distributions over the bodies as these compliment each other in the understanding of the interference regions.

In the present tests, as there are up to 4800 pressure readings used in the analysis of each test condition of the complete configuration, it was decided that it was not economical to present the C_p data in both ways and the data would be presented only in the form of contour plots.

In order to produce the contour plots, it was necessary for the C_p data to be presented as heights at defined points over a rectangular area. The x-axis represented the distance from the nose of the body, the y-axis represented the angle of the line of pressure tappings from a datum position and the z-axis the C_p value.

As it is obviously impossible to reproduce the three dimensional positioning of the pressure tappings on the overlapping bodies as a two-dimensional diagram, further distortions in the presentation were necessary in order to present the contour plots for all three bodies so that the relationship between the interference pattern can be better studied, albeit imperfectly. Firstly, the distance apart of the diagrams is arbitrary. Secondly, in order to position the regions of maximum interference on the bodies so that corresponding regions are adjacent, it was necessary to change the datum angular position and the positive direction of rotation of the body generator containing the pressure tappings as indicated in Fig 3. Thirdly, because

of the small size of the contour plots, the small C_p interval and the relatively large size of contour labels, the labelling of the contours is somewhat haphazard and the contours tend to merge together in regions of large pressure gradients, especially when these are not normal to the x or y axes.

In spite of all these limitations, it is considered that the diagrams present a good qualitative picture of the extent and character of the interference regions and how they vary with change of attitude.

A brief description of the C_p distribution over the single body may assist further in the interpretation of the contour-plots.

At zero pitch, C_p does not vary around the body and the only variation occurs in an axial direction. Thus the contour-plots will consist of a series of straight lines parallel to the y-axis whose distance apart varies with the axial pressure gradient, ref 1.

The C_p variation along the body varies as follows:-

a) Just aft of the nose, C_p has a value of approximately 0.3

b) C_p initially falls rapidly to become zero at x/L = 0.18 and then falls increasingly slowly to reach a minimum value of C_p = -0.12 at x/L = 0.394 which is the position of maximum body diameter and also the position of maximum interference on the 3-body configuration

c) Aft of this, C_p rises rapidly to about -0.02 at x/L = 0.5 after which the rate of increase falls off steadily until C_p becomes zero at x/L = 0.65 and reaches a maximum value of 0.01 at x/L = 0.83 which is maintained to about x/L = 0.93.

d) Aft of this, C_p decreases at an increasing rate to reach a value of -0.007 at x/L = 0.99

When pitch is increased, C_p decreases on the upper surface of the nose and increases on the lower. The initial difference in

C_p between the top and bottom centre-lines gradually reduces with x/L to become zero, irrespective of attitude, at the position of maximum body diameter. Aft of this, C_p on the top of the body becomes greater than on the bottom of the body and the difference in C_p between the top and bottom centre-lines gradually increases with x/L to reach a maximum value at x/L = 0.8 before decreasing to a small value at the base of the body.

Thus the maximum interference between the bodies, which is at the position of maximum diameter, occurs in a region where the interference-free pressure is a minimum and does not vary circumferentially at pitch angles up to 2 degrees and only slightly at greater angles. In addition, it is also at the beginning of a region of rapidly increasing pressure, i.e. an unstable pressure gradient.

In the following discussions, it is convenient to describe the features of the contour-plots by using topographical terms, i.e. "hollow", "ridge", "valley", "col", etc. It is also important to remember that the area mapped is a distorted representation of the actual body surfaces and the Ø = 0 and Ø = 360 degree generators are physically the same generator.

10.1 The C_p distributions at datum attitude

The experimental and estimated C_p distributions over the bodies are presented as contour plots in Fig 15.

The contour-plots of the experimental C_p distributions over the bodies are shown in Fig 15 a). Because of the lack of contour labelling, some additional information is required.

As the body combination is symmetrical about the vertical centre-line of the central body, the C_p distributions over the port and starboard bodies are identical but handed.

The extent of the regions of interference on the starboard body are clearly distinguished. The main interference region is indicated by a feature consisting of a series of closed contours centered at x/L = 0.4. These represent a region of reduced C_p, a "hollow", in the pressure surface with a minimum value of C_p of approximately -0.46 as compared with -0.12 for the interference-free value. The bottom of the "hollow" is approximately oval in shape with the major axis twisted very slightly in an anti-clockwise direction relative to the x-axis and is centred on the Ø = 126 degree generator instead of on the Ø = 135 generator as might have been expected from the configuration geometry. At x = 0.4, this "hollow" extends past the Ø = 360/0 degree generator and affects the C_p distribution over the whole circumference of the body. In fact, the axial C_p distribution along the Ø = 300 degree generator, i.e. the one directly opposite the centre of the "hollow", is the only one that closely resembles that of the single body and thus is relatively interference-free.

Initially the shape of the contours of the "hollow" alter little as C_p increases but soon the contours are distorted by two additional features.

The first is due to the constriction in the flow between the bodies at the position of minimum gap causing a 2 degree upflow and a 4 degree outflow near the nose of the body, Sections 4.1 and 4.3. This results in a region of higher C_p in the form of a "ridge" protruding from the pressure surface which starts at the nose of the body on the Ø = 112 degree generator and gradually gets smaller until it blends into the walls of the "hollow" near the bottom. The axis of the "ridge" moves round the body as the distance from the nose increases with its generator angle, increasing slightly to Ø = 122 degrees, i.e. the generator moves towards the bottom of the body. The "ridge" blends into the "hollow" very slightly off-centre and thus is the probable cause of the slight twist in the orientation of the "hollow as mentioned above. As the contours are parallel to the y-axis outside the "ridge", C_p does not vary circumferentially outside the "ridge". Thus the pressures

inside the ridge are responsible for the normal-force and side-force interference loadings on the forebody.

The second feature is a "valley" of lower C_p that leads downstream from the rear of the "hollow" and is inclined slightly towards the bottom of the diagram. This "valley" seems to split in traversing the steep "slope" of the rapid increase in C_p at the beginning of the afterbody to leave a central "ridge" located along the $\emptyset$ = 122 degree generator. The "valleys" are slightly asymmetric in that the one nearest the bottom of the diagram is slightly better defined. By the base, however, these circumferential variations in C_p have died away leaving an uniform distribution.

The C_p distribution over the central body shows clearly the interference regions from both the port and starboard bodies. Even though the axes of the regions are separated by only 90 degrees, both interference regions have the distinctive pattern described above and blend together with a minimum of distortion.

The two "hollows" are joined together by a small "col" near the bottom of the "hollow". The two forebody "ridges" leave the "hollows" separately, but blend together near the nose of the body. Likewise the two "valleys" are separate when they leave the "hollows" and are kept separate by the "ridge" that comes from the "col" between the two "hollows" and acts as a plane of symmetry. Thus, for different reasons, the C_p distribution over the centre of the afterbody is similar to that behind the maximum interference region on the outer bodies. These features in the C_p distribution gradually disappear as the base approaches so that an uniform circumferential distribution is present at the base of the body.

The contour-plots of the estimated C_p distributions over the bodies is shown in Fig 15 b).

The estimated C_p distributions agree well with the experimental results in the prediction of the main interference region, the "hollow", and the general features of the contour plots. However, there are some minor disagreements in the prediction of the forebody and afterbody features. These are:-

a) the "ridge" feature on the forebody of the starboard body is predicted to be centred on the Ø =122 generator over its whole length rather than moving slightly around the body.

b) the "valleys" coming from the rear of the "hollows" are not present and variations in the circumferential distributions over the afterbody are greater.

10.2 Effect of pitch on the C_p distributions.

The contour-plots of both the estimated and experimental C_p distributions over the bodies at pitch angles of 2, 4 and 6 degrees are presented in Fig 16. The experimental distributions are presented in Figs 16 a), c) and e) and the estimated distributions in Figs 16 b), d) and f).

Consider first the starboard body C_p distribution.

As pitch increases, the "ridge" extending from the nose into the main interference "hollow" moves towards the bottom of the body, increases in height and tries to extend further into the "hollow". As the depth of the "hollow" increases slowly with pitch from C_p = -0.47 to -0.53, the net effect of the changes is to rotate the major axis of the base of the "hollow" further clockwise thus distorting the shape of the "hollow" and deflecting an increasing part of the "hollow" towards the top of the body.

An increase in pitch also affects the "valley" that left the rear of the "hollow". As pitch increases, the "valley" progressively penetrates farther into the steep slope to the rear of the "hollow" and eventually breaks through the crest. The "valley" is quite

narrow and deep until it breaks through the "crest" when it spreads out into a complicated arrangement of undulations which, in turn, blend into each other as the base approaches.

The changes that take place in the C_p distribution over the central body are rather different.

The main feature of the experimental forebody contourplots at zero pitch is the twin "ridges" extending forward from the "twin hollow" and blending together into a single, flat ridge forward of x/L = 0.1. As pitch is increased, this single "ridge" gets flatter and then changes to a shallow "valley" which joins the "valley" between the twin "ridges". At 2 degrees pitch, the contours immediately behind the nose are straight and parallel to the y-axis indicating that the extreme nose of the body is accurately aligned to the oncoming airstream at this attitude. This is rather different to what had been deduced in Section 4.1 where, on the basis of the size of the forebody loading peak, it had been estimated that there was a mean downwash of 6 degrees over the forebody. However if the distributions are re-examined, Fig 4, it can be seen that the loadings nearest the nose are zero at 2 degrees confirming the above analysis and showing the dangers of trying to estimate local effects by analysing effects over a much greater area.

Analysis of the effect of change of pitch on the main interference region, the "twin hollow" shows that not only does its depth increase slowly as pitch is increased, but considerable changes also take place in its planform. This is caused by the two "ridges" leading into the front of the "twin hollow" becoming more prominent and joining the outer side walls of the "hollow". This process exerts a squeezing effect on the front of the base of the "hollows" so that they become less wide than the rear. The "valley" between the two front ridges also extends forward as pitch increases and blends into the general pressure field around the nose of the body.

The "valleys" that extend rearwards from the two "hollows" penetrate farther into the steep slope and eventually penetrate the crest and spread out over the afterbody. The formation of these "valleys" also makes the central "ridge" between them appear more prominent although its overall height does not alter greatly with increase in pitch.

As in the zero pitch case, the agreement between the estimated and experiment is very good at all pitch angles. The main differences are in the prediction of the shape of the the "hollows", where the estimated shapes tend to be more circular in planform, and in the distribution over the rear of the afterbody where the experimental distribution is more even.

10.3 Effect of yaw on the C_p distributions

The contourplots of the estimated and experimental C_p distributions over the three bodies at yaw angles of 2, 4 and 6 degrees yaw are shown in Fig 17. The experimental distributions are presented in Figs 17 a), c) and e) and the corresponding estimated distributions are shown in Figs 17 b), d) and f).

It should be noted that some of the experimental results for the central body are in error. In the distribution over the central body at 2 degrees yaw there are two axial distributions, Ø = 126 and 153 degrees, in which all the C_p values are high, probably due to a consistent error in the measurement of the static reference pressure, and thus these distributions should be ignored.

10.3.1 Starboard (leeward) body

As has been seen already, Section 10.1, at zero yaw, the presence of the other bodies induce an upflow of about 2 degrees and an outflow of about 4 degrees, i.e. in the same direction as positive yaw, at the nose of the body which leads to an appreciable loading over

the forebody. This is represented on the contourplot by the "ridge" running aft from the nose and blending into the main interference "hollow". At zero yaw the axis of the "ridge" goes through the centre of the "hollow", but moves slightly closer to the top of the body at angles of yaw greater than 2 degrees. The explanation of this is as follows:-

When yaw is increased, the side-force loadings increase, but the normal-force loadings hardly alter. As a result, the resultant loading, and therefore the axis of the "ridge", moves towards the horizontal centre-line of the body, the Ø = 90 degree generator and the "ridge" becomes more prominent

The main feature of the contourplot, the "hollow", becomes deeper, alters in shape, extends around the body, moves circumferentially slightly towards the bottom of the body and twists slightly as yaw increases.

The position of the centre of the base of the "hollow", x/L = 0.394, does not alter as yaw varies, but the minimum value of C_p varies almost linearly from -0.47 to -0.53 as yaw varies between Ø and 6 degrees. This is exactly the same variation as when pitch is altered from Ø to 6 degrees yaw and is not unexpected because of the geometry of the body combination.

As yaw increases, the shape of the contours forming the "hollow" alters because of the increase in size and alteration of position of the "ridge". Because the axis of the "ridge" is nearer the top of the body than the axis of the "hollow", the alterations in the characteristics of the "ridge" as yaw increases results in the front of the "ridge" penetrating further into the "hollow" and "squeezing" it so that the front part becomes elongated and twisted towards the bottom of the body. This twist is in the opposite direction to that of the oncoming flow and has been previously observed with the two-body configurations, refs 4 and 5. The result of this twist is to distort the shape of the "hollow" so that the shape of the front of the "hollow" becomes different on each side of the "ridge". On the side nearest the

bottom centre-line, the Ø = 180 degree generator, the axis of the "hollow" is swept in contrast to that of the other side which is unswept. The general shape of the rear of the "hollow" is not altered so markedly because of the constraint of the large rise in C_p at the rear of the "hollow".

Because of the increased interference as yaw increases, the size of the "hollow" increases circumferentially and increasingly spreads past the top of the body thus altering appreciably the shape of the region diametrically opposite the "hollow" in which C_p varies little. The presence of large increase in C_p at the beginning of the afterbody ensures that most of the change in shape takes place over the front of the region and affects the forebody C^p distribution diametrically opposite the "ridge".

The "valley" that comes from the rear of the "hollow" on the side nearest the top of the body becomes more prominent as yaw increases and, together with the associated "ridge" system, further distorts the rapid increase in slope to the rear of the "hollow" and the "crest" that marks the beginning of the large region extending over the whole surface of the body aft of x/L = Ø.6 where C_p varies relatively little.

At zero yaw, the main features on this region are the "ridge" coming from the rear of the "hollow", two small closely spaced "hills" to the rear of the "ridge" which are located at located at x/L = Ø.9, and the sudden reduction of C_p at the rear of the body. The smaller "hill" is positioned nearer the top of the body and the larger does not extend as far as the bottom of the body.

At 2 degrees yaw, the "ridge" has become less prominent and has moved towards the bottom of the body. The two "hills" have coalesced into one larger, vaguely egg-shaped "hill" whose larger end is to the rear of the "ridge". The "hill" extends around the bottom of the body to the horizontal centre-line, the 270 degree generator.

With further increase in yaw, the distinct "ridge" feature disappears and, while C_p remains approximately zero over the bottom part of the body,the value of C_p measured at the beginning of the afterbody on the top centre-line falls gradually as yaw increases. This results in the shape of the constant C_p region changing from rectangular to triangular as yaw increases. In addition, the "hill" again divides into two. These are in the same axial position as previously with the smaller located on the port-upper side of the body and the larger starting on the port-lower side and extending past the bottom of the body so that the major part is located on the starboard-lower side.

The estimated contourplots reproduce the experimental results very well as far as the general features of the C_p distributions are concerned and their variation with yaw but disagree somewhat in the finer detail of the distributions at the rear of the "hollow" and, in particular, the "hills" present in the afterbody C_p distributions.

10.3.2 Central body

For this body, it should be noted that the y-axis for the contour diagrams has been changed and Ø' = 180 is now the top centre-line of the body and the 0/360 degree generator is the bottom centre-line. It should also be remembered that the diagrams are distorted representations of the actual pressure distributions over the surface as Ø' is an *angle* and not a *distance*. Thus, although the axes of the "ridges" appear to be parallel on the diagrams, they actually get closer to each other as they approach the nose of the body because the local radius gets smaller.

As yaw is increased the following changes take place in the contourplots:-

a) The axes of the two "ridges" on the forebody remain parallel and the same distance apart, but move around the body slightly for yaw angles greater than 2 degrees, (Ø' decreases).

b) As yaw increases from zero, the windward "ridge" becomes more pronounced whilst the leeward "ridge" blends into it near the nose where the physical separation is small. The rear of the leeward "ridge" however remains separate and is comparable in size with the windward "ridge". The position at which the "ridges" separate move further aft as yaw increases

c) Initially the two "hollows are approximately circular in planform with a blending region between them with their centres being the same distance apart as the forebody "ridges. There is very little change in character up to 2 degrees yaw.

d) Above 2 degrees yaw, considerable geometric changes start to take place. The centres of the two "hollows" remain in the same positions but, because of the circumferential movement of the two "ridges" to port, the growth of the "ridges" causes the front of the "hollows" to be rotated to starboard and the planform of the bottom of the "hollows" to be elongated slightly. Because of the movement of the "ridges", the resultant interaction is not symmetrical and a "valley" pushes forward from front of the starboard "hollow" into the distribution on the starboard side of the starboard "ridge" while the "valley" trailing from the port "hollow" is much more prominent than that from the starboard body and extends to the base of the body at the higher angles of yaw.

e) Regardless of the angle of yaw , the depth of both "hollows" is the same. Their depth initially increases slowly with angle of yaw and then more rapidly, varying from C_p = -0.47 at 0 degrees yaw to -0.50 at 6 degrees.

f) At zero yaw, the distribution over the afterbody aft of x/L = 0.6 is relatively uniform with a centrally placed wedge-shaped "hill" projecting with a circular summit region. As yaw increases, this projection initially increases in size and is deflected to port. However at 6 degrees yaw, the "valley" trailing from the starboard "hollow" is sufficiently powerful to split the "hill" into two of which the one to starboard is the larger and higher.

The estimated distribution agrees very well with experiment in that all the main characteristics of the distributions are predicted although there are some regions to the rear of the "hollows" were there are differences in detail and the distributions are markedly less uniform.

10.3.3 Port (windward) body

For these contourplots, the y-axis reverts to that used for the starboard body, i.e. it represents Ø with Ø = 0 and 360 representing the top centre-line of the body where Ø is the anti-clockwise angle of rotation as seen from the rear, Fig 3.

At zero yaw, the C_p distribution is the mirror image of that of the starboard body, Fig 15 a) and is that due to the basic interference between the bodies. When the bodies are yawed, the C_p distributions due to yaw are superimposed on the basic interference distribution. These imposed distributions are different for the port and starboard bodies as a leeward yaw C_p distribution is superimposed on the main interference region of the port body whilst a windward distribution is imposed in the case of the starboard body.

Due to the interference from the other bodies, the direction of the flow approaching the nose of the port body has components of -4 degrees in yaw and +2 degrees in pitch as previously determined. Looking at how the contours in the forebody region vary as yaw increases, it can be seen that the forebody "ridge" does not alter greatly with yaw aft of x/L = 0.2, but, in the nose region, the "ridge gradually flattens and, by 6 degrees yaw, it has been replaced by a slight "valley" centred on the 270 degree generator and joining the side of the "ridge". In addition a small local "ridge" has started to appear diametrically opposite. This confirms that the outflow at the nose of the body is about 4 degrees and also shows that aft of x/L = 0.2, the variations in side-force must come mainly from the changes in C_p distributions over the windward side of the forebody. Up to 2 degrees

yaw, the axis of the "ridge" does not alter its location, but at larger angles it moves slightly downwards towards the bottom of the body.

The centre of the "hollow" does not alter in position as yaw increases and the minimum value of C_p in the " hollow" varies only slightly as yaw alters, varying between C_p = 0.46 and 0.48. The orientation of the axes of the "hollow" does not alter up to 2 degrees yaw, but above this the axes twist slightly clockwise due to the slight movement downwards of the "ridge" relative to the "hollow". Because of the differences in the flow conditions, the upper contours vary in a different way from the starboard body as they are much more symmetrical. As in the case of the other "hollows", there is a well defined "valley" trailing back from the bottom of the "hollow" along its tilted major axis.

When the bodies are yawed, the estimated C_p distributions over the afterbody predict the form of the experimental distributions very well, but there are some features that are less well predicted such as the "valleys" to the rear of the "hollows" and the uniformity of the afterbody distributions.

11.0 ESTIMATION OF THE AERODYNAMIC CHARACTERISTICS OF THE BODY COMBINATION AT NEGATIVE PITCH

Due to the asymmetry of the body combination, it had been intended to test the 3-body configuration at both positive and negative pitch. However, the original test programme had to be truncated for a variety of reasons and only one partial set of data was obtained at negative pitch, i.e. that for the central body at -2 degrees pitch. As the results from this test did not conform to the trend indicated at positive pitch, it seemed possible that the aerodynamic characteristics at positive and negative pitch were significantly different.

The results obtained so far in the test series had shown that it as possible to estimate the pressure distributions over the nose of the body and the interference region with a high degree of accuracy, but the accuracy was less good over the interference-free parts of the afterbody due to the inability of the method to predict accurately the effects of the base-cavity flow on the pressure distribution over the afterbody when it was not dominated by interference effects.

Once the configuration had been modelled to obtain the estimates for comparison with the experimental results, it was easy to extend the estimates to cover the negative pitch range and also some some selected combinations of pitch and yaw. Accordingly, estimates were made of the local loading distributions, the aerodynamic coefficients and the C_p distributions over the bodies at the following attitudes:-

a) pitch angles of -2, -4 and -6 degrees at zero yaw

b) yaw angles of 2, 4 and 6 degrees at 6 degrees pitch

c) yaw angles of 2, 4 and 6 degrees at -6 degrees pitch

The variation of the aerodynamic coefficients with pitch and yaw are presented in Figs 18 and 19. The variation of the local loading distributions with pitch and yaw are shown in Figs 20, 21 and 22. These figures include the estimates previously obtained for

comparison with the experimental results so that the general trends over the total range of attitude could be assessed.

Contour-plots of the C_p distributions over the bodies are presented in Fig 23.

11.1 Variation of C_N, C_Y and C_A with pitch at zero yaw

The variation of C_N with pitch over the range of -6 to +6 degrees is shown in Fig 18 a) for the port and central bodies and also for the 3-body configuration. In all cases the variation with pitch is smooth throughout the range, but varies appreciably in character between positive and negative pitch in the case of the individual bodies.

As pitch increases from -6 degrees, C_N for the central body decreases at a decreasing rate from its initial value of 0.29 to reach a minimum value of 0.22 near -2 degrees pitch and then increases at an increasing rate to reach a value of 0.40 at +6 degrees pitch.

The variation of C_N with pitch for the port body is almost the opposite. As pitch increases from -6 degrees, C_N increases at a decreasing rate from its initial value of -0.23 to reach a maximum value of -0.10 at about +3 degrees pitch and then decreases slowly to reach a value of -0.11 at +6 degrees pitch.

When these values of C_N are combined together to obtain the variation of C_N with pitch for the 3-body configuration, it is found that the variation of C_N with pitch is linear over the whole pitch range and varies from -0.056 at -6 degrees to 0.058 at +6 degrees pitch.

The variation of C_Y with pitch for the bodies is shown in Fig 18 b). Because of the symmetry of the bodies about the vertical plane through the centre-line of the central body, C_Y for the central body = 0.0 at all pitch angles and is equal and opposite for the port

and starboard bodies. C_Y for the outer bodies varies little in magnitude from the mean value of 0.21 over the pitch range of +/- 4 degrees but then decreases slightly.

The values of C_A for the port and central bodies vary smoothly with pitch but in opposite ways, Fig 18 c).

C_A for the port body has a value of -0.038 at -6 degrees pitch and increases at a decreasing rate with increase in pitch to reach a value of +0.066 at 6 degrees pitch

In the case of the central body, C_A = +0.036 at -6 degrees pitch and decreases at an increasing rate with increase in pitch to reach a value of -0.016 at +6 degrees pitch.

When the values of C_A for the three bodies are combined to give C_A for the 3-body combination, it is found that the maximum value of C_A, +0.015, occurs at zero pitch and then decreases symmetrically about zero pitch to reach a value +0.011 at +/- 6 degrees pitch.

It is interesting that large but completely different variations of C_N and C_A with pitch for the central and outer bodies result in much smaller variations in the quantities for the complete configuration.

11.2 Variation of C_N, C_Y and C_A with yaw

The variation of C_N, C_Y and C_A with yaw at pitch angles of -6, 0 and +6 degrees are presented in Fig 19.

At zero pitch, the variation in yaw has only a small effect on C_N on all three bodies with C_N decreasing slightly in magnitude in all cases, Fig 19 a). This reduction in magnitude is the same for both the port and starboard bodies up to 4 degrees yaw, but, at

greater angles, the magnitude of C_N falls off slightly more rapidly in the case of the port body. The value of C_N for the complete configuration remains approximately zero at all yaw angles.

At a pitch angle of -6 degrees, the variations of C_N with yaw show several differences. These are:-

a) Although C_N for the central body has increased at zero yaw even though the pitch angle is more negative, see Fig 18, the variation with yaw is very similar to that at zero pitch.

b) The zero yaw values of C_N for the port and starboard bodies are more negative than at zero pitch. The variation of C_N with yaw for the port and starboard bodies is much greater than at zero pitch with the differences becoming apparent immediately. As at zero pitch, C_N for the port body becomes less negative with increase in yaw with the rate increasing steadily with yaw. On the other hand, C_N for the starboard body becomes more negative with increase in yaw with the rate being quite large initially, but decreasing steadily with increase in yaw.

c) In spite of these changes, the value of C_N for the complete configuration remains constant throughout the yaw range at a value of approximately -0.056.

At a pitch angle of +6 degrees, at first sight it seems that the variations of C_N with yaw for the various bodies are very similar to those at -6 degrees pitch although the values at zero yaw are rather different. However, on closer examination, it is seen that the sense of the variations of C_N with yaw for the bodies has been reversed as the values of C_N for the starboard body now become less negative with increase in yaw instead of more negative and those of the port body become more negative with increase in yaw instead of less negative.

The variation of C_Y with yaw for the three bodies at pitch angles of -6, 0 and +6 degrees pitch is shown in Fig 19 b). At all pitch angles, the variation of C_Y with yaw is approximately linear for all three bodies and the slope of the variation for the port body is

more positive than that for the starboard body. In addition, the values of C_Y at zero yaw change little with change of pitch.

At zero pitch, the slope of all the variations is positive with the slope of the central-body variation being approximately the mean of that of the port and starboard bodies and the same as that of the 3-body combination.

At -6 degrees pitch, the variation of C_Y with yaw is slightly negative for the port and starboard bodies but that of the central body is positive and nearly five times the magnitude of either that of the 3-body combination or the starboard body. The variation of C_Y with yaw for the 3-body combination however remains approximately the same as at zero pitch.

At +6 degrees pitch, the variation of C_Y with yaw for the port and starboard bodies is now positive, and approximately three times that of the 3-body combination whilst the variation for the central body is negative and double the magnitude of that of the 3-body combination.

It is interesting that the changes in flow that occur as pitch is varied are sufficient to cause all the bodies to produce a negative variation in side-force at some pitch angle when the bodies are yawed positively and yet, the variation of side-force with yaw for the 3-body combination hardly alters as pitch is varied.

The variation of C_A with yaw for the three bodies at pitch angles of -6, 0 and +6 degrees pitch is shown in Fig 19 c).

Although the values of C_A at zero yaw vary appreciably with both the body and pitch angle, the variation of C_A with yaw alters little.

For the port and starboard bodies, the variation of C_A with yaw is linear at all pitch angles and the slope of the variation for the port body is positive and about 15% less in magnitude than the negative slope of the starboard body with typical values of the slope being -0.0082/degree and +0.007/degree for the starboard and port bodies respectively.

In the case of the central body, C_A initially varies little up to 4 degrees yaw, but becomes less positive with further increase in yaw.

At zero yaw, the values of C_A for the port and starboard bodies vary from +0.036 at -6 degrees yaw to +0.018 at 0 degrees and then to -0.016 at +6 degrees yaw, i.e. the variation from 0 to +6 degrees yaw is 1.34 the variation from -6 to 0 degrees yaw. In the case of the central body, C_A varies from -0.038 at -6 degrees yaw to +0.018 at 0 degrees and then to +0.066 at +6 degrees yaw so that the variation from 0 to +6 degrees yaw is now only 0.87 the variation from -6 to 0 degrees yaw.

In spite of these wide variations in C_A when yaw varies, the value of C_A for the complete configuration reduces slowly and linearly with change in yaw although the slope varies somewhat irregularly with variation of pitch. The value of C_A at zero yaw is constant at -6 and 0 degrees pitch at a value of +0.015 and then reduces to +0.011 at +6 degrees pitch.

11.3 Variation of the loading distributions with pitch and yaw.

The variation of the normal-force, side-force and axial-force loading distributions with pitch at zero yaw are presented in Fig 20 a), b) and c) respectively.

11.3.1 Normal-force loading distributions

The variation of the normal-force loadings over the central and port bodies vary in a consistent manner as pitch is altered.

The negative forebody loadings over the central body reduce linearly with increase in pitch and eventually become positive at +6 degrees pitch.

The positive loading distributions in the neighbourhood of the position of minimum gap between the bodies do not remain constant as might be expected, but increase with increasing pitch. The rate of change is small at negative pitch, but is considerably greater at positive pitch.

At +6 degrees pitch the loading distributions over the afterbody are negative. As pitch is reduced, the negative loadings reduce gradually and eventually become completely positive below -2 degrees pitch, with the rate at which the loadings change being rather greater at negative pitch angles. It should be noticed that, at a given pitch angle, the afterbody loadings remain constant over much of the afterbody.

Although the loading distributions over the port body are different in shape from those over the central body, the general characteristics are very similar, as is the variation with pitch. However the differences in the rate of change in the distributions at positive and negative pitch angles is much smaller than those noted on the central body.

11.3.2 Side-force loading distributions

As the outer bodies are symmetrically located relative to the vertical centre-line of the central body, the side-force loadings on the central body are zero and do not vary with change of pitch.

The general shape of the side-force loading distributions over the port body is very similar to that of the normal-force distributions over the central body, but the variations as pitch varies are rather different as these variations are due to the changes in interference between the bodies.

Close to the nose of the body and at the position of maximum interference, there is very little change in loading as pitch varies. Between these positions, the loadings at a given station increase positively at a constant rate as pitch increases and the magnitude of the increase varies with distance along the body.

There is only a small variation with pitch in the side-force loading at the rear of the afterbody, but there is a considerable variation in loading along the afterbody as pitch varies. The change in loading at a given station along the afterbody becomes linearly more negative as pitch increases and the magnitude of the change increases up to x/L = 0.6 and then decreases as the base of the body approaches.

11.3.3 Axial-force loading distributions

The variation of the axial-force loadings distributions with pitch for the central and port bodies are shown in Fig 20 c). The general character of the distributions for the two bodies is very similar although the proportions and values differ between the two bodies. The changes in distribution as pitch varies are likewise similar, namely:-

a) There is a region between x/L = 0.3 and 0.5 where there is little variation in loading as pitch changes.

b) Between x/L = 0.0 and 0.3 the loading at both positive and negative pitch increases linearly with increase in pitch, but the rate of increase is considerably greater at negative pitch.

c) The afterbody loadings at both positive and negative pitch decrease linearly with increase in pitch, but more slowly than the

forebody loadings. As before the rate of change is greater at negative pitch.

11.4 Variation of loading distributions with yaw

11.4.1 Normal-force loading distributions

The variation of the normal-force loading distributions with yaw at pitch angles of -6, 0 and +6 degrees are shown in Figs 21 a), b) and c).

The variation of the normal-force loading distributions at zero yaw for the three pitch angles have already been described in Section 11.2. The changes in the loading distributions with increases in yaw are as follows:-

a) Central body.

There is little change in the distributions at any pitch angle as yaw is increased up to 4 degrees, but, by 6 degrees yaw, the loadings near the main interference peak at x/L = 0.4 have decreased slightly.

b) Starboard body.

Although the zero yaw distributions are very different at the chosen pitch angles, the variation of the distributions with yaw have some common features in that there is little variation of the loadings with yaw at between x/L = 0.0 and 0.1, in a region near x/L = 0.4 and also at the rear of the body. In between these positions, the loadings over the forebody become more negative and those over the afterbody become more positive as yaw increases.

At -6 degrees pitch, the forebody loadings rapidly become more negative between x/L = 0.1 and 0.2 as yaw increases. The

change remains constant to x/L = 0.3 and then reduces so that the change in loading is zero at x/L = 0.4. These changes in loading vary linearly with yaw and are appreciable. The changes in loading over the afterbody with variation of yaw are small in comparison.

At 0 degrees pitch, the changes in forebody loading as yaw varies are very similar to those at -6 degrees yaw but are rather smaller. The changes in the afterbody loadings are now significant and are of nearly the same magnitude as the changes in the forebody loadings, with the maximum change occurring near x/L = 0.6 before reducing slowly as the base is approached.

At +6 degrees pitch, the increments in the forebody due to change of yaw are still approximately the same as before, but the afterbody loading increments have increased so that the maximum increase is now the same in magnitude as that over the forebody.

c) Port body

The changes in loading from that at zero yaw are approximately the same as those over the starboard body but with the sign reversed and it is this that accounts for the apparent difference in character between the port and starboard loading distributions.

11.4.2 Side-force loading distributions

The variations in the side-force loading distributions as yaw is varied are shown in Fig 22 a), b) and c) for pitch angles of -6, 0 and +6 degrees pitch.

As the side-force loading distributions at zero yaw at pitch angles of -6, 0 and +6 degrees have already been described in section 11.2, the discussion will discus only the changes that occur in the loading distributions as yaw is varied.

a) Central body.

For reasons of symmetry, the side-force loadings at zero yaw are zero. As yaw increases, a positive loading distribution develops over the forebody. The peak in this loading distribution is comparable in magnitude to that for the single-body although the peak is rather flatter and further aft. At the same time a negative loading distribution develops over the afterbody which takes the form of an increase in loading until about x/L = 0.6 followed by the loadings either remaining constant over the rest of the afterbody or falling slowly and then remaining constant over the last part of the afterbody.

Although the general shape of the distributions remain similar, the relative size of the forebody and afterbody distributions varies as pitch is altered.

At +6 degrees pitch, Fig 22 c), the peak in the (positive) forebody distribution increases linearly with increase in yaw and remains in the same position, x/L = 0.2, with the loading distributions at all yaw angles being approximately symmetrical about this position. The peak in the (negative) afterbody loading distributions occurs at about x/L = 0.5 at all yaw angles, increases linearly with yaw and is the same magnitude as the forebody loading peak. Because of the widely different shapes of the forebody and afterbody loading distributions, the negative side-force generated by the afterbody will be considerably greater than the positive side-force produced by the forebody. Thus the net side-force generated by the body will be negative at positive yaw as previously noted, Section 11.3.2.

At 0 degrees pitch, Fig 22 b), although the general shapes of the distributions are similar to those at 6 degrees yaw, the forebody peak loadings have increased by about 20%. The initial part of the distribution is as previously, but the increase in the peak loading has been achieved by the movement of the peak loading farther aft to x/L = 0.22. As the afterbody loadings, and thus the afterbody side-force,

have been decreased by about 40%, the result of these changes is that the net side-force on the body is now positive at positive pitch.

The loading distributions continue to change in the same way as pitch is reduced to -6 degrees. The forebody loading peak increases by a further 35% of the initial value and moves aft to x/L = 0.26 whilst the afterbody loadings decrease to approximately 30% of the initial values. These changes result in a further increase in the rate that side-force changes with increase in yaw.

b) Starboard body

The forebody side-force loading peaks at +6 degrees pitch increase linearly with increase in yaw as do the loadings at the other positions along the forebody. Over the first part of the afterbody, between x/L = 0.4 and 0.6, there is no increase in loading with change in yaw but, aft of this, the afterbody loading peaks near x/L = 0.65 decrease linearly with yaw but at about 30% the rate that the forebody peak loadings increase. Aft of the afterbody peak, the increase in loading with change in pitch is nearly constant.

At 0 degrees pitch, the increase in loading over the first part of the forebody with change in yaw is is the same as at 6 degrees pitch, but is rather less over the second half. There is now a change in loading as yaw varies over the front of the afterbody which increases with distance from the front of the afterbody, reaches a maximum near x/L = 0.65 and then remains constant over the rest of the afterbody. The rate of increase in loading at the afterbody loading peak has now increased slightly to 40% of that at the forebody loading peak.

These changes in loading distribution continue as pitch decreases further. At -6 degrees pitch, the increase in loading over the front half of the forebody is still unaltered, but the increase in loading with change of pitch decreases rapidly and becomes zero over the last quarter of the forebody. The afterbody loadings now increase

more rapidly with change of yaw than at 0 degrees pitch and the change in loading at the position of the afterbody loading peak has now increased to 50% of the increase in loading at the forebody loading peak.

c) Port body.

The changes in loading distributions with yaw at pitch angles of 6, 0 and -6 degrees are the same as for the starboard body, but because the sign of the loading distributions at zero yaw are inverted, the distributions look rather different.

11.5 The estimated C_p distributions over the extended range of pitch and yaw

The contourplots of the estimated C_p distributions are presented in Fig 23 a) - i).

11.5.1 Extended pitch range at zero yaw

A cursory examination of the additional results at negative pitch angles, Fig 23 d) - f), showed that they differed significantly from those at positive pitch, Fig 16 b), d) and f), but that the change in character takes place when pitch is altered from zero, Fig 15 b). For briefness, the contourplots will only be compared at pitch angles of 0, +6 and -6 degrees pitch as these best show the differences in character of the distributions.

11.5.1.1 Pitch = 0 degrees

At zero pitch, Fig 15 b), the region of maximum interference on the outer bodies is represented by the "hollow" in the pressure surface whose basic form is symmetrical about its y-axis. A narrow "ridge" parallel to the x-axis protrudes from the pressure surface between the nose and the centre of the "hollow" but blends

smoothly into the pressure surface at either end. Over most of the afterbody, the C_p distribution is uniform except for a slight "ridge" trailing behind the "hollow". These features on the outer bodies are reproduced on the central body, but, because of the closeness of the interference patterns, some merging of the features is present, i.e. the "ridges" blend together at the nose of the body, the "hollows" blend together except near the regions of maximum depth and the "ridges" in the afterbody distributions are almost completely blended.

11.5.1.2 Pitch = +6 degrees

At +6 degrees pitch, Fig 16 f), the contourplots are more complicated as the main features have altered appreciably.

In the case of the central body, the main interference "hollows" near the top centre-line of the body are unaltered in position but are now deeper, somewhat egg-shaped and twisted slightly so that the bluff front ends are inclined towards the top centre-line, Ø' = 180. Because the bodies are at positive pitch, the C_p value near the nose is less on the top centre-line than on the bottom centre-line, Ø' = 0/360 and this shows up on the contourplot as a "valley" along the Ø' = 180 generator and a "ridge" along the Ø' = 0 generator. As x/L increases, the "valley" narrows and steepens before blending into the "col" between the two "hollows" but the "ridge" rapidly becomes less pronounced and has blended into the basic interference pattern by x/L = 0.2.

The "ridges" leading into the "hollows" that were a feature of the general interference pattern at zero pitch, are now less prominent and blend into the sides of the "hollows" that are remote from the top centre-line.

The C_p distribution over the afterbody has altered appreciably. There is now a pronounced elongated "hill" trailing back from the "col" along the top centre-line. This is flanked on either side by a "valley" which originates from the rear of the "hollows". These

"valleys" are separated over the rear of the afterbody by a small "hill" which is symmetrical along the bottom centre-line and extends between x/L = 0.6 and 0.95. In addition, the rapid rise in C_p that took place over the beginning of the afterbody is now present only to the rear of the "col" and has been replaced over the bottom half of the body by a region of slowly increasing pressure.

The contourplots for the outer bodies differ somewhat from that for the central body because the interference region, being on the lower half of the body, is modified differently when pitch is increased.

The main feature of the forebody distribution is now the marked "ridge" extending rearwards from the nose of the forebody near the bottom centre-line which results from the generation of positive normal-force over the forebody. This intersects the side of the " hollow" nearest the bottom centre-line. As a result the front of the "hollow" is twisted slightly towards the top of the body and the side adjacent to the central body is squeezed forward whilst the small part of the "hollow" on the other side of the "ridge" is little effected with the result that there is a region on that side of the body between x/L = 0.25 and 0.4 where C_p is virtually constant.

The afterbody distribution is also extensively modified. There is a well defined "valley" trailing axially behind the "hollow" and another, less well-defined, which is formed at the beginning of the afterbody on the horizontal centre-line of the body on the side remote from the central body. These are separated by a) a "ridge" originating on the beginning of the afterbody on the bottom centre-line and b) by a much larger one located near the top of the body nearest the central body.

11.5.1.3 Pitch = -6 degrees

The C_p distributions over the bodies at a pitch angle of -6 degrees, Fig 23 f), is markedly different from those at 0 and +6 degrees which have been described above.

Because the bodies are at negative pitch, the C_p values along the top centre-line of the bodies near the noses are now greater than those along the bottom centre-lines. As a result, there is now a pronounced "ridge" extending rearwards from the nose along the top centre-line of the central body, Ø' = 180, to join the "col" between the two "hollows". This "ridge" has a major effect on the geometry of the "hollows". Firstly, the centres of the bottoms of the "hollows" are now further apart. Secondly the "hollows" are no longer symmetrical about the line joining their centres, but have become elongated and swept forward towards the nose of the body. As a result, the "hollows" have become more akin to "valleys" along the bottom of the main forebody "ridge" with the front of the "valley" pointing towards the outer bodies.

The "ridge" and "valley" features extending rearwards from the "hollows", are markedly less pronounced than those at +6 degrees pitch and more pronounced than those at 0 degrees, but the distribution over the rear of the afterbody is more uniform than either.

The distributions over the outer bodies have also altered considerably. The bottom part of the "hollow" is very similar to those of the central body with the front inclined towards the bottom centre-line. There is a "ridge" along the inner side of the body starting from the top of the body near the nose and blending into the top side of the "hollow" with the elongated "hollow" forming a "valley" along the bottom side of the "ridge" as with the central body. The "valley" from the bottom of the body at the nose interacts with the top of the "hollow" to result in a region of almost constant C_p over the outer half of the body near the position of maximum diameter. A "valley" from the rear of the "hollow" moves towards the top of the body along the line of

the major axis of the "hollow". This and the shallow "valley" which starts at the beginning of the afterbody and runs along the horizontal centreline on the outer half of the body, separate two "ridges" that run along the top and bottom of the afterbody of which the bottom "ridge" is the highest.

11.5.2 Variation of C_p distributions with yaw, pitch = +6 degrees

The contourplots of the C_p distributions at yaw angles of 0, 2, 4 and 6 degrees are shown in Figs 16 f), 23 c), b) and a) respectively. From these diagrams it can be seen that, although there are significant alterations to the various features in the contourplots as yaw is varied, the general form of the contours does not alter greatly.

11.5.2.1 Central body

As yaw increases, the position of the centres of the "hollows" does not alter but the following changes in geometry occur:-

a) In the case of the "hollow" on the port (windward) side of the body, the depth increases and the planform becomes more elongated although the inclination of the major axis hardly alters. In addition, the "valley" that comes from the rear of the "hollow" becomes deeper and narrower and runs in a more axial direction.

b) The depth of the "hollow" on the starboard side of the body decreases, its planform becomes more circular and the major axis rotates rapidly in an anti-clockwise direction so that it is pointing nearly circumferentially when the bodies are at +6 degrees yaw. The "valley" that comes from the rear of the "hollow" becomes rather less well-defined as yaw increases. It starts in the direction of the major axis of the "hollow" but rapidly changes direction until it runs axially along the body aft of $x/L = 0.5$.

c) The contours to the rear of the starboard "hollow" gradually straighten, becoming more circumferential and closer together as yaw

increases. The resultant rapid rise in C_p is slightly to the rear of the base region of the starboard "hollow", is in line with the rear of the elongated base of the port "hollow" and is only present over the starboard half of the twin "hollow". The "valley" coming from the rear of the "hollow" seems to deflected towards the bottom of the body by this feature which also seems responsible for the twisting of the "hollow".

d) As yaw increases, the distribution over the nose of the body is modified in order to generate the required side-force and results in the rotation of the basic "ridge" - "hollow" distribution pattern around the body. At +6 degrees yaw, the distribution has rotated by about 30 degrees in a clock-wise direction.

e) Over the rear half of the forebody, the distribution is largely controlled by interference effects and thus changes relatively little as yaw increases. However, the large changes that take place in the geometry of the starboard "hollow" do cause the "ridge" leading into it to become less prominent.

f) The general form of the afterbody distribution changes little with increase in yaw except that it also rotates clockwise around the body by approximately the same amount as the forebody distribution.

11.5.2.2 Starboard body

As yaw increases the following changes take place in the contourplots of the C_p distributions:-

1) The position of the centre of the "hollow" remains unaltered as yaw increases but the depth of the "hollow" decreases, the shape of the bottom contours become more circular and its major axis twists so that the front of the "hollow" moves towards the top of the body in concert with similar changes in the characteristics of the starboard "hollow" on the central body. As a result of this rotation of the base, the general shape of the forward extension of the "hollow" alters with its axis becoming less swept forward initially but sweeping forward more rapidly as the nose is approached.

2) At zero yaw, little of the "hollow" extends to the starboard side of the body and thus there is little interference effect from the

"hollow" on the pressure distribution over the starboard side of the body. As yaw increases, the extent of the "hollow" increases and it expands past the top and bottom centre-lines into the starboard side of the body.

3) The "ridge" along the forebody becomes more prominent and moves anti-clockwise around the port half of the body from near the bottom centre-line to becoming almost aligned with the centre of the "hollow".

4) As yaw increases, the marked "valley" trailing from the rear of the "hollow" becomes less prominent and finally disappears leaving a small circumferential region in which C_p rises rapidly in an axial direction.

5) The disappearance of this "valley" as yaw increases, causes considerable changes in the afterbody distribution. Initially, the small "hill" located on the bottom centreline at the rear of the afterbody is absorbed into the larger "hill" in the same axial position whose centre is positioned initially on the port side of the body near the top centre-line. As this happens, the "hill" moves anti-clockwise around the body. The small "hill" is never completely absorbed however and as yaw increases, it becomes a separate entity again and continues to grow and rotate around the body until, by 6 degrees yaw, there are two well defined "hills" at the rear of the afterbody. The smaller, which is derived from the original small "hill" and is fairly flat, is positioned on the lower port side of the body near the centre-line while the larger, more prominent one is located on the top starboard side of the body near the centre-line.

11.5.2.3 Port body

As yaw increases, the following changes in the pressure distribution takes place:-

i) The "ridge" from the nose becomes more prominent and rotates anti-clockwise around the body from being slightly to starboard of the bottom centre-line to being slightly to port.

ii) The centre of the "hollow" does not alter in position, but the "hollow" deepens, elongates and rotates to become more closely aligned with the axis of the body and also extends around the top of the body to form a small, subsidiary "hollow" on the top port surface.

iii) The "valley" that trails from the rear of the "hollow" becomes deeper and extends further along the body.

iv) The afterbody distribution becomes more irregular as the "valleys" and "hills" become more pronounced with increase in yaw. The small "hill" slightly to the port of the bottom centre-line becomes longer and larger and apparently more prominent although this is the result of the C_p value at the base of the "hill" becoming more negative. It has also rotated anti-clockwise around the body by about 30 degrees at 6 degrees yaw. The larger "hill" positioned slightly to starboard of the top centre-line at zero yaw similarly extends forward and rotates anti-clockwise with increase in yaw.

11.5.3 Variation of the C_p distributions with yaw, pitch = -6 degrees

The contourplots of the C_p distributions over the bodies at 0, 2, 4 and 6 degrees yaw are presented in Figs 23 f) - i). Looking at the diagrams, it can be seen that the variation of the contourplots with yaw is somewhat similar to that already described at +6 degrees yaw with the important difference that the interference "hollow" that decreases in depth as yaw becomes more positive is now the one on the port, (windward), side of the bodies.

11.5.3.1 Central body

As yaw is increased, the following changes take place in the contour plots:-

a) Although the front of the "ridge" that runs along the top of the body, $\emptyset' = 180$, from the nose to the "col" between the two "hollows", rotates around the body in an anti-clock direction, the rear part of the "ridge" still runs along the body axis.

b) The centres of the "hollows" do not alter in position but the "hollows" alter differently in character as yaw increases. At this pitch angle it is the "hollow" on the starboard side of the body that elongates and deepens as yaw increases and also twists to align itself more closely to the body axis. However, the swept-forward planform of the "hollow" does not alter greatly in extent. The port "hollow" decreases in depth and its bottom becomes more circular in planform as yaw increases whilst, at the same time, its axis twists markedly in a clockwise direction. In addition, the planform of the "hollow"" increases in size as it twists and eventually extends around the bottom of the body into the starboard side.

c) At zero yaw, there is only a very minor "ridge" and "valley" system extending rearwards behind the "hollows" and the C_p distribution over the rear of the body is reasonably uniform. As yaw increases, a narrow "valley" first forms from the rear of the starboard "hollow" and then deepens with further increase in yaw. In addition a much less well-defined "valley" forms which seems to originate in the region where the contours forming a "hollow" extend past the bottom centre-line of the body. As these "valleys" form, they cause two "hills" of unequal size to appear in the afterbody distribution with their "tops" positioned at x/L = 0.85. The major "hill" is located on the bottom centre-line of the body at zero yaw and gradually rotates anti-clockwise around the starboard side of the body as yaw increases and the "hill" becomes more prominent. The minor "hill" only begins to form at about 2 degrees yaw and is then located diametrically opposite the major "hill". Once this "hill" has formed, it is similar in extent to the other, but not as high and rotates around the body in the same way as yaw increases.

11.5.3.2 Starboard body

The changes in the C_p distribution over the starboard body that occur as yaw is increased are as follows:-

1) The front of the "ridge" extending from the top centre-line of the body near the nose into the port side of the "hollow" rotates anti-

clockwise around the body whilst the rear rotates clockwise around the body to blend into the side of the "hollow" rather further aft.

2) The position of the centre of the "hollow" does not alter, but the "hollow" deepens, becomes narrower and rotates to become more aligned with the axis of the body and, at the same time extends over less of the circumference and more along the body.

3) The "valley" that extends from the rear of the "hollow" becomes deeper and, reflecting the movement of the rear of the "hollow", twists anti-clockwise around the body.

4) The "hills" that are the main feature of the afterbody distribution become more prominent and likewise move anti-clockwise around the body as yaw increases.

11.5.3.3 Port body

The changes in the characteristics of the C_p distribution due to change in yaw are much greater in extent than those over the starboard body. Although the "hollow", the main feature of the distribution created by interference between the bodies, decreases in depth, becomes more circular in planform and twists as yaw increases, it also becomes larger in extent and more diffuse so that it extends around virtually the complete circumference of the body at the position of maximum diameter, x/L = 0.39.

As yaw changes, features of the forebody and afterbody distributions change in the usual way, i.e. they rotate around the body in an anti-clockwise direction and the "hills" in the afterbody distributions become more prominent.

12.0 AN EMPIRICAL METHOD OF IMPROVING THE AGREEMENT BETWEEN THE ESTIMATED AND EXPERIMENTAL LOADS

The estimated values of C_N and C_Y do not generally agree well with the experimental values when the attitude of the bodies is appreciable, Figs 6 and 9. A previous investigation on the body used in the present body combination, ref 1, had deduced that this was because the panel method could not reproduce the effect of the base cavity flow on the afterbody C_P and loading distributions regardless of the base closure used to close the bluff base of the body.

It was suggested that the main cause of the disagreement was that the flow inside the base cavity imposed the condition that there should be negligible variation in the pressures measured around the circumference of the afterbody at the base and thus the local loading at the end of the afterbody should be zero.

The panel method predicted that, when the body was pitched, the normal-force loadings remained constant aft of a point near the beginning of the afterbody. The experimental loading distributions agreed well with estimate as far as the beginning of the conical afterbody but then decreased almost linearly to become zero at the base of the body. As a result the load over the afterbody was about half of that estimated.

When the body is pitched, the forebody produces a positive load but the afterbody produces a negative load which is a considerable proportion of the forebody load. Thus the total load is the difference between two large loads and so is very sensitive to differences between the estimated and experimental afterbody loads. Thus the halving of the afterbody load will produce very large changes in the total load.

12.1 Corrections to the estimates for the single body

The estimated and measured variation of C_N with pitch for the single body is shown in Fig 24. Three differences between the variations are immediately apparent:-

a) The experimental value of C_N at zero pitch is not zero as would be expected for reasons of symmetry. This is probably due to misalignment of the model in the windtunnel and can be allowed for by a shift in zero.

b) The experimental variation is slightly non-linear.

c) The estimated variation is linear and only half of the mean experimental variation.

In view of these large differences between the experimental and estimated value of C_N, it was decided to see whether a simple empirical correction based on the observed differences between the experimental and estimated loading distributions would eliminate or at least significantly reduce the error in the prediction of C_N.

The proposed correction is applicable when the estimated local-loading is constant for some distance in front of the bluff base of a body. The load over this region is the area under the (rectangular) loading distribution, i.e. proportional to the product of the (constant) local-loading coefficient and the length over which the loading is constant. Experiment has demonstrated that the loading in this regional actually decreases linearly to become zero at the base of the body and thus the actual load over the region is proportional to half the product of the local-loading at the front of the region and the length of the region and thus is also equal to the required correction.

Initially it was decided to apply this correction to the simple case of the single body.

Examination of the loading distributions, ref 1, showed that the estimated loadings remained constant aft of x/L = 0.45 at all

non-zero pitch angles. Thus the correction was based on a length of 0.55L and the value of the local loading at x/L = 0.45.

The corrected estimate is shown in Fig 24. After making allowance for the zero-shift on the experimental results, it is seen that the estimated results are now non-linear in the same way as the experimental results and the estimated values of C_N are now within 5% of the measured values.

12.2 Corrections to the estimates for the 3-body configuration

In the case of the 3-body configuration, it is not so obvious as to the extent of the region over which is legitimate to apply the proposed correction because of the effect of the mutual interference between the bodies on the loading distributions. Looking at the comparisons between the experimental and estimated loading distributions for the 3-body configuration over a limited range of pitch or yaw, Figs 13 and 14, it can be seen that the interference effects are dominant until approximately x/L = 0.65. Aft of this, the base effects become dominant and the estimated loadings mostly did not vary greatly over the rear of the afterbody.

When the estimated loading distributions were obtained for the extended range of pitch and yaw, Figs 20, 21 and 22, it was found that there were many cases where the loadings over the rear of the body were neither constant or negligible. In these cases, the loading at the end of the body could vary from zero to a value greater than that at x/L = 0.65 and thus the present method could give corrections that were considerably in error.

As a first stage, it was decided to apply the above correction method to all the normal-force and side-force loading distributions calculated for the extended pitch and yaw range to see the magnitude of the corrections and how the corrected estimates agreed with

the available experimental results. The correction used was of the same form as before but based on the front of the "correction" region being positioned at x/L = 0.6625,(the first station aft of x/L = 0.65 at which the loadings were estimated) and the loading at that station.

Both the original and corrected estimates of C_N and C_Y for the bodies over the extended attitude range are shown in Figs 18 and 19. Also included are the available experimental values so that the accuracy of the estimates can be assessed over at least some part of total range.

The predicted variations of C_N with pitch are shown in Fig 18 a). It can be seen that they do not agree very well with the available experimental results. However, with the exception of the value at zero pitch for the central body, the agreement between the corrected estimates and the experimental results is excellent.

When the basic distribution for the condition in error was examined, it was found that, as the loading at the base of the body was very small and that at x/L = 0.66 was appreciable, no correction was really required and, in fact, there was excellent agreement between the estimated and experimental values at this condition.

The variation of C_Y with pitch for the bodies is shown in Fig 18 b). In this case, the values of C_Y for the central body are always zero for reasons of symmetry, but neither the predicted or corrected values of C_Y for the outer bodies agree very well with the experimental values which are approximately mid-way between them.

If the estimated loading distributions are examined, Fig 20 b), it is seen that all the cases at positive pitch are in the "doubtful" category, i.e. the loading at the beginning of the "correction length" is appreciable, but it reduces to a smaller loading at the base of the body. In these particular cases, the loading at the rear of the body is approximately half that at the beginning of the correction

length so the correction should be approximately halved and thus agree with the experimental results.

The variation of C_N and C_Y with yaw for the various bodies at pitch angles of -6, 0 and +6 degrees is shown in Fig 19 and the corresponding loading distributions are shown in Figs 21 and 22.

Consider first the variation of C_N with yaw at zero pitch where experimental comparisons are available. The corrections made to the estimated results are appreciable and, in the case of the outer bodies, the corrected results are closer to experiment. In the case of the central-body, the reverse is true as the estimated results agree very closely with experiment.

If the central-body loading distributions are examined, Fig 21 b), it can be seen that the central body distributions reduce to approximately zero at the rear of the body and thus no corrections to the estimated results should be necessary as is indeed the case.

The afterbody loading distributions for the outer bodies are very similar in character and so it would have been expected that no correction to the estimates would have been required. However this was not so and some other reason had to be sought to explain why a correction was necessary. If the comparisons between the experimental and estimated loadings are examined, Fig 14 a), c) and e), it will be seen that there is good agreement between the central-body loadings over the whole length of the body. On the other hand, in the case of the outer bodies, there is good agreement over the afterbodies, but the agreement between the forebody loadings is less good with the experimental loadings being less than estimated. It would appear that the good agreement between the experimental and corrected loads is due to the co-incidence that the correction to the afterbody loads happens to be equal to the difference between the estimated and experimental forebody loads

At the other pitch angles, the corrections are large and approximately constant at a given condition. However examination of the loading distributions, Figs 21 a) and c), indicate that they come in the "doubtful" category as far as the correction criteria are concerned and thus the estimated corrections will be in error.

Comparison of the variation of C_Y with yaw for the experimental, estimated and corrected results at zero pitch, Fig 19 b), shows that the experimental results do not agree consistently with either the estimated or corrected variations. Examination of the loading distributions showed that relatively few of the distributions satisfied the correction criteria and thus the correction applied would be in error.

Looking at the side-force loading distributions over the whole of the extended attitude range, it became obvious that relatively few of the distributions satisfied the criteria for the correction in its present form to be accurate. This was because :-

a) Many of the loading distributions over the afterbody varied smoothly without any well-defined region in which the loadings remained constant.

b) In practice, the loading at the end of the body could be zero or greater, equal or less than the loadings in the region of the nominal position from which the correction was calculated.

12.3 Revised correction method

Re-examination of the original error analysis showed that the analysis was basically correct but was incorrectly formulated because it assumed, on the evidence of the investigation of tests on the single body, ref 1, that the estimated loadings would always be constant over a considerable length of the afterbody and thus the loading at the end of the body would invariably be the same as that at the beginning of the "correction region".

The correction that is actually required is one that corrects the overall load on the body to allow for the difference between the estimated loading distribution and one that assumes that the loading varies linearly between that at the beginning of the "correction region" and zero at the end of the body. If the estimated distribution over the afterbody is approximately linear, as it is in most cases, the load correction becomes ½ x loading at the end of the body x length of the region thought to be affected by the base-cavity. This correction is the same as previously used except the loading at the beginning of the "correction region" is replaced by the loading at the end of the body.

Using this revised correction, the accuracy of the prediction method should be greatly improved as the revised method should deal with those conditions where the original method failed to predict the experimental results as described previously.

The accuracy of the load correction depends on two judgements which are:-

1) the length of the afterbody affected by the base-cavity flow

2) whether the estimated afterbody loading distribution can be adequately represented by a line between the loadings at the beginning and end of the length defined in 1).

When an estimate of the loads over a body or body configuration is being made as part of a project assessment, it is suggested that the afterbody loading distributions should be examined over a small range of conditions to assess where the loadings are first influenced by the base-cavity flow. In the absence of any other reason, this could be taken as the position where the distribution is nearest tangential to a straight line from zero loading at the end of the body.

If the estimated afterbody distribution cannot reasonably be represented by a linear distribution, the accuracy of the simple correction will be poor and some other method will need to be used to increase the accuracy of the correction.

13.0 FLOW VISUALISATION

Sufficient time was available at the end of the test period to obtain one oil-flow visualisation pattern of the flow over the three-body combination at the datum attitude, pitch = 0 degrees = yaw, before the models had to be de-rigged.

Because of the closeness of the bodies to each other, it was difficult to see the main interference regions simultaneously and thus get an adequate appreciation of the flow patterns. Some photographs were taken of the flow patterns of which the two most informative are shown in Fig 25. These both show mainly the flow patterns over the central body and are therefore complemented by the contourplot of the corresponding C_p distribution over the central body.

The upper picture shows the flow along the central body towards the position of maximum interference. The flow lines on the body closely approximate to the streamlines over the surface of the body which in turn are at right-angles to the pressure contours. The region of maximum interference is shown on the diagram by the rather confused region near the top of the bottom, (central), body and is also shown by a similar pattern just visible in the corresponding position on the top, (port), body. The flow lines show the flow from the top of the central body being initially deflected towards the centre-line because of the down-flow induced over the nose and then bending upwards towards the low-pressure region that marks the position of maximum interference. The well-defined boundary between the dark and light parts of the picture marks the boundary between the "ridge" of high pressure caused by the induced flow over the nose of the body.

The lower picture shows a top view of the flow over the central body with the main feature of interest being the well-marked streamwise filaments coming from the "valleys" at the rear of the regions of maximum interference. Also shown is the flow along the fore-bodies bending towards these regions.

4.0 DISCUSSION

The main features of the analysis of the interference effects on the three bodies when the attitude of the 3-body configuration is varied over a range of pitch and/or yaw are summarised below.

14.1 Experimental results

a) Basic interference at datum attitude, pitch = 0 degrees = yaw

There are two types of interference present, one due to the close proximity of the bodies to each other and the other due to changes in the incident flow induced by the presence of the bodies.

The interference due to the close proximity of the bodies is concentrated about the positions where the gap between the bodies is a minimum. At these positions, the speed of the flow is a maximum and thus C_p is a minimum, but because of the three-dimensional nature of the body surfaces, the region of maximum interference is quite small and very three-dimensional. However, the whole interference region is much larger and extends circumferentially over more than half the body and axially over approximately +/- 0.25 L.

For this three-body configuration, there are four main centres of interference which are located at a distance of 0.392 L behind the nose of the bodies, i.e. at the position of maximum diameter. In the case of the central body, there are two centres located at +/- 45 degrees from the top centre-line of the body. The main centre of interference on the starboard body is located at 135 degrees anti-clockwise from the top centre-line of the body, i.e. in the centre of the quadrant facing the central body, and that on the port body is in the corresponding position. The port and starboard bodies also interfere with each other, but the interference is smaller and is barely distinguishable on the C_p distributions as a separate entity.

The minimum pressure in these four interference regions is C_p = -0.46 as compared with the minimum value of C_p = -0.12 present on a single body at the same attitude.

Because of these interference regions, the local loadings are high, especially on the central body which has two regions of low pressure on the top half of the body. As these regions are centred at +/- 45 degrees from the top of the body, there will be an effect on both the normal and side-force loadings, but the side-force components cancel each other. The maximum local normal-force loading measured on this body was +2.35 as compared with a maximum local loading of +0.78 measured on a single body at 6 degrees pitch

The local loadings measured on the outer bodies are rather different because of the different positions of the interference regions. The main interference region is centred on a generator at 45 degrees from the bottom centre-line of the body and so its effect has to be resolved through +/- 45 degrees to give a component to both the normal-force and side-force loadings. The component to the normal-force loading will be negative and the side-force component will be towards the plane of symmetry of the configuration. The secondary interference region, (from the other outer body), is centred on the horizontal centre-line of the body and so will contribute only to the side-force loading in the direction of the plane of symmetry of the combination. The maximum local normal-force loading measured on the port body was -1.06 with a maximum side-force loading of 1.83, i.e 56% of the side-force loading comes from the interference from the central body and 44% from the starboard body.

Besides the changes in the loading distribution resulting from the proximity of the bodies forming the body combination, there are changes in the loading distribution that are a result of changes in the angle of the incident flow induced by the presence of the bodies. These changes in incident flow result in loading distributions over the nose and rear of the bodies that are similar to those over a

single body. By matching these distributions to those of a single body, the following estimates of the mean flow directions over the front of the forebody and rear of the afterbody were made:-

Central body

Front of forebody	6 degrees downflow
Rear of afterbody	2 degrees upflow

Outer bodies

Front of forebody	2 degrees upflow,	4 degrees outflow
Rear of afterbody	1 degree downflow,	1 degree inflow

When the loading distributions are integrated to give the values of C_N and C_Y due to interference, the following load coefficients were obtained :-

Central body	C_N = 0.230	
Port body	C_N = -0.128,	C_Y = 0.215

In comparison, the measured value of C_N for a single body at 6 degrees pitch is 0.12.

The axial-force loading distributions are similar in character to those on a single body. The positions of the various peaks seem to be dictated purely by body geometry as they vary little with the attitude of the body or whether the body is in its own or forms part of a body combination. The absolute and relative magnitudes of the peaks however do vary appreciably with attitude and configuration, particularly the first two peaks which are located on the forebody.

When the loading distributions are integrated to obtain the values of C_A for the fore-body, afterbody and whole body, it is found that, compared with a single body, the interference causes a large decrease forebody C_A and a slightly larger increase in afterbody C_A with the result that there is a small increase in total C_A which,

however, is relatively large in percentage terms because the total C_A is the small difference between two much larger quantities.

b) Change in interference with change in attitude

If the interference loadings do not change with change in attitude, the loading at a given station will be the sum of the interference loading and the loading on a single body at the required attitude. However, if this is not the same as the measured loading, then the interference loading must have changed and the change in the interference loading, the "additional interference", is the measured loading minus the expected loading.

It was found that large changes in the "additional interference" loadings occurred as attitude was varied. When measured as a percentage of the maximum interference present at the datum attitude, the maximum "additional interference" loadings were large, up to 40% in normal-force, 25% in side force and 70% in axial force, Table 2. The largest changes generally did not occur at the positions where the basic interference was a maximum, but where there were large changes in interference loading, the changes varied linearly with change in attitude. From these observations it may be concluded that the shape of the loading distributions over the bodies altered in a different manner from those of a single body as attitude was varied and particularly when yaw was varied.

The character of the changes in interference varies appreciably with the type of loading, position of the body and whether the bodies were pitched or yawed. In general, most of the large changes in interference loading that occur when pitch or yaw is increased, take place over the forebodies with the maximum change occurring near x/L = 0.25. However, an exception to this is the change in the normal-force interference loading on the central body where the changes occur over a region of approximately +/- 0.25 L on either side of the end of the

forebody, x/L = 0.39, which is the position at which the change is a maximum.

As attitude changes, the minimum values of C_p in the maximum interference regions and the shape of the contours defining the regions change appreciably. The minimum value of C_p in all four regions decreases to approximately -0.53 at a pitch angle of +6 degrees at zero yaw. When the bodies are yawed at zero pitch, the minimum pressures in the interference regions on the bodies still become more negative but by different amounts in the different regions. The minimum values of C_p in the interference regions on the port, (windward), and starboard, (leeward), sides of the central body are the same, C_p = -0.49 This is also the minimum value of C_p in the interference region on the leeward side of the port, (windward), body. However, the minimum value of C_p in the interference region on the windward side of the starboard, (leeward), body is rather more negative, C_p = -0.54.

The changes in the forebody C_p distributions that take place as attitude changes, interact with the changes in the C_p distributions in the main interference region on all the bodies and result in considerable changes in their shape as attitude changes. The planform of the C_p contours in this region become more elongated as attitude increases and, in addition, twists about the position of minimum C_p when yaw varies and also suffers considerable distortions in planform.

These alterations in the main interference region spread downstream and distort the normal changes in the afterbody distributions that occur as the result of a change in attitude.

c) Variation of C_N, C_Y and C_A with attitude

When the loadings are integrated to obtain the variations of C_N, C_Y and C_A with pitch and yaw for the individual bodies and the body combination, it is found that, although the

individual coefficients can be considerably greater and also vary in a completely different way with change in attitude from the comparable values and variations for a single body, the aerodynamic characteristics for the body combination are very similar to those of a single body.

C_N

As already mentioned, the value of C_N at zero pitch for the central body is approximately twice that of a single body at 6 degrees pitch. When pitch is increased, C_N increases at a steadily increasing rate and doubles between 0 and 6 degrees pitch. Thus the change in interference between 0 and 6 degrees pitch is equal to the increase in C_N for a single body over the same range of pitch. The value of C_N at zero pitch for the outer bodies is negative and equal to that of a single body at -6 degrees pitch. As pitch is increased C_N becomes less negative but at a decreasing rate and thus C_N has only increased by about 2/3 that of a single body when pitch has increased by 6 degrees, i.e the interference on the outer bodies has become more negative as pitch becomes more positive.

When yaw is varied at zero pitch, C_N for the central body decreases at a steadily increasing rate so that it has reduced by 26% by +6 degrees yaw. The variation of C_N with yaw is different for the port and starboard bodies. C_N for the port, windward, body becomes less negative with increase in yaw and although the shape of the variation is very similar to that of the central body, the change in C_N between 0 and 6 degrees yaw is slightly greater in absolute terms with the result that the value of C_N at 6 degrees yaw is only 44% of that at zero yaw. On the other hand, C_N for the starboard, leeward body becomes slightly more negative initially and then remains approximately constant with further variation in yaw, with the change in C_N between 0 and +6 degrees being 8%. As the value of C_N at zero yaw of the central body is double that of the outer bodies, the overall value of C_N for the 3-body combination remains approximately zero as yaw varies, but there will be

a slight rolling moment present due to the different variations of C_N with yaw for the outer bodies.

C_Y

The variation of C_Y with pitch at zero yaw is small. For reasons of symmetry, C_Y for the central body remains zero as pitch varies. As the interference region on the port and starboard bodies is not symmetric about their y-axes, C_Y is not zero at zero pitch and there is a side-force of magnitude $C_Y = 0.21$ on each body directed towards the other. Due to the changes in the C_P distribution in the interference region as pitch varies, C_Y for the port and starboard bodies increases linearly in magnitude by approximately 8% as pitch increases from 0 to +6 degrees.

In the absence of any change in interference as yaw is varied, it would be expected that the change in C_Y would the same as that for a single body. This is indeed the case for the central body where the change in C_Y between 0 and 6 degrees yaw is only slightly less than that of a single body. However, the changes for the outer bodies are considerably less, the changes in C_Y for the port, (windward), body and starboard, (leeward), bodies being approximately 80% and 60% respectively of that of the single body. Thus the corresponding change for the 3-body configuration is approximately 80% of that for the single body.

C_A

The variation of C_A with attitude is considerably different from that of the single body.

The total C_A for the single body at zero pitch is 0.0042 and this decreases slowly by 0.004 as pitch increases to +6 degrees. As the corresponding values of forebody C_A are -0.0032 and

0.0122, the afterbody C_A is +0.0072 at zero pitch and increases to +0.0154 at 6 degrees pitch.

Not only is the value of the total C_A at zero pitch for the central body approximately double that of the single body but the increment between 0 and 6 degrees pitch is positive, (opposite in sign), and 11½ times greater in magnitude than that of the single body. The value of the forebody C_A at zero pitch is negative and 6.3 times greater than that of the single body while the increment in C_A between 0 and 6 degrees pitch is positive and approximately double that of a single body. Thus the afterbody C_A at zero pitch is 4 times that of the single body and the increase between 0 and 6 degrees is 2.5 times greater.

The variation of C_A with pitch for the port and starboard differs from that of the central body. At zero pitch the total C_A of the port/starboard body is slightly less than that of the central body and is 1.7 times that of the single body. However C_A now reduces with increase in pitch and the decrement in C_A between 0 and 6 degrees pitch is 7 times that of the single body. The forebody C_A at zero pitch is negative and 6.4 times that of the single body, i.e. approximately the same as that of the central body. However C_A again decreases with increase in pitch, but the decrease between 0 and 6 degrees pitch is about 2.6 times that of the single body. The resulting afterbody C_A is 3.3 times that of the single body but the increase between 0 and 6 degrees pitch is only about 40% of that of the single body.

The variation of C_A with yaw is different from that with pitch.

In the case of the central body the variation of C_A with yaw is now very similar to that of the single body. The value of the total C_A falls very slightly with increase on yaw, with the amount of the decrease being only about 75% of that of the single body. Whilst the value of the forebody C_A at zero yaw is considerably more negative

than that of the single body, the forebody C_A decreases slightly as yaw varies between 0 and +6 degrees, the amount of the decrease being about 15% greater than that of the single body. As a result, the afterbody C_A increases slightly as yaw increases,with the change being some 35% greater than that of a single body.

The variations of C_A with yaw for the outer bodies differ not only from each other but are completely different from the central body.

The total C_A of the port body increases linearly and that of the starboard body decreases linearly as yaw is varied between 0 and +6 degrees. The change in C_A between 0 and +6 degrees yaw for the starboard body is some 7% greater than that for the port body, but both changes are an order of magnitude greater than that occurring on either the central body or a single body. The changes in the forebody C_A of the port and starboard bodies with yaw are similar in character to those of the total C_A but are smaller in magnitude. There is now a much larger difference between the two bodies with the ratio (change in forebody C_A / change in total C_A) being 0.6 for the port body and 0.9 for the starboard body. As a result of these differences, the afterbody C_A increases by about 60% between 0 and +6 degrees yaw in the case of the port body, while that of the starboard body decreases by 15%.

14.2 Estimated characteristics

The C_P distributions over the bodies were estimated using the same inviscid panel method, SPARV, that had been used previously to determine the interference characteristics of other body configurations. The loading distributions over the bodies and the load coefficients were then obtained by successive integration of the C_P distributions.

14.2.1 Comparison with experimental results

As previously, there was good agreement between the estimated and experimental C_p and loading distributions over the fore-bodies and the regions on the bodies where the interference effects were large. However, the estimated C_p distributions over the afterbodies did not agree too well with experiment in the regions, at the rear of the afterbody, where the interference effects were not large and where the loadings were appreciable because the estimated C_p distributions were not very uniform. In the regions where these conditions applied, the experimental loadings tended towards zero at the base of the body, but the estimated loadings were generally constant because the estimation method did not allow an adequate representation of the effects of the flow in the base-cavity on the C_p distribution over the rear of the afterbody.

Although the differences between the experimental and estimated C_p distributions over the rear of the body did not appear to be very significant, the differences in the afterbody loading distributions could be quite large at the larger attitudes. As the overall normal-force and side-force on these particular bodies were the relatively small difference between a large fore-body load and a smaller afterbody load, a relatively small difference between the estimated and experimental afterbody loadings could lead to large differences between the estimated and experimental overall loads.

As it was impracticable to correct the afterbody C_p distributions, a method of correcting the afterbody normal-force and side-force loadings was developed that resulted in close agreement between the estimated and experimental load coefficients for a single body. The good agreement was the result of an individual assessment of each condition to decide whether the proposed form of correction was applicable.

As the ultimate objective was to develop a form of correction that could be applied automatically in the computation of the loads, it was decided to apply the correction method to all conditions that were computed for the 3-body configuration to see how the corrected results compared with experiment. It was found that the correction method considerably improved the accuracy of prediction at large attitudes when the afterbody loadings were high, but at the expense of the agreement at low attitudes when the correction was not required.

By a small alteration to the correction method a new correction method was evolved which should give good estimates of the loads for most types of loading distributions provided that a rough estimate could be made of the length of the afterbody over which the correction should be applied.

14.2.2 Extension of the estimates to a greater range of attitudes

Whilst the estimated C_{p_s} distributions at -2, -4 and -6 degrees pitch at zero yaw followed the general pattern present at positive pitch, the distributions as yaw was varied at pitch angles of +6 and -6 degrees pitch differed appreciably from those at 0 degrees pitch.

The central body has two adjacent interference regions centred about the positions where the gap between the bodies is a minimum. When the bodies are yawed at zero pitch the contours defining the regions alter in shape and depth in the same way.

This is not so when the bodies are yawed at +6 degrees pitch as the centre part of the interference region on the starboard (lee), side of the body remains approximately the same as yaw varies while that on the port side of the body elongates, twists and deepens appreciably with considerable down-stream changes in the C_{p_s} distribution.

When the bodies are yawed at -6 degrees pitch, the interference regions alter in a somewhat similar way, except that it is the port, (windward), interference region that alters little as yaw increases and the starboard interference region that alters appreciably.

When the C_{lp} distributions are integrated to give the local loadings, the loading distributions alter smoothly with change in pitch and yaw. At large angles of pitch and/or yaw, the side-force and normal-force loadings over the rear of the afterbodies become appreciable and so a correction would be required to the estimated loads if the normal-force and side-force loads were to be estimated accurately. However, in many cases, the loadings were not very constant over the afterbodies and so a revised correction method was developed that should give better results than the method used in this report which, in some cases, will over-estimate the correction required.

It was found that the calculated corrections were large but, as the corrected results agreed well with the available experimental results, the corrected results could be used with reasonable confidence in the extended attitude range. In most cases, the results over the extended attitude range followed the trend established by the experimental data. The exception to this is the variation of C_N with pitch for the central body where C_N varies little at negative pitch, although the variation with pitch is appreciable at constant pitch.

15.0 ACKNOWLEDGEMENT

The author would like to thank Attack Weapons Department, Defence Research Agency (Aerospace Division), RAE Farnborough, Hants for sponsoring this investigation.

SYMBOLS

A	Axial-force (due to body pressures only)
C_A	Axial-force coefficient (A/qS)
C_m	Pitching-moment coefficient (M/qSL)
C_N	Normal-force coefficient (N/qS)
C_n	Yawing-moment coefficient (N'/qSL)
C_p	Pressure coefficient $(p-p_\infty)/q$
C_Y	Side-force coefficient (Y/qS)
D	Maximum body diameter
$dC_A/d(x/L)$	Local axial-force loading
$dC_m/d(x/L)$	Local pitching-moment loading
$dC_N/d(x/L)$	Local Normal-force loading
$dC_n/d(x/L)$	Local yawing-moment loading
$dC_Y/d(x/L)$	Local side-force loading
L	Overall length of the body
M	Pitching-moment (measured about the nose)
N	Normal-force
N'	Yawing-moment (measured about the nose)
p	Local static pressure
p_∞	Free-stream static pressure
q	Free-stream dynamic pressure
r	Body radius
S	Maximum body cross-sectional area ($\pi D^2/4$)
x	Distance from the nose of the body
X_N	Distance ahead of the nose of the line of action of C_N
X_Y	Distance ahead of the nose of the line of action of C_Y
Y	Side-force
$\emptyset$	Anti-clockwise angle of pressure generator from top centre-line
$\emptyset'$	Clockwise angle of pressure generator from bottom centre-line

REFERENCES

1 Llewelyn-Davies, D.P. A comparison between the experimental and estimated pressure and loading distributions over an axisymmetrical body with a bluff base over a small of pitch at subsonic speed.
C.I.T. Cranfield
CoA Report No 9105, February 1991

2 Christopher, P.A.T
Hussain Z. An investigation into the aerodynamic characteristics of bodies of revolution.
C.I.T. Cranfield
CoA Report No 8436, December 1984

3 Llewelyn-Davies, D.P. The effect of longitudinal stagger on the aerodynamic interference between two axi-symmetrical bodies whose centrelines are parallel, at zero pitch and separated by 1.05 body diameters.
C.I.T. Cranfield
CoA Report No 8900, January 1989

4 Llewelyn-Davies, D.P. The effect of pitch and yaw on the aero-dynamic interference between two identical unstaggered axisymmetrical bodies whose centrelines are parallel and separated by 1.11 body diameters.
C.I.T. Cranfield
CoA Report No 8909, August 1989.

REFERENCES (continued)

5 Llewelyn-Davies, D.P. The effect of pitch and yaw on the aerodynamic interference between two identical staggered axisymmetrical bodies whose centrelines are parallel and separated by 1.11 body diameters.
C.I.T. Cranfield
CoA Report No 8912, Deecember 1989

6 Petrie, J.A.H. Development of an efficient and versatile panel method for aerodynamic problems.
Ph.D Thesis, University of Leeds, 1979.

x/L	r/L	slope (degrees)
0.01875	0.006258	17.987
0.03750	0.012177	17.055
0.05625	0.017763	16.127
0.07500	0.023071	15.203
0.09375	0.027955	14.283
0.11250	0.032570	13.368
0.13125	0.036868	12.455
0.15000	0.040854	11.546
0.16875	0.044530	10.640
0.18750	0.047900	9.736
0.20625	0.050965	8.835
0.22500	0.053729	7.936
0.24375	0.056194	7.039
0.26250	0.058360	6.144
0.28125	0.060231	5.250
0.30000	0.061807	4.358
0.31875	0.063089	3.467
0.33750	0.064079	2.576
0.35625	0.064777	1.686
0.37500	0.065183	0.797
0.39375	0.065298	-0.093
0.41250	0.065122	-0.982
0.45000	0.063897	-2.761
0.48750	0.061941	-3.000
0.52500	0.059975	-3.000
0.56250	0.058010	-3.000
0.60000	0.056045	-3.000
0.65000	0.053424	-3.000
0.68750	0.051459	-3.000
0.72500	0.049494	-3.000
0.77647	0.046796	-3.000
0.80000	0.045563	-3.000
0.83750	0.043598	-3.000
0.87500	0.041633	-3.000
0.91250	0.039667	-3.000
0.95000	0.037702	-3.000
0.96250	0.003705	-3.000
0.98125	0.036064	-3.000
0.99025	0.035921	-3.000

a) Body ordinates and slope at pressure-plotting points

Overall length = 60.56 in.
Maximum diameter (D) = 7.9091 in. (0.13060 L)
L/D ratio = 7.6645
Forebody length = 23.7273 in. (0.39290 L)
End of ogive = 27.5562 in. (0.45502 L)

b) Body dimensions

TABLE 1 Details of revised configuration

Central body

Component	extent	peak value	position
Maximum change in interference at 6 degrees pitch			
Normal-force	0.2 → 0.7	+0.38 (16%)	0.35
Axial-force	0.0 → 0.4	-0.008 (3%)	0.11
Maximum change of interference at 6 degrees yaw			
Normal-force	0.2 → 1.0	-0.18 (8%)	0.41
Side-force	0.2 → 0.4	0.197	0.30
Axial-force	0.2 → 0.4	-0.009 (3%)	0.11

Port and starboard bodies

Component		extent	peak value	position
Maximum change in interference at 6 degrees pitch				
Normal-force		0.1 → 0.35	+0.20 (20%)	0.26
Side-force	a)	0.0 → 0.39	0.46 (25%)	0.26
	b)	0.4 → 1.0	-0.21 (11%)	0.56
Axial-force		0.0 → 0.4	-0.008 (3%)	0.11

Port body

Component	extent	peak value	position
Maximum change in interference at 6 degrees yaw			
Normal-force	0.0 → 0.4	0.40 (39%)	0.26
Side-force	0.0 → 0.4	-0.237 (13%)	0.21
Axial-force	0.0 → 0.4	0.164 (71%)	0.16

Starboard body

Component	extent	peak value	position
Maximum change in interference at 6 degrees yaw			
Normal-force	0.0 → 0.4	-0.339 (33%)	0.26
Side-force	0.0 → 0.4	-0.297 (16%)	0.20
Axial-force	0.0 → 0.4	0.127 (55%)	0.16

Table 2. Change in interference with change of attitude

N.B % means % of maximum interference for coefficient at datum attitude

FIGURES 1 - 25

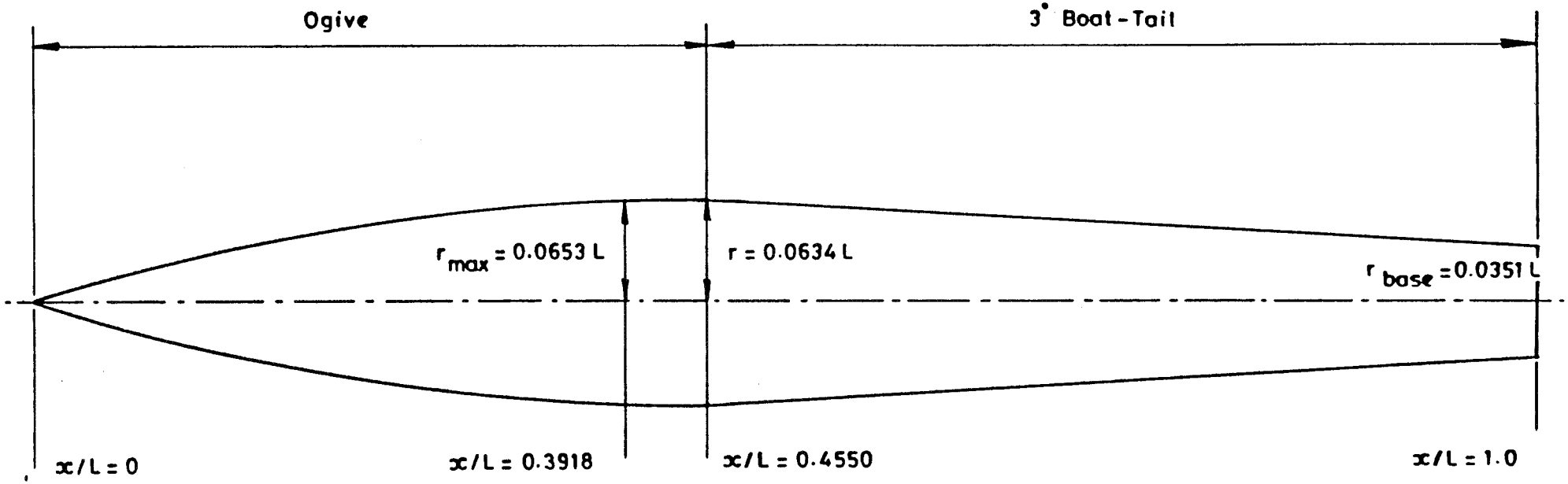

Fig 1. Model Geometry.

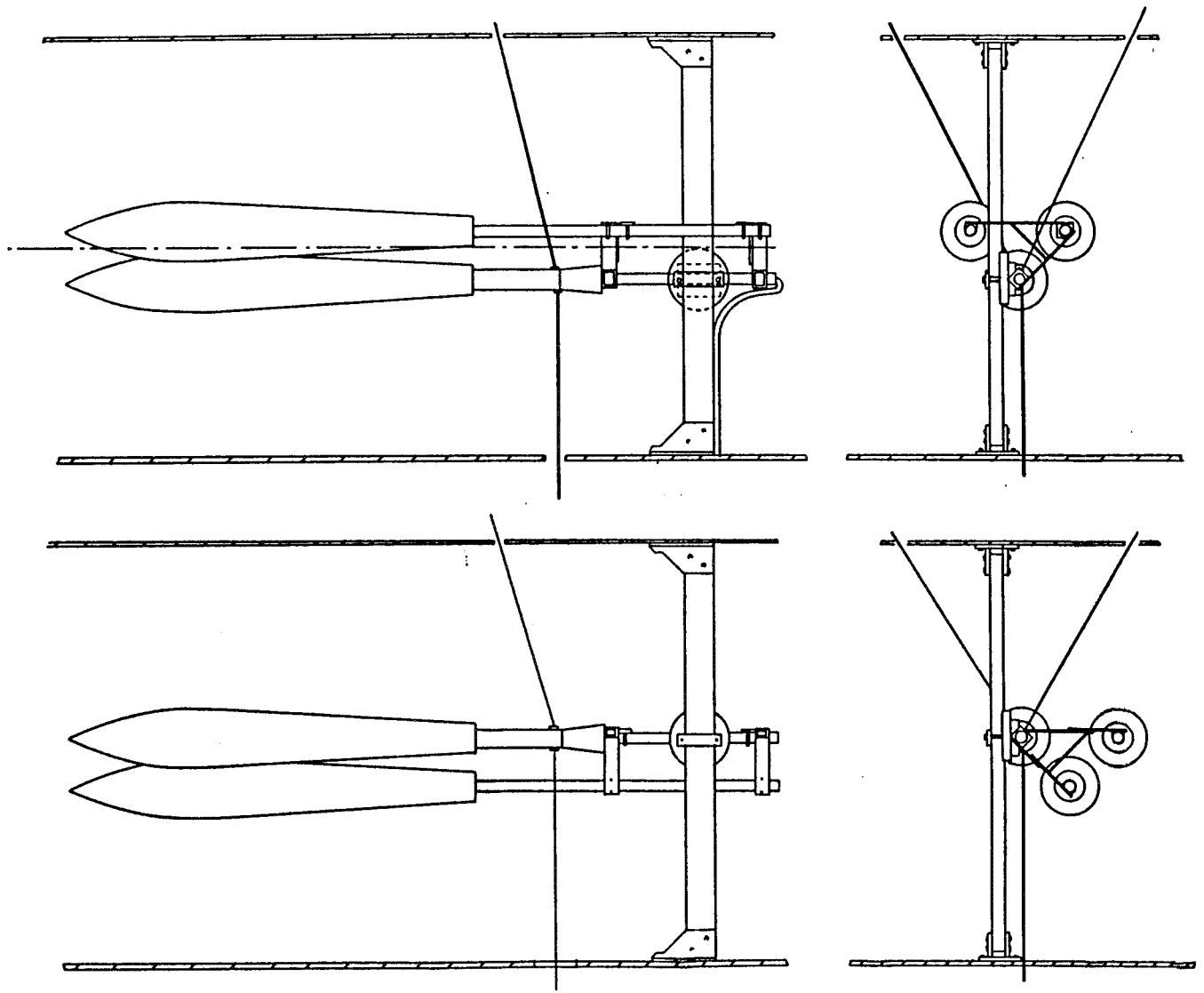

(a) Alternative positions for instrumented body

Fig. 2. Model Rigging Arrangements.

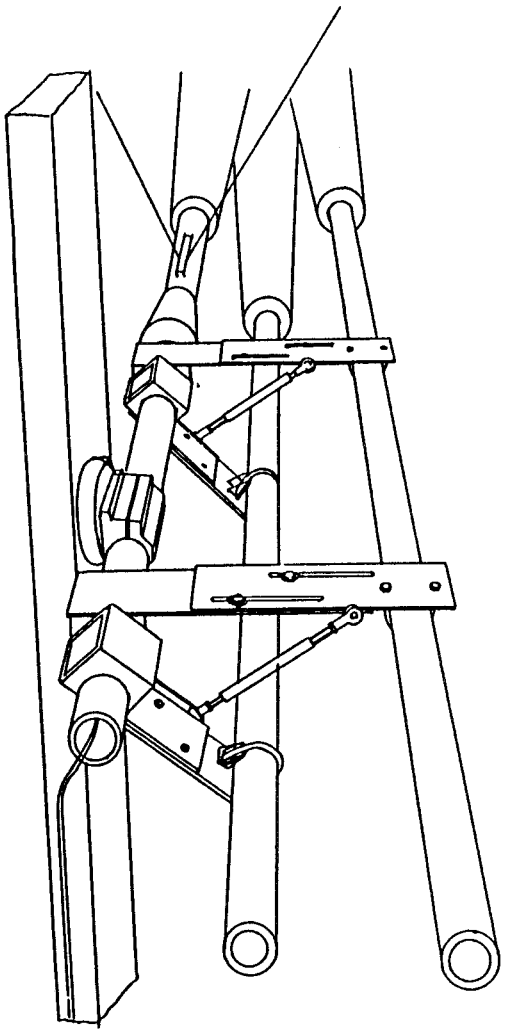

(b) Support system details

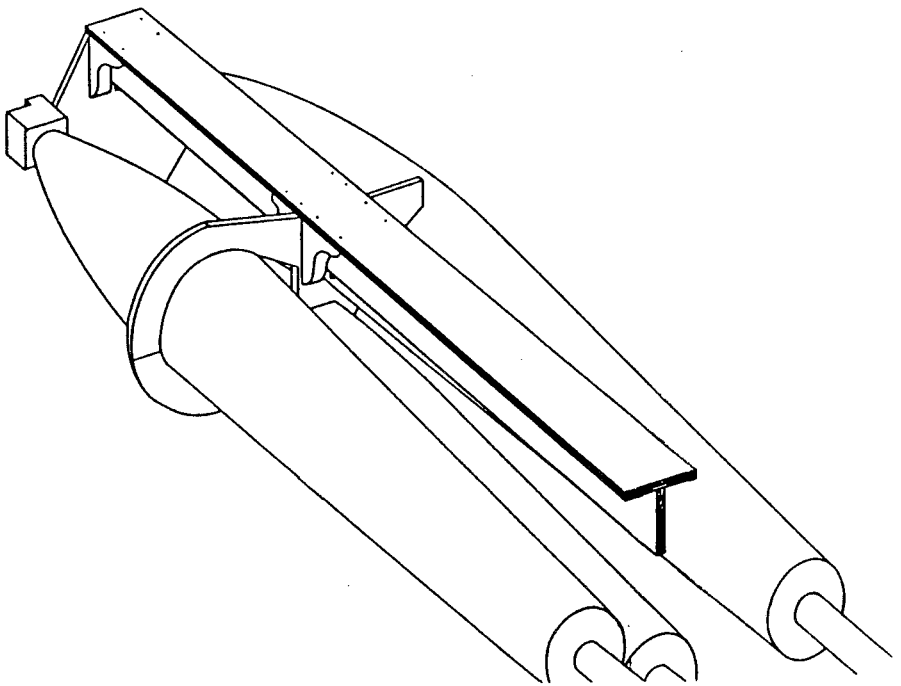

(c) Model alignment rig.

Fig. 2. Cont.

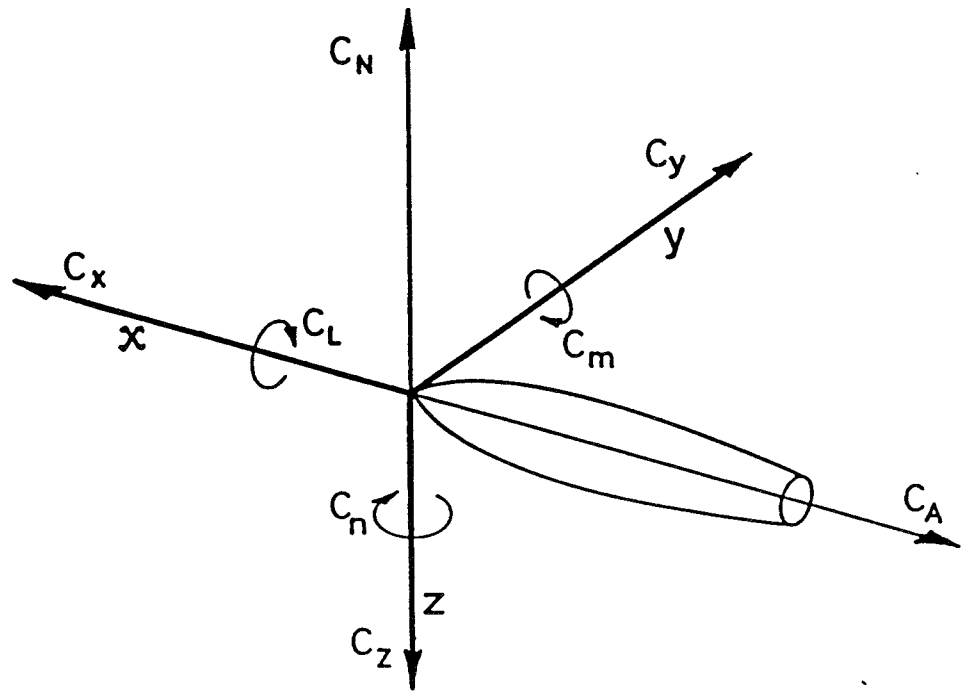

(a) Body axis system of forces and moments.

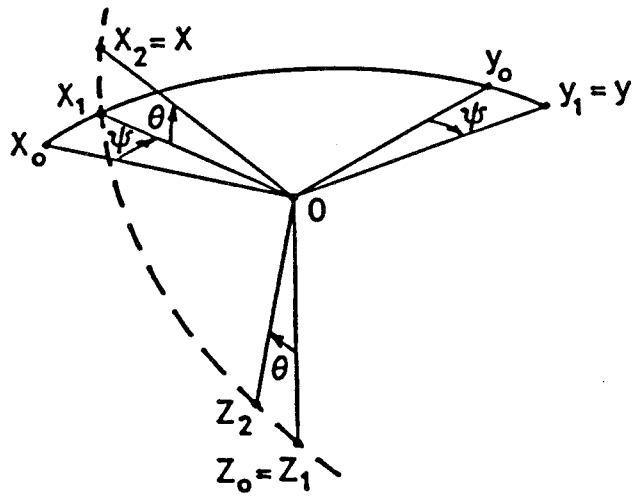

(b) Definition of incidence (θ) and yaw (ψ) in non-rolling body axes.

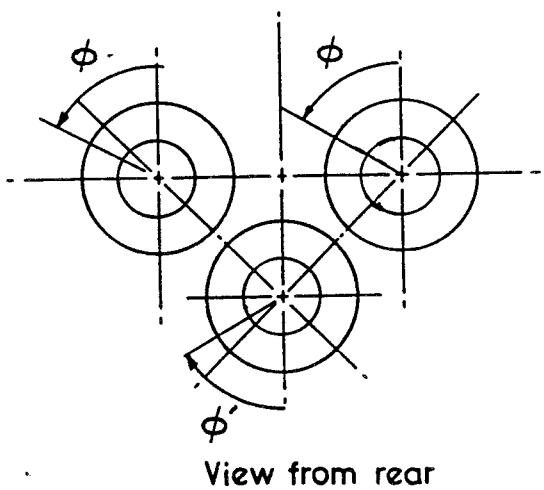

View from rear

(c) Definition of generator angles

Figure 3. Definition of axis system.

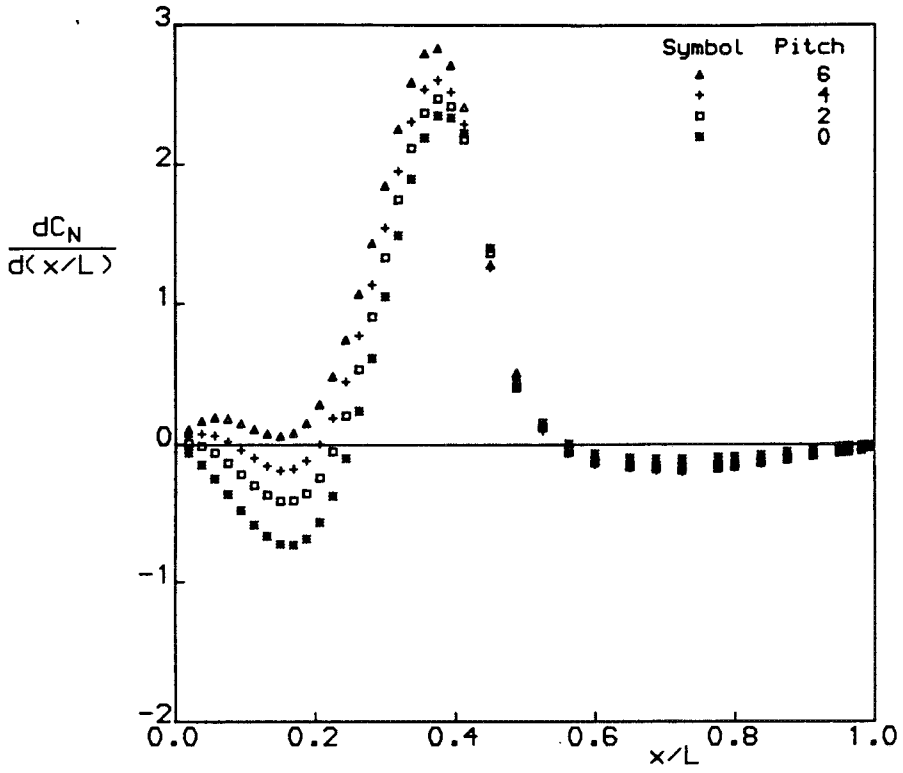

Central body

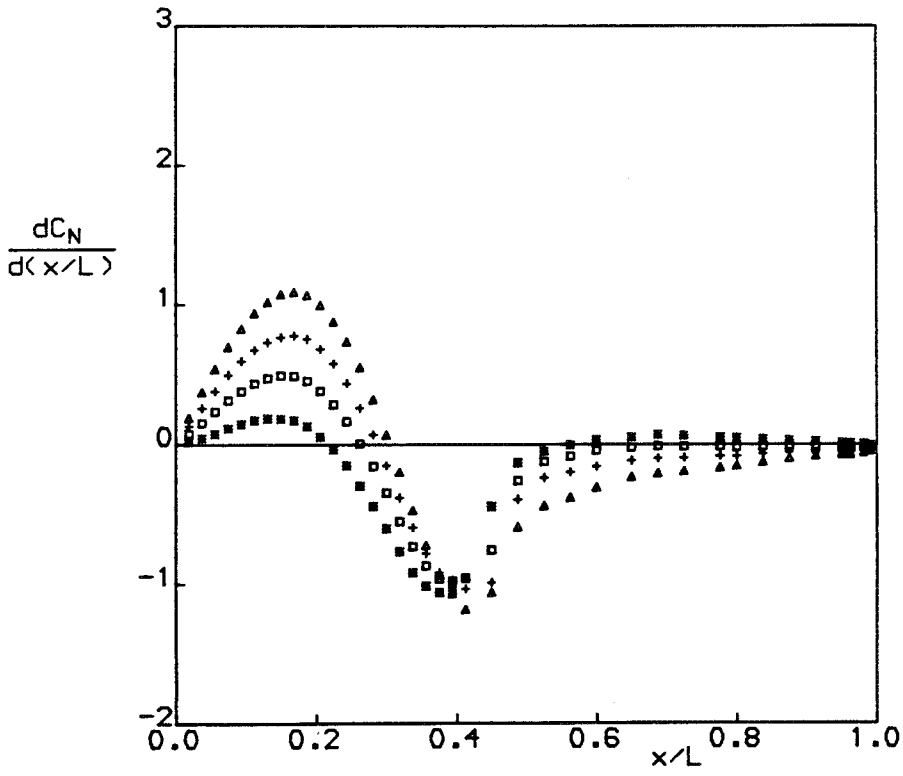

Port body

a) Normal-Force loadings

Figure 4. Variation of experimental loadings with pitch

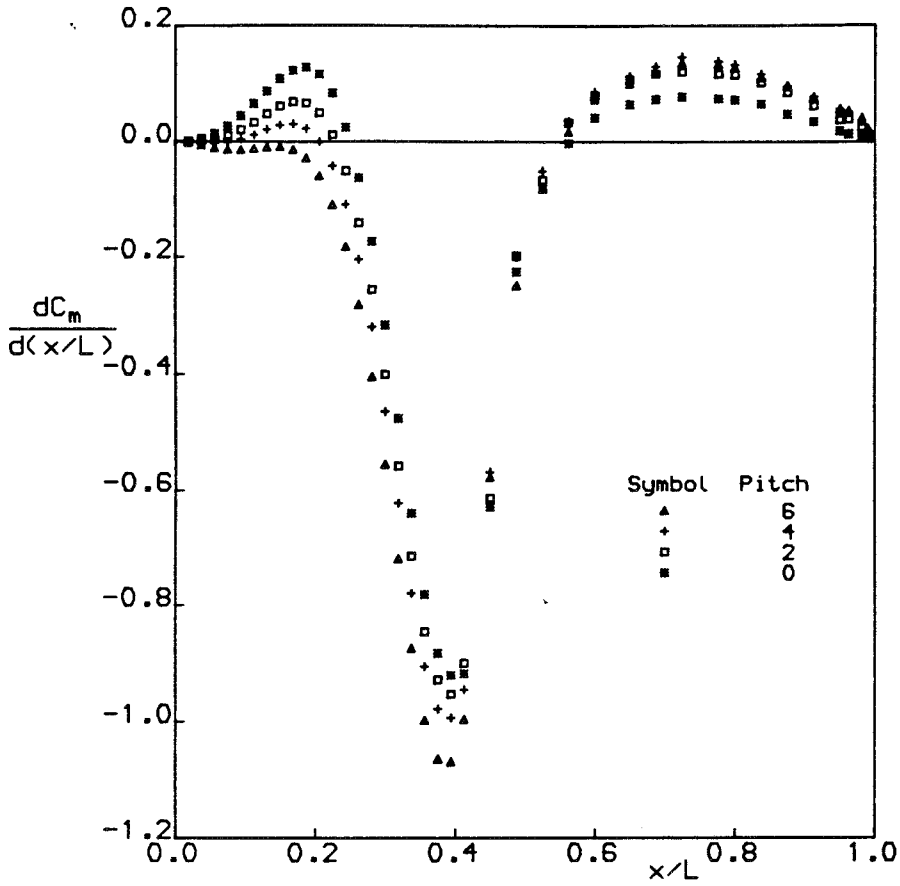

Central body

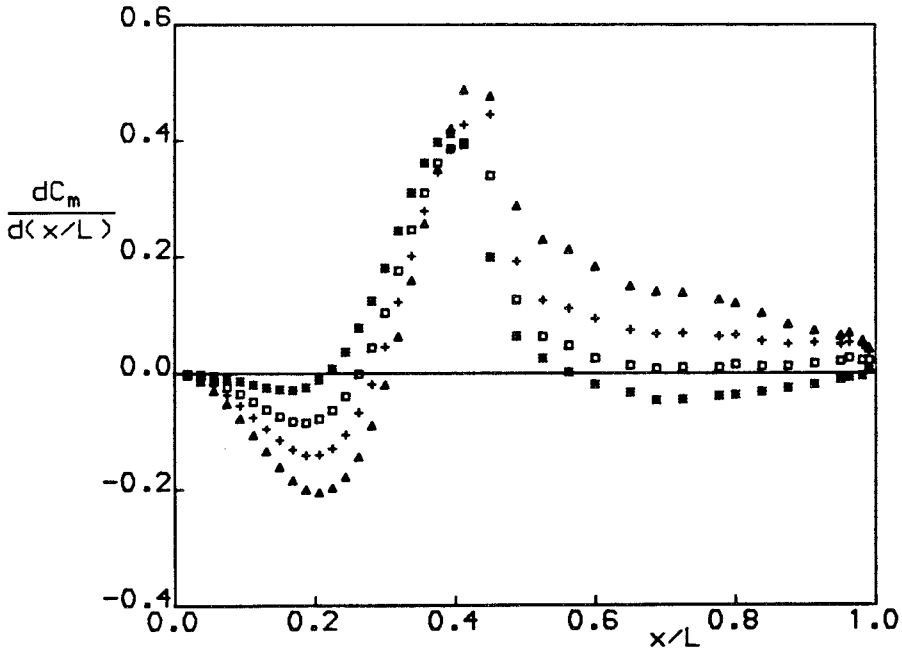

Port body

b) Pitching-moment loadings

Figure 4 continued

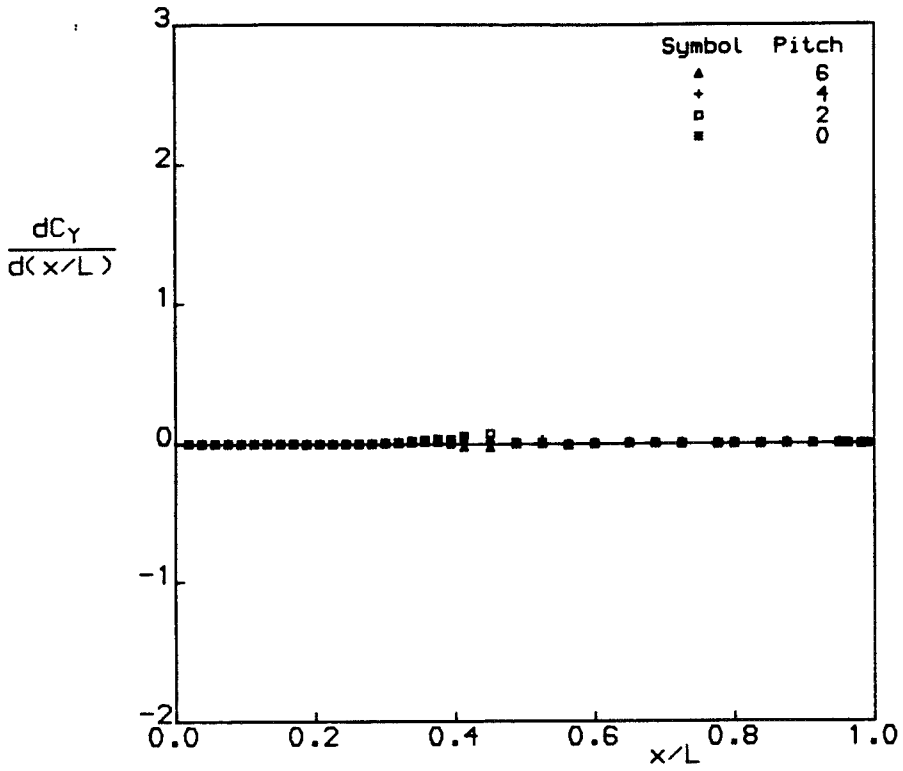

Central body

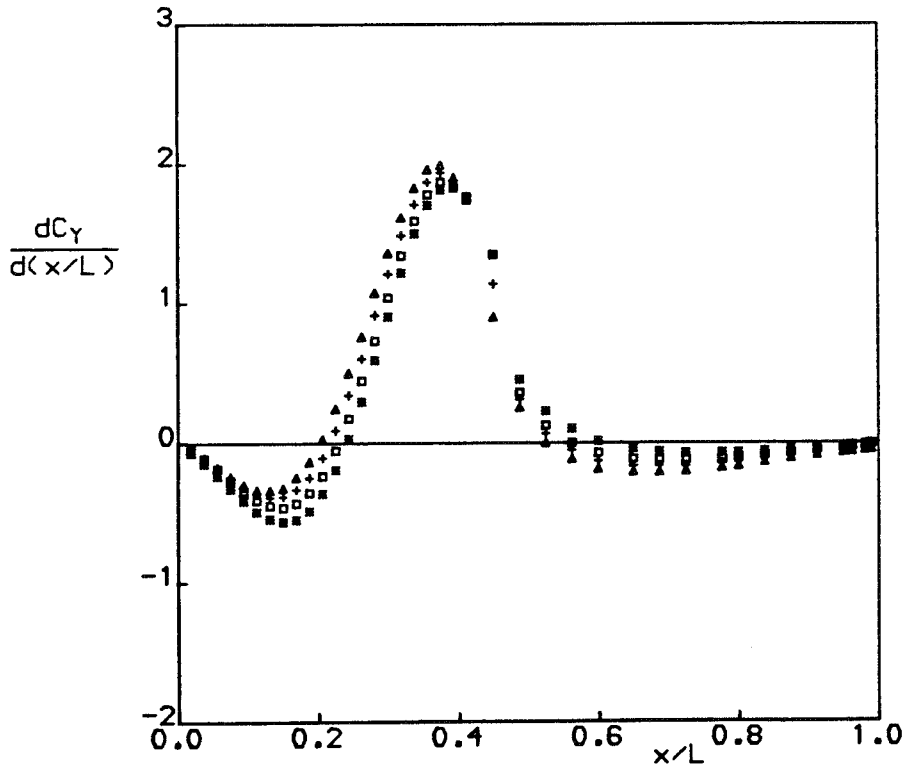

Port body

c) Side-Force loadings

Figure 4 continued

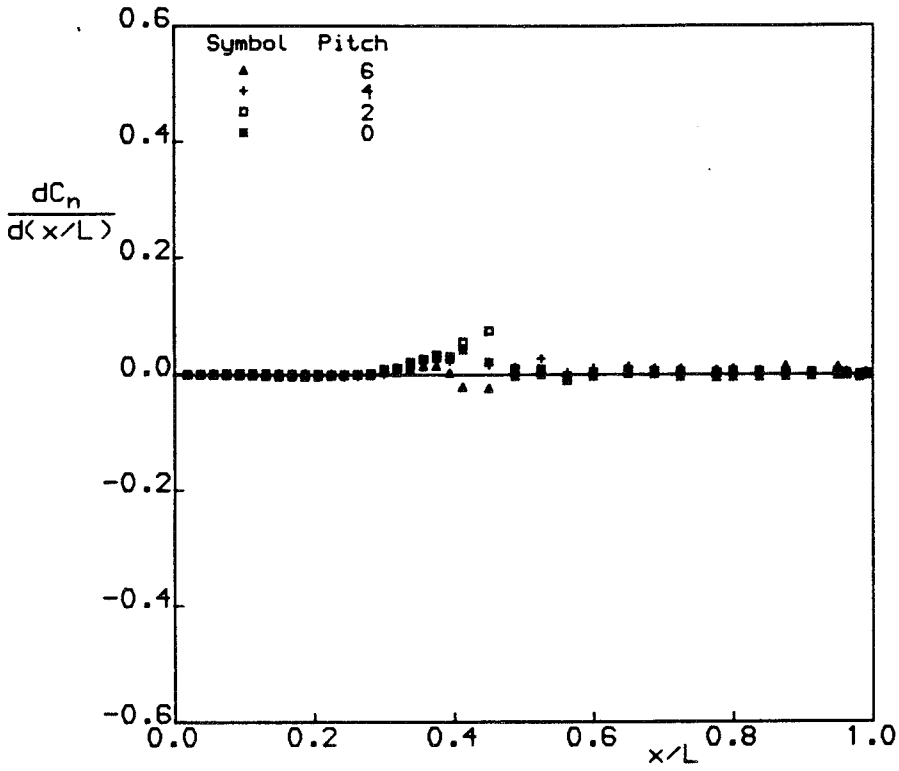

Central body

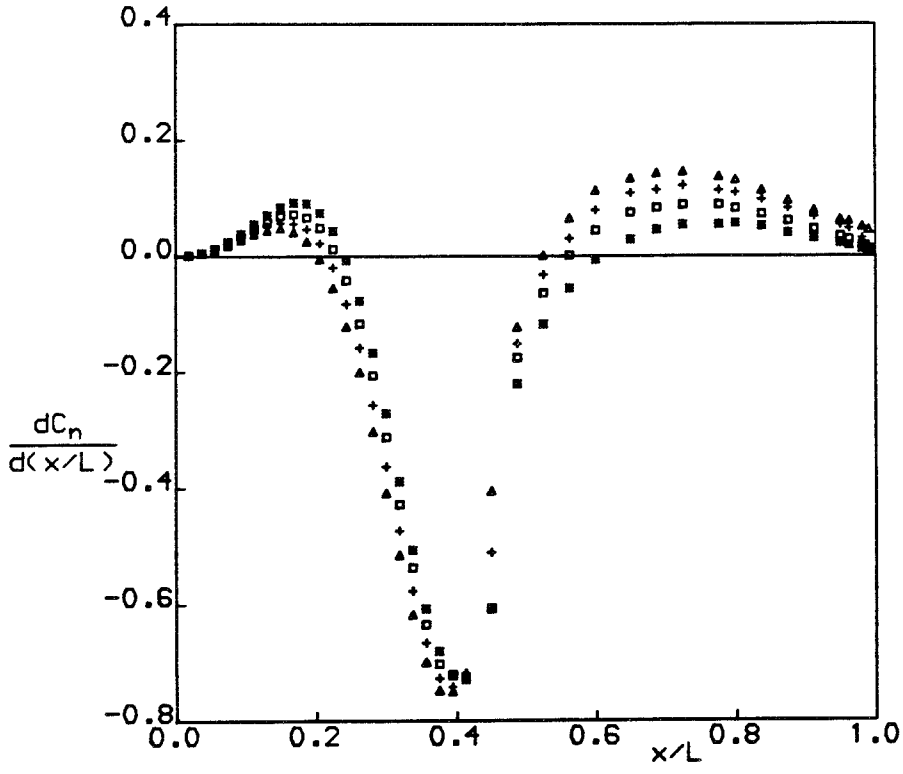

Port body

d) Yawing-moment loadings

Figure 4 continued

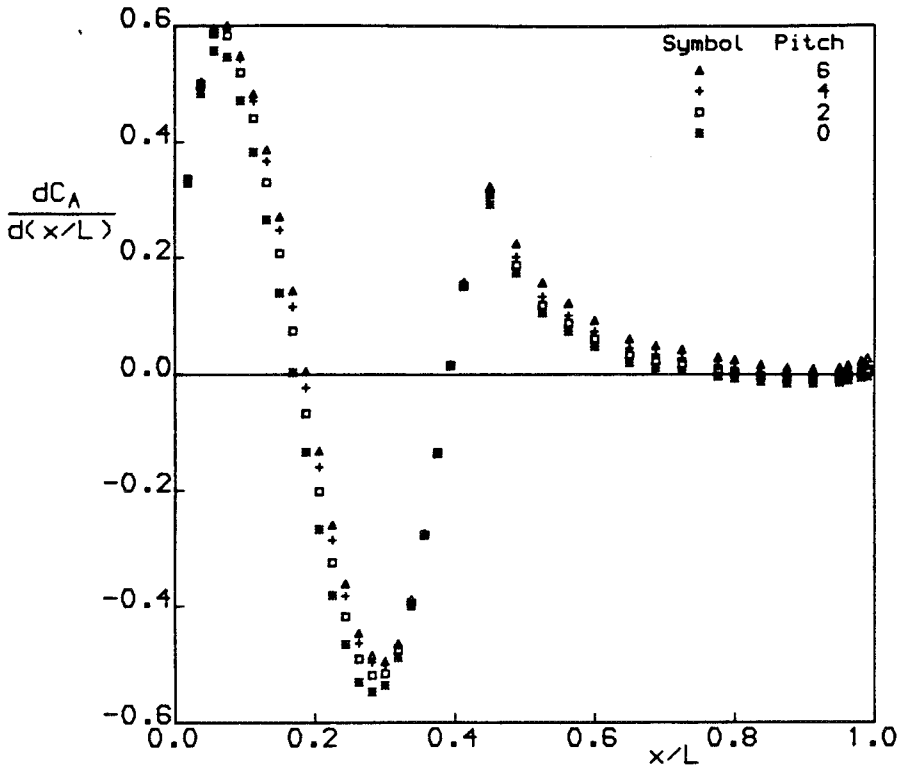

Central body

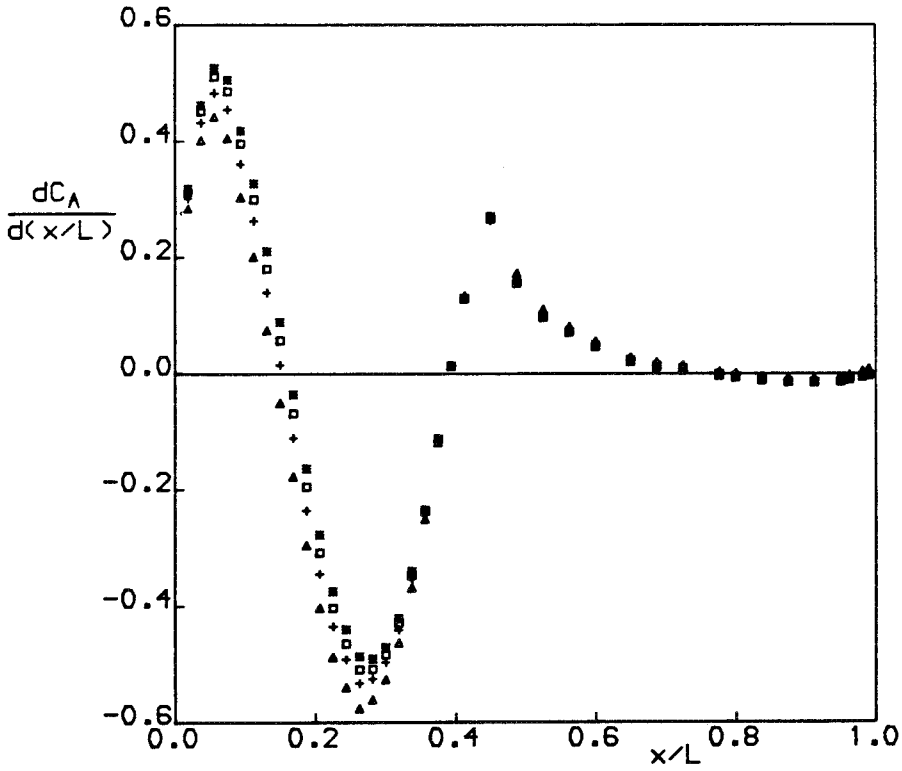

Port body

e) Axial-force loadings

Figure 4 concluded

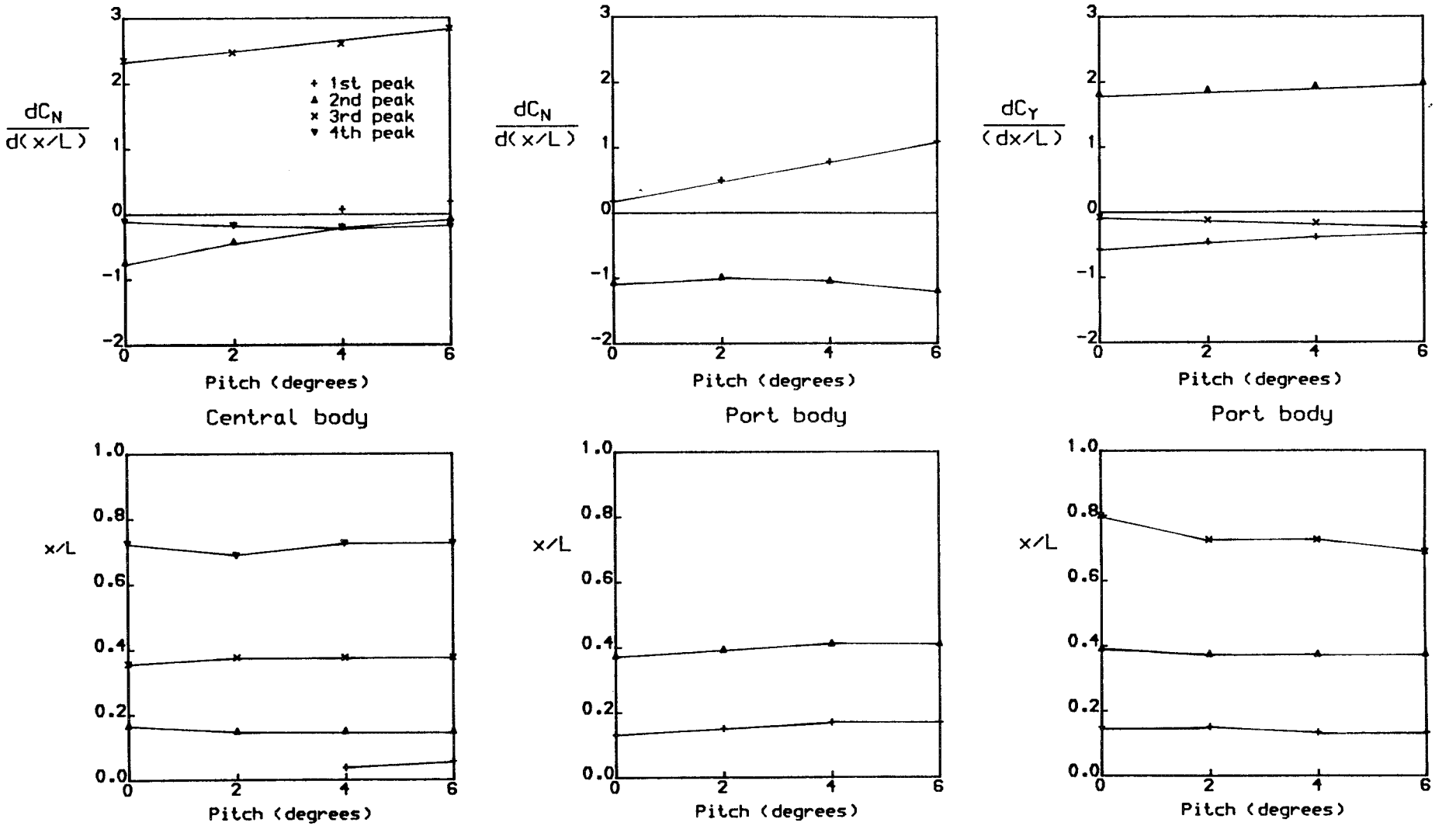

Figure 5. Variation of the magnitude and position of the loading peaks with pitch

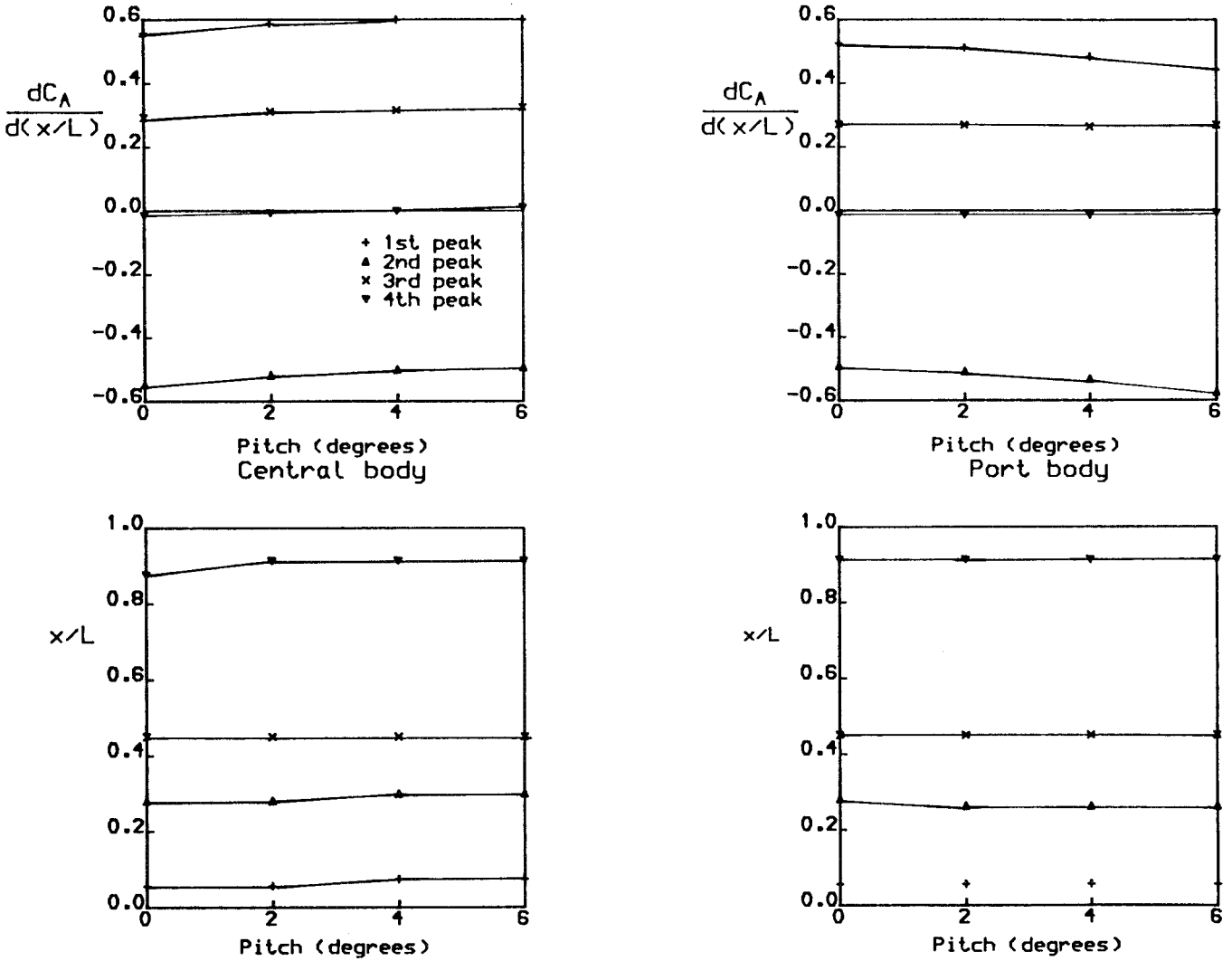

c) Axial-Force loading

Figure 5 concluded

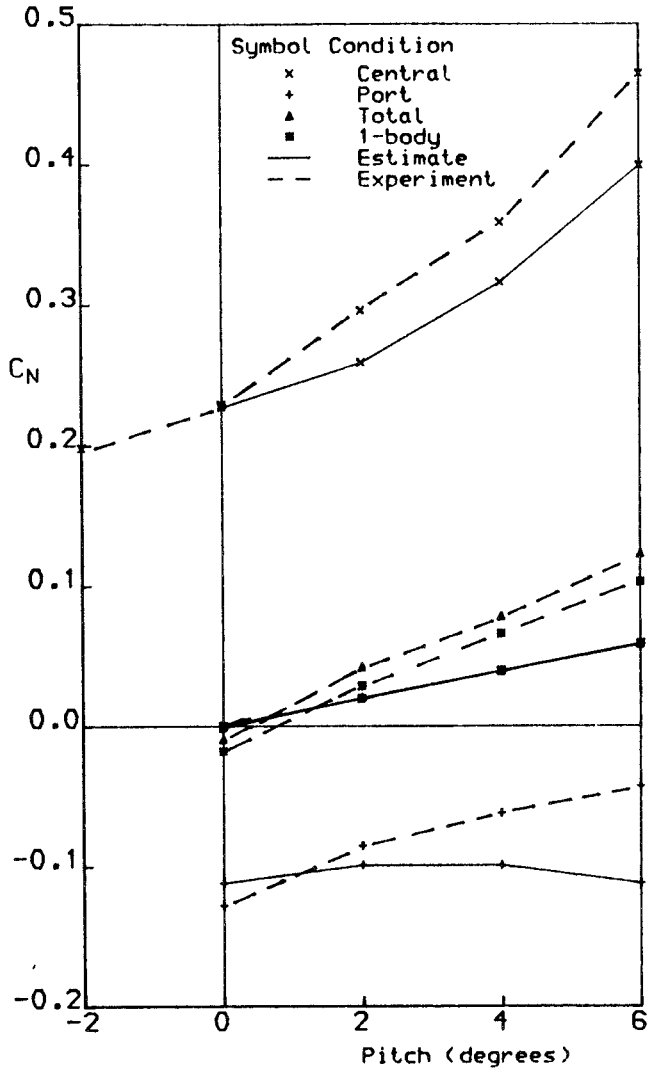

a) C_N

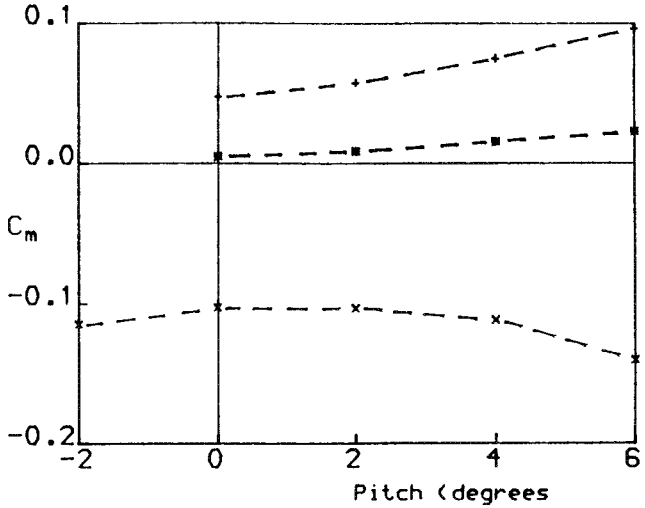

b) C_m

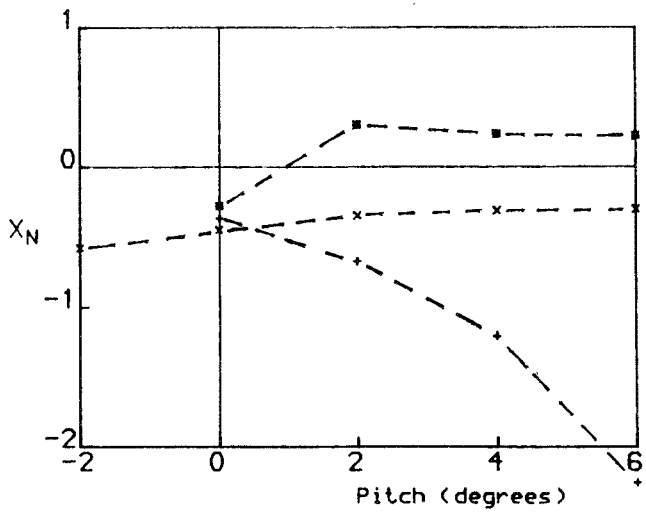

c) X_N

Figure 6. Variation of aerodynamic characteristics with pitch

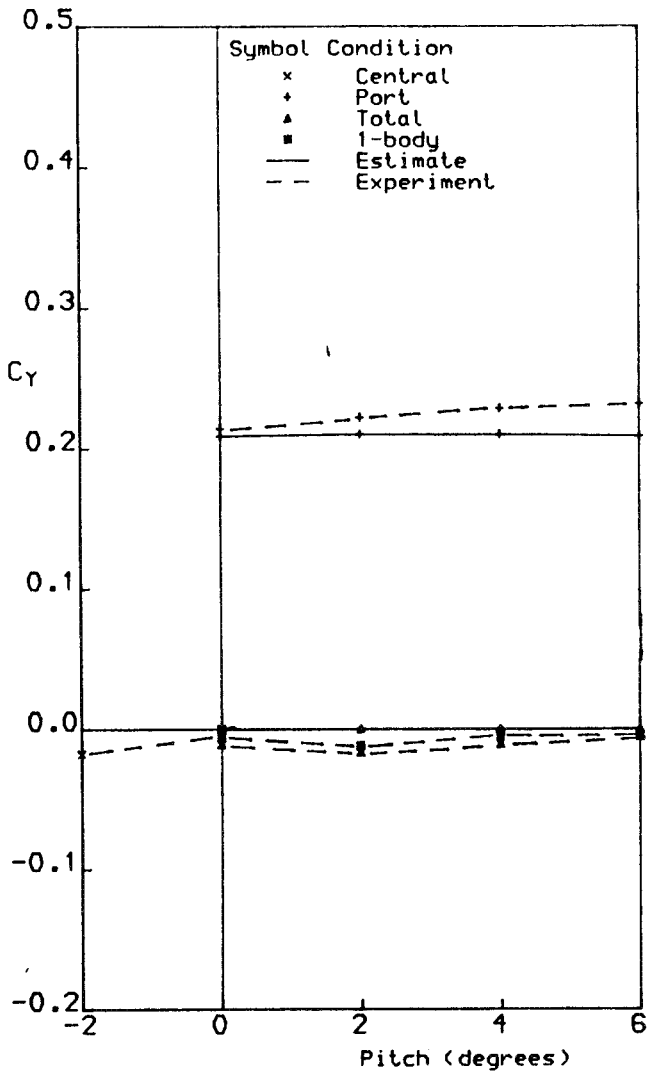

d) C_Y

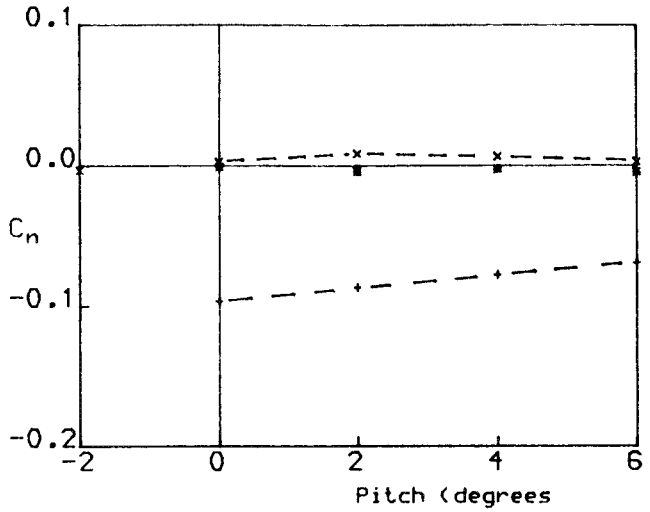

e) C_n

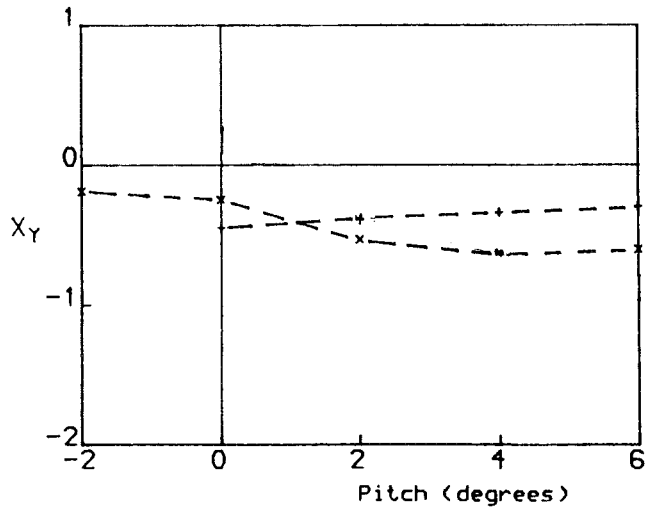

F) X_Y

Figure 6 continued

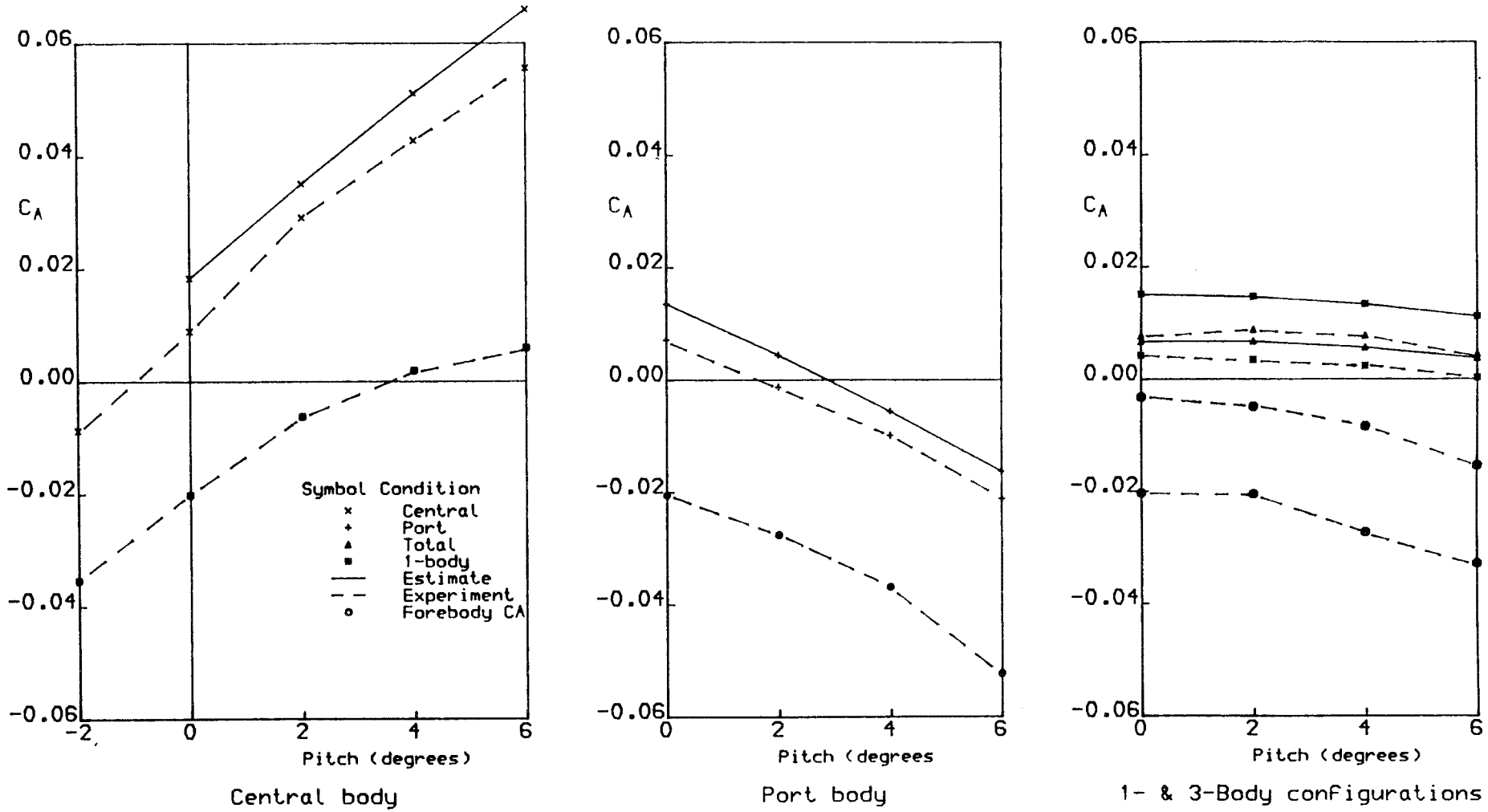

g) C_A

Figure 6 concluded

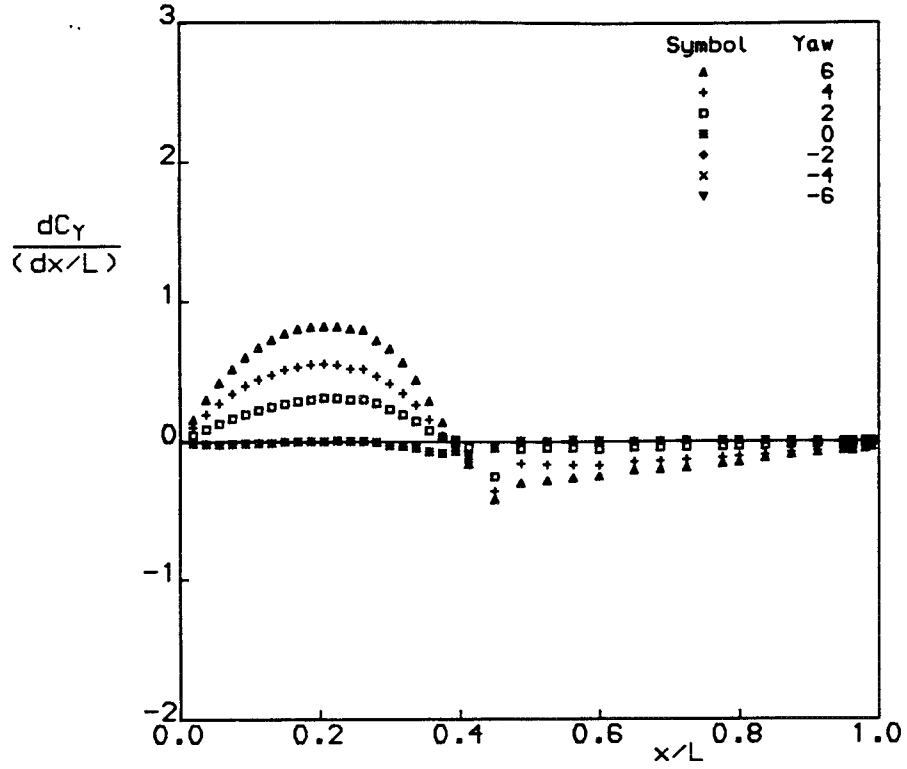

Central body

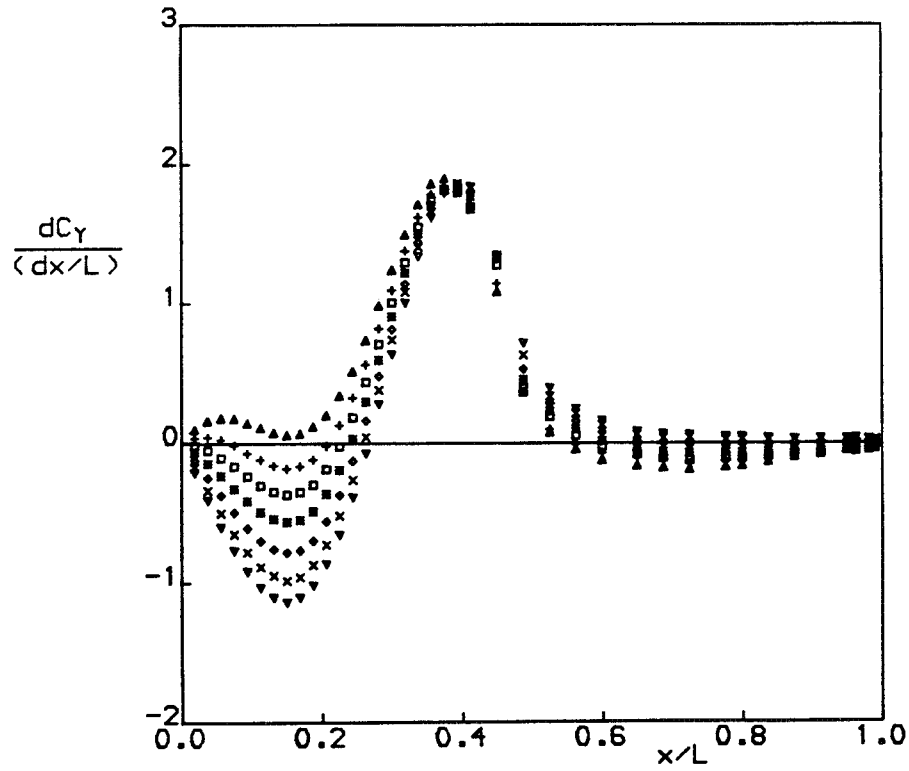

Port body

a) Side-force loadings

Figure 7. Variation of experimental loadings with yaw

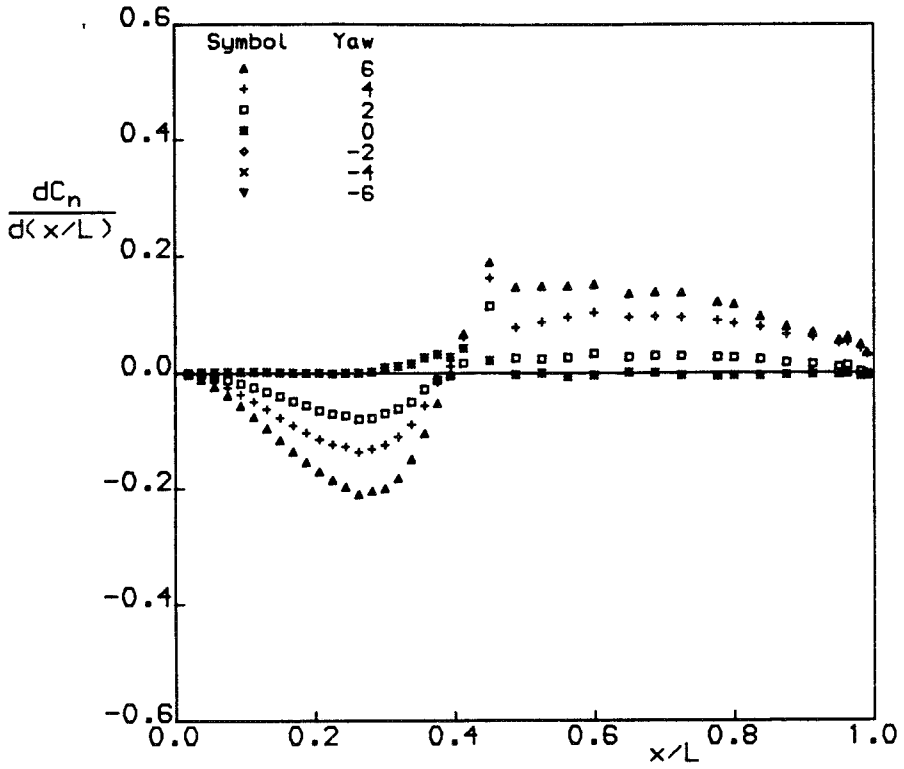

Central body

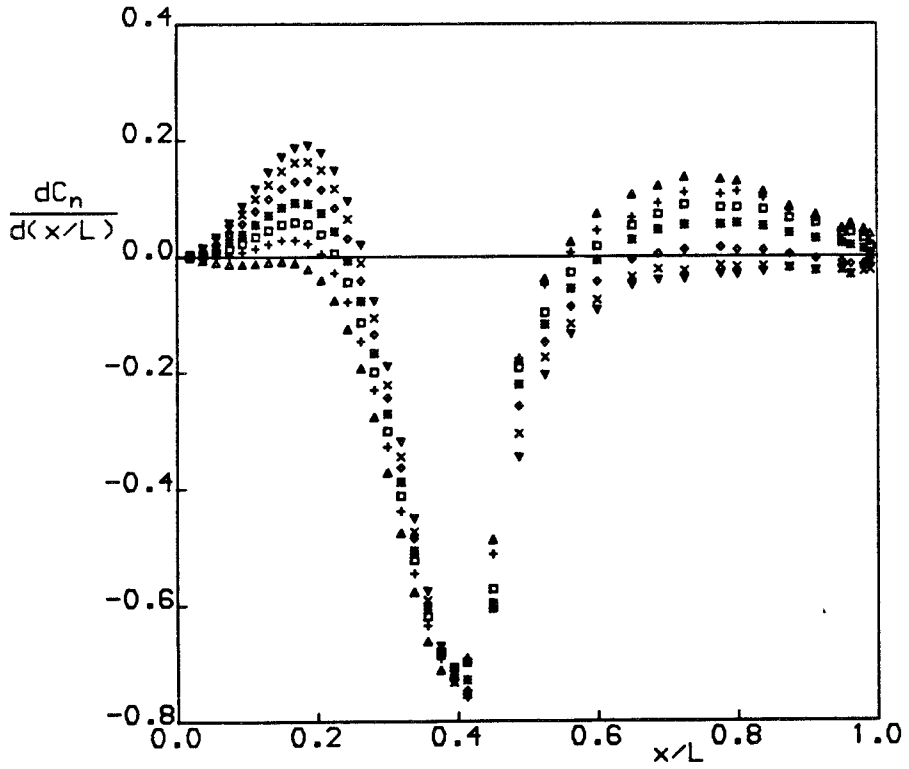

Port body

b) Yawing-moment loadings

Figure 7 continued

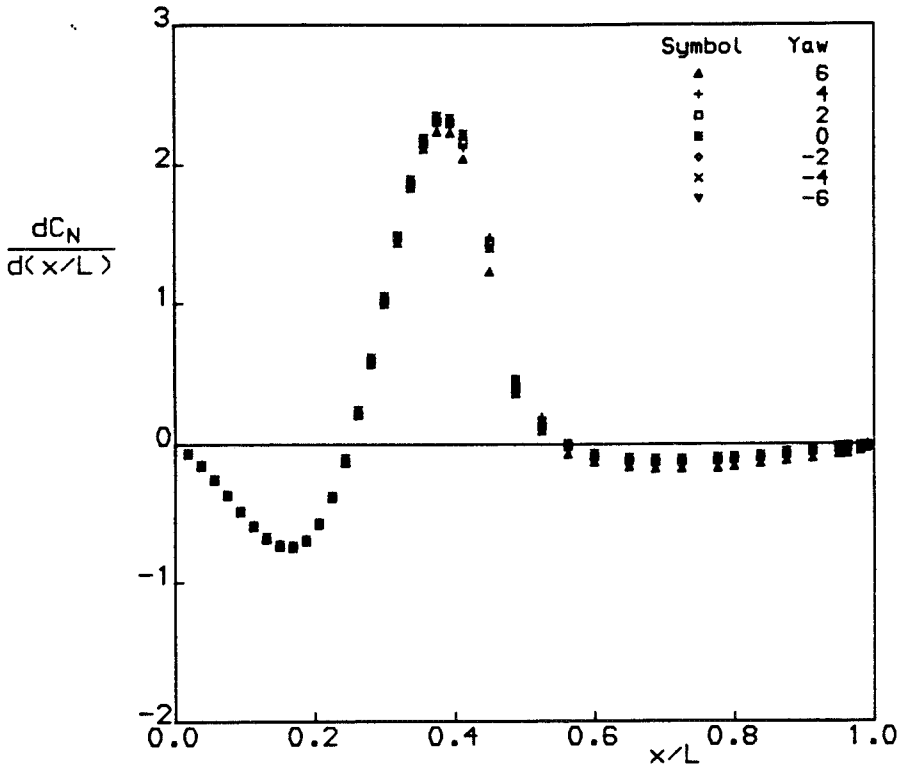

Central body

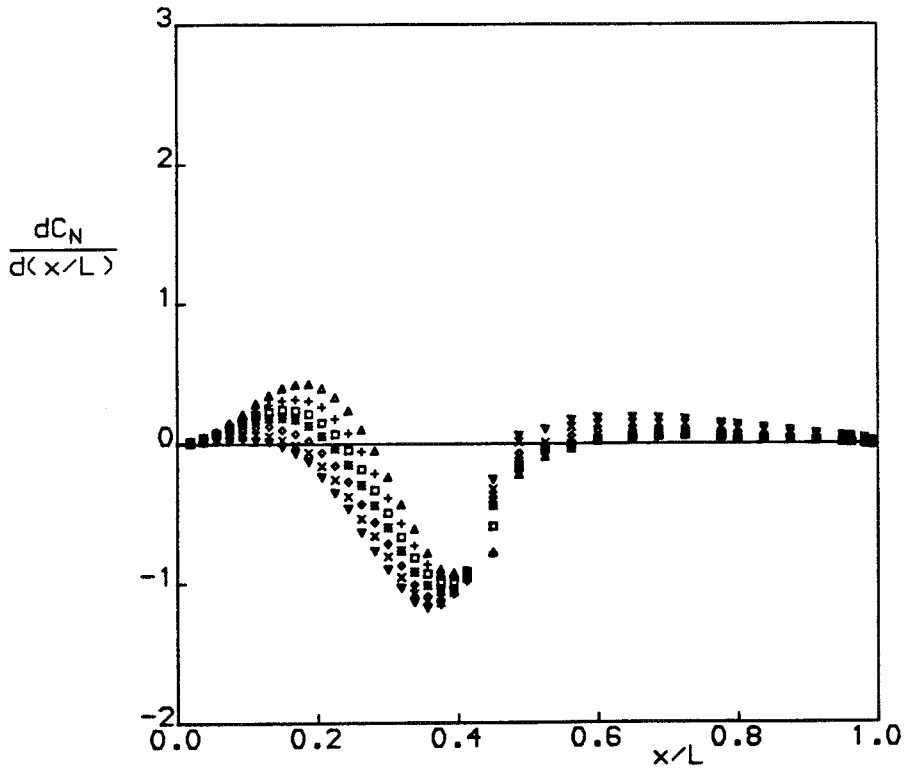

Port body

c) Normal-Force loadings

Figure 7 continued

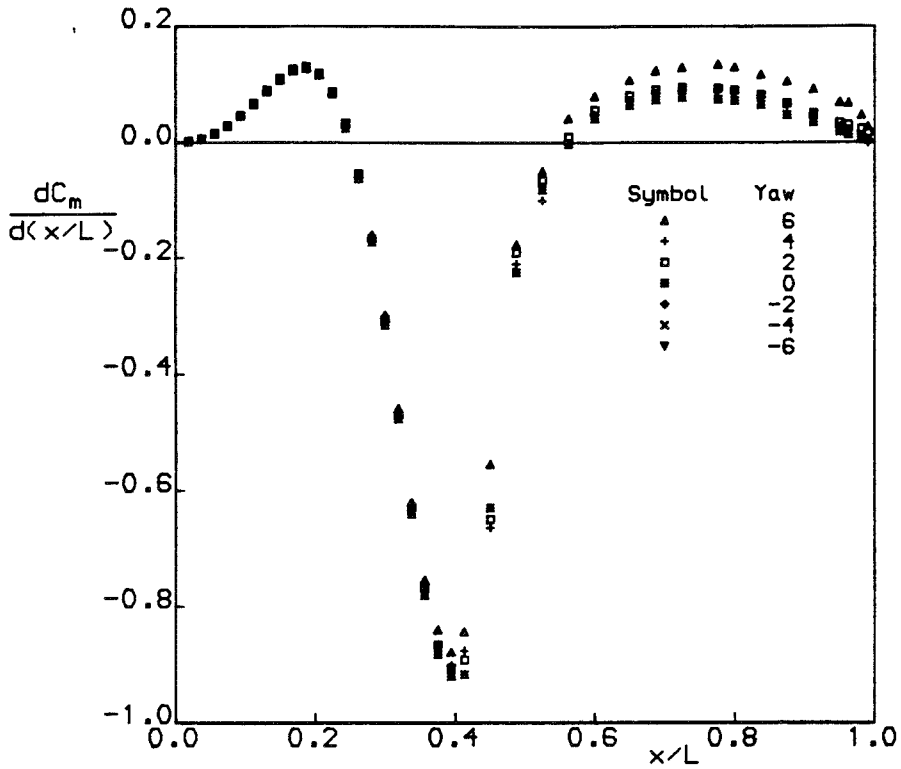

Central body

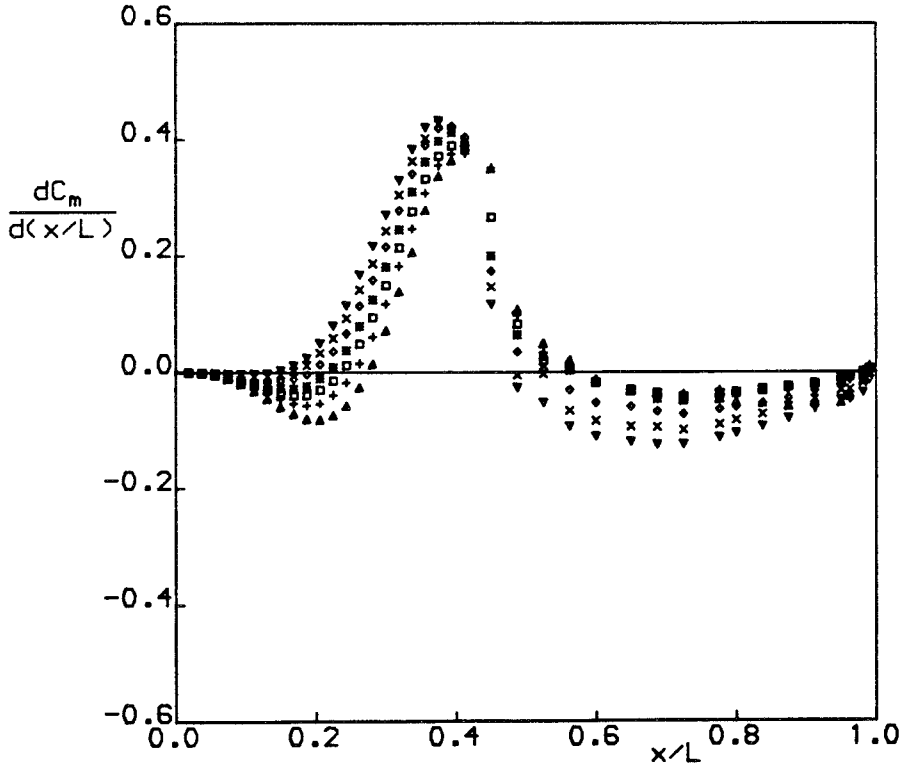

Port body

d) Pitching-moment loadings

Figure 7 continued

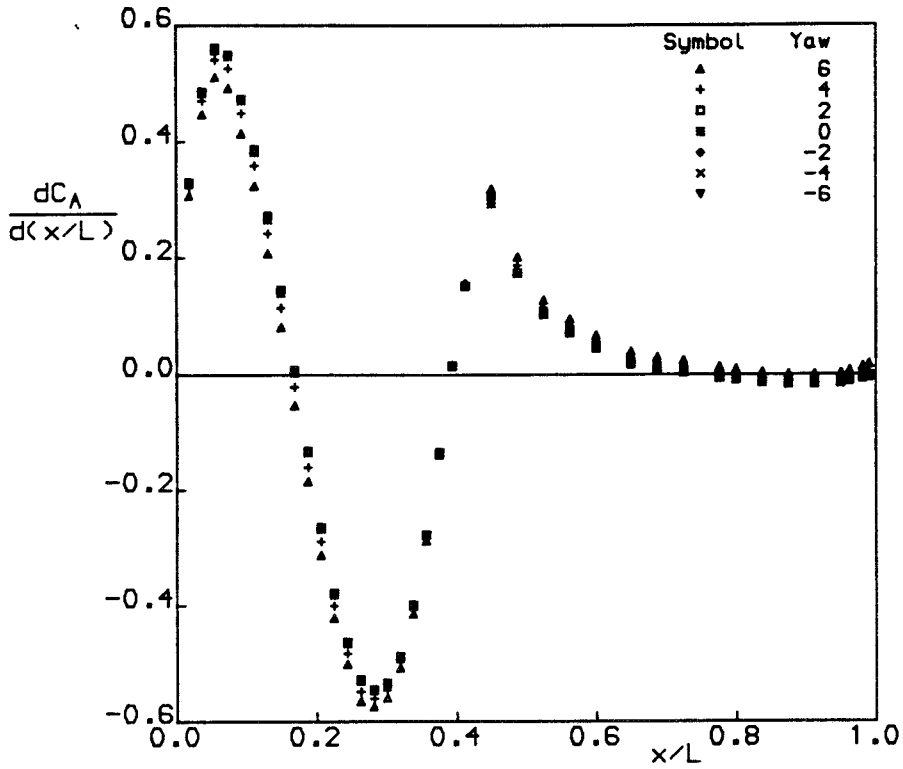

Central body

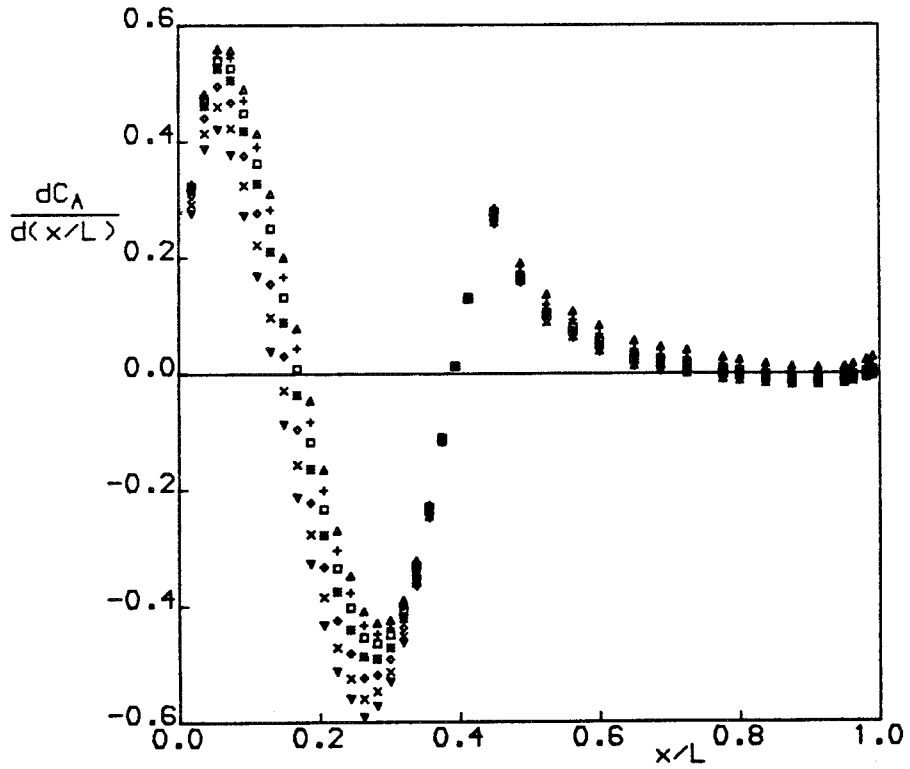

Port body

e) Axial-Force loadings

Figure 7 concluded

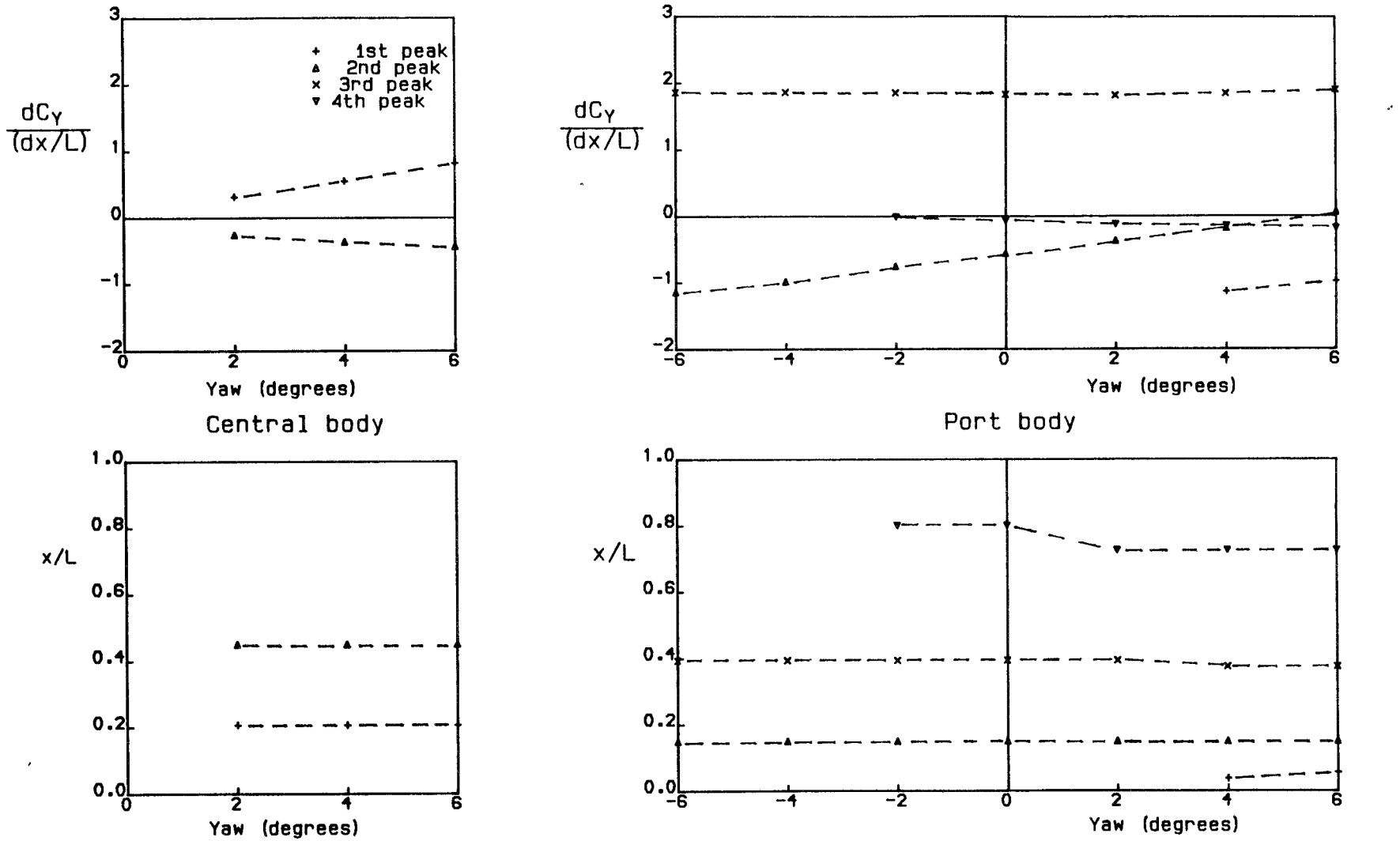

Figure 8.Variation of the magnitude and position of the loading peaks with yaw

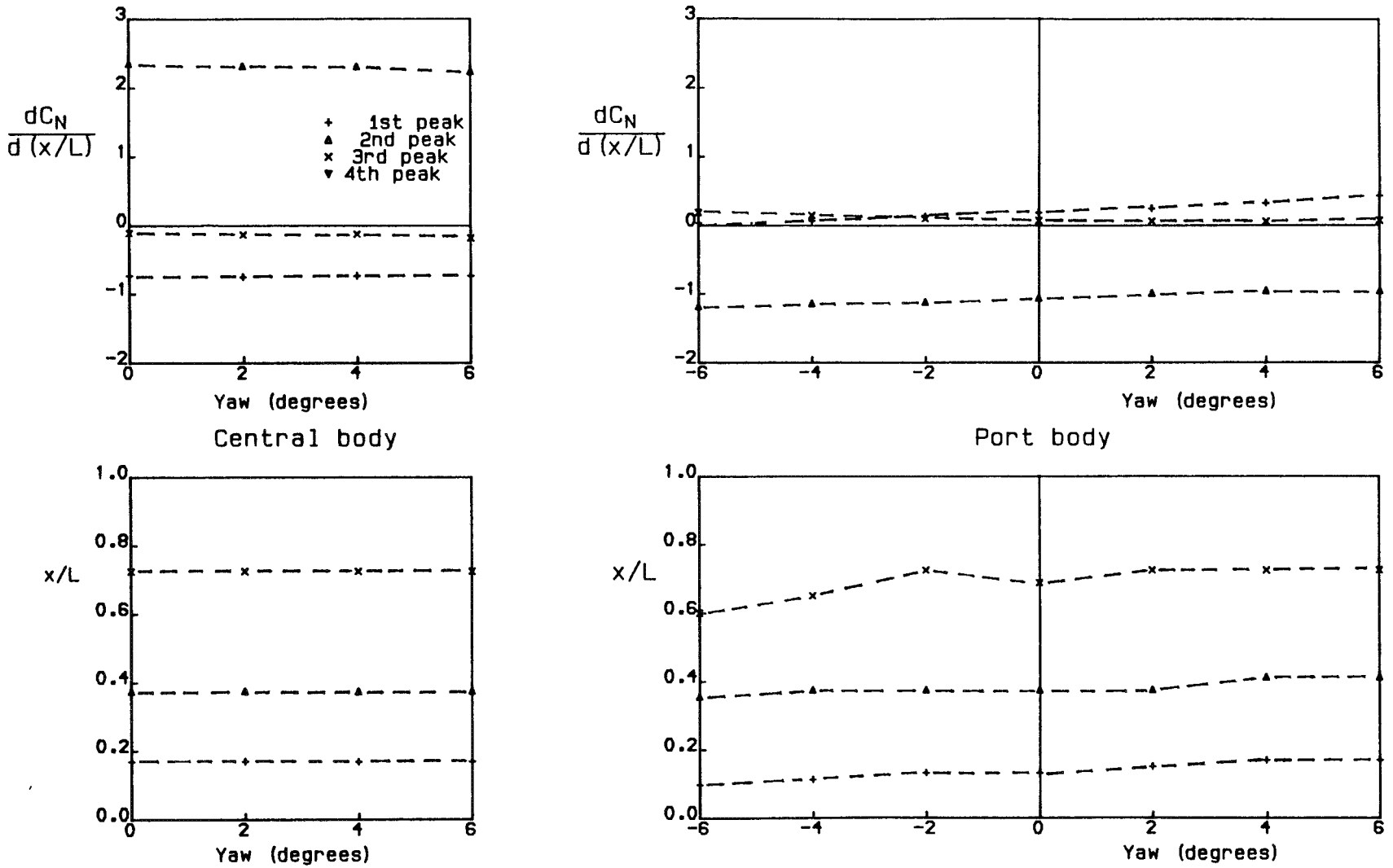

b) Normal-force loadings

Figure 8 continued

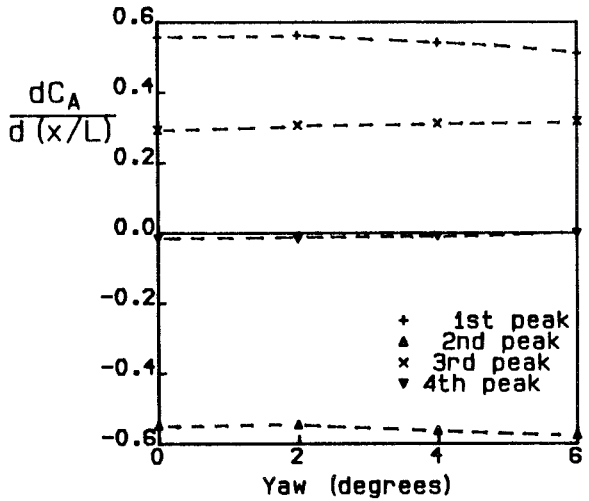

Central body

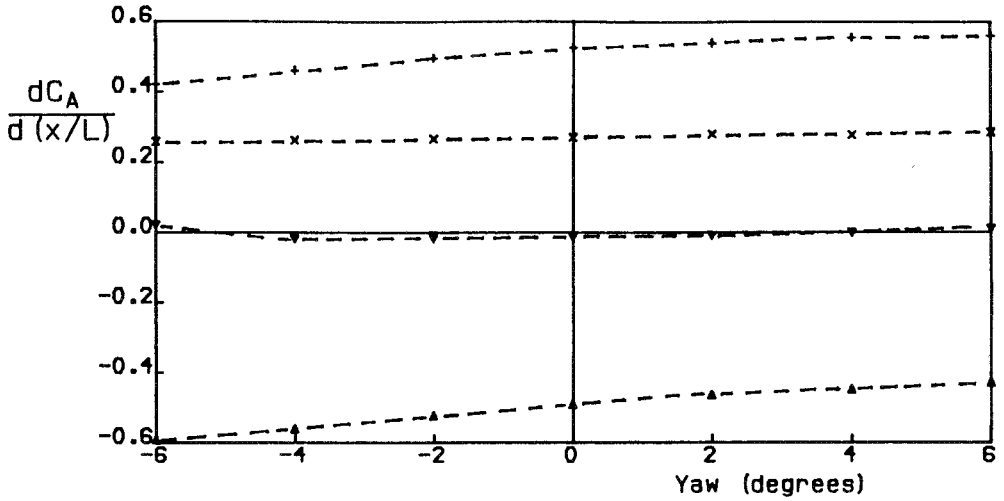

Port body

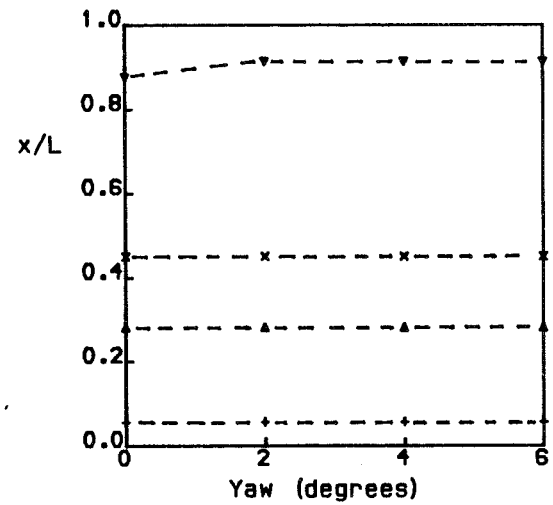

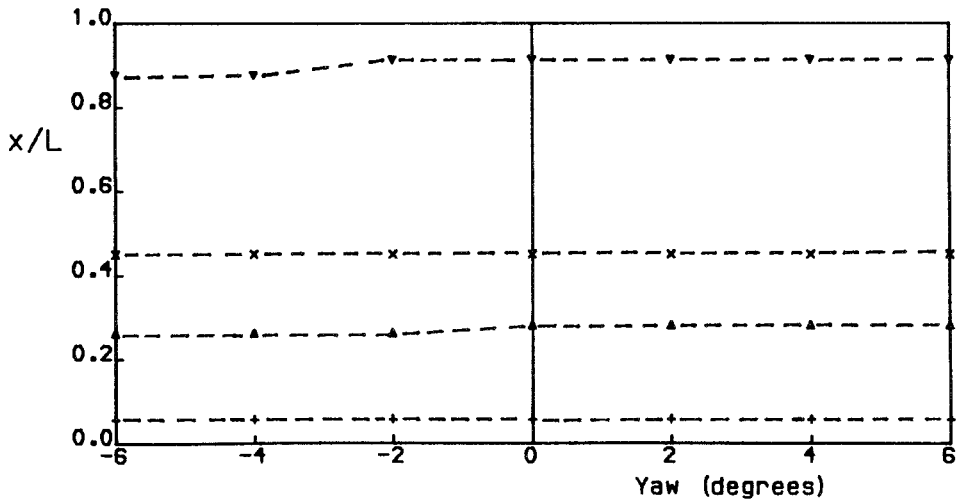

c) Axial-force loadings

Figure 8 concluded

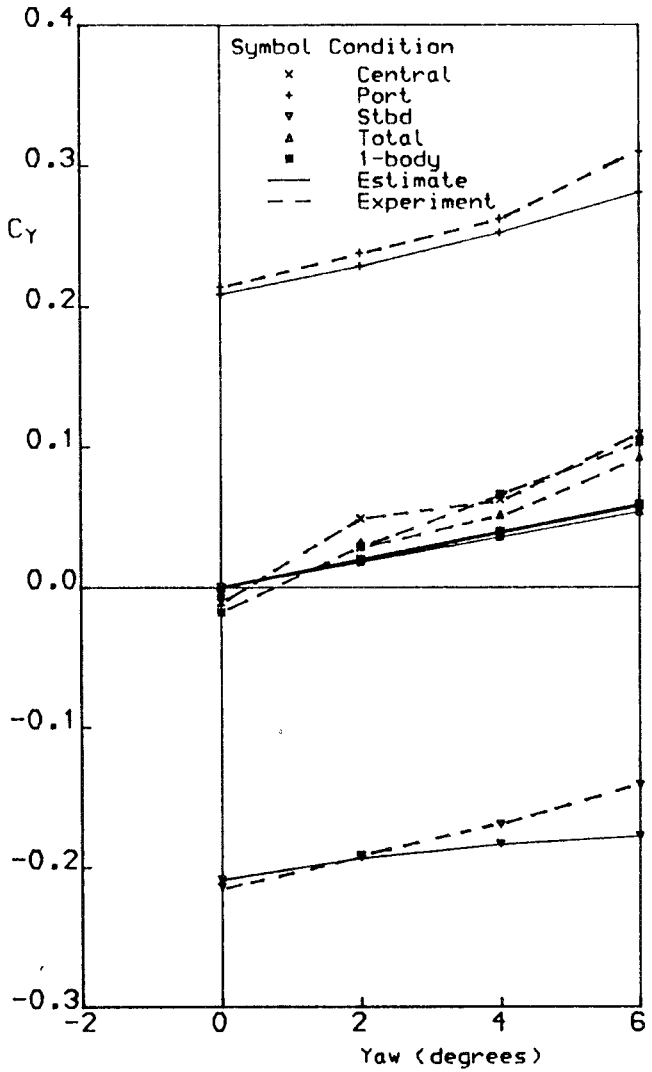

a) C_Y

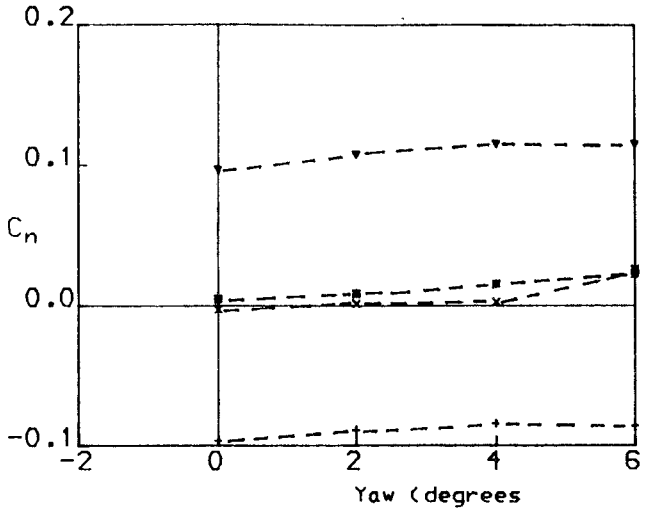

b) C_n

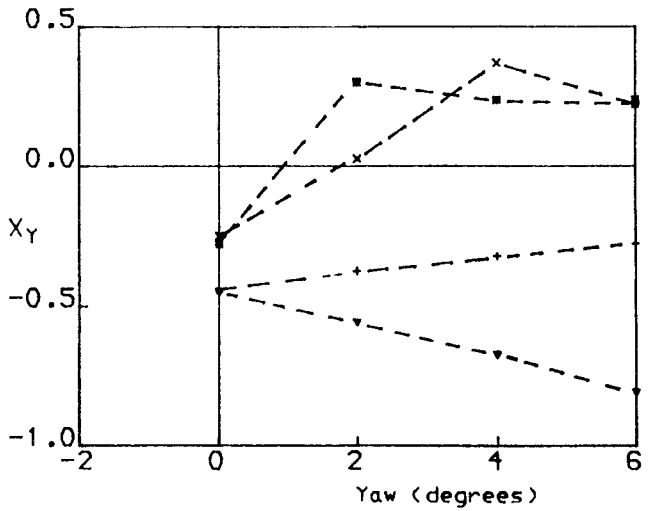

c) X_Y

Figure 9. Variation of aerodynamic characteristics with yaw

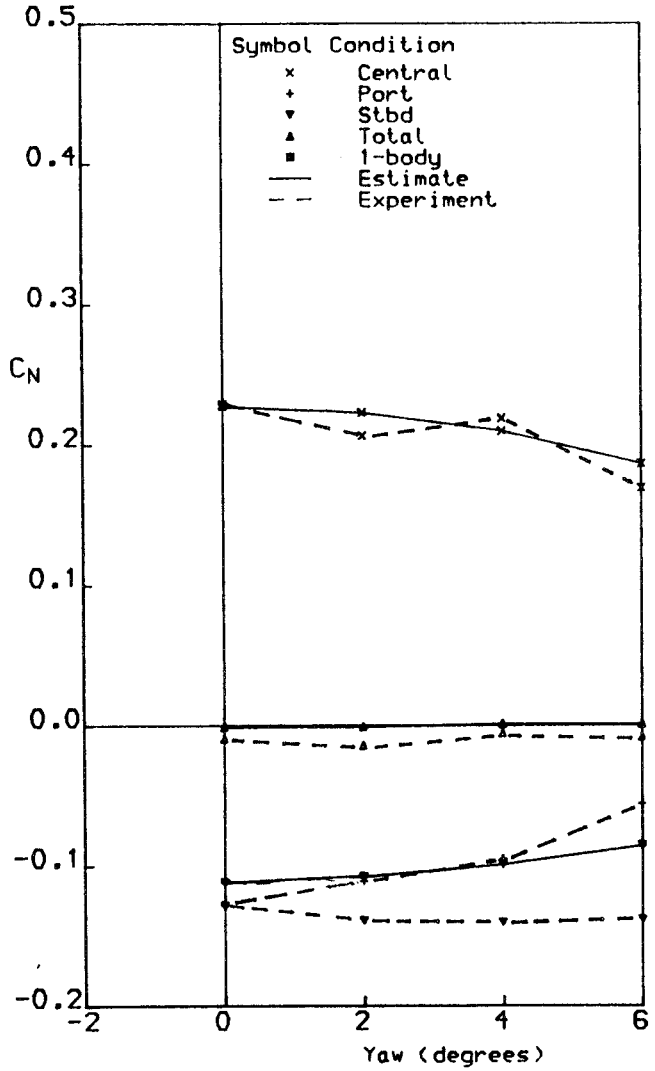

d) C_N

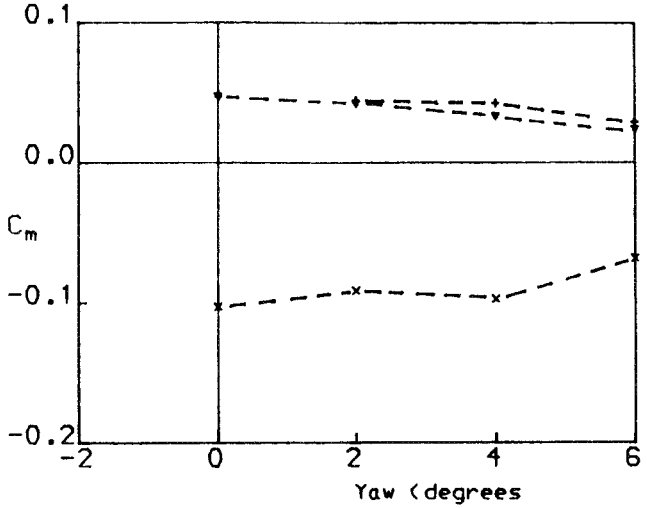

e) C_m

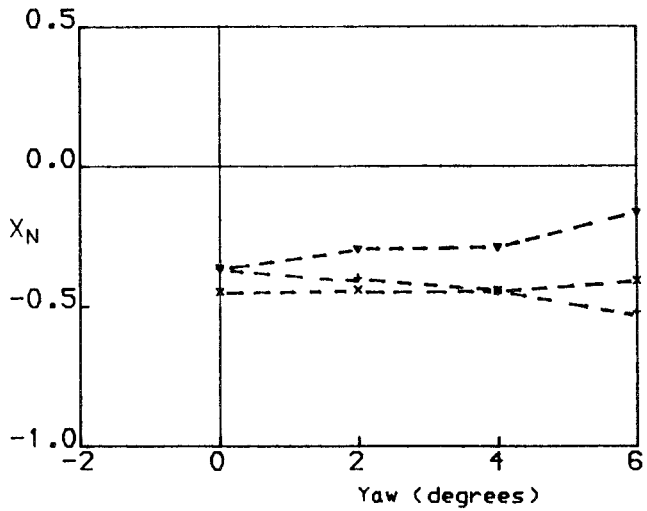

F) X_N

Figure 9 continued

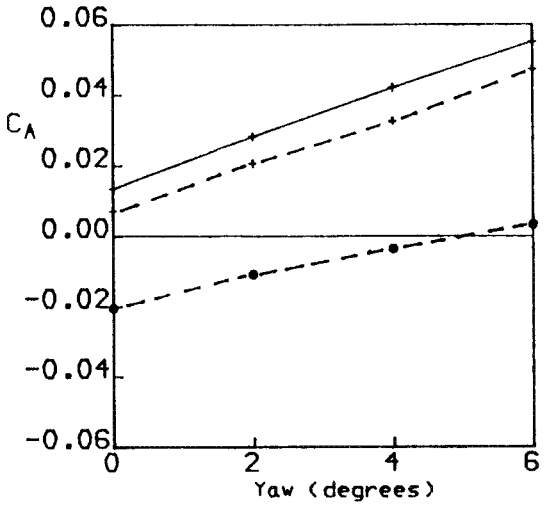

Port body

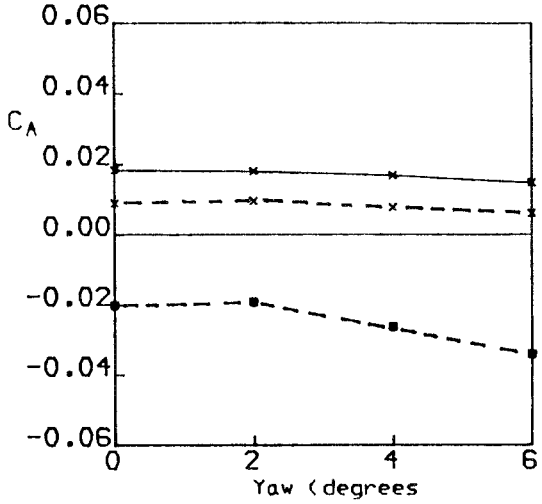

Central body

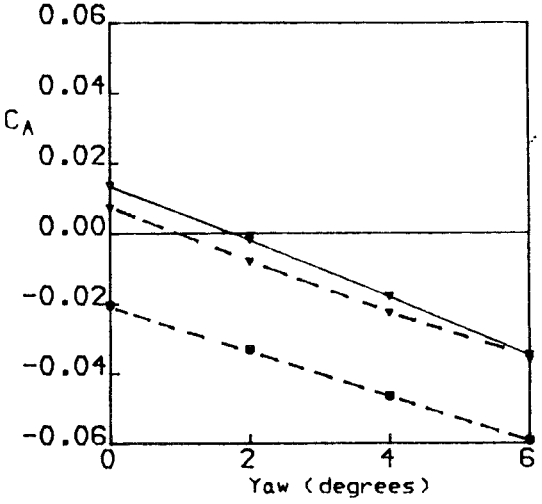

Starboard body

Symbol	Condition
×	Central
+	Port
▼	Stbd
▲	Total
■	1-body
——	Estimate
– –	Experiment
o	Forebody CA

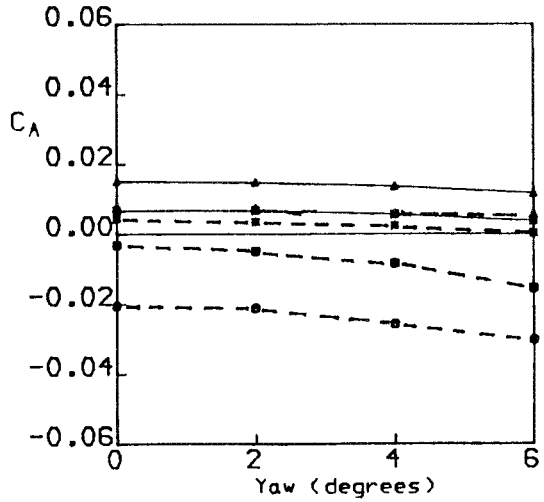

1- & 3-body configurations

g) C_A

Figure 9 concluded

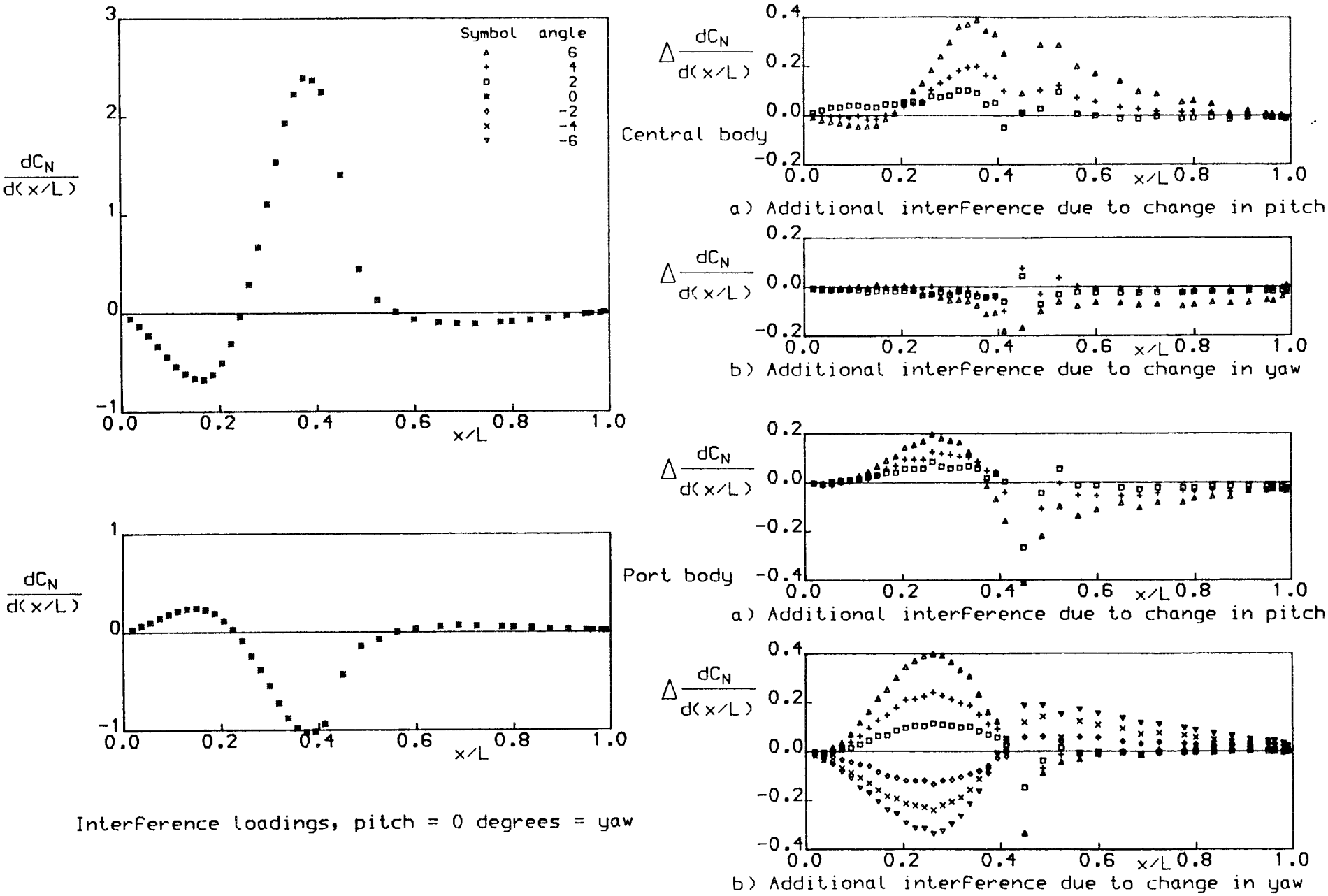

Figure 10. Variation of normal-force interference loadings with pitch and yaw

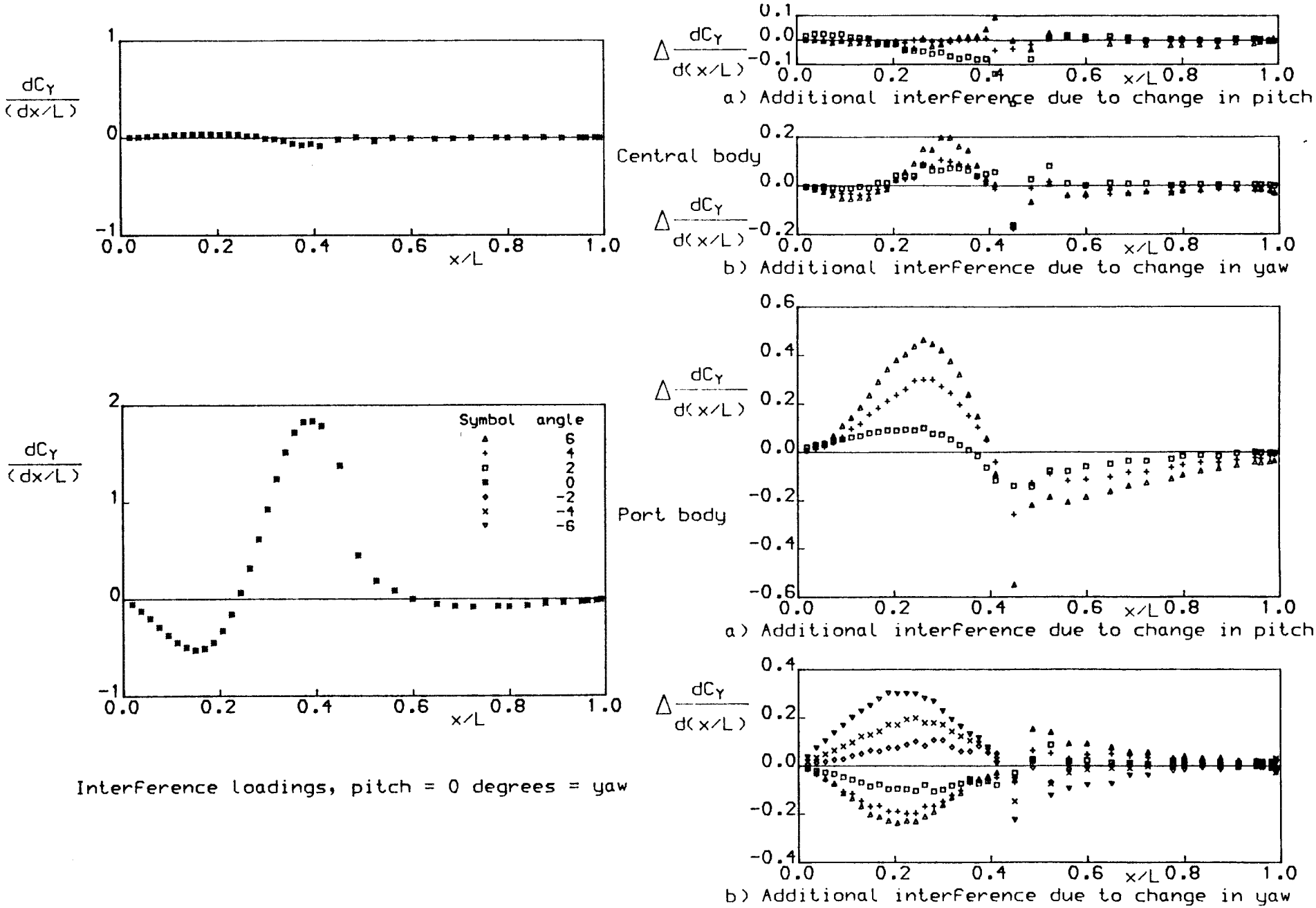

Figure 11. Variation of side-force interference loadings with pitch and yaw

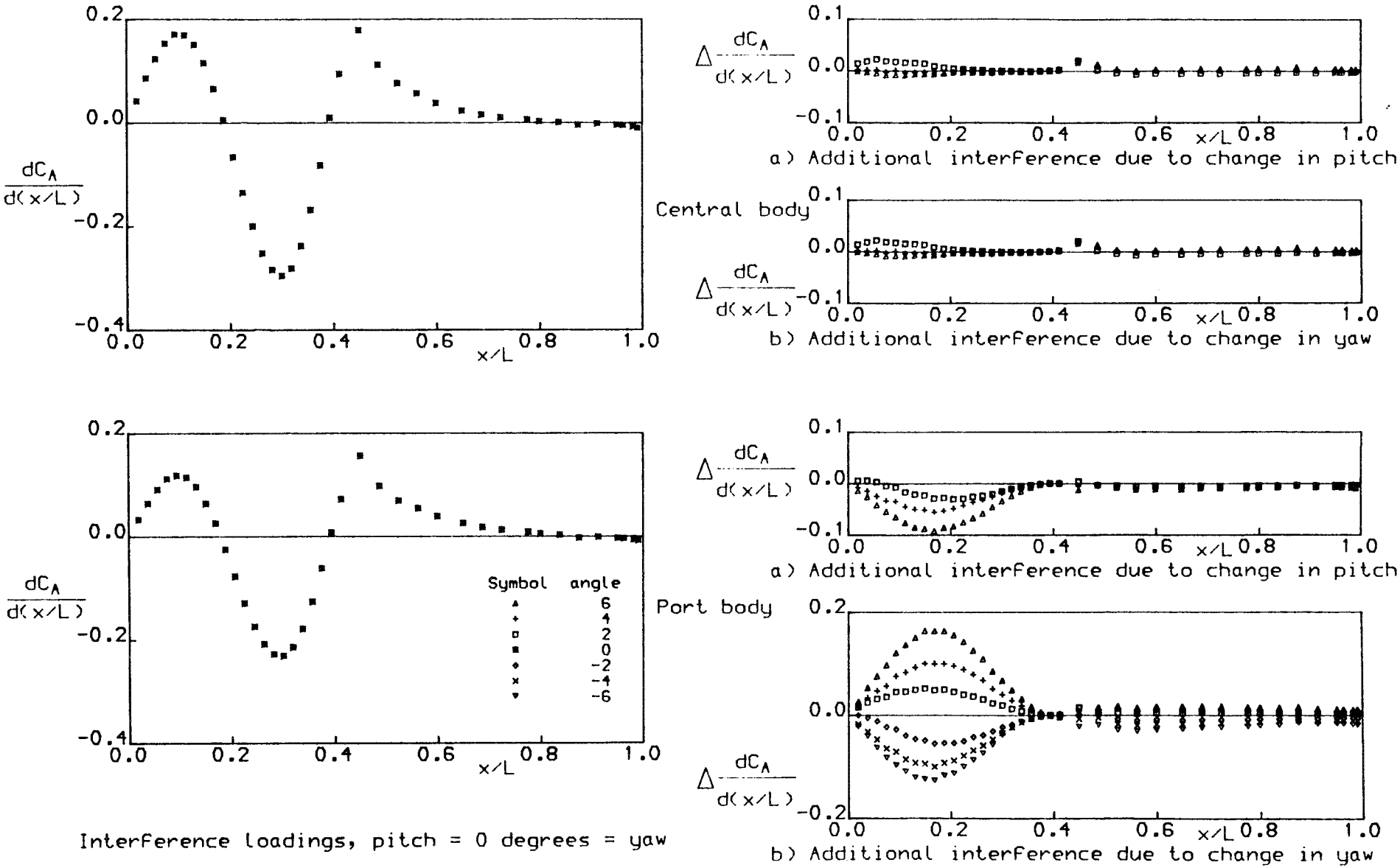

Figure 12. Variation of axial-force interference loadings with pitch and yaw

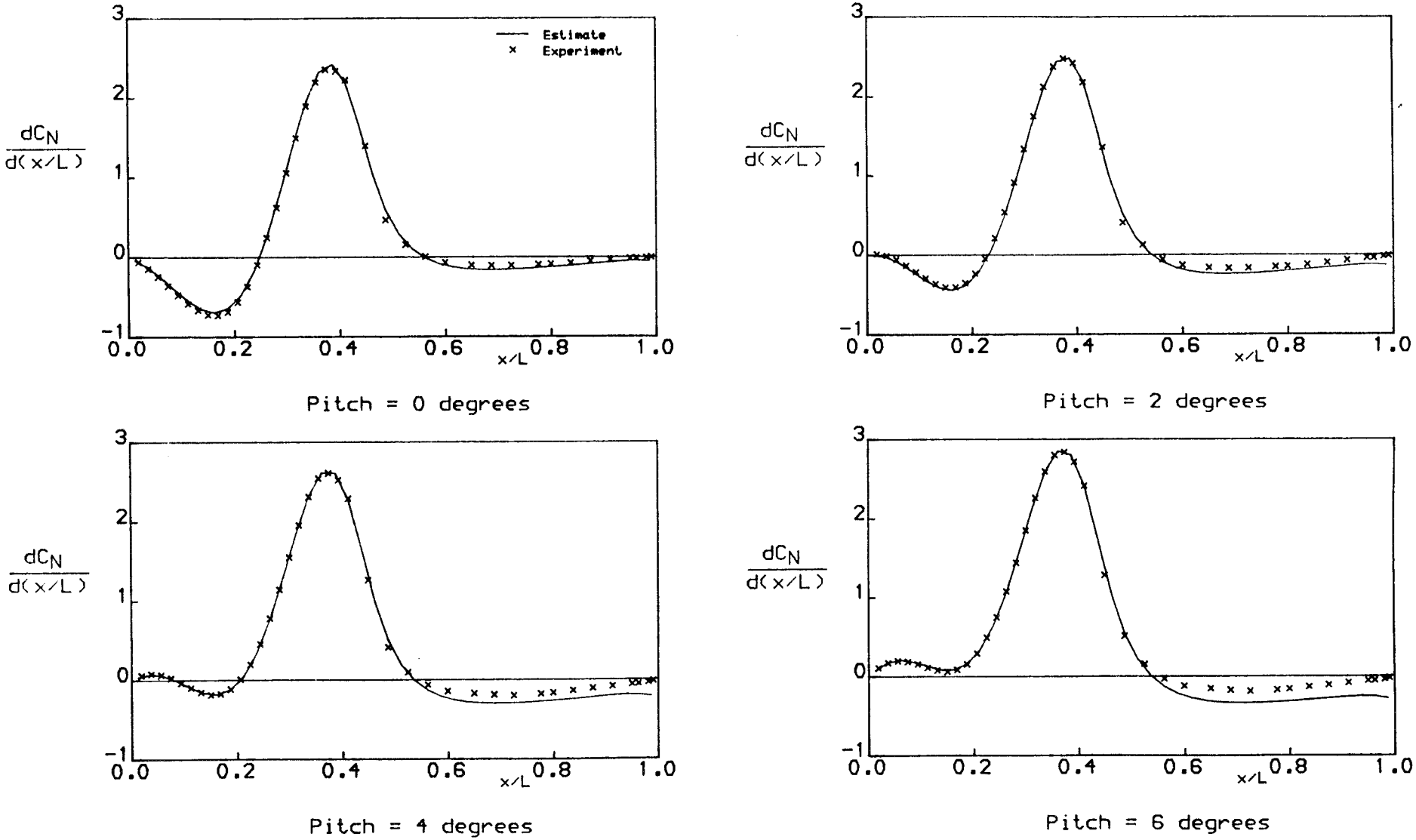

a) Normal-force loading distributions on central body

Figure 13. Comparison of estimated and experimental loading distributions as pitch varies

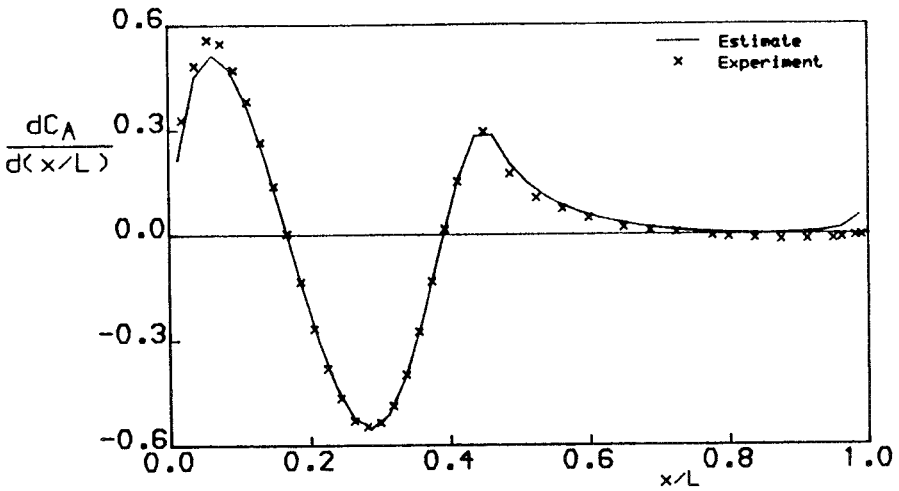

Pitch = 0 degrees

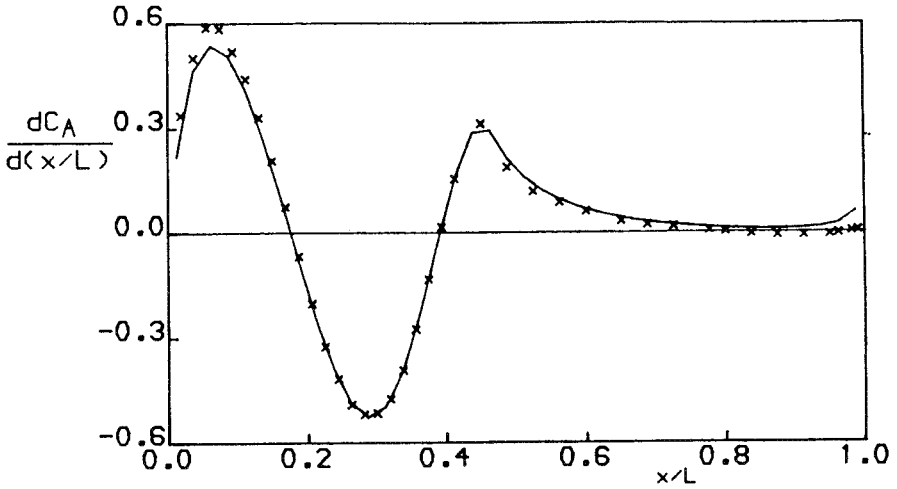

Pitch = 2 degrees

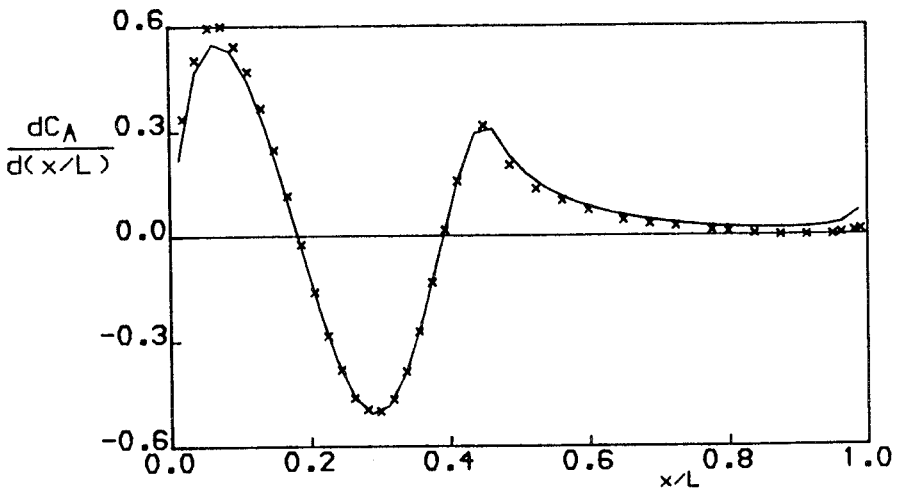

Pitch = 4 degrees

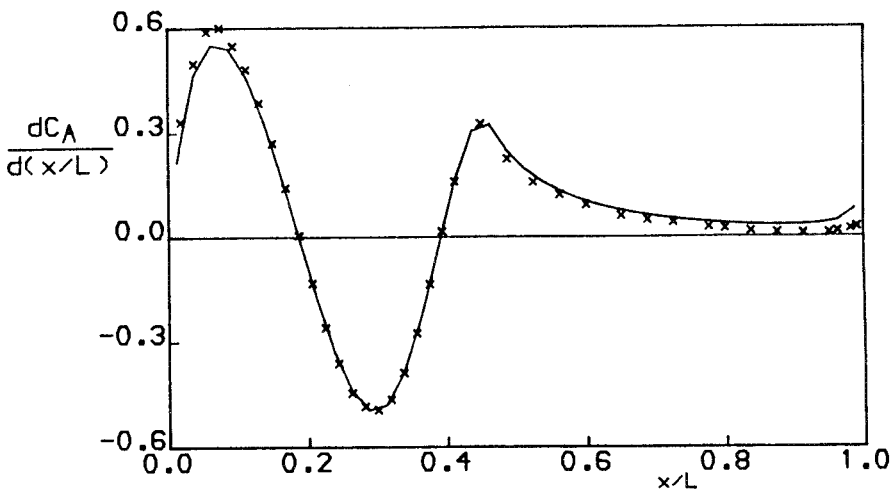

Pitch = 6 degrees

b) Axial-Force loading distributions on central body

Figure 13 continued

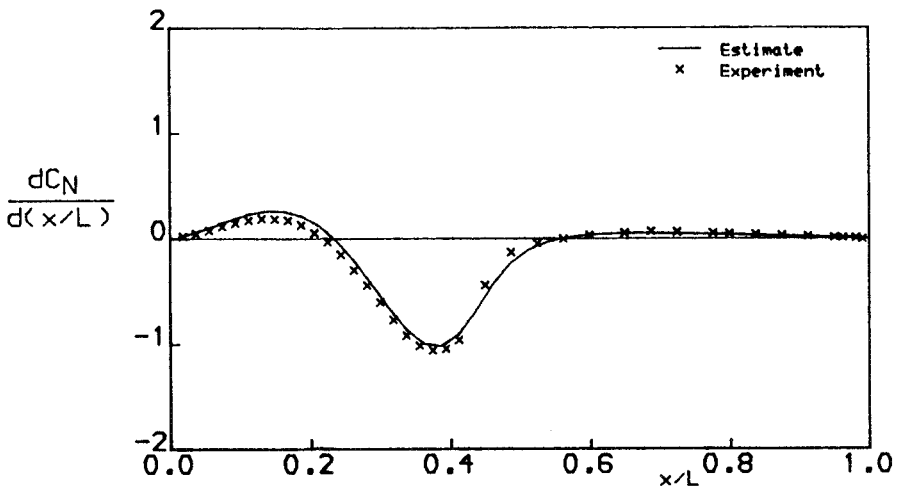

Pitch = 0 degrees

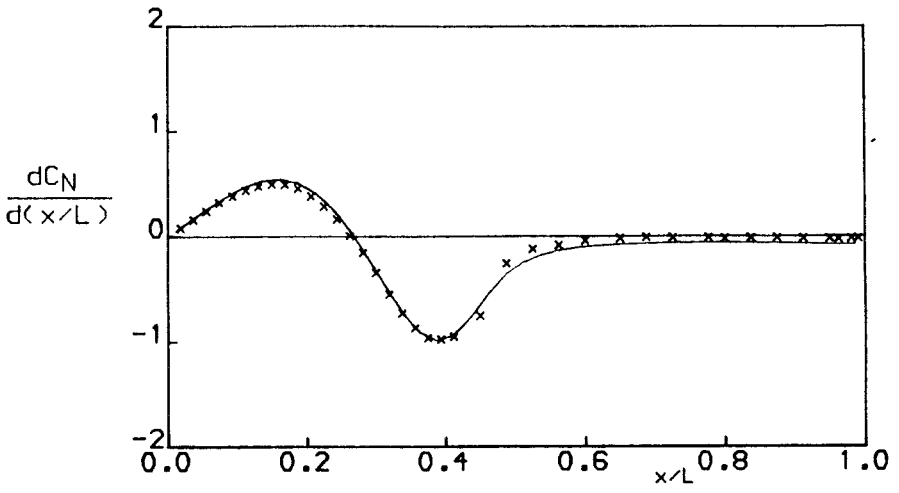

Pitch = 2 degrees

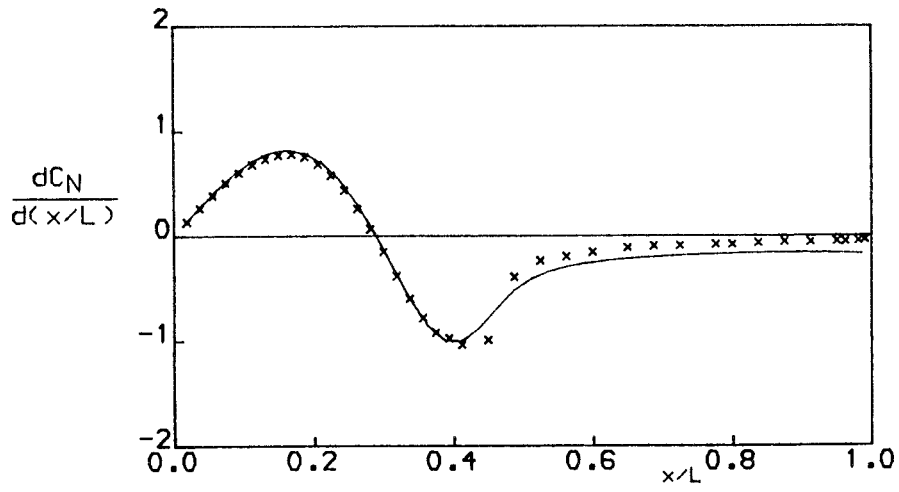

Pitch = 4 degrees

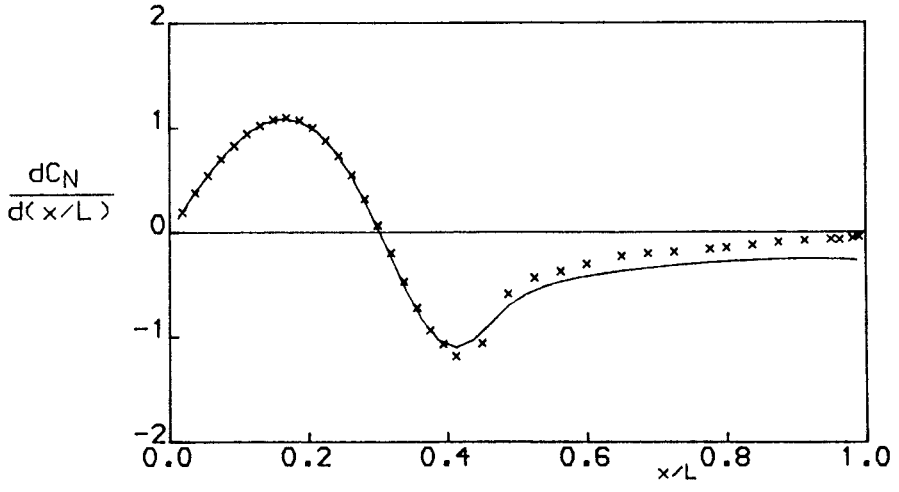

Pitch = 6 degrees

c) Normal-Force loading distributions on port body

Figure 13 continued

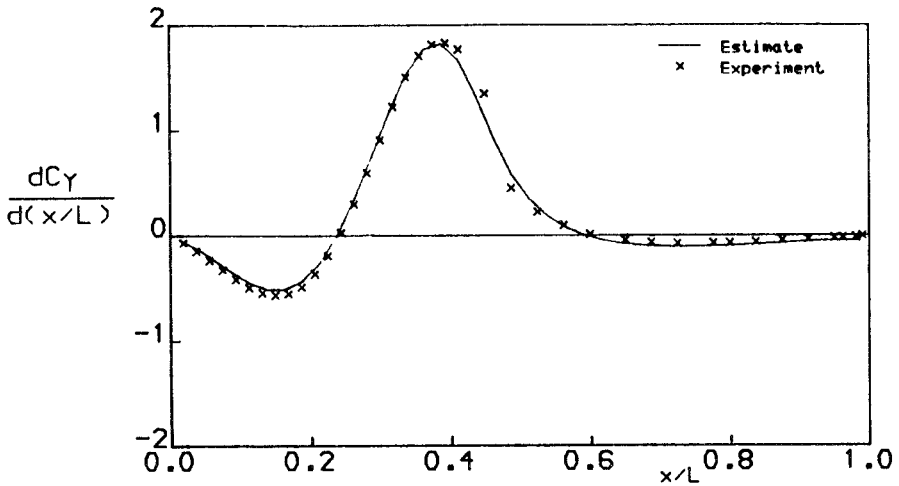

Pitch = 0 degrees

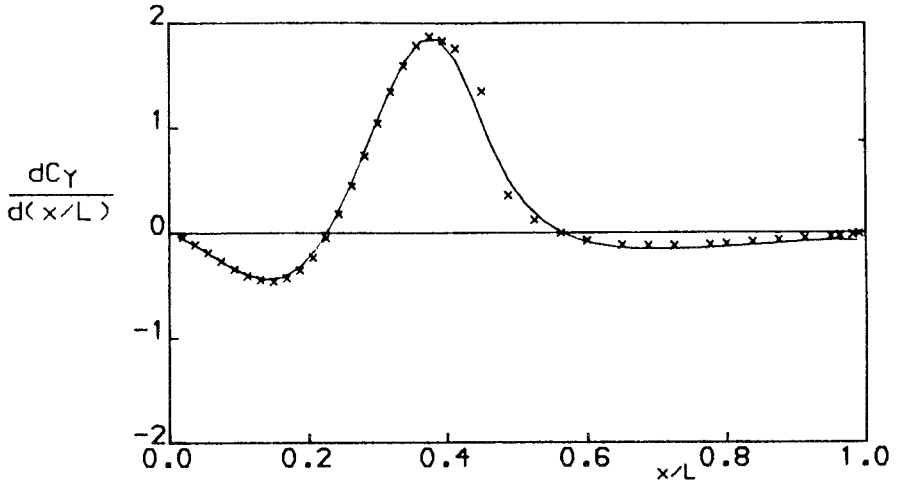

Pitch = 2 degrees

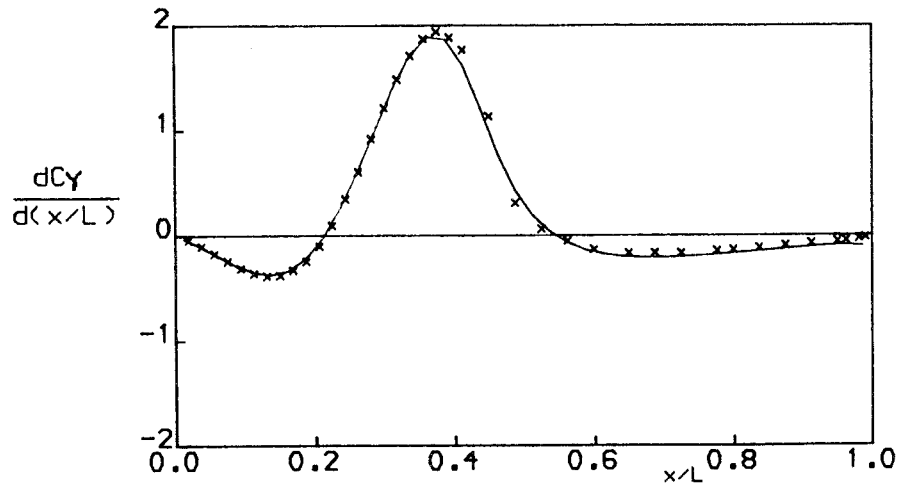

Pitch = 4 degrees

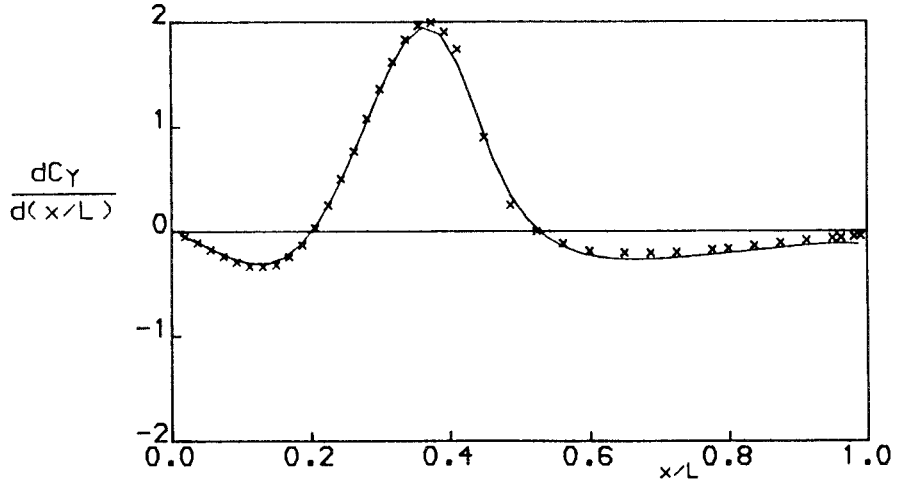

Pitch = 6 degrees

d) Side-Force loading distributions on port body

Figure 13 concluded

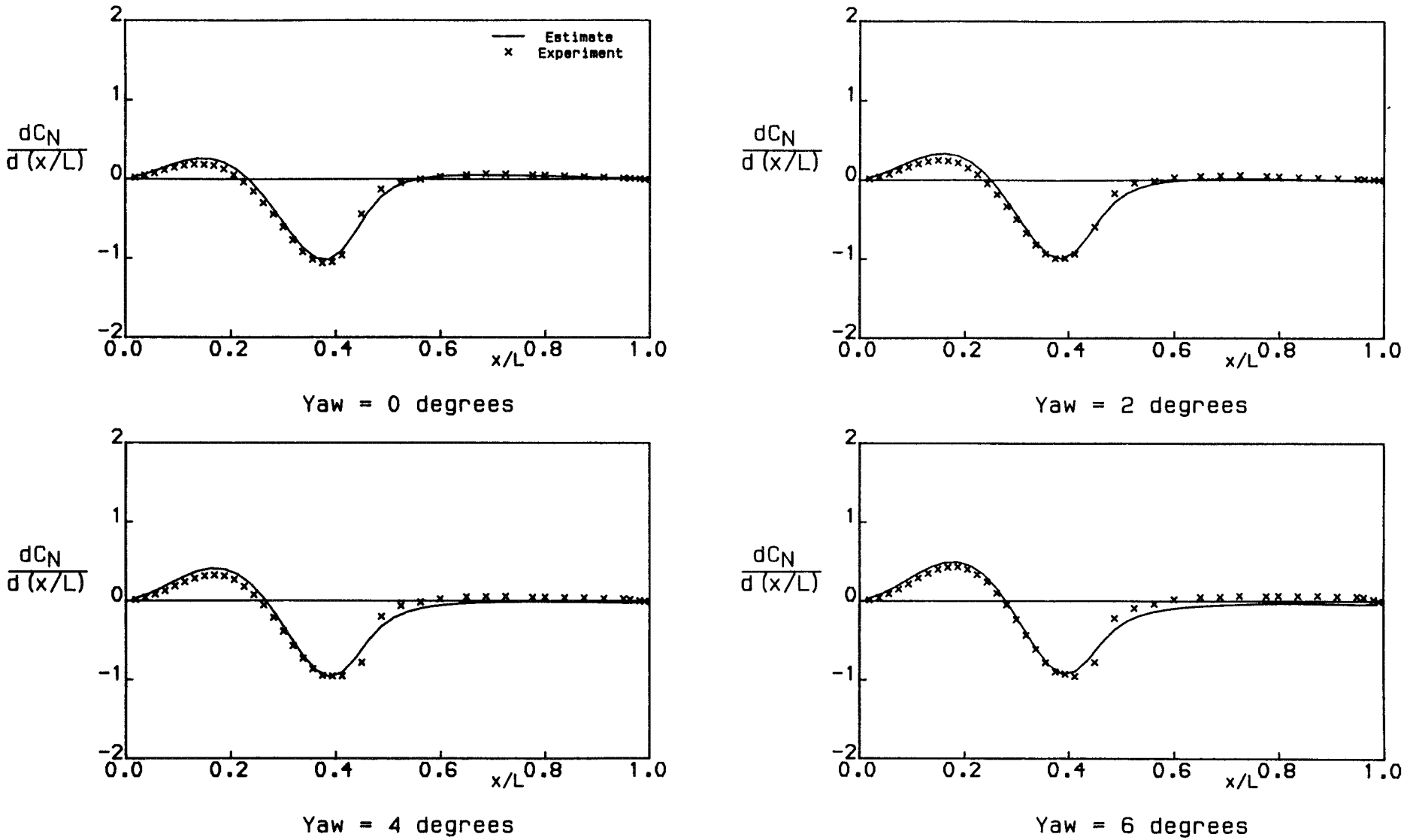

a) Normal-force loading distributions on port body

Figure 14. Comparison of estimated and experimental loading distributions as yaw varies

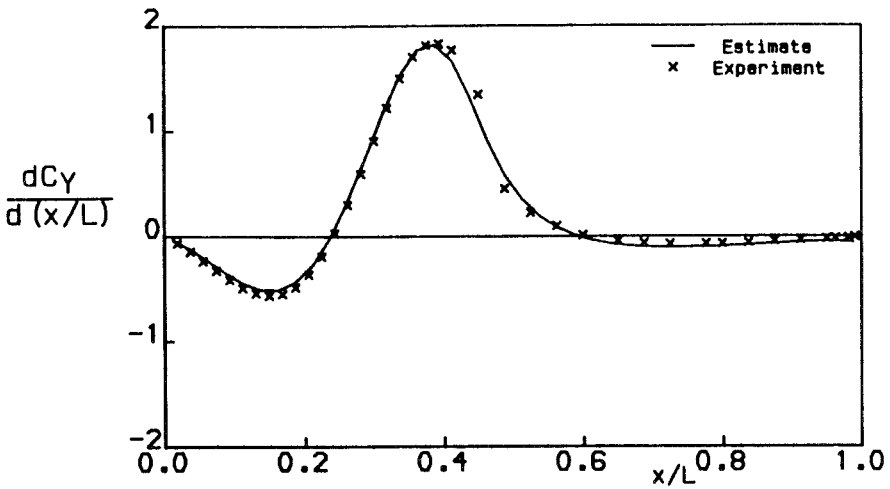

Yaw = 0 degrees

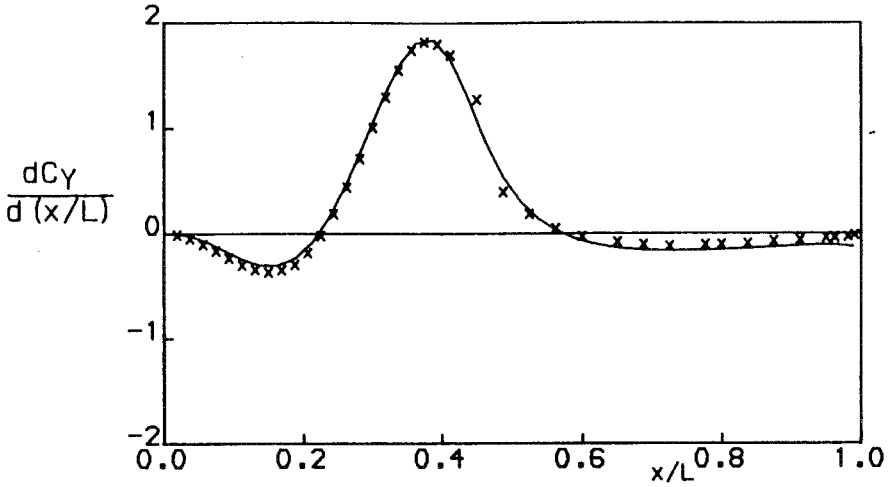

Yaw = 2 degrees

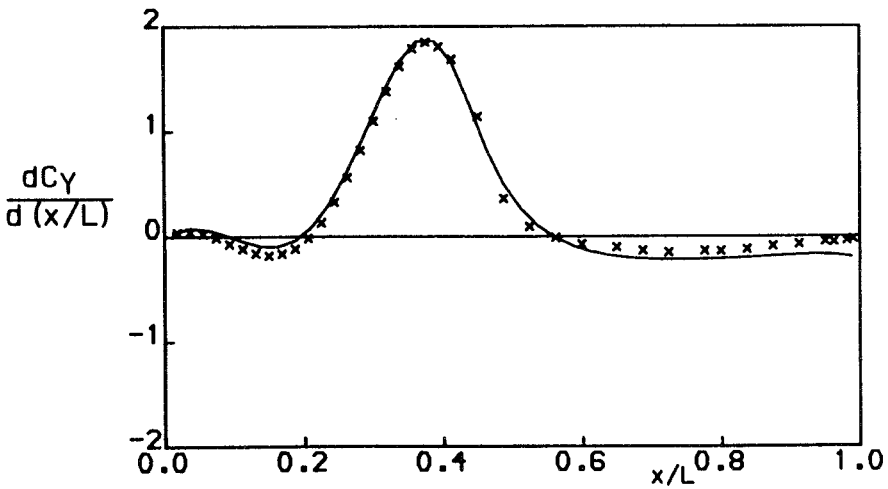

Yaw = 4 degrees

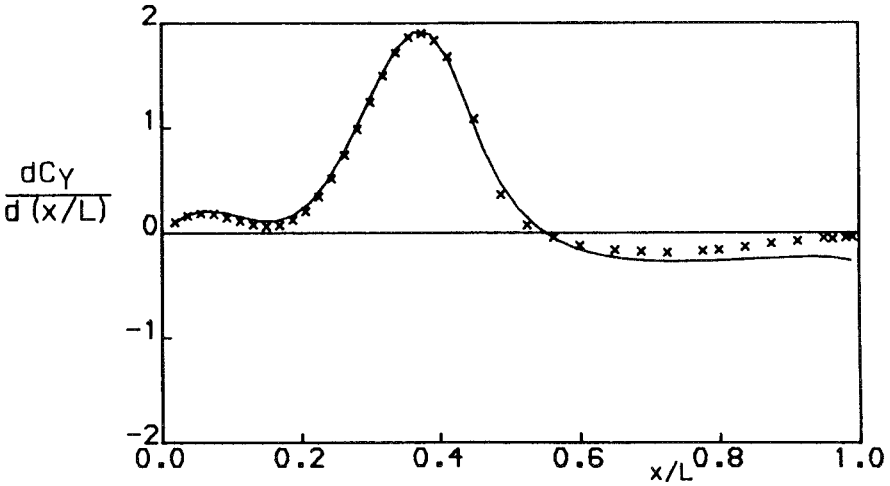

Yaw = 6 degrees

b) Side-force loading distributions on port body

Figure 14 continued

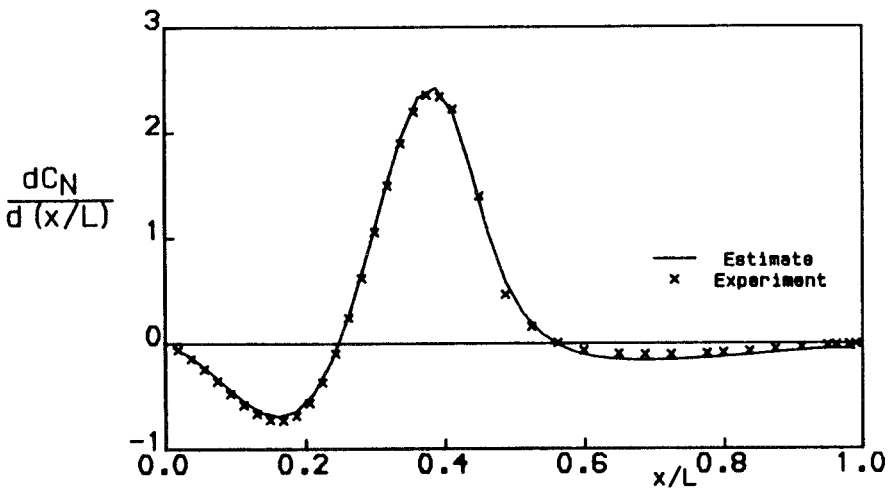

Yaw = 0 degrees

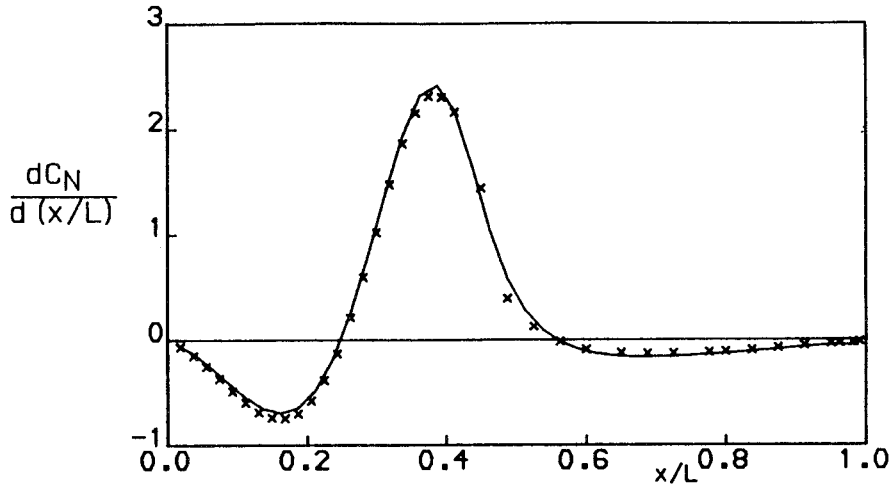

Yaw = 2 degrees

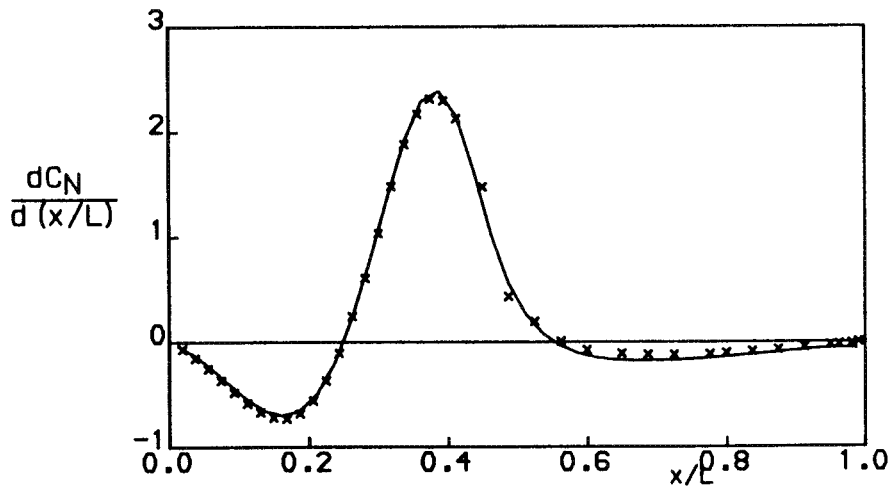

Yaw = 4 degrees

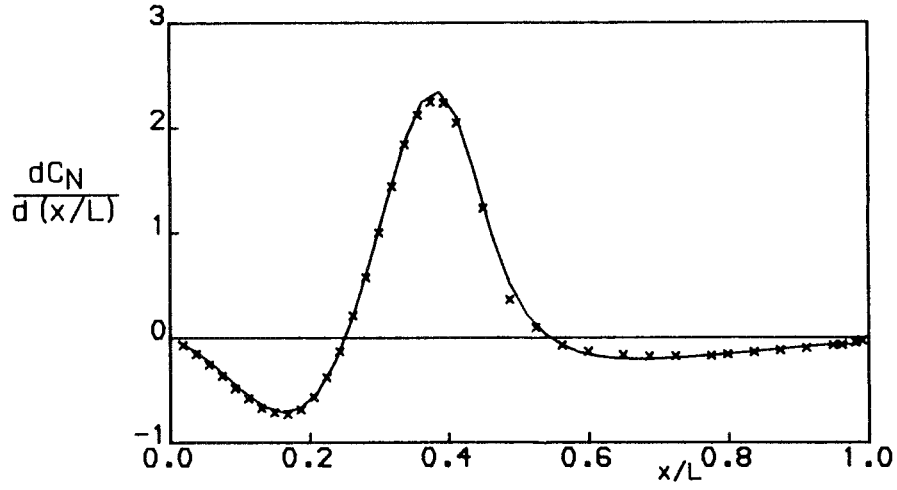

Yaw = 6 degrees

c) Normal-force loading distributions on central body

Figure 14 continued.

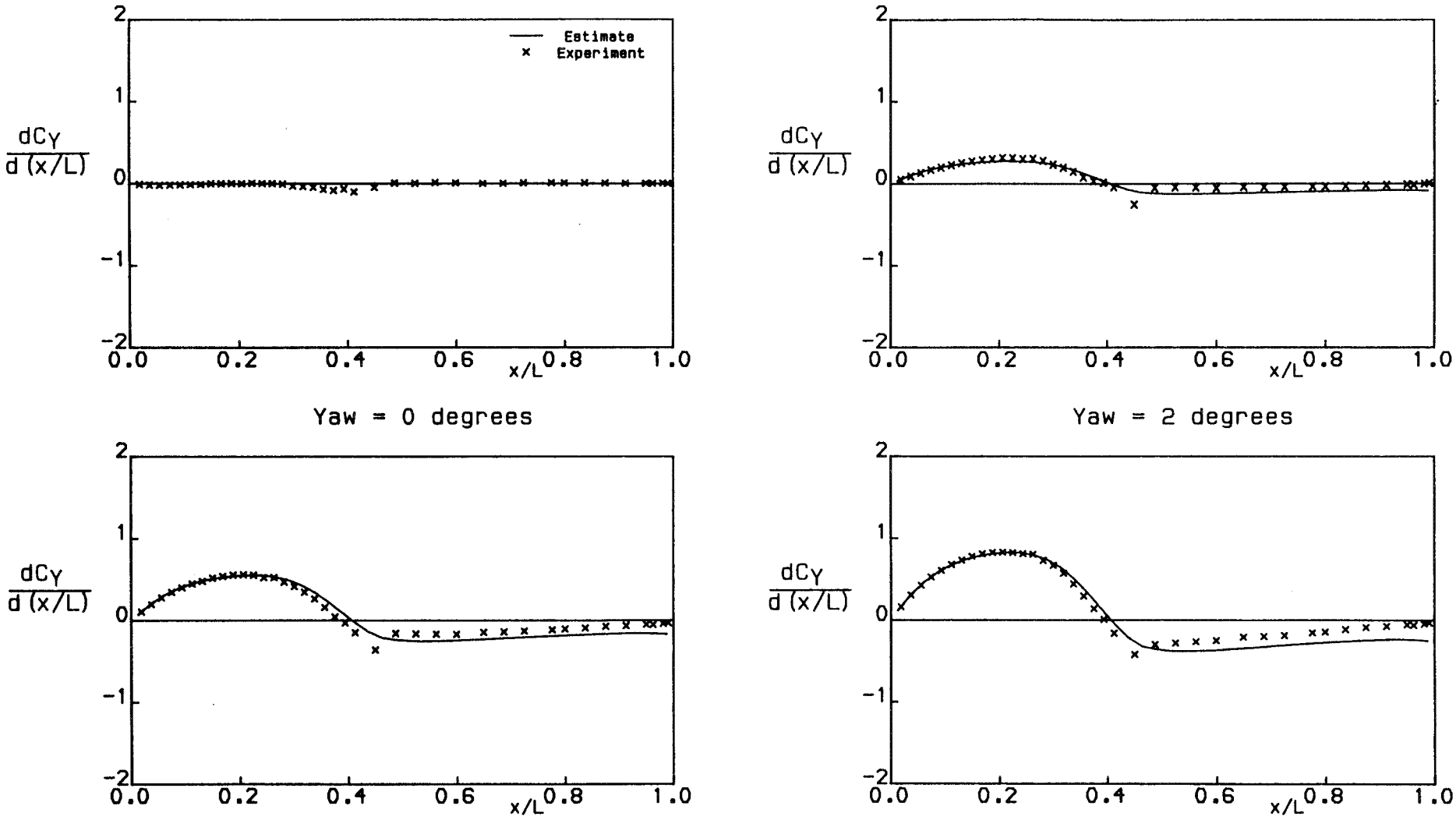

Yaw = 0 degrees

Yaw = 2 degrees

Yaw = 4 degrees

Yaw = 6 degrees

d) Side-force loading distributions on central body

Figure 14 continued

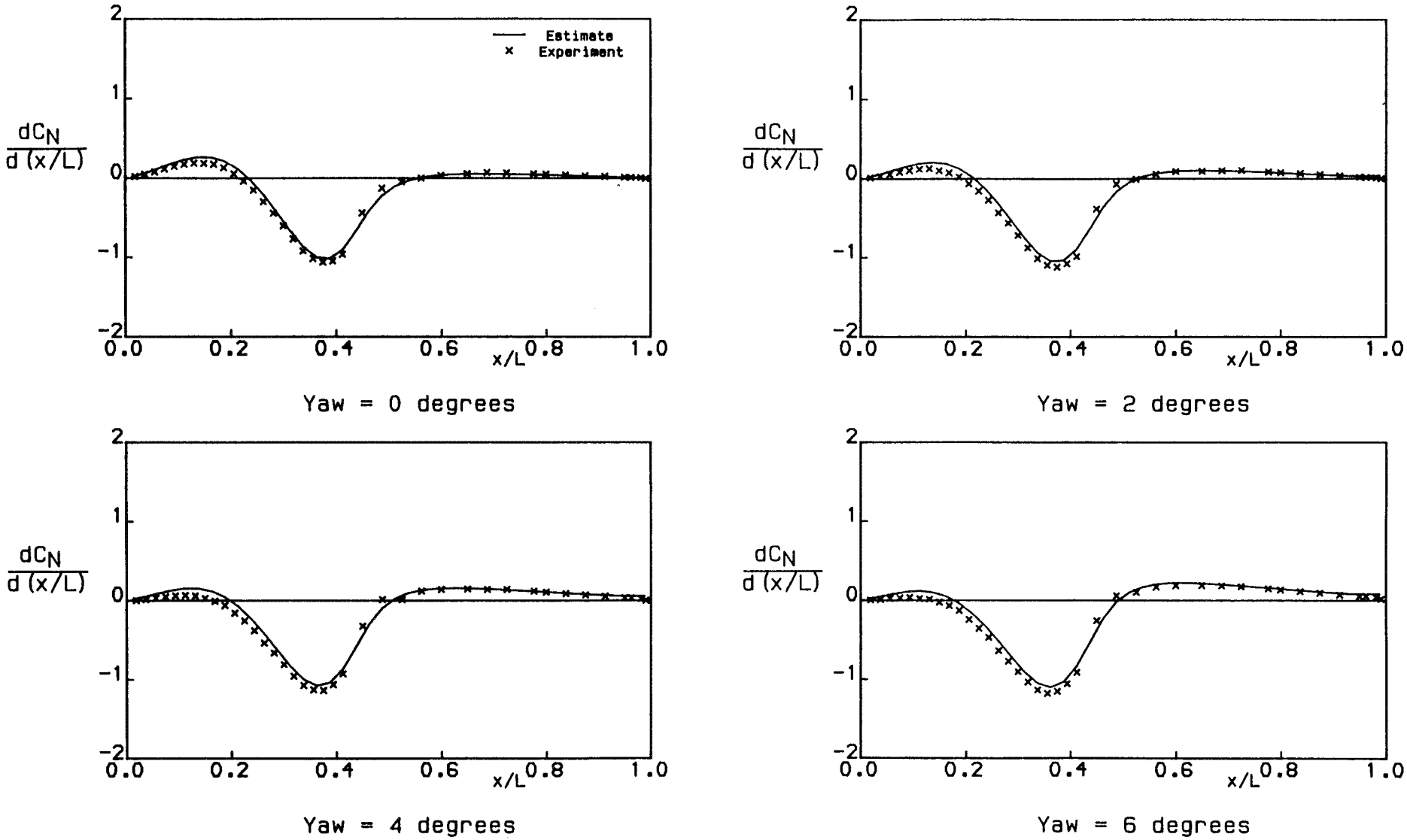

e) Normal-force loading distributions on starboard body

Figure 14 continued.

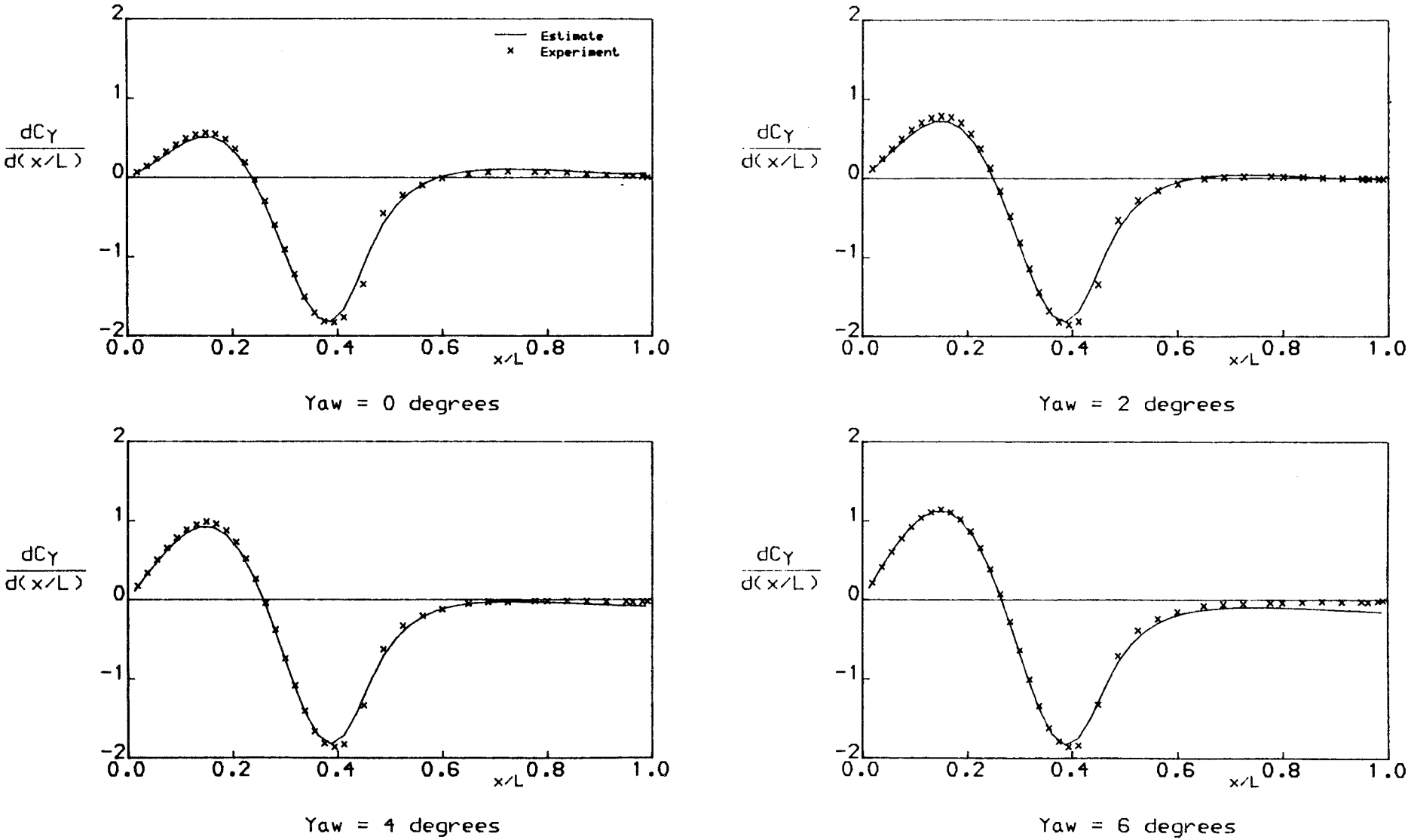

F) Side-Force loading distributions on starboard body

Figure 14 concluded

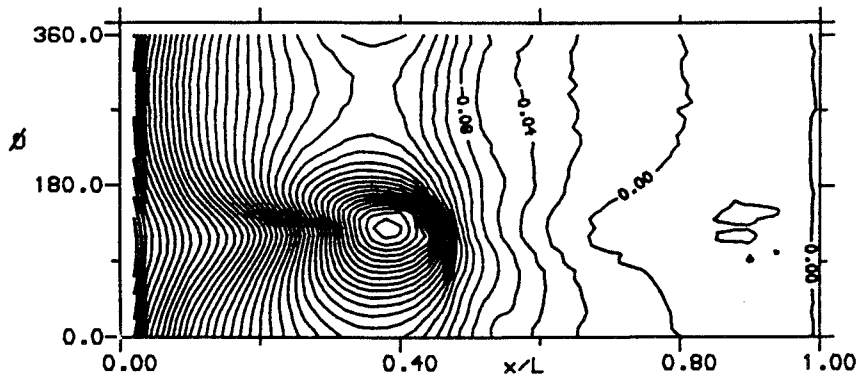

Stbd body

Contour Step 0.02

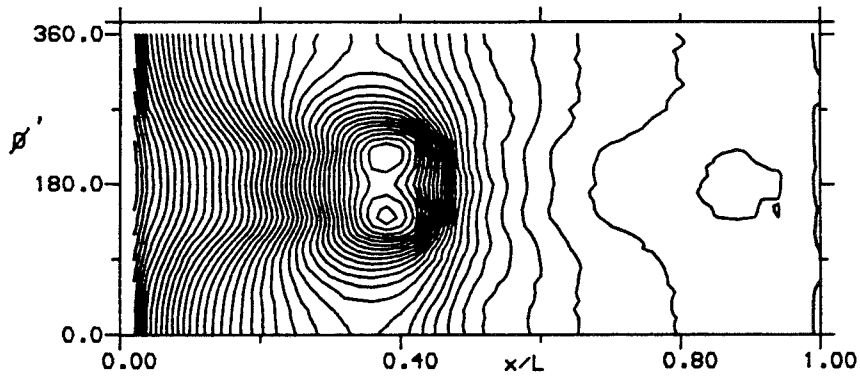

Central-body

Contour Step 0.02

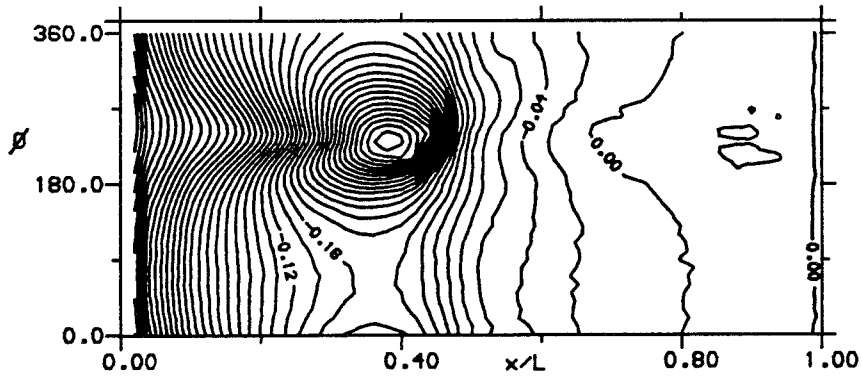

Port body

Contour Step 0.02

a) Experiment - Pitch = 0 degrees, Yaw = 0 degrees

Figure 15. Contour plots of zero pitch Cp distributions

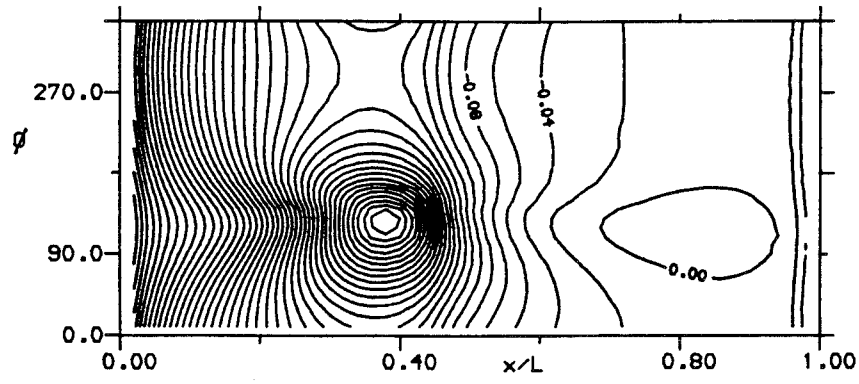

Stbd body

Contour Step 0.02

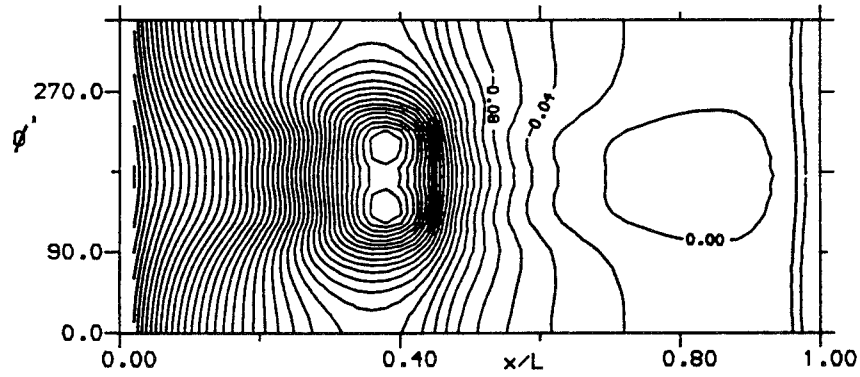

Central body

Contour Step 0.02

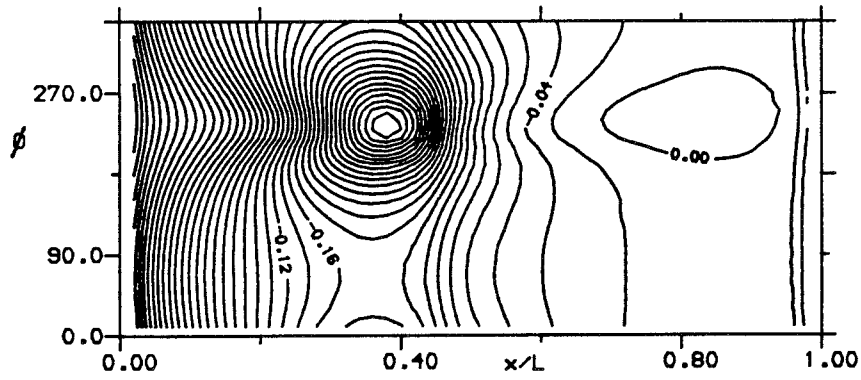

Port body

Contour Step 0.02

b) Estimate - Pitch = 0 degrees, Yaw = 0 degrees

Figure 15 concluded

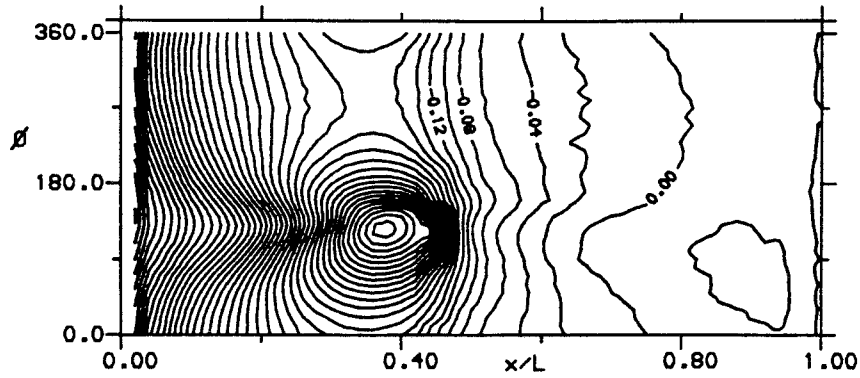

Stbd body

Contour Step 0.02

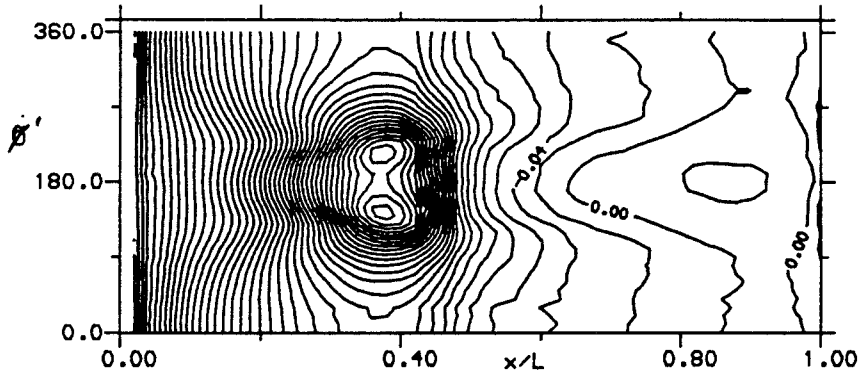

Central-body

Contour Step 0.02

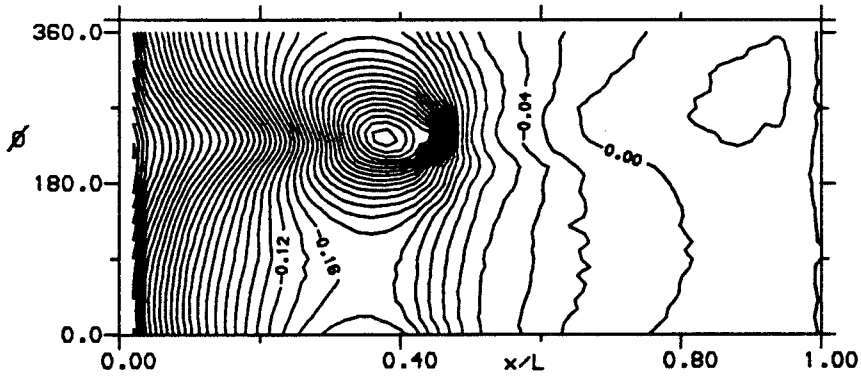

Port body

Contour Step 0.02

a) Experiment - Pitch = 2 degrees, Yaw = 0 degrees

Figure 16. Comparison of experimental and estimated Cp distributions - Variation with pitch

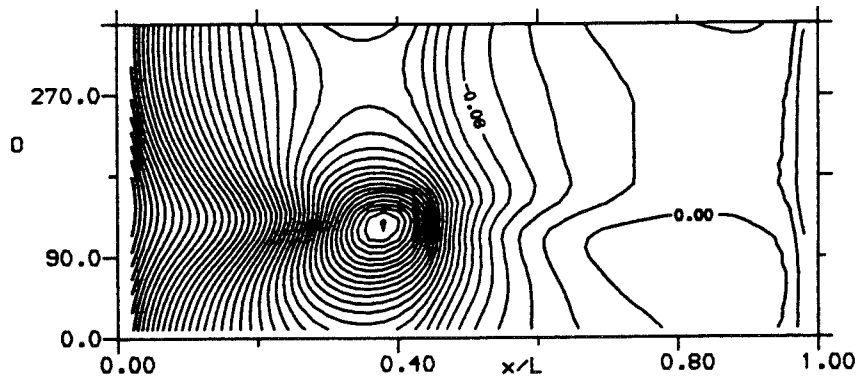

Stbd body

Contour Step 0.02

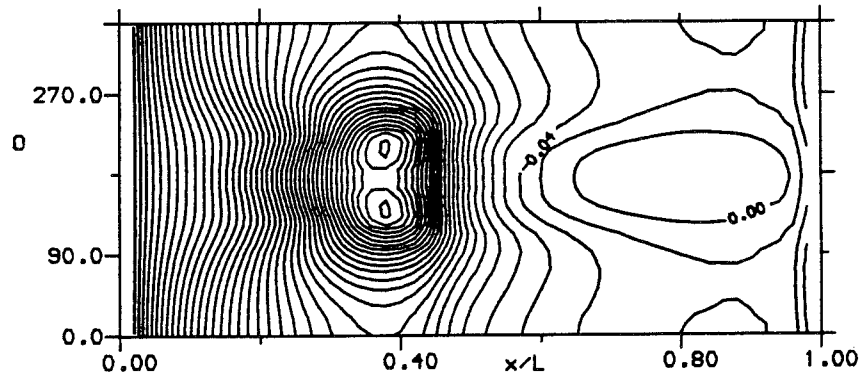

Central body

Contour Step 0.02

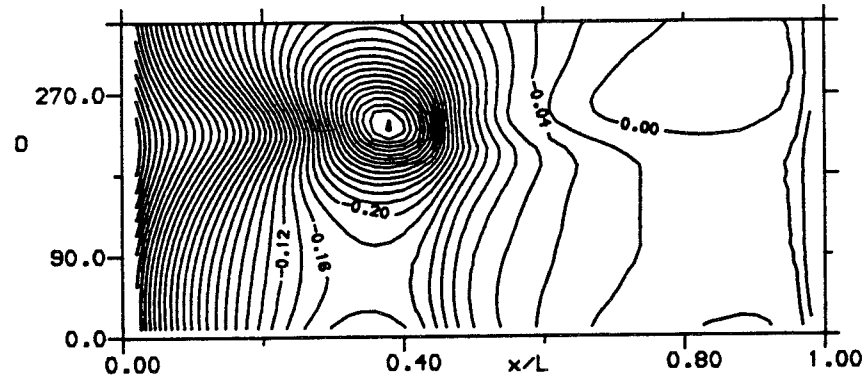

Port body

Contour Step 0.02

b) Estimate - Pitch = 2 degrees, Yaw = 0 degrees

Figure 16 continued

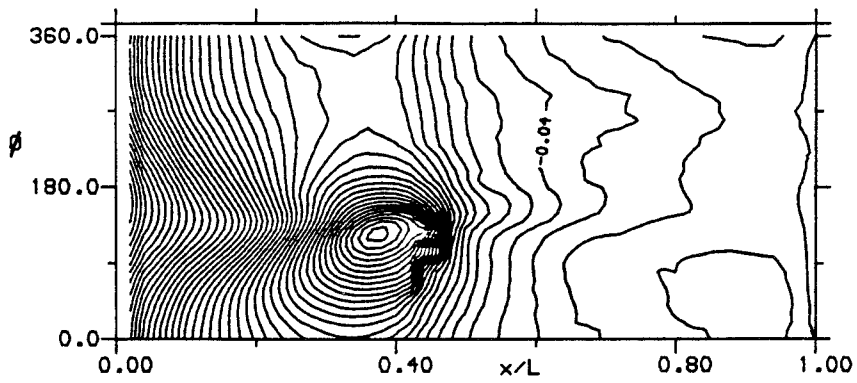

Stbd body

Contour Step 0.02

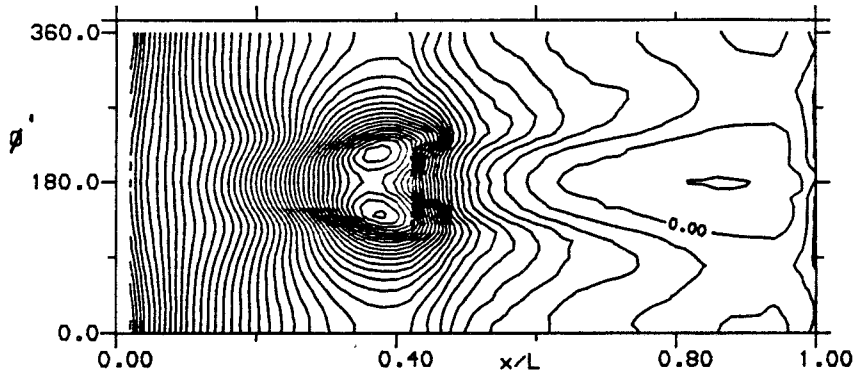

Central-body

Contour Step 0.02

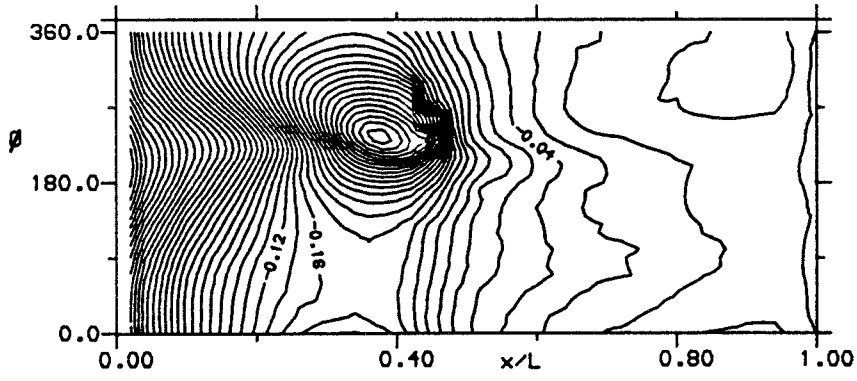

Port body

Contour Step 0.02

c) Experiment - Pitch = 4 degrees, Yaw = 0 degrees

Figure 16 continued

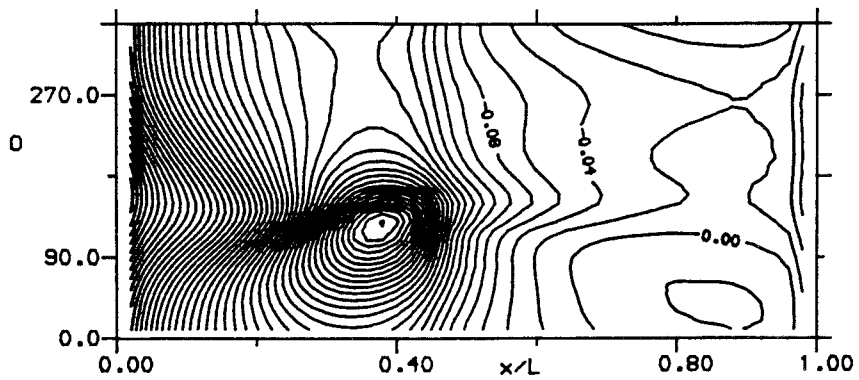

Stbd body

Contour Step 0.02

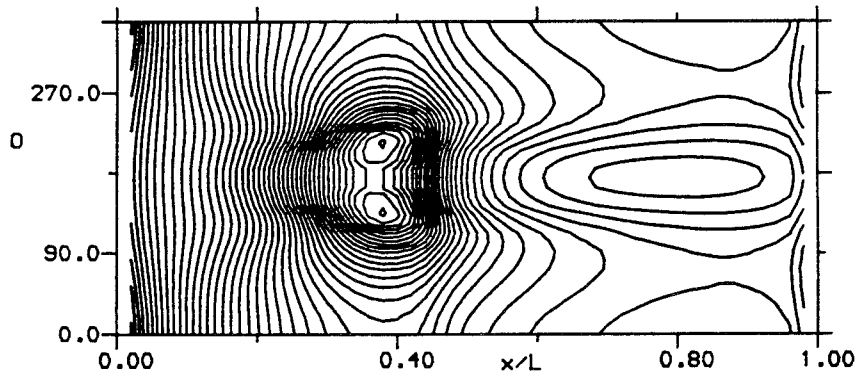

Central body

Contour Step 0.02

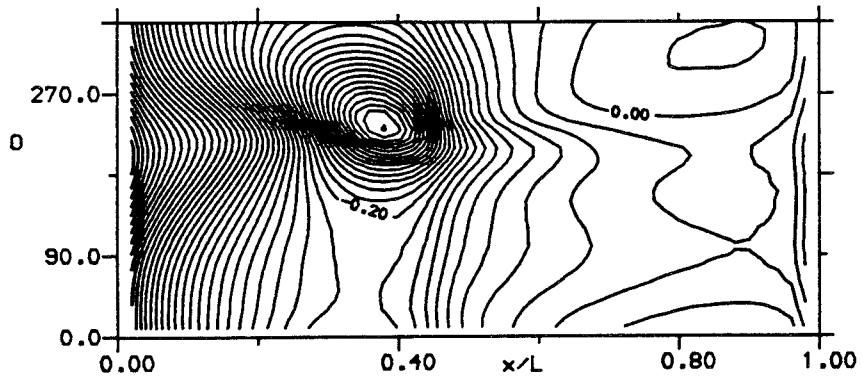

Port body

Contour Step 0.02

d) Estimate - Pitch = 4 degrees, Yaw = 0 degrees

Figure 16 continued

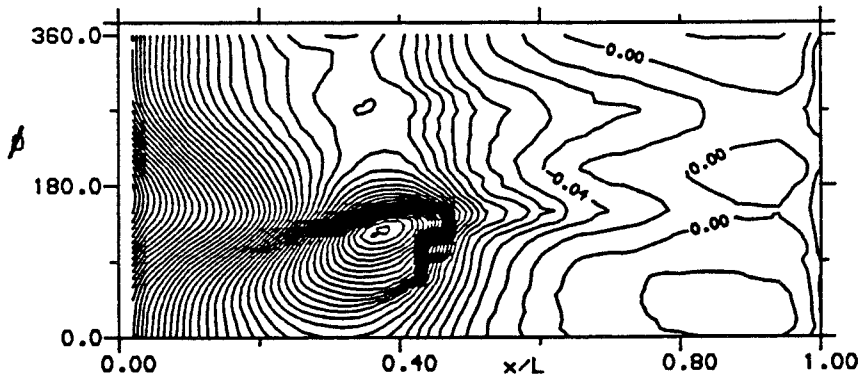

Stbd body

Contour Step 0.02

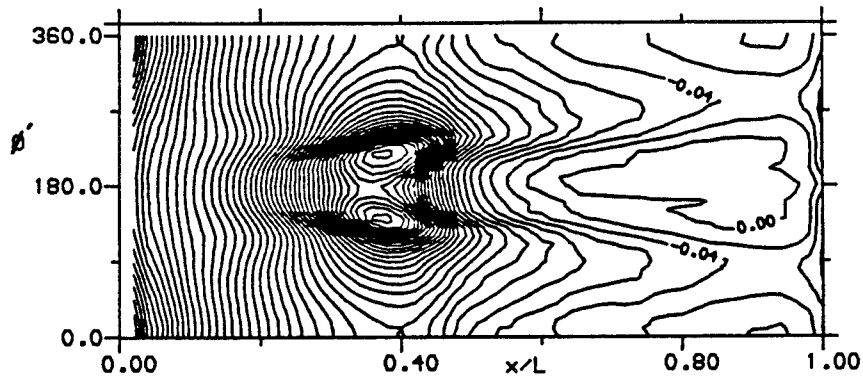

Central-body

Contour Step 0.02

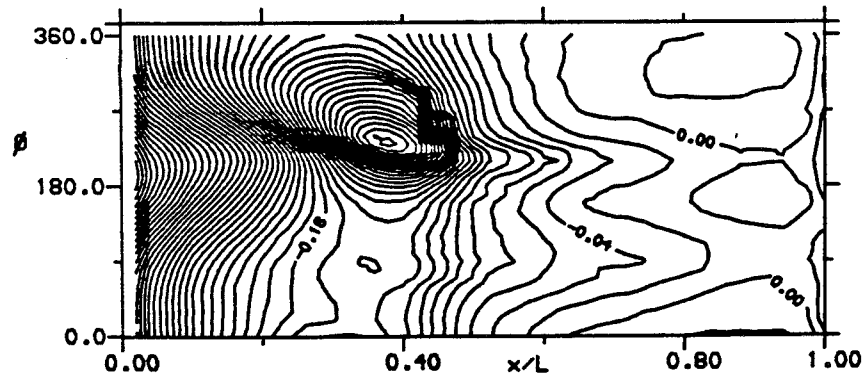

Port body

Contour Step 0.02

e) Experiment - Pitch = 6 degrees, Yaw = 0 degrees

Figure 16 continued

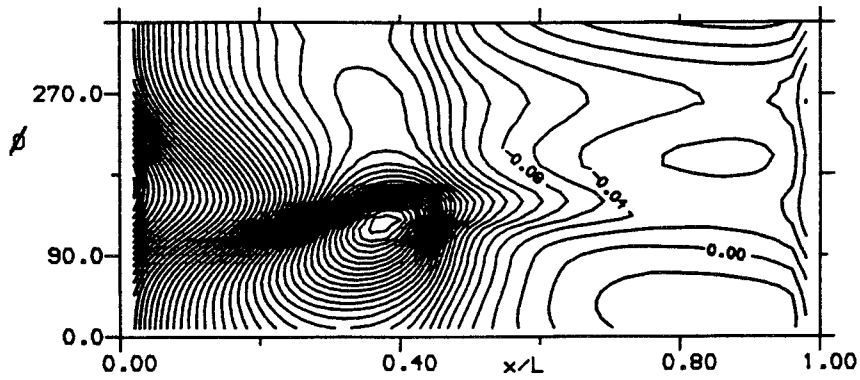

Stbd body

Contour Step 0.02

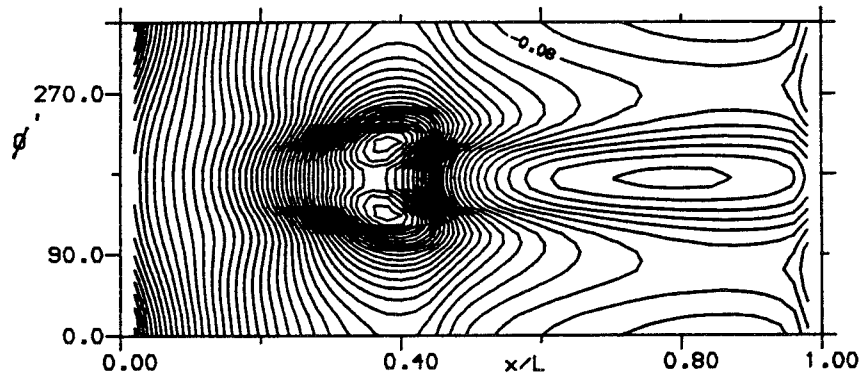

Central body

Contour Step 0.02

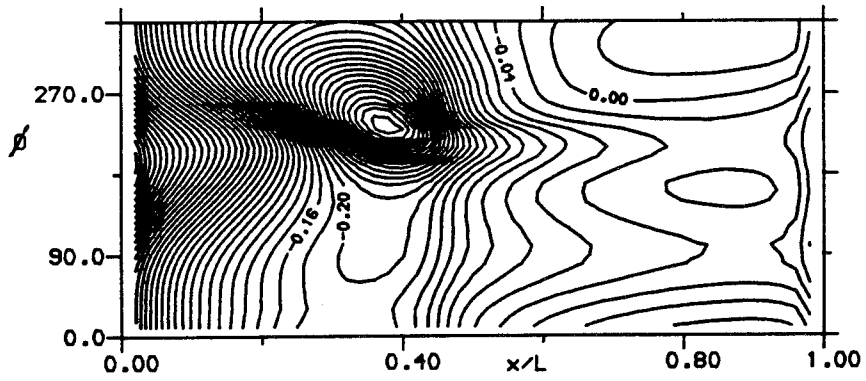

Port body

Contour Step 0.02

F) Estimate - Pitch = 6 degrees, Yaw = 0 degrees

Figure 16 continued

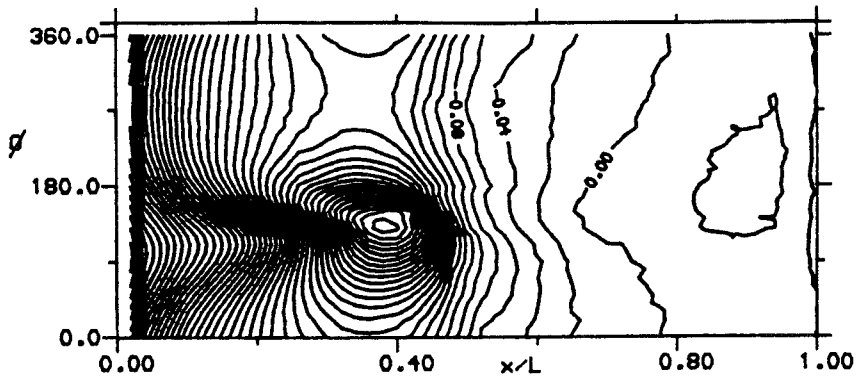

Stbd body

Contour Step 0.02

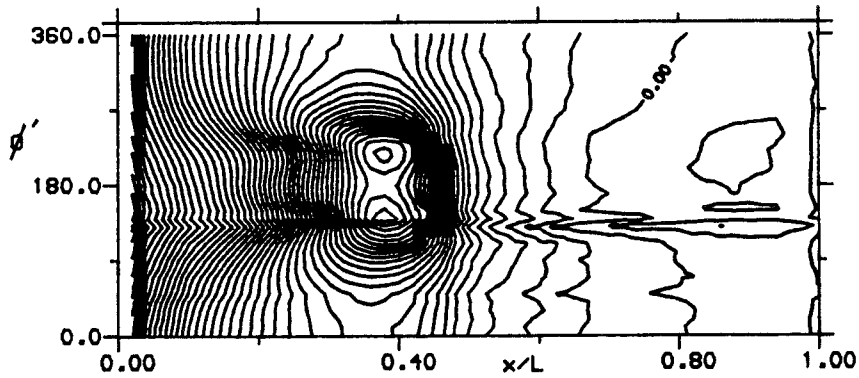

Central-body

Contour Step 0.02

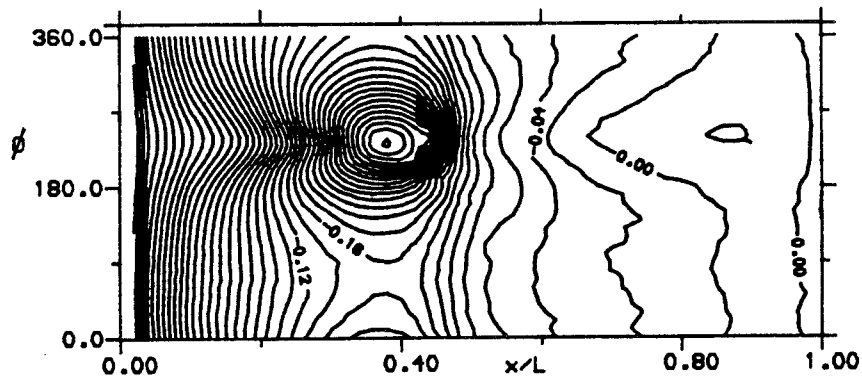

Port body

Contour Step 0.02

a) Experiment - Pitch = 0 degrees, Yaw = 2 degrees

Figure 17. Comparison of experimental and estimated Cp distributions - Variation with yaw

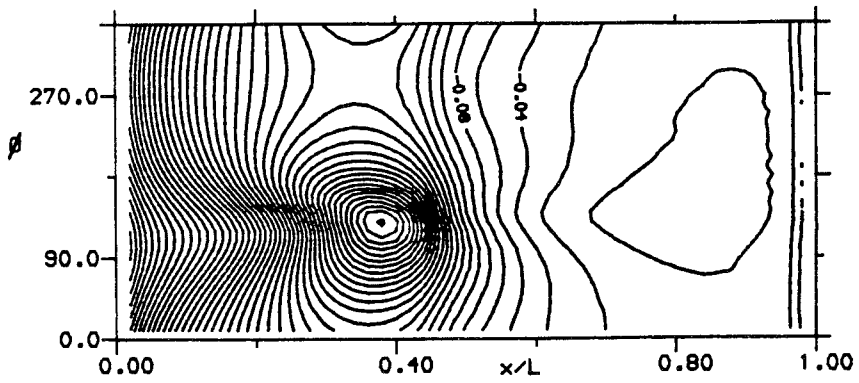

Stbd body

Contour Step 0.02

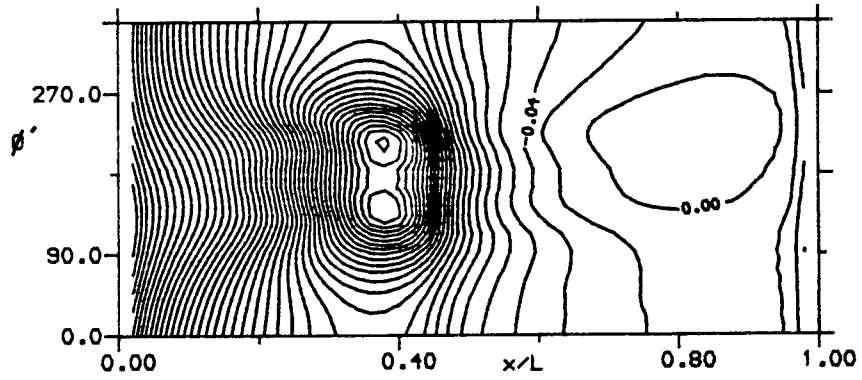

Central body

Contour Step 0.02

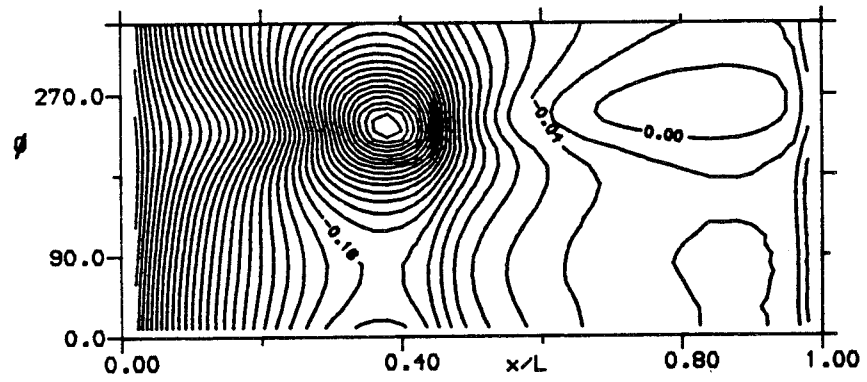

Port body

Contour Step 0.02

b) Estimate - Pitch = 0 degrees, Yaw = 2 degrees

Figure 17 continued

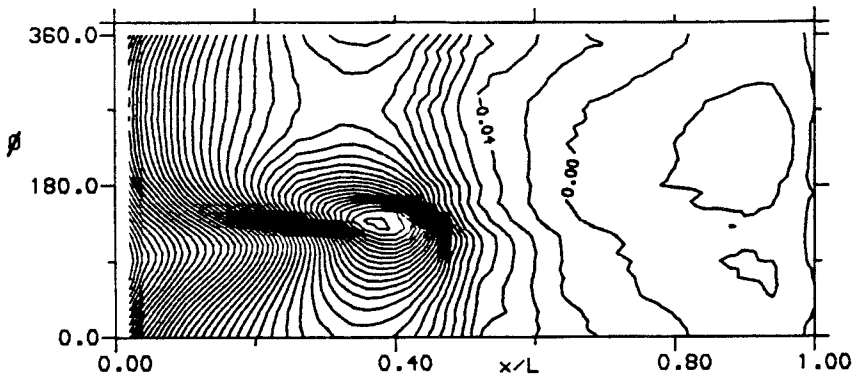

Stbd body

Contour Step 0.02

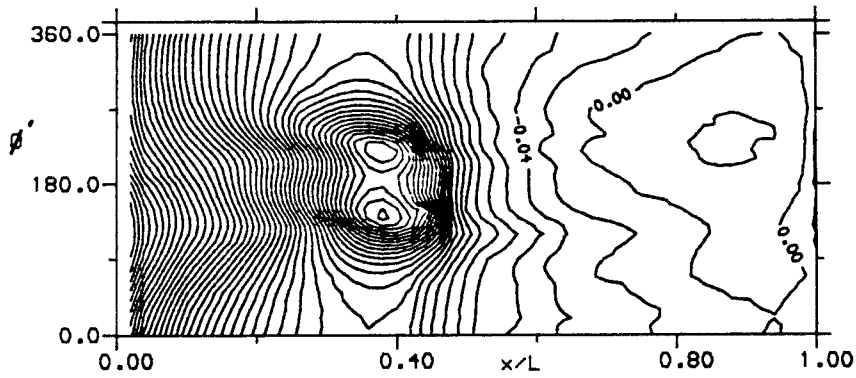

Central-body

Contour Step 0.02

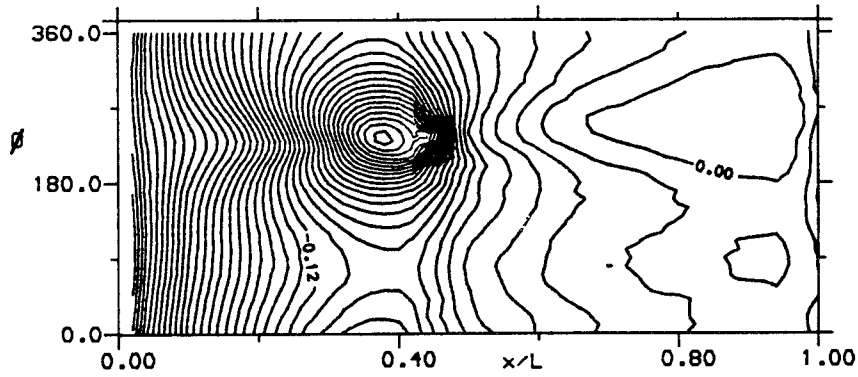

Port body

Contour Step 0.02

c) Experiment - Pitch = 0 degrees, Yaw = 4 degrees

Figure 17 Continued

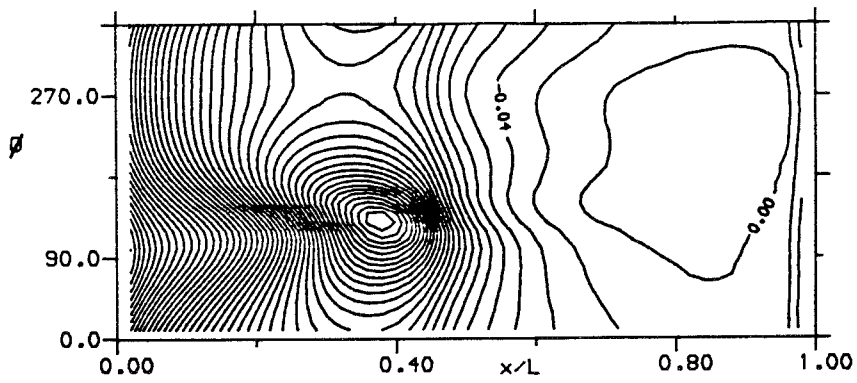

Stbd body

Contour Step 0.02

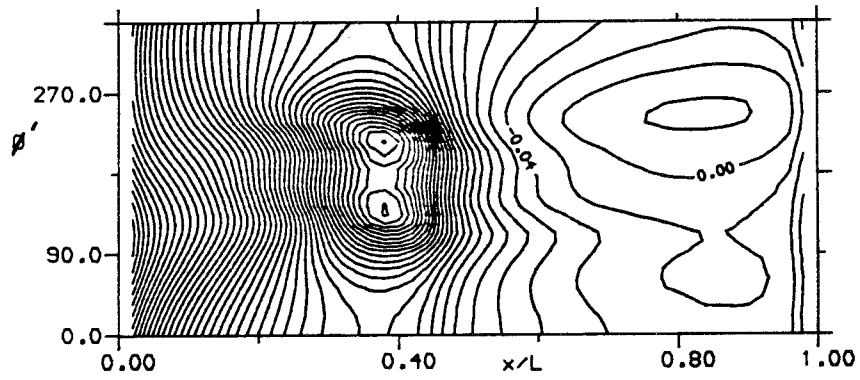

Central body

Contour Step 0.02

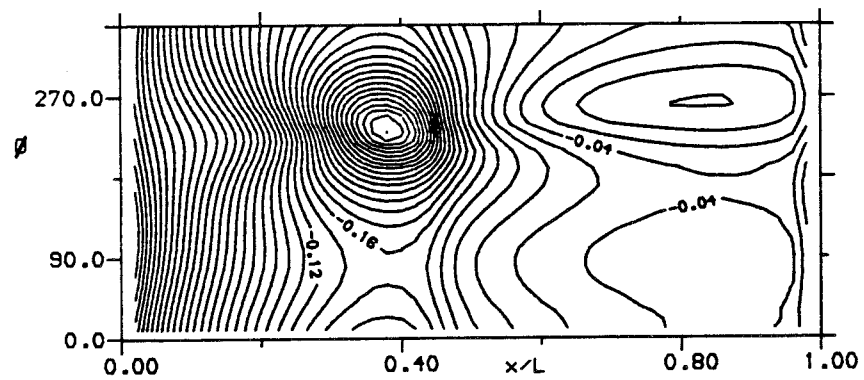

Port body

Contour Step 0.02

d) Estimate - Pitch = 0 degrees, Yaw = 4 degrees

Figure 17 continued

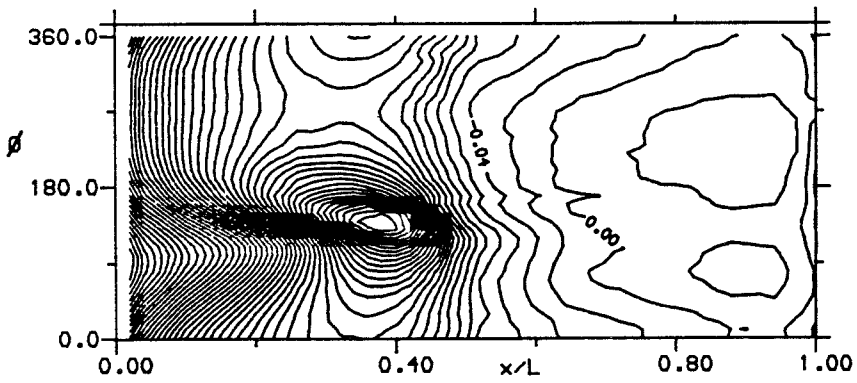

Stbd body

Contour Step 0.02

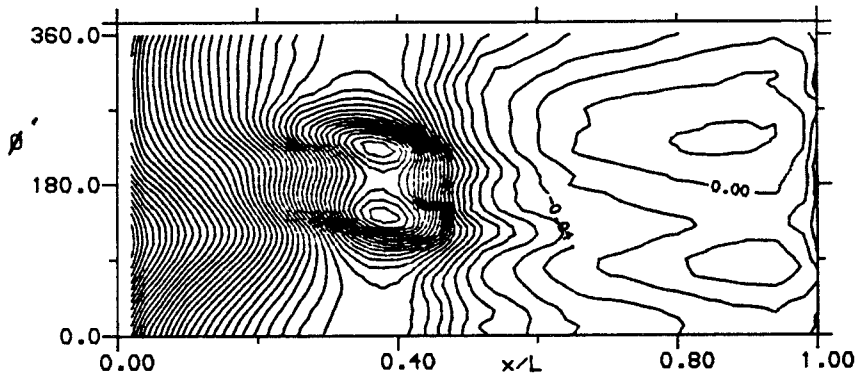

Central-body

Contour Step 0.02

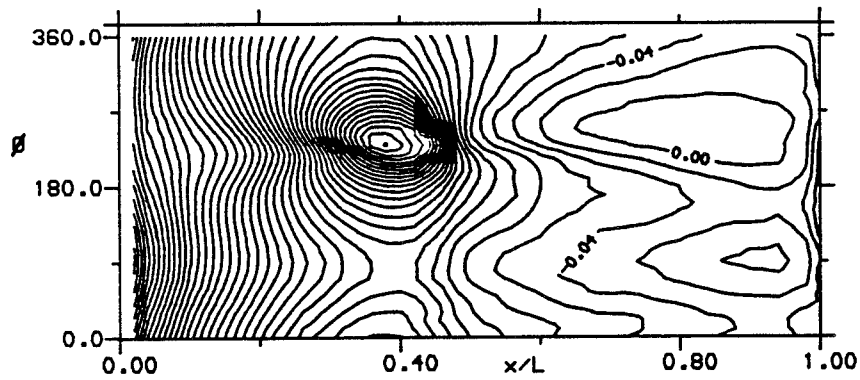

Port body

Contour Step 0.02

e) Experiment - Pitch = 0 degrees, Yaw = 6 degrees

Figure 17 continued

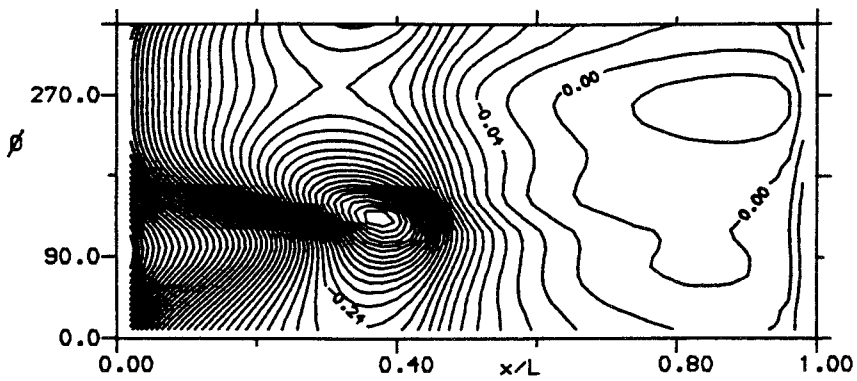

Stbd body

Contour Step 0.02

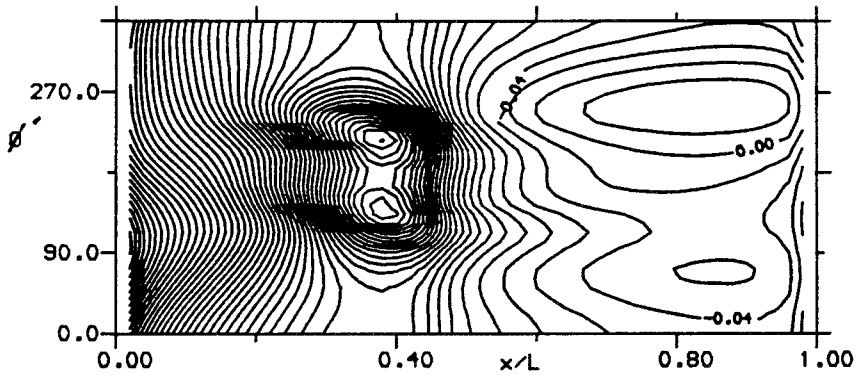

Central body

Contour Step 0.02

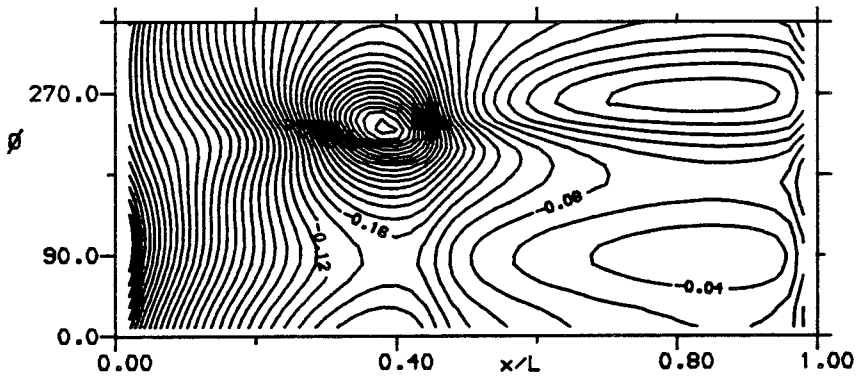

Port body

Contour Step 0.02

F) Estimate - Pitch = 0 degrees, Yaw = 6 degrees

Figure 17 continued

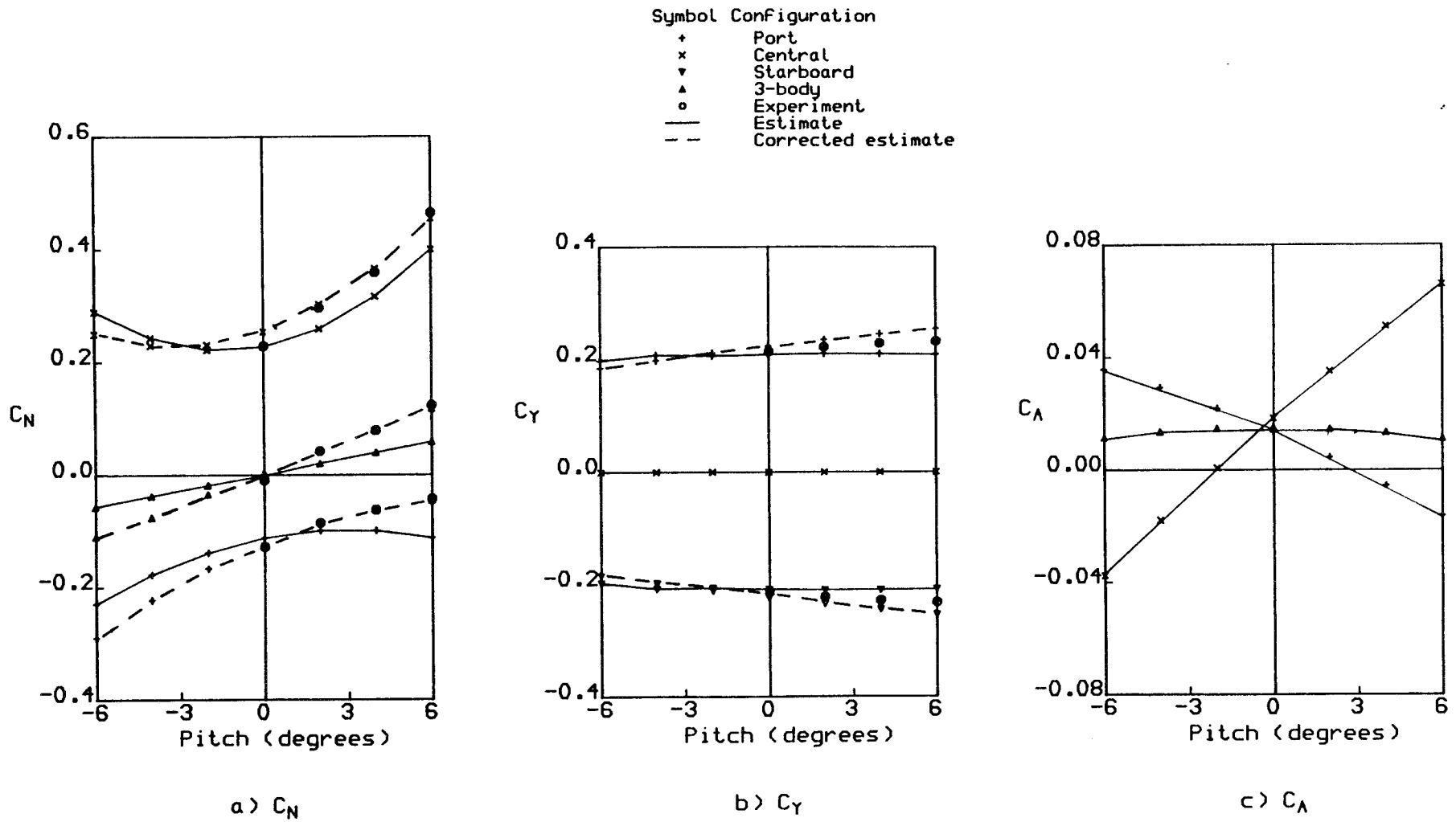

Figure 18. Variation of estimated aerodynamic coefficients with pitch (extended range)

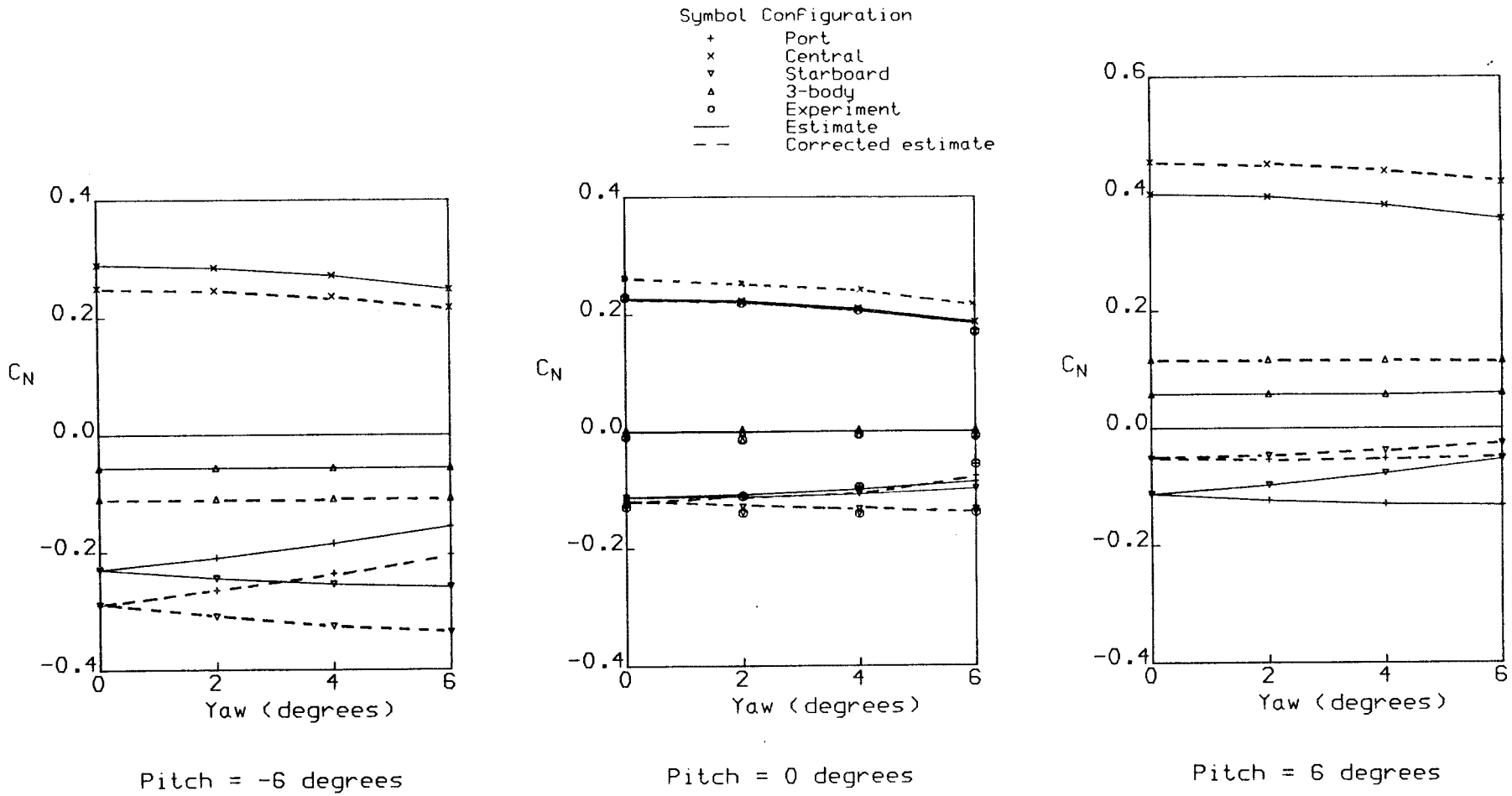

a) Variation of C_N with yaw

Figure 19. Variation of estimated aerodynamic coefficients with yaw (extended range)

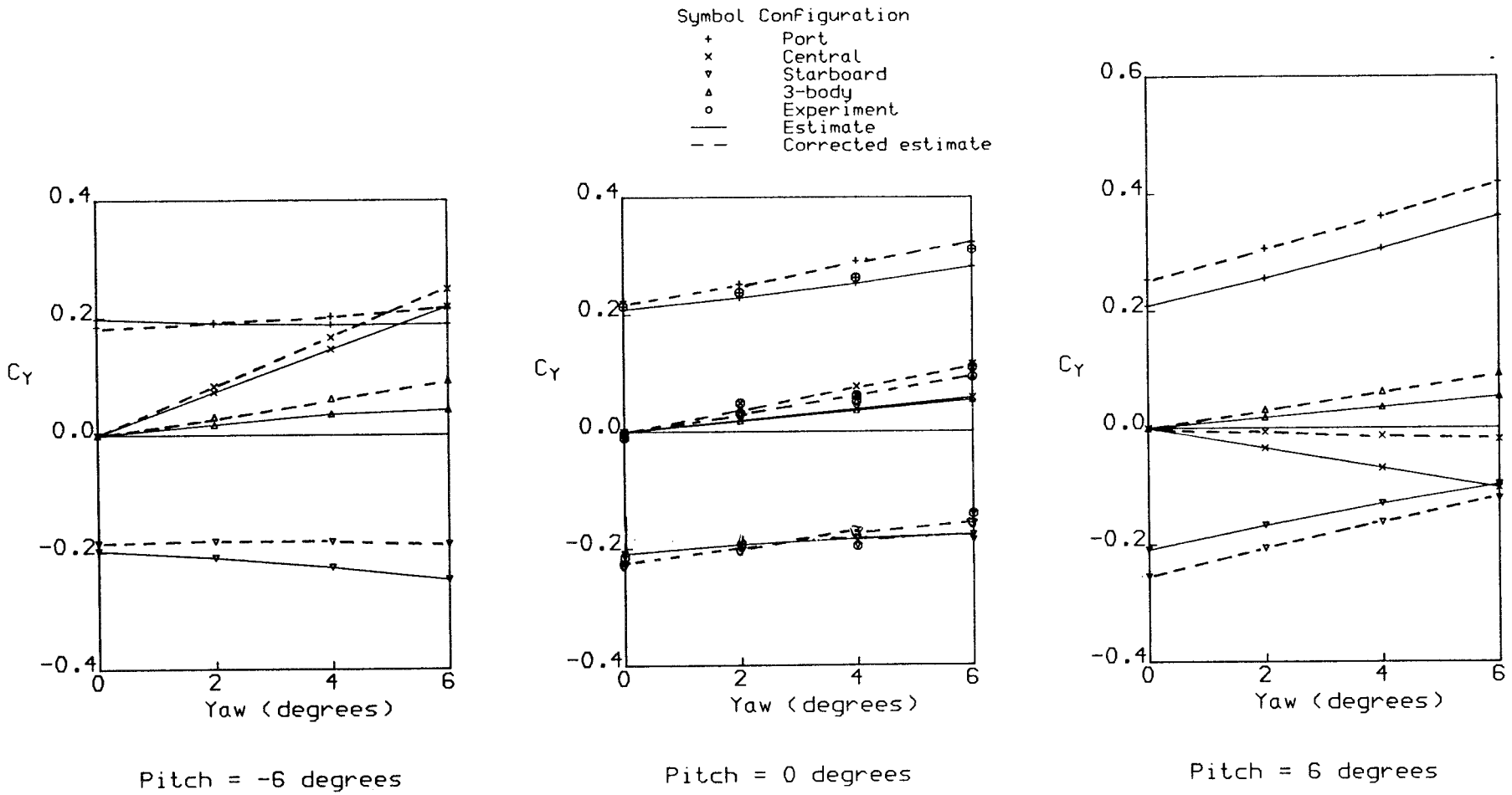

b) Variation of C_Y with yaw

Figure 19 continued

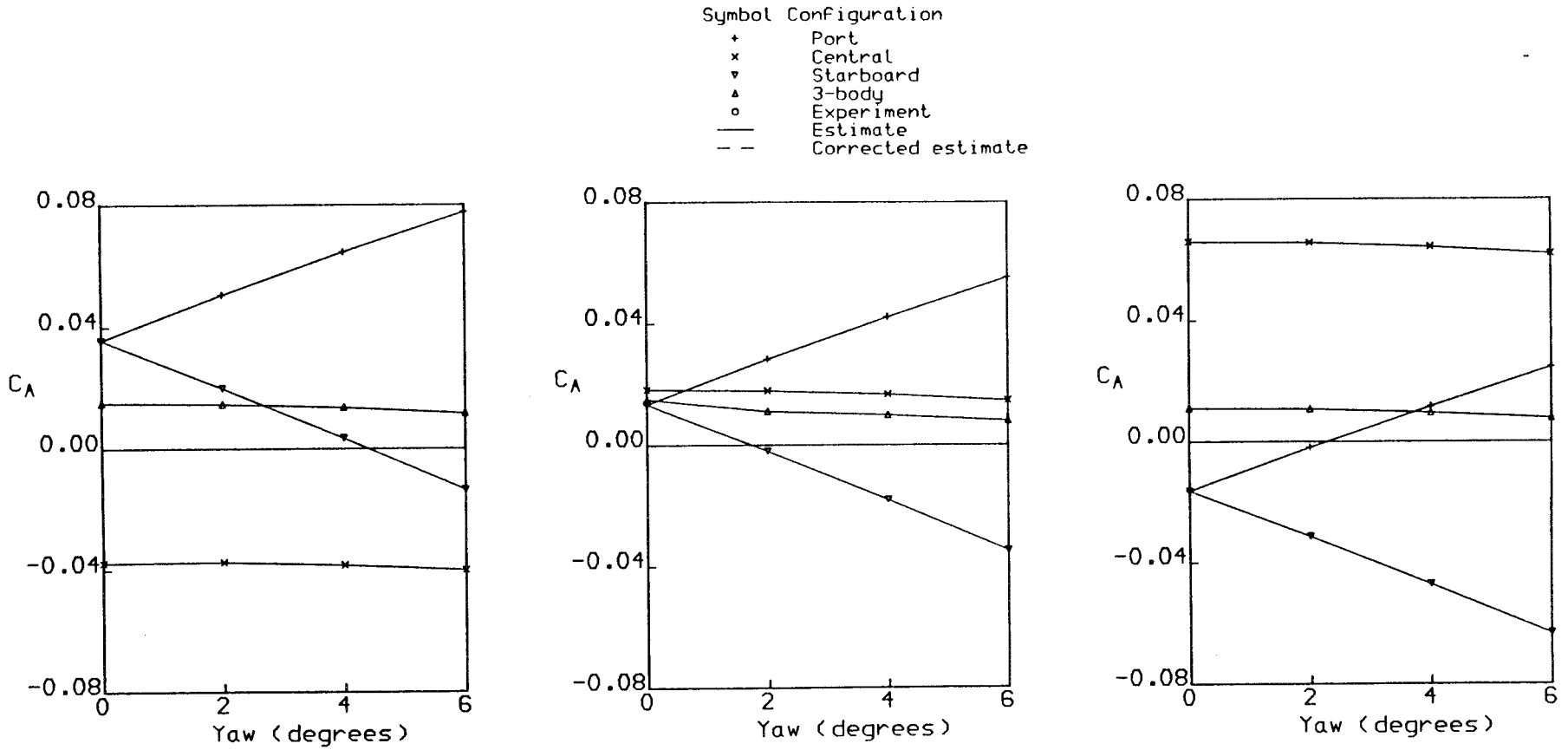

c) Variation of C_A with yaw

Figure 19 concluded

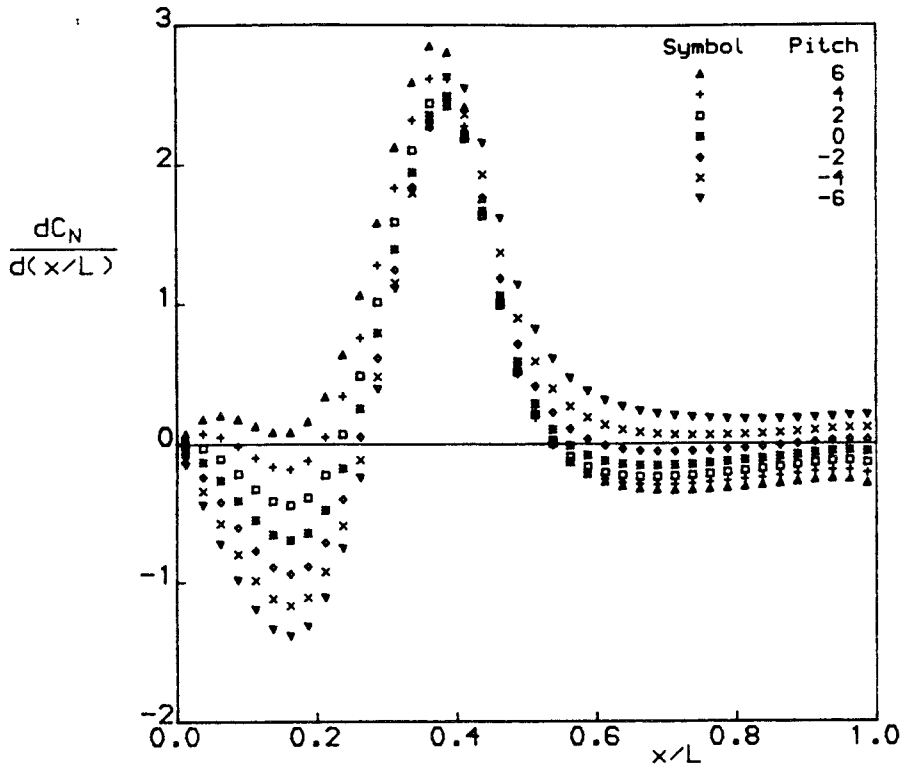

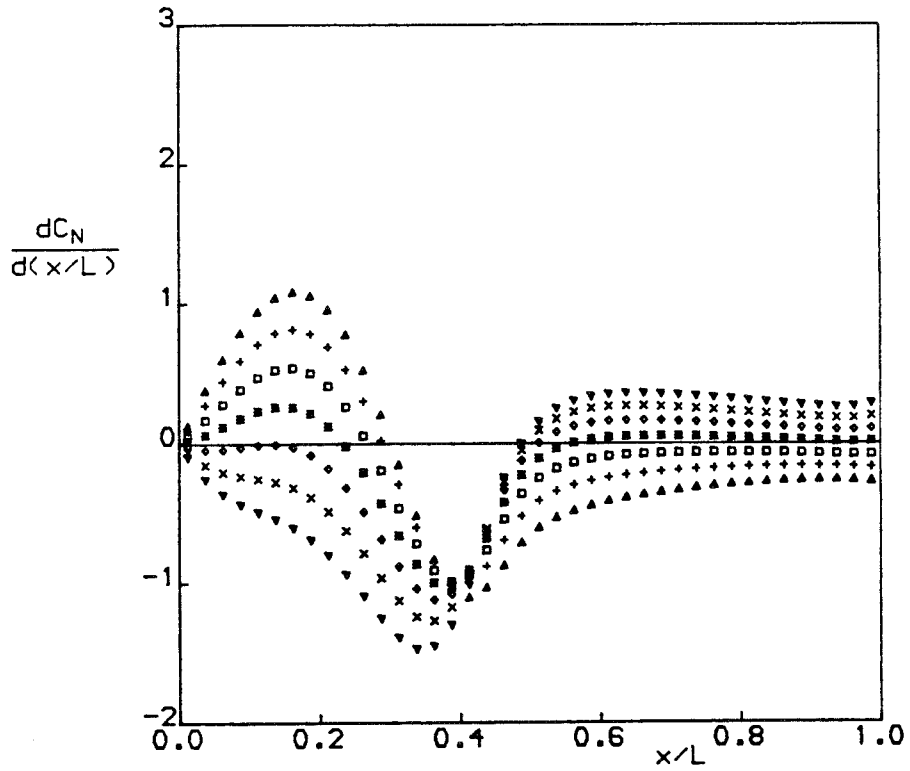

a) Normal-Force loadings

Figure 20. Variation of estimated loadings with pitch

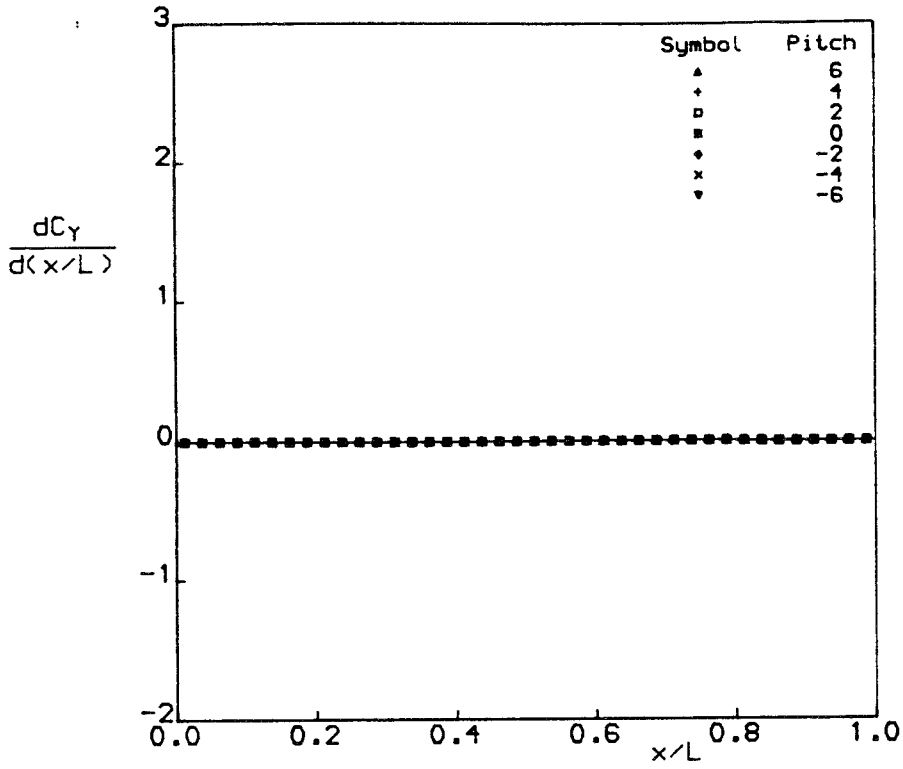

Central body

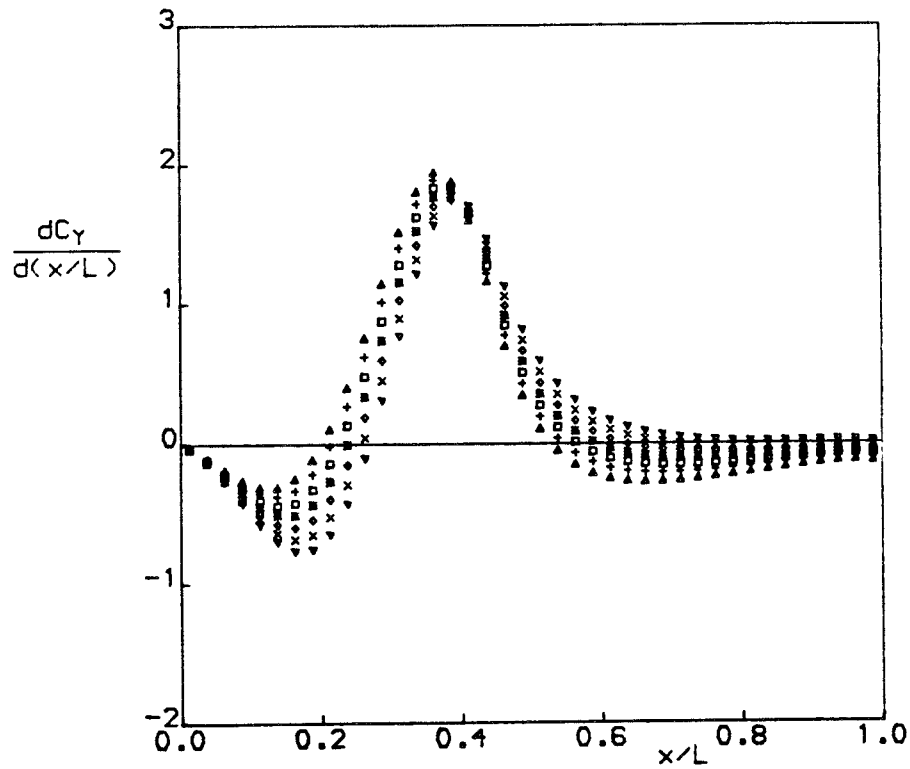

Port body

b) Side-Force loadings

Figure 20 continued

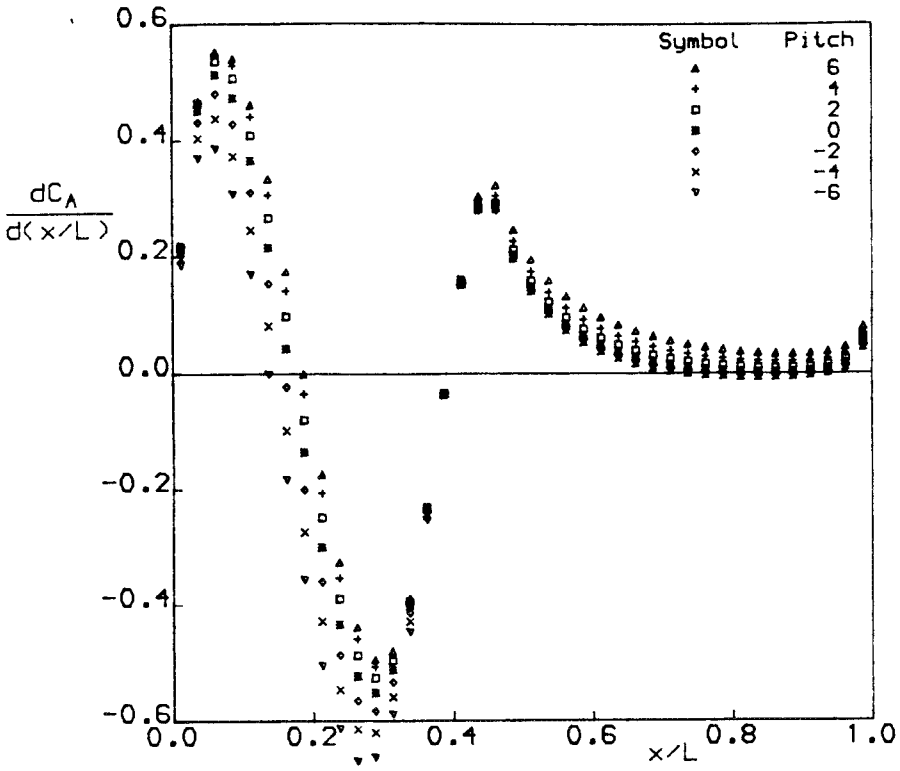

Central body

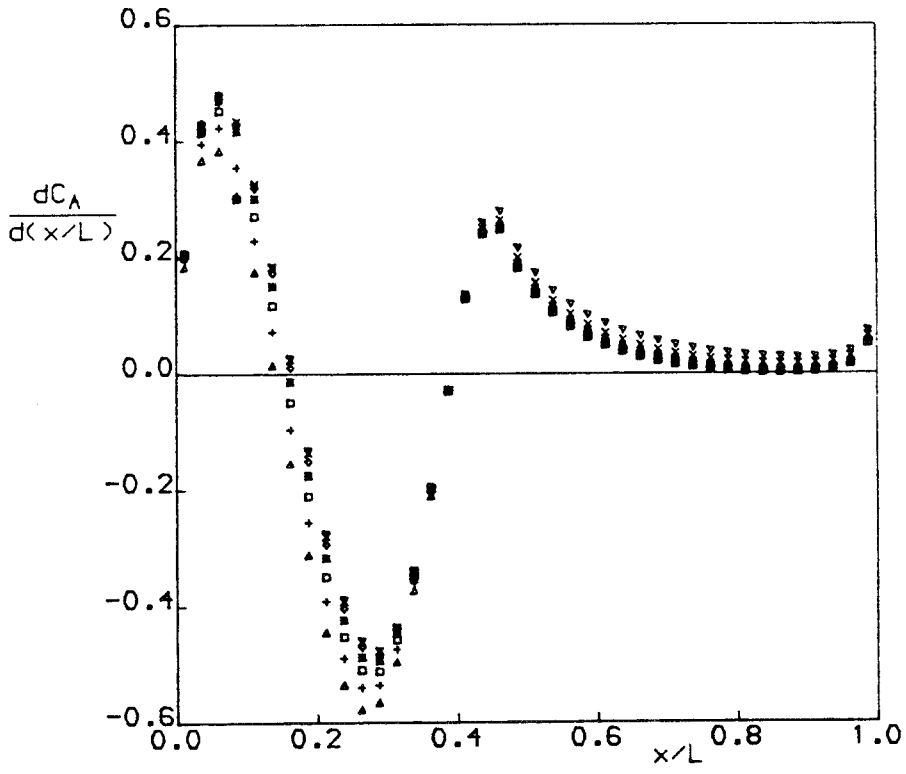

Port body

c) Axial-Force loadings

Figure 20 concluded

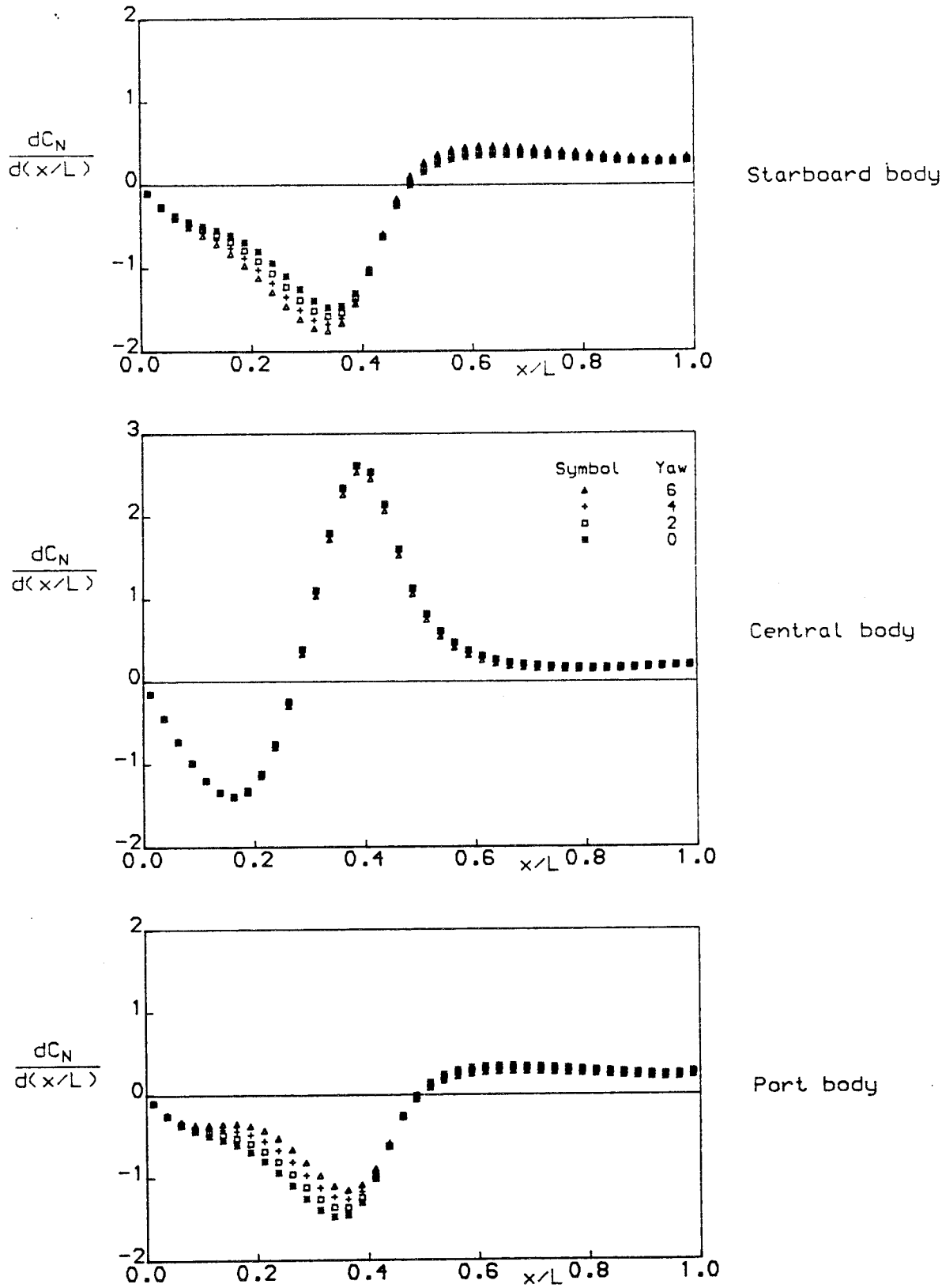

a) Pitch = -6 degrees

Figure 21. Variation of estimated normal-force loading distribution with yaw

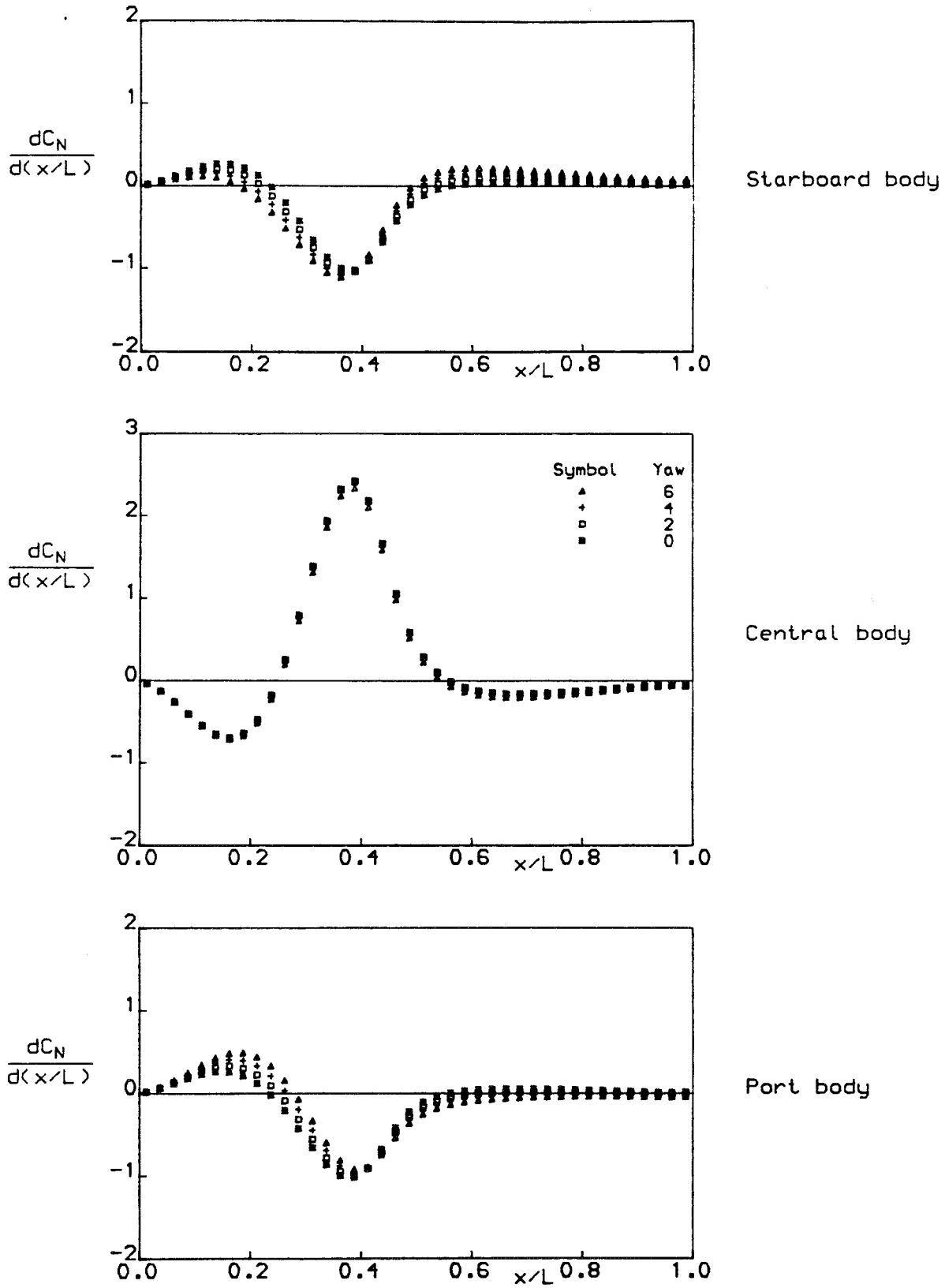

b) Pitch = 0 degrees

Figure 21 continued

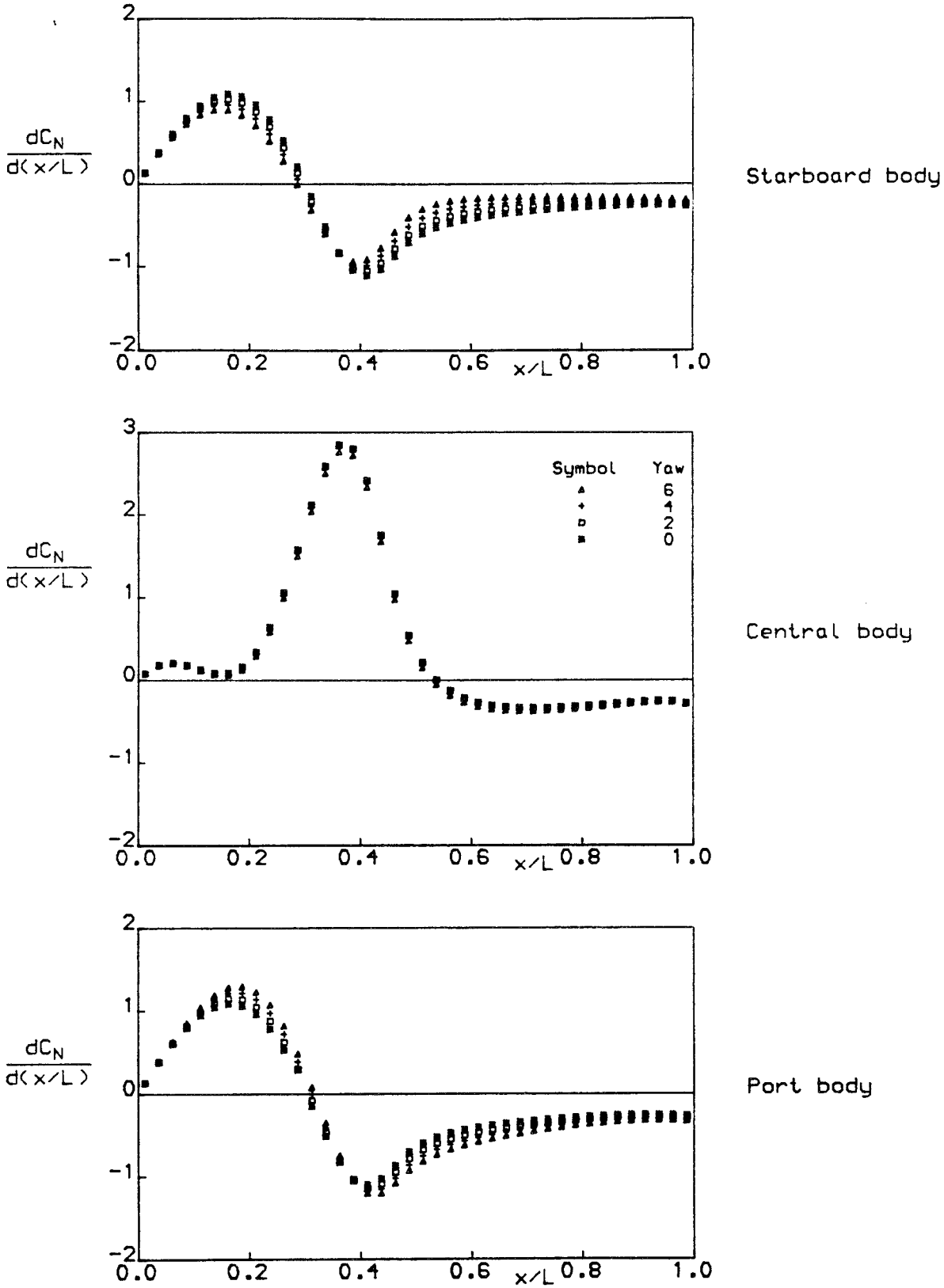

c) Pitch = 6 degrees

Figure 21 concluded

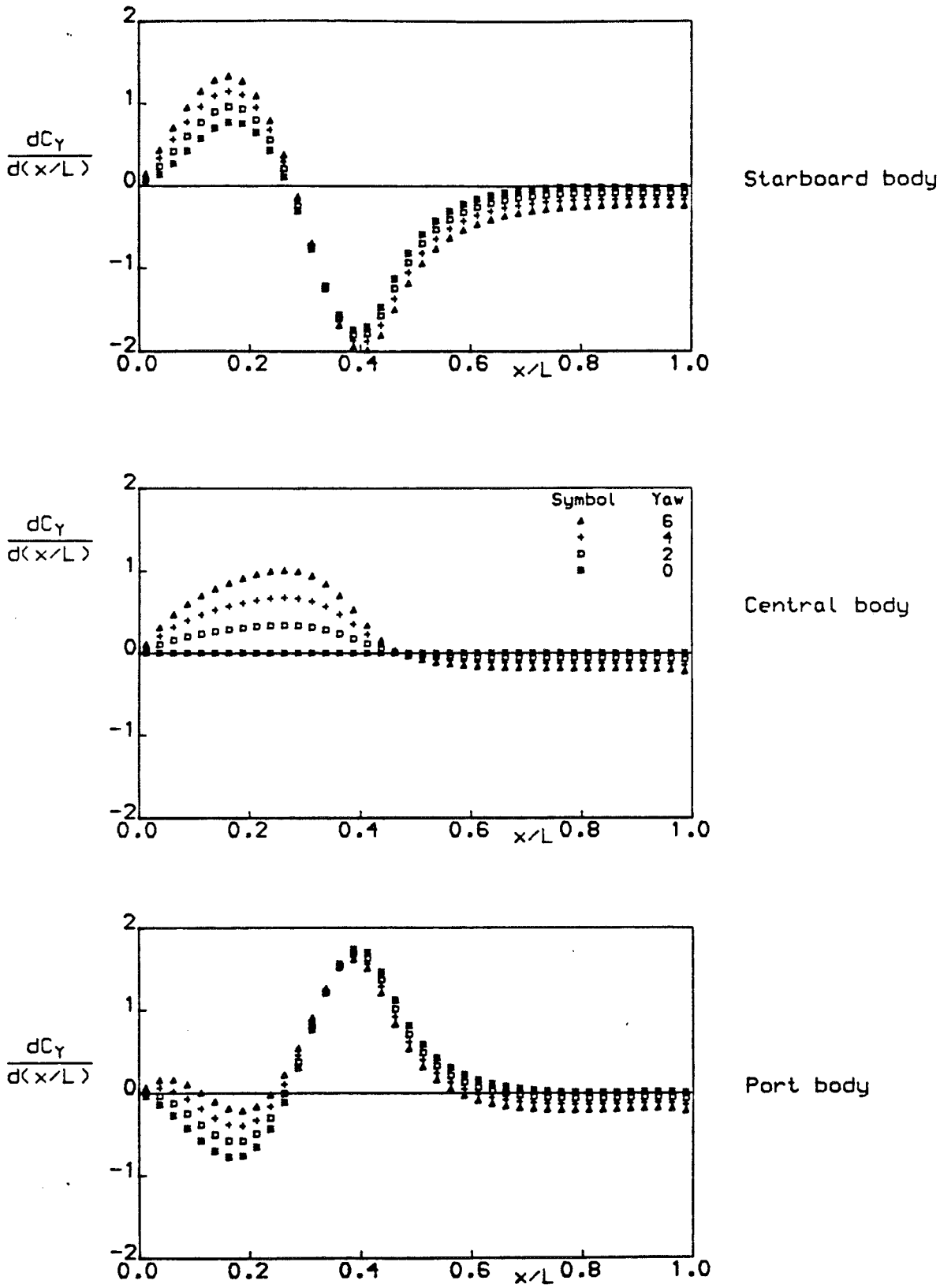

a) Pitch = -6 degrees

Figure 22. Variation of estimated side-force loading distributions with yaw

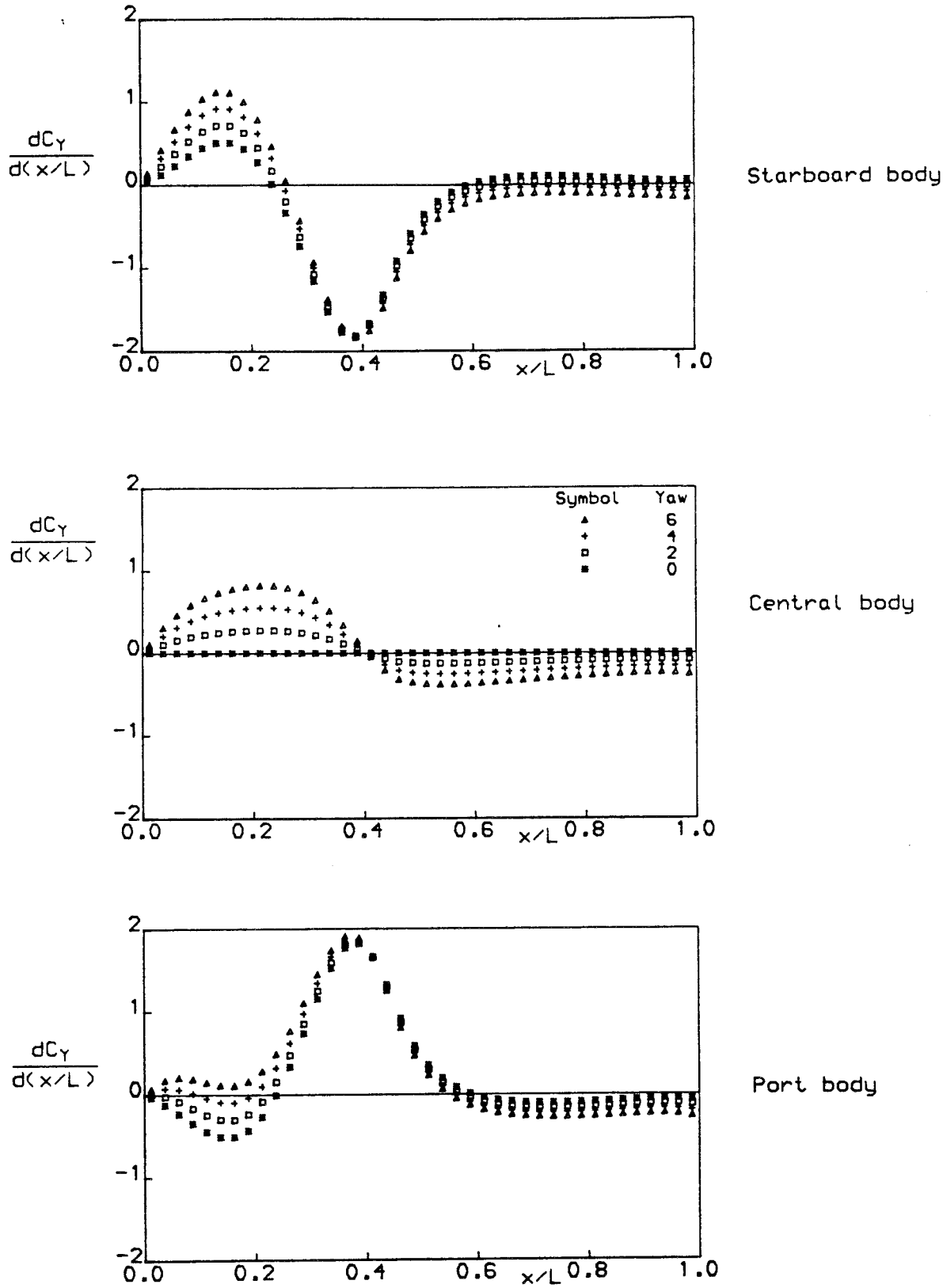

b) Pitch = 0 degrees

Figure 22 continued

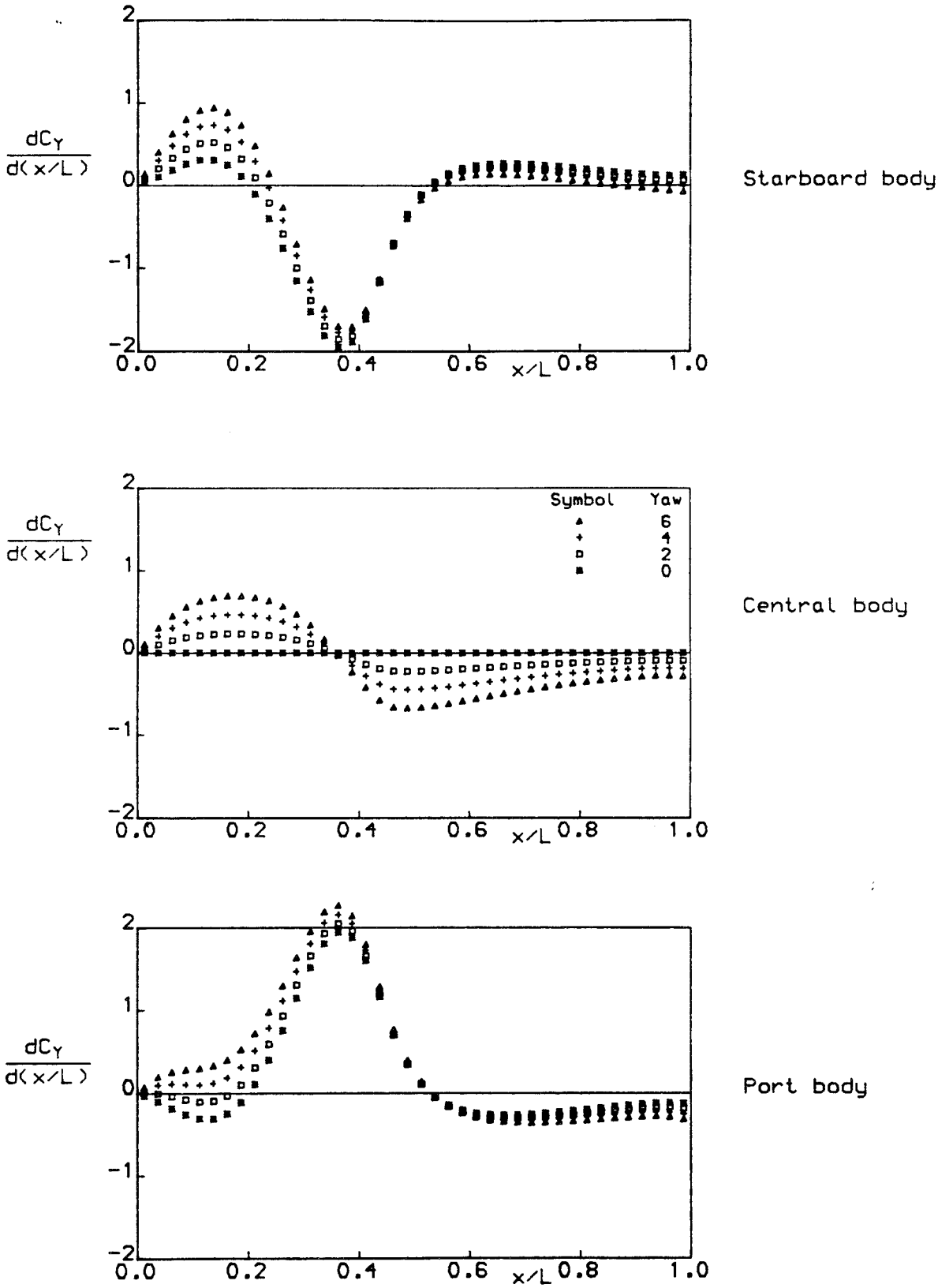

c) Pitch = 6 degrees

Figure 22 concluded

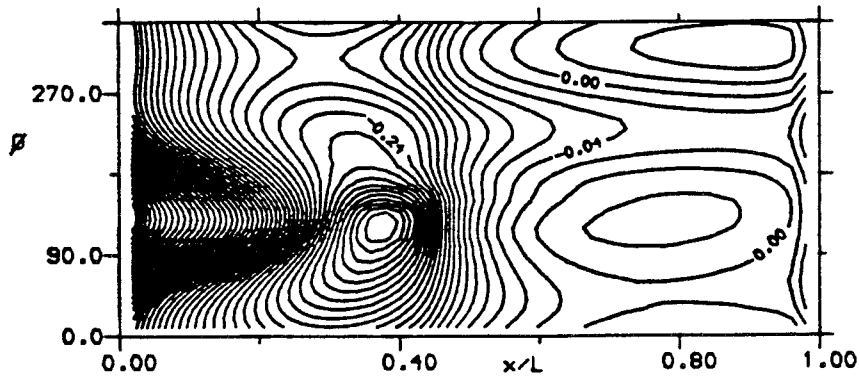

Stbd body

Contour Step 0.02

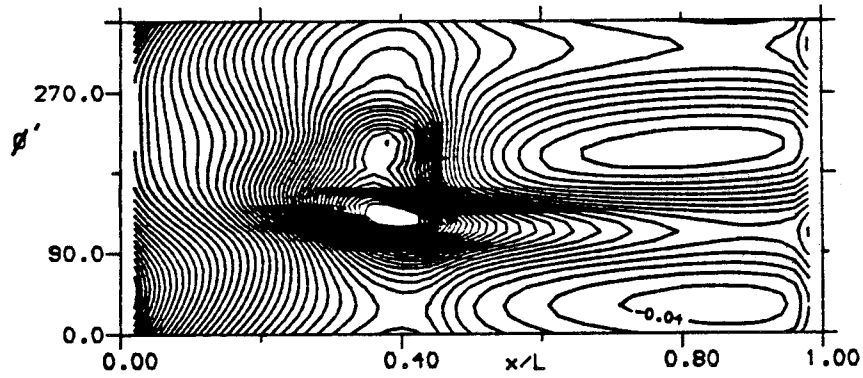

Central-body

Contour Step 0.02

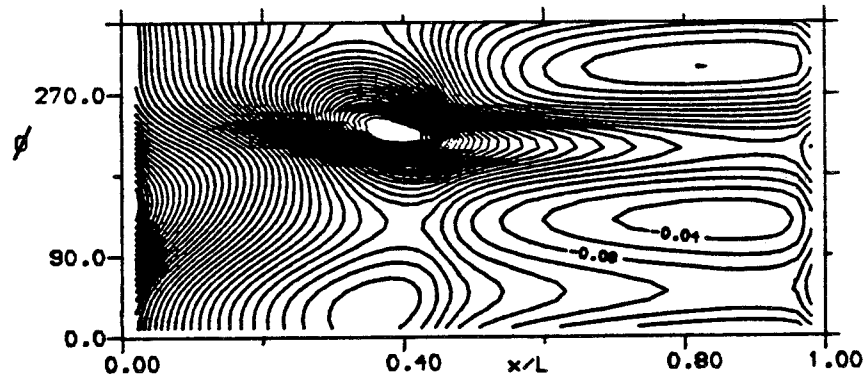

Port body

Contour Step 0.02

a) Pitch = 6 degrees, Yaw = 6 degrees

Figure 23. Contour plots of estimated Cp distributions

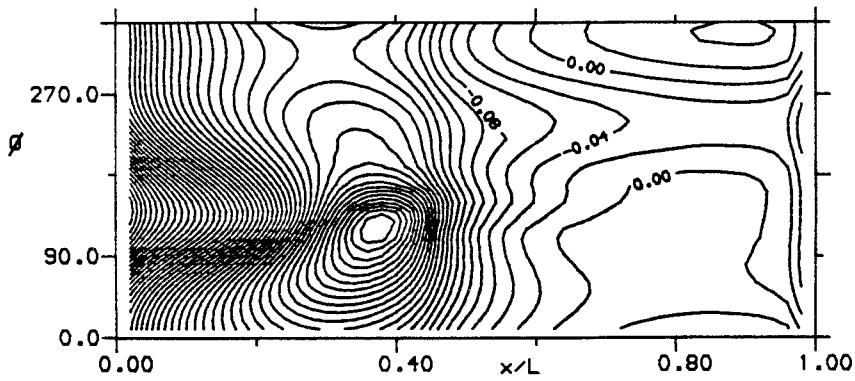

Stbd body

Contour Step 0.02

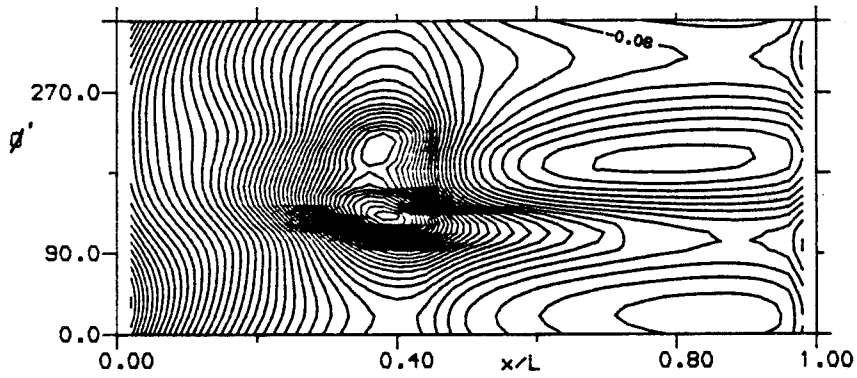

Central-body

Contour Step 0.02

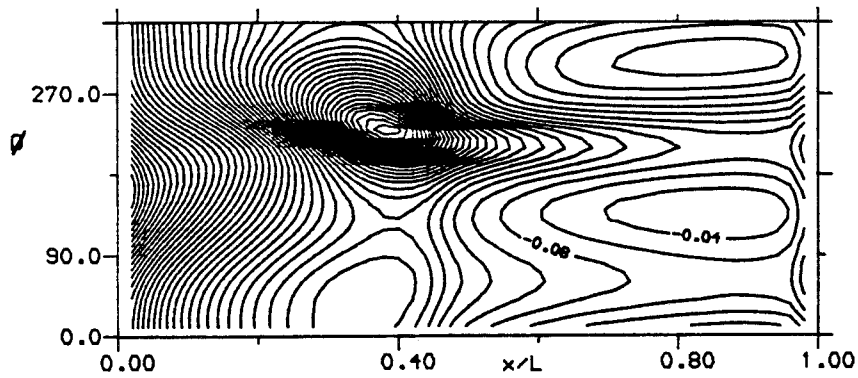

Port body

Contour Step 0.02

b) Pitch = 6 degrees, Yaw = 4 degrees

Figure 23 continued

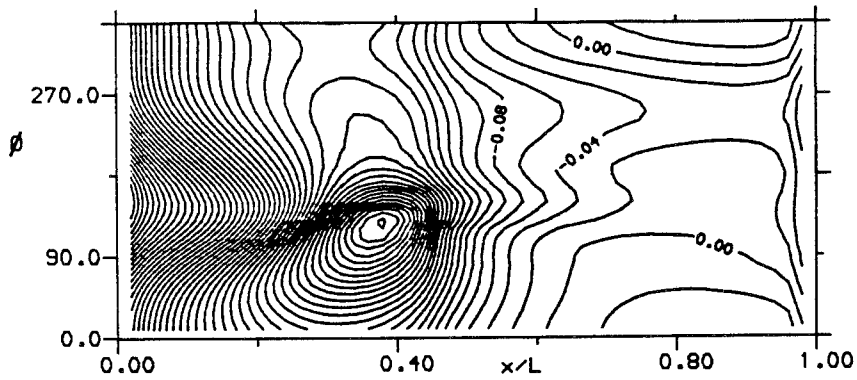

Stbd body

Contour Step 0.02

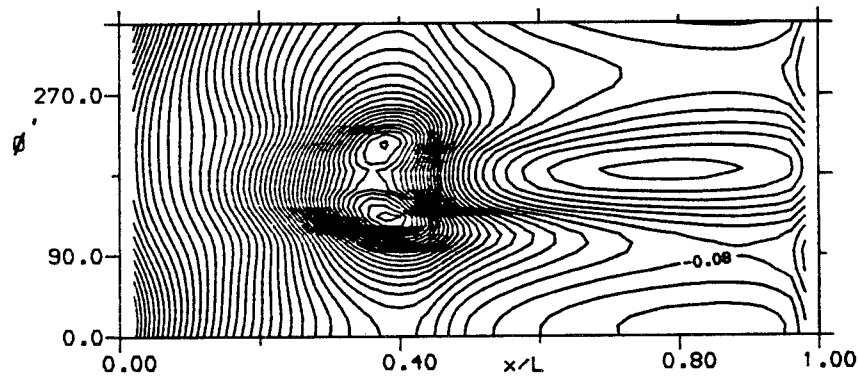

Central-body

Contour Step 0.02

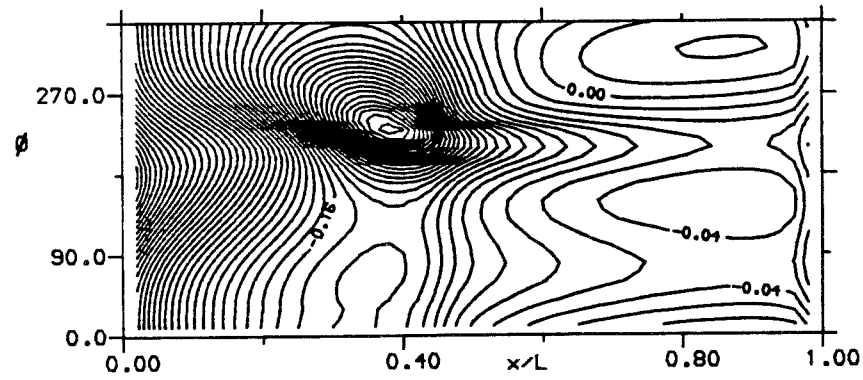

Port body

Contour Step 0.02

c) Pitch = 6 degrees, Yaw = 2 degrees

Figure 23 continued

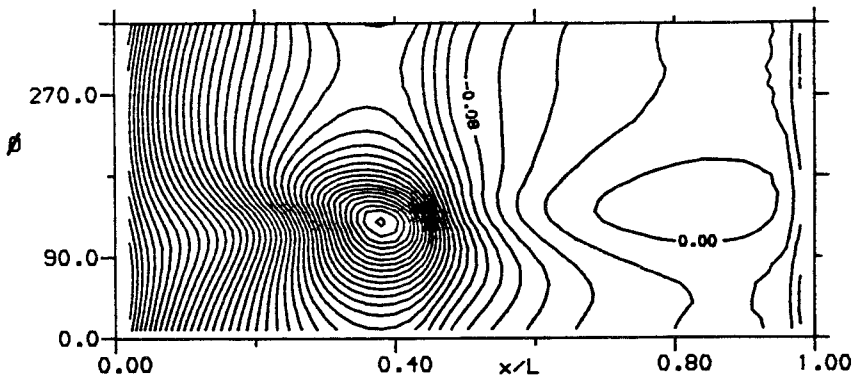

Stbd body

Contour Step 0.02

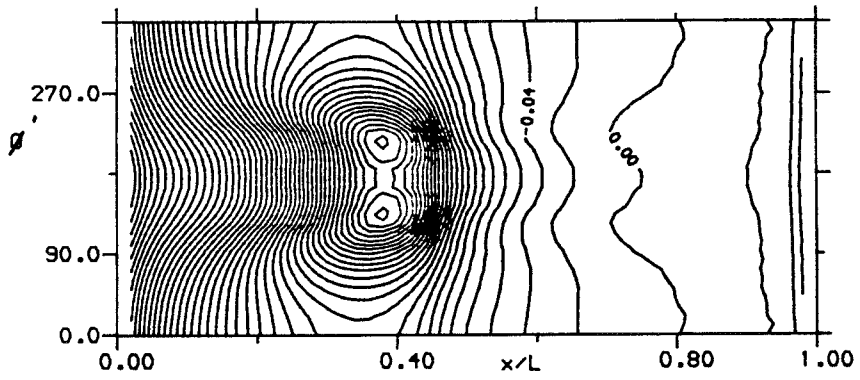

Central-body

Contour Step 0.02

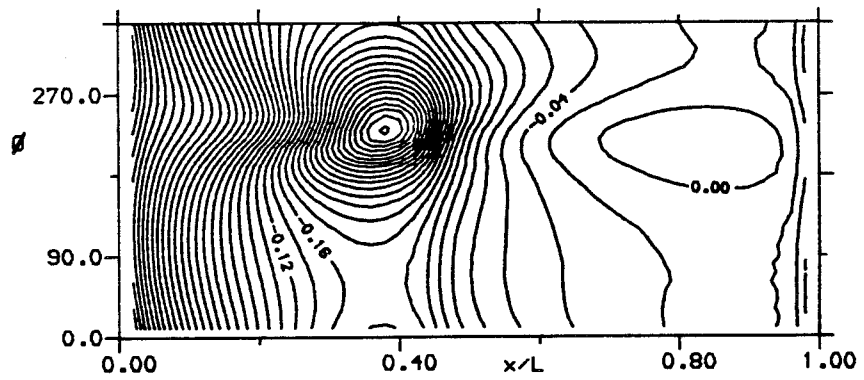

Port body

Contour Step 0.02

d) Pitch = -2 degrees, Yaw = 0 degrees

Figure 23 continued

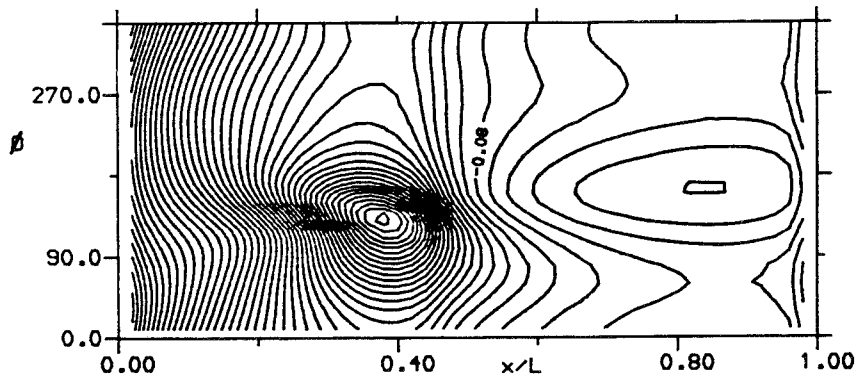

Stbd body

Contour Step 0.02

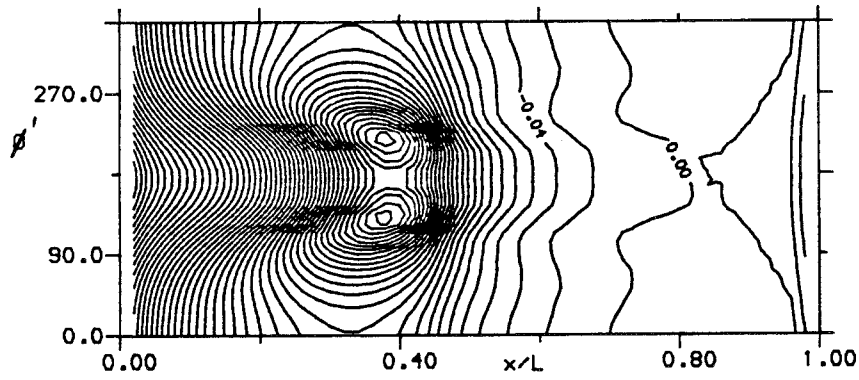

Central-body

Contour Step 0.02

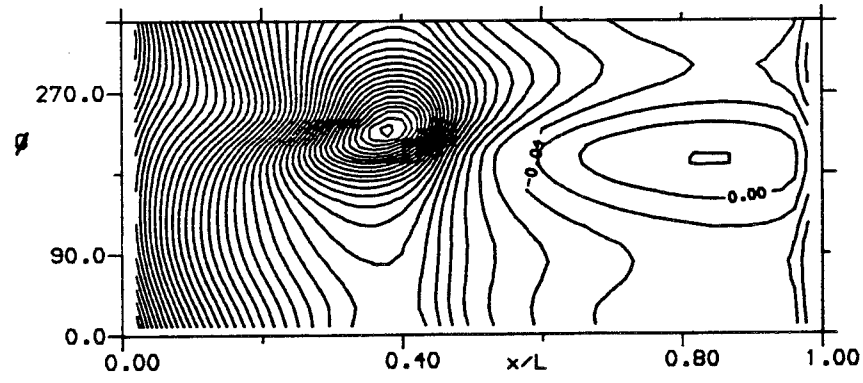

Port body

Contour Step 0.02

e) Pitch = -4 degrees, Yaw = 0 degrees

Figure 23 continued

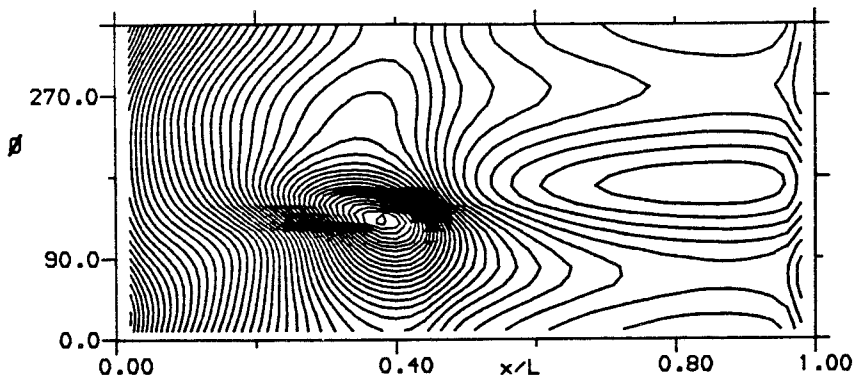

Stbd body

Contour Step 0.02

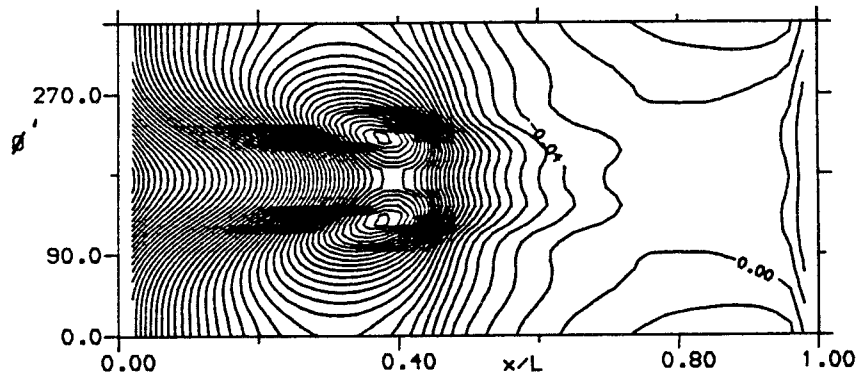

Central-body

Contour Step 0.02

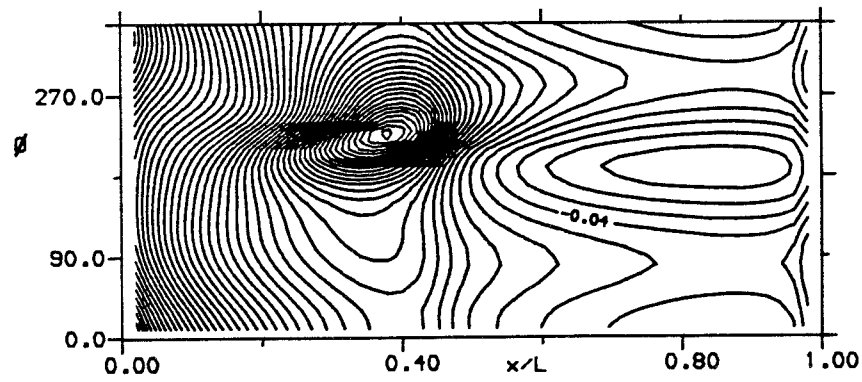

Port body

Contour Step 0.02

F) Pitch = -6 degrees, Yaw = 0 degrees

Figure 23 continued

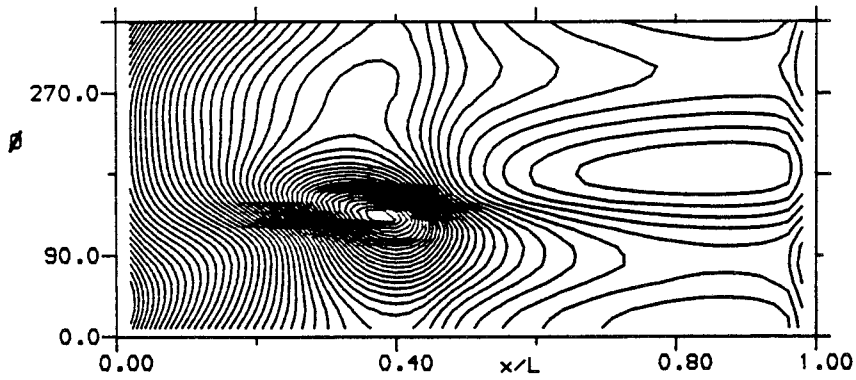

Stbd body

Contour Step 0.02

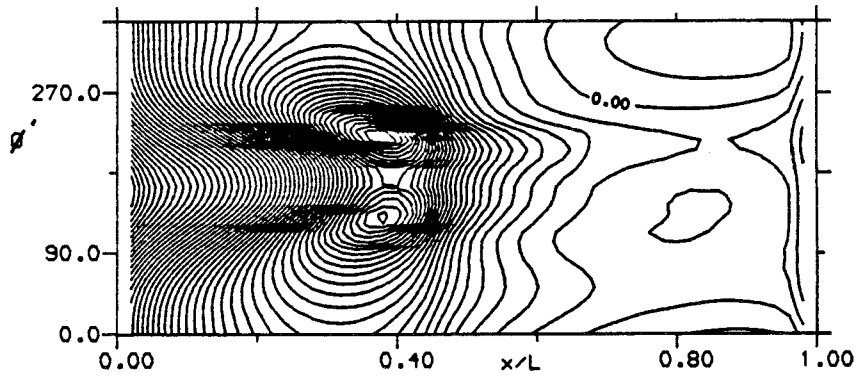

Central-body

Contour Step 0.02

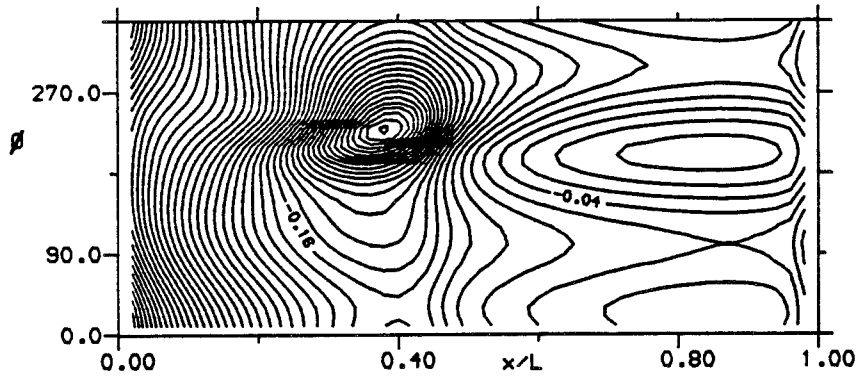

Port body

Contour Step 0.02

g) Pitch = -6 degrees, Yaw = 2 degrees

Figure 23 continued

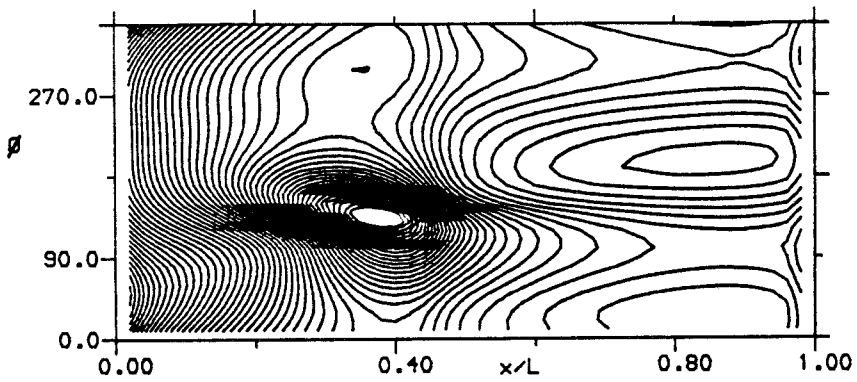

Stbd body

Contour Step 0.02

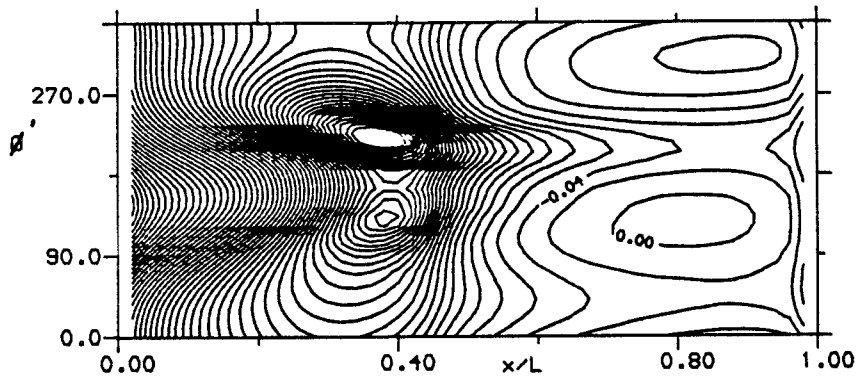

Central-body

Contour Step 0.02

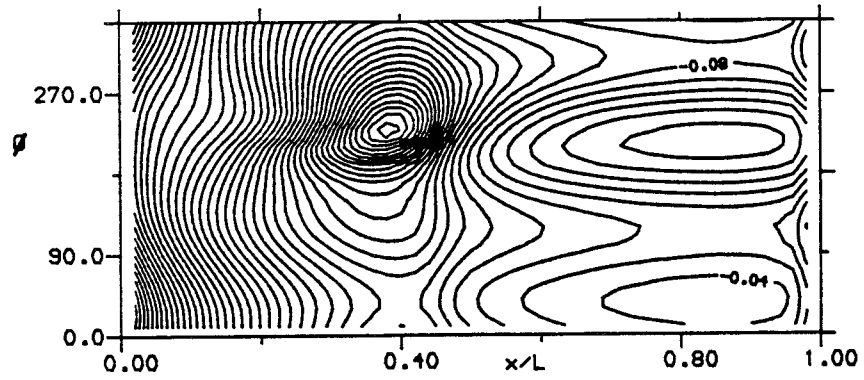

Port body

Contour Step 0.02

h) Pitch = -6 degrees, Yaw = 4 degrees

Figure 23 continued

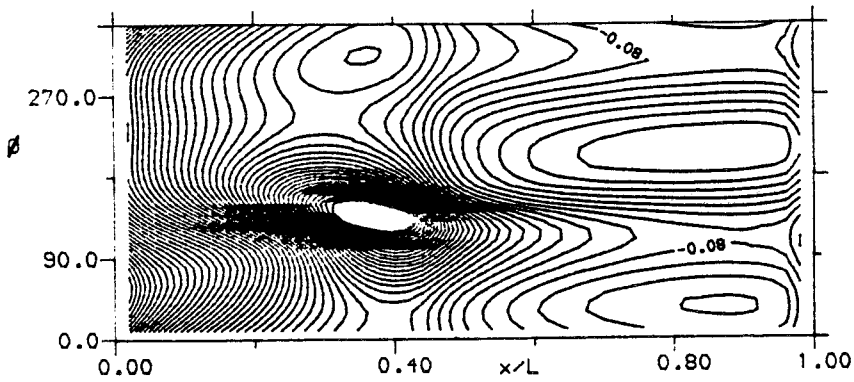

Stbd body

Contour Step 0.02

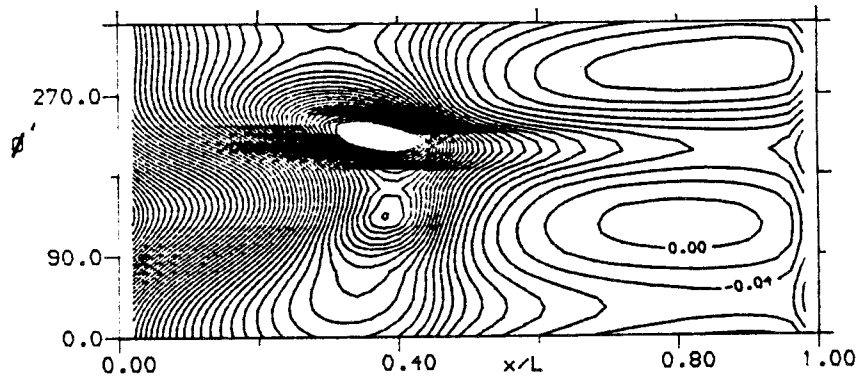

Central-body

Contour Step 0.02

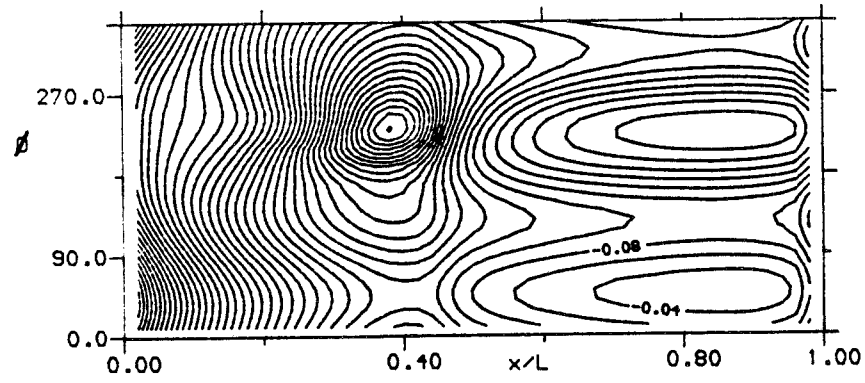

Port body

Contour Step 0.02

i) Pitch = -6 degrees, Yaw = 6 degrees

Figure 23 continued

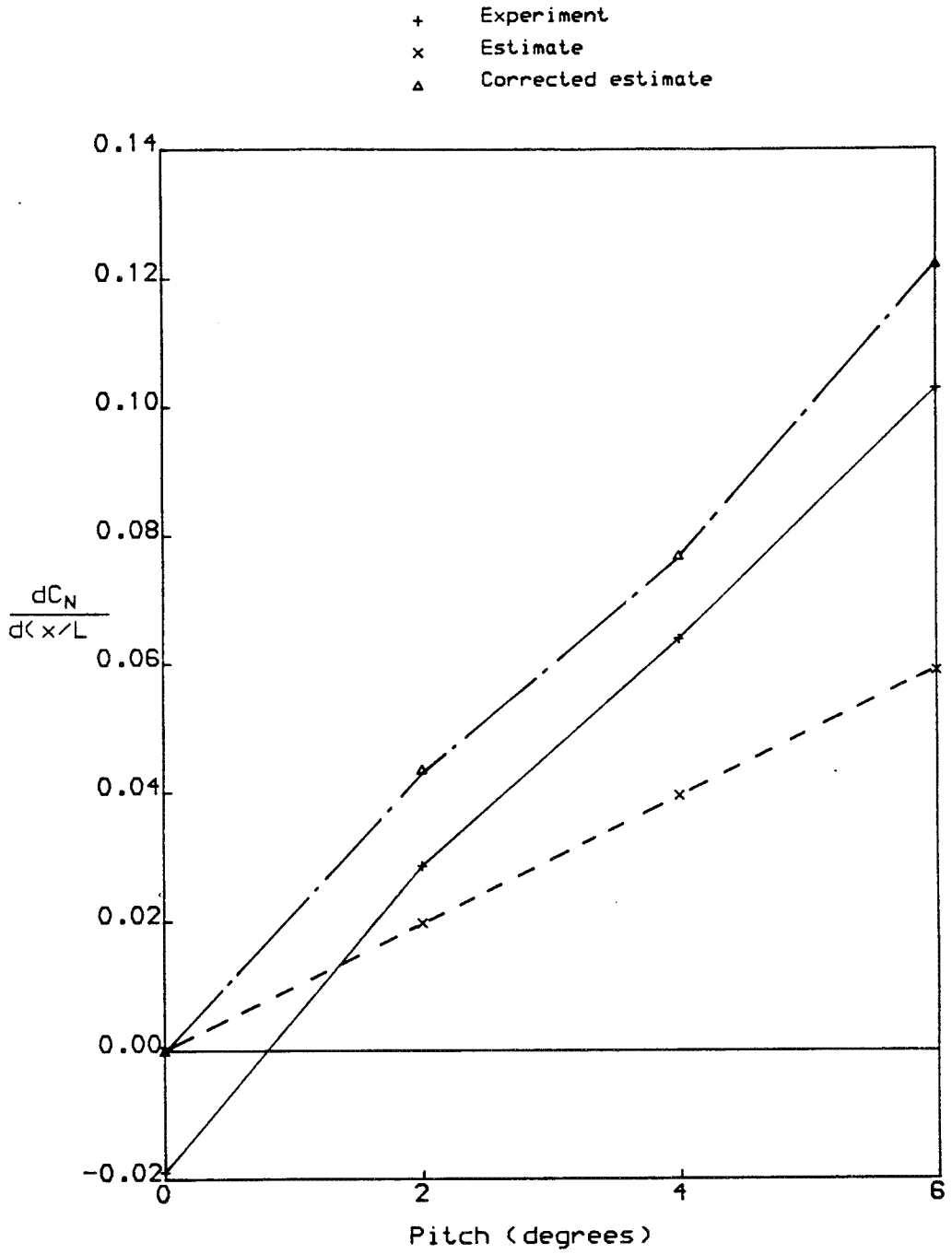

Figure 24. Single body. Comparison of estimated and experimental variations of C_N with pitch

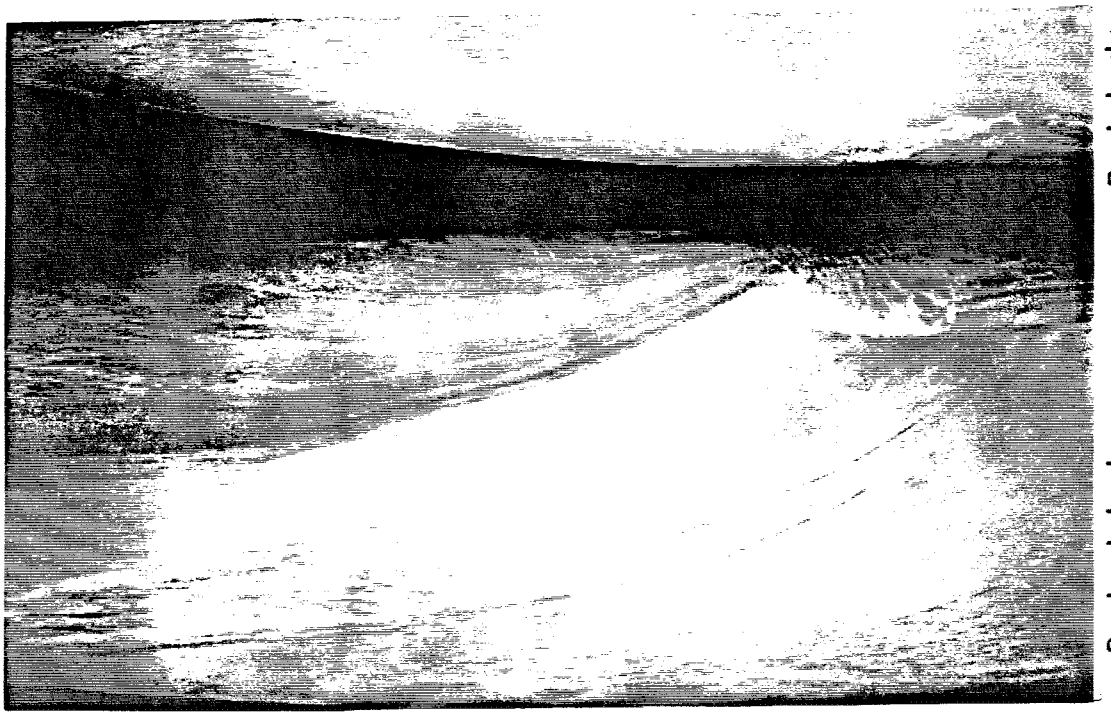

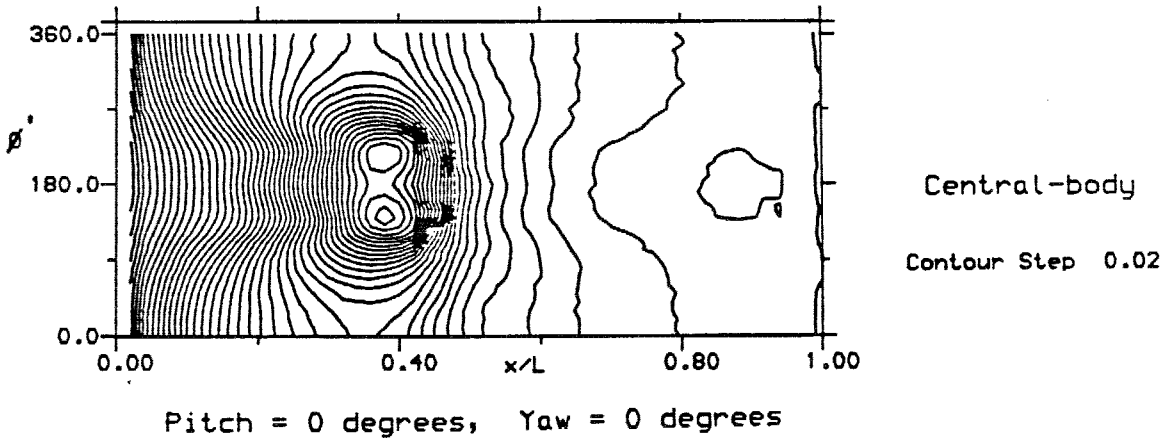

Pitch = 0 degrees, Yaw = 0 degrees

Figure 25. Oil-flow visualisation patterns